How to formulate for structure and texture via 3D-Printing – Design and characterisation of edible biopolymer gels to act as release vehicles

by

Michael-Alex Kamlow

A thesis submitted to the University of Birmingham for the degree of

DOCTOR OF PHILOSOPHY

School of Chemical Engineering

College of Physical and Engineering Sciences

The University of Birmingham

March 2022

Abstract

3D printing of edible materials has seen a surge of interest within the last decade. However, there exists a shortage of printable materials and the understanding of parameters that must be controlled to facilitate successful print jobs that are appealing to consumers and reproducible to prevent waste and keep costs down. 3D printed objects are created one layer at a time, with subsequent layers deposited on top of the previous one. This requires the shape to set quickly and be able to support the weight of the new layers above it. Most research on the 3D printing of edible materials has focused on extruding pre-gelled samples which maintain their shape due to yield stress, with no sol-gel transition taking place. This work aims to address the gaps in the literature present surrounding hot-extrusion 3D printing. Hydrocolloid gels that gel rapidly, with a high gel strength and recovery that allows it to maintain its shape after printing are ideal for this method. This work examined agar and kappa-carrageenan (κC) as candidate hydrocolloids.

Initially these gels had their thermal characteristics analysed through rheology and micro differential scanning calorimetry (DSC), as the gel temperatures were a key parameter for hot-extrusion 3D printing. The storage modulus (G′) was also used to determine printability of the gels. Above their gel temperature, gels should have a low G′ which should rapidly rise below the gel temperature. 3% w/v κC with 2% w/v vitamin B1 had a G′ of around 100,000 Pascals and was found to be printable. 2% w/v agar was not printable with the printing setup being used. Hereafter, agar was no longer used. Texture profile analysis showed that 3D printed gels were weaker than cast gels, undergoing delamination at the weak semi-fused sites between printed layers. Release tests were carried out and the 3DP were found to release more vitamin B1 compared to cast gels (78% vs 66% after 6 hours at 37 ˚C) owing to the layering allowing water to penetrate more quickly into the gel network.

Sunflower oil (SFO) was then added into the systems by creating oil-in-water emulsions and then dispersing the κC within them to produce emulsion gels. This gave a system with controllable energy content and the ability to encapsulate lipophilic molecules in a

straightforward manner. Two emulsifiers were used, tween 20 (T20) and whey protein isolate (WPI). T20-stabilised emulsions underwent flocculation upon addition of the κC, but the WPI-stabilised emulsion gels did not. DSC showed that if the concentration of κC was fixed at 3% w/w in the aqueous phase, then addition of up to 40% w/w sunflower oil did not affect the gelling temperatures (36-37 ˚C). This was reflected in the printability not being affected by varying the oil phase from 0-40% w/w. Post-printing rheology and texture profile analysis found that increasing the oil fraction did not affect the tested mechanical characteristics of the 3D printed gels as they still failed along the semi-fused sites between layers.

Finally, to build on this work the emulsion gels were tested for stability and it was found that the oil droplet size remained constant over 8 weeks. Cinnamaldehyde, a lipophilic molecule was added to the oil phase and release tests were carried out. Unlike the vitamin B1 there was no significant difference in the final amount of cinnamaldehyde released over six hours between cast and 3D printed κC-emulsion gels. Lastly, erioglaucine disodium salt (EDS) was added and co-release was carried out. The EDS was found not to interfere with the release of the cinnamaldehyde and it released faster from the 3D printed gels compared to the cast gels. Overall κC-gels were found to be suitable for 3D printing under a narrow range of parameters with and without sunflower oil. The 3D printed gels perform differently to cast gels in terms of mechanical properties owing to the presence of semi-fused sites running throughout them. They can be utilised as customisable release vehicles that release hydrophiles at a faster rate and lipophiles at a similar rate compared to the equivalent cast gels.

Acknowledgements

Well, with the completion of this thesis, the time has come to close the book on this period of my life. Part of that involves expressing some gratitude to the people who were alongside me for the journey.

I want to thank my primary supervisor Dr. Tom Mills, not only for all of his help during my time in the lab, in supervisor meetings and group meetings; but also for accepting me for study onto a PhD and being willing to take a chance on someone coming from a different background to chemical engineering, I would also like to express my gratitude to my secondary supervisor, Dr. Fotis Spyropoulos. His help in formulating ideas of where to next direct my research, understanding results and in my writing were invaluable and he went above and beyond what I had expected from a secondary supervisor! Thank you to you both, I will always be indebted to the two of you.

I want to thank my post-doctoral researcher Dr. Saumil Vadodaria for the time spent helping me in and out of the lab, as well as always having time for a chat. I was honoured to spend most of my time as a member of the postgraduate researcher student committee, and I'd like to thank everyone who served with me.

I want to thank all the students who were with me as part of the food microstructure group, not only as fellow researchers but as people to spend time with outside of the lab. I especially want to thank Kilian Daffner for helping me obtain the printing system from Germany, as well as being a great housemate and friend for two years. I want to thank Nelli Chourmouziadi Laleni for many helpful discussions around my work and fun discussions over lunch. I'd also like to thank Tom Holt for giving me a place to stay during the final four months of my PhD, helping me in the lab and always being available to go out for a drink after work.

I also want to thank my family for supporting me through this time of my life and beyond. Your love and care will always be appreciated. Many thanks to you Mum, Dad, Mark, Charlotte, Nadine, Chris, Tom, Rosie and Maya! I'd also like to thank my friends Saul, Andy, Tommy as well as all my other friends from home and from the time of my first degree.

Semper paratus

Table of Contents

List of tables

List of figures

List of equations

List of abbreviations and initialisations

3DP	Three-dimensional printing
δ	Phase angle
ΔH	Enthalpy change
κC	Kappa-carrageenan
ω	Angular frequency
ζ-potential	Zeta potential
ABS	Acrylonitrile butadiene styrene
AM	Additive manufacturing
C_0	Critical minimum concentration
C*	Critical overlap concentration
CAD	Computer aided design
CLSM	Confocal laser scanning microscopy
$D_{3,2}$	Surface weighted mean
$D_{3,3}$	Geometric weighted mean
$D_{4,3}$	Volume weighted mean
DSC	Differential scanning calorimetry
µDSC	Micro differential scanning calorimetry
EBAM	Electron beam additive manufacturing
EDS	Erioglaucine disodium salt

F	Fickian diffusion constant
FDM	Fused deposition modelling
FFF	Fused filament fabrication
Fill	Fill space
Flow	Flow percentage
G′	Storage modulus
G″	Loss modulus
HCl	Hydrochloric acid
H_L	Layer height
KCl	Potassium chloride
LVER	Linear viscoelastic region
N_s	Nozzle size
O/W emulsion	Oil-in-water emulsion
PBS	Phosphate buffer solution
PLA	Polylactic acid
R	Relaxational constant
R_s	Syneresis ratio
SFO	Sunflower oil
SLS	Selective laser sintering
T20	Tween 20
TD-NMR	Time domain nuclear magnetic resonance

T_{gel}	Gel temperature
T_H	Hold temperature
T_{HWB}	Water bath temperature on feed pipes
T_{melt}	Melt temperature
T_{NWB}	Water temperature on the nozzle
TPA	Texture profile analysis
T_{PB}	Printer bed temperature
UV vis-spec	Ultraviolet visible spectrophotometry
V_p	Print speed
WPI	Whey protein isolate

Chapter 1

Introduction

1.1 Context and Motivation

In the future, the production of nutritionally tailored and fortified foods at the point of consumption, for specific target groups such as athletes, the elderly or malnourished people is expected to see increased demand (McClements, et al., 2021). One means of achieving this is through additive manufacturing, also known as 3D printing (3DP). 3DP entails the build-up of parts in a layer-by-layer manner, by using image files that are digitally sliced into layers by software and then transmitted to the printer. Generally, 3DP entails the production of building materials such as plastic polymers, ceramics and metals (Gebler, Schoot Uiterkamp, & Visser, 2014) However, from around the start of the previous decade, more and more research started to explore 3DP's potential for use as a means of pioneering food manufacture.

3DP enables the production of food with a tightly controlled structure, with very little waste (Diaz, Noort, & Van Bommel, 2017). This presents the possibility of creating foods with specialised characteristics, such as softer foods for people with swallowing difficulties, or unique release characteristics for flavours or pharmaceuticals (Kouzani, et al., 2017; Vithani, et al., 2019). However, food 3DP is still seen as a niche technology, with various issues to overcome including slow throughput compared to traditional means of manufacture (Lipton, Cutler, Nigl, Cohen, & Lipson, 2015), issues with consumer perception (Lupton & Turner, 2018) and a limited library of food "inks" restricting what can be printed (Sun, et al., 2015). Furthermore, the multi-component nature of food systems is another major challenge, often containing several materials in varying ratios and phases; as well as micro- and nanostructural features that affect structural and sensory properties, with many of these features being temperature, ion and processing dependent.

Various foodstuffs have been the subject of research in food 3DP including chocolate (Lanaro, Desselle, & Woodruff, 2019), dough (Yang, Zhang, Prakash, & Liu, 2018), dairy gels (Daffner, Ong, Hanssen, Gras, & Mills, 2021), mashed potato (Liu, Zhang, Bhandari, & Yang, 2018) and more. Many studies have focused on hydrocolloid gels as materials for food 3DP. These have

various advantages that make them ideal for use. Many are biocompatible, renewable and are well understood in both food and pharmaceuticals. Hydrocolloid gels can be printed through either cold or hot extrusion. Cold extrusion does not undergo a phase transition *in situ*, produces shapes with a superior fidelity and requires no temperature control (Gholamipour-Shirazi, Norton, & Mills, 2019). Hot extrusion 3DP can print highly viscous gels with less difficulty, as they are still in the sol-state when within the printer (Azam, Zhang, Bhandari, & Yang, 2018). Hot extrusion 3DP requires hydrocolloid gels that rapidly solidify below their gelation temperature (T_{gel}), with a high recoverability and stiffness being desirable (Warner, Norton, & Mills, 2019).

Despite plenty of research into the 3DP of hydrocolloid gels, there still exist gaps within the current literature that this project looks to address. One issue is that most of the existing literature does not examine how the 3DP hydrocolloid gels perform compared to their cast equivalents. Most research groups tend to present formulations and parameters that result in successful prints. Without examining how these compare to the equivalent cast material, it is difficult to overcome issues with consumer perception, as well as meaning they can only speculate on the unique textural and structural characteristics of 3DP foods. Furthermore, despite there being plenty of review papers looking to the future and talking about functional foods created through 3DP, there exists little literature examining the release of active molecules from 3DP hydrocolloid matrices. With most research into molecular release from 3DP devices being from a pharmaceutical perspective, taking in tablets and other oral dosage forms, that while being edible are not traditionally considered foodstuffs.

For 3DP to become the disruptive technology that it has threatened to be, a detailed understanding of the processing parameters and the feedstock characteristics will be required. Understanding these, will make it clearer what future formulations will be printable, as well as whether certain formulation manipulations such as the addition of an oil phase to hydrocolloid gels, or incorporating a charged molecule will be doomed from the outset. Anything that interferes with the printability, such as increasing viscosity or decreasing gel stiffness and recoverability might not be suitable without altering processing or formulation characteristics

(Kim, Bae, & Park, 2017). Plenty more work is required to build up a suite of suitable feedstocks, which have a degree of customisation and a printer or group of printers suitable for use in people's homes.

1.2 Research objectives

The overarching objective of this project was to continue to expand the library of available feedstocks for food 3DP within an extrusion context. Not only would hydrocolloid gels be investigated, but whether emulsion gels containing a stabilised oil phase could be produced and how they affected the printability of the materials, and the mechanical properties of the printed gels. This work was framed in the context of utilising these gels as molecular release vehicles and comparing how they performed against a traditional cast gel both texturally and as a release vehicle. The main objectives included:

- Investigate the thermal and rheological characteristics of candidate hydrocolloid gels, and assess their suitability for hot-extrusion 3DP
- Establish printing parameters that can be transferred between different 3D printing systems
- Carry out post-printing characterisation of printed gels and compare them to cast gels
- Assess the performance of 3DP gels as release vehicles for model molecules and compare them to cast gels

1.3 Thesis layout

This thesis comprises six chapters, covering the introduction, an examination of current literature, three results chapters, all of which have been published in peer-reviewed journals and a chapter covering overall conclusions and future work. The details of these publications can be found on the cover page of the corresponding chapter.

Chapter 1 – The introduction to the project, covering the project background, and the objectives of this research

Chapter 2 – A literature review covering the state of the art, within 3D printing, examining different 3DP techniques both within and without a food setting. It then continues to examine the background knowledge of hydrocolloid gels, emulsions and emulsification routes, as well as emulsion gels as foods and release vehicles.

Chapter 3 – This chapter carries out pre-printing characterisation on kappa-carrageenan (κC) and agar hydrocolloid gels, to assess their suitability for hot-extrusion 3DP with and without a model molecule, vitamin B1, otherwise known as thiamine. Following this, several printing parameters were tested in order to determine the printability of the thiamine-hydrocolloid gels. Then post-printing characterisation involving compression texture profile analysis (TPA) and light microscopy were carried out to examine the bulk- and microstructural characteristics of the 3DP gels and compare them to their cast equivalents. Finally release tests were carried out to assess the performances of cast and 3DP gels, with simple mathematical modelling based on the Peppas-Sahlin model being carried out (Peppas & Sahlin, 1989).

Chapter 4 – This work involved the formulation of emulsion gels, as a natural progression of the simple, water-based gels investigated in the previous chapter. Since only κC was found to be printable in the previous chapter, these were the only hydrocolloid systems examined from here on out. Sunflower oil (SFO) at varying concentrations (0-40% w/w) were added to the gel systems along with one of two different emulsifiers (whey protein isolate and Tween 20). These were then assessed to see if varying SFO concentration or emulsifier type affected the printability of the κC-emulsion gels. Finally, mechanical characterisation (oscillation rheology and compression TPA) and confocal laser scanning microscopy was carried out on the 3DP κC-emulsion gels, as well as the cast equivalents to see what effect the SFO and emulsifiers had on their bulk- and microstructural properties.

Chapter 5 – This work further builds upon the systems examined in the previous chapter. The κC-emulsion gels had micron and sub-micron emulsions distributed through them. Their stability characteristics were examined in terms of water loss and droplet size over time. Penetration TPA was carried out to examine the bulk structure in a different manner to the

previous chapters. Then, a lipophilic model molecule (cinnamaldehyde) was added to the oil phase and release tests were carried out for micron and sub-micron scale emulsion gels stabilised by either whey protein isolate or Tween 20 in a range of release media. Finally, a hydrophilic model molecule (erioglaucine disodium salt) was added, and dual release studies were carried out.

Chapter 6 – The final chapter recaps all the major findings within the project, and some avenues for future work are proposed.

1.4 Publications and presentations

The results of this project have been per-reviewed, and/or presented at conferences.

1.4.1 Publications

- Gholamipour-Shirazi, A., **Kamlow, M.-A.,** T Norton, I., & Mills, T. (2020). How to formulate for structure and texture via medium of additive manufacturing-a review. Foods, 9(4), 497
- **Kamlow, M.-A.,** Vadodaria, S., Gholamipour-Shirazi, A., Spyropoulos, F., & Mills, T. (2021). 3D printing of edible hydrogels containing thiamine and their comparison to cast gels. Food Hydrocolloids, 116, 106550
- **Kamlow, M.-A.,** Spyropoulos, F., & Mills, T. (2021). 3D printing of kappa-carrageenan emulsion gels. Food Hydrocolloids for Health, 1, 100044
- **Kamlow, M.-A.,** Holt, T., Spyropoulos, F., & Mills, T. (2022). Release and co-release of model hydrophobic and hydrophilic actives from 3D printed kappa-carrageenan emulsion gels. Food Hydrocolloids, 132, 107852

1.4.2 Presentations

1.4.2.1 Oral Presentations (Speaker in bold)

- **Kamlow, M.-A.,** Vadodaria, S., Gholamipour-Shirazi, A., Spyropoulos, F., & Mills, T. 3D printing of edible hydrogels containing thiamine and their comparison to cast gels. 15th International Hydrocolloids Conference, Melbourne, Australia, 2020.

- **Kamlow, M.-A.,** Spyropoulos, F., & Mills, T. Assessing the suitability of kappa-carrageenan for the 3D printing of complex gel structures. International Conference on Formulations in Food and Healthcare, 2021.

1.4.2.2 Poster presentations (Speaker in bold)

- **Kamlow, M.-A.,** Spyropoulos, F., & Mills, T. Studying the release of functional molecules from 3D printed hydrocolloid gels. 4th UK Hydrocolloids Symposium - From Food to Bioprocessing, University of Leeds, School of food science, 2019.
- **Kamlow, M.-A.,** Spyropoulos, F., & Mills, T. Formulation for 3D printing: Creating a plug and play platform for a disruptive UK industry. Food Layered Manufacturing of edible and printable materials – hydrocolloid gels. Formulation for 3D Printing Annual review meeting, Nottingham, 2019

1.5 References

Azam, R. S. M., Zhang, M., Bhandari, B., & Yang, C. (2018). Effect of Different Gums on Features of 3D Printed Object Based on Vitamin-D Enriched Orange Concentrate. *Food Biophysics, 13*(3), 250-262.

Daffner, K., Ong, L., Hanssen, E., Gras, S., & Mills, T. (2021). Characterising the influence of milk fat towards an application for extrusion-based 3D-printing of casein− whey protein suspensions via the pH− temperature-route. *Food Hydrocolloids*, 106642.

Diaz, J. V., Noort, M. W.-J., & Van Bommel, K. J. C. (2017). Method for the production of an edible object by powder bed (3d) printing and food products obtainable therewith. In: Google Patents.

Gebler, M., Schoot Uiterkamp, A. J. M., & Visser, C. (2014). A global sustainability perspective on 3D printing technologies. *Energy Policy, 74*, 158-167.

Gholamipour-Shirazi, A., Norton, I. T., & Mills, T. (2019). Designing hydrocolloid based food-ink formulations for extrusion 3D printing. *Food Hydrocolloids, 95*, 161-167.

Kim, H. W., Bae, H., & Park, H. J. (2017). Classification of the printability of selected food for 3D printing: Development of an assessment method using hydrocolloids as reference material. *Journal of Food Engineering, 215*, 23-32.

Kouzani, A. Z., Adams, S., Whyte, D. J., Oliver, R., Hemsley, B., Palmer, S., & Balandin, S. (2017). 3D printing of food for people with swallowing difficulties. In *DesTech 2016: Proceedings of the International Conference on design and technology* (pp. 23-29): Knowledge E.

Lanaro, M., Desselle, M. R., & Woodruff, M. A. (2019). 3D Printing Chocolate. In *Fundamentals of 3D Food Printing and Applications* (pp. 151-173).

Lipton, J. I., Cutler, M., Nigl, F., Cohen, D., & Lipson, H. (2015). Additive manufacturing for the food industry. *Trends in Food Science & Technology, 43*(1), 114-123.

Liu, Z., Zhang, M., Bhandari, B., & Yang, C. (2018). Impact of rheological properties of mashed potatoes on 3D printing. *Journal of Food Engineering, 220*, 76-82.

Lupton, D., & Turner, B. (2018). "I can't get past the fact that it is printed": consumer attitudes to 3D printed food. *Food, Culture & Society, 21*(3), 402-418.

McClements, D. J., Barrangou, R., Hill, C., Kokini, J. L., Lila, M. A., Meyer, A. S., & Yu, L. (2021). Building a Resilient, Sustainable, and Healthier Food Supply through Innovation and Technology. *Annual review of food science and technology, 12*, 1-28.

Peppas, N. A., & Sahlin, J. J. (1989). A simple equation for the description of solute release. III. Coupling of diffusion and relaxation. *International Journal of Pharmaceutics, 57*(2), 169-172.

Sun, J., Zhou, W., Huang, D., Fuh, J. Y. H., Hong, G. S. J. F., & Technology, B. (2015). An Overview of 3D Printing Technologies for Food Fabrication. *8*(8), 1605-1615.

Vithani, K., Goyanes, A., Jannin, V., Basit, A. W., Gaisford, S., & Boyd, B. J. (2019). An overview of 3D printing technologies for soft materials and potential opportunities for lipid-based drug delivery systems. *Pharmaceutical Research, 36*(1), 1-20.

Warner, E. L., Norton, I. T., & Mills, T. B. (2019). Comparing the viscoelastic properties of gelatin and different concentrations of kappa-carrageenan mixtures for additive manufacturing applications. *Journal of Food Engineering, 246*, 58-66.

Yang, F., Zhang, M., Prakash, S., & Liu, Y. (2018). Physical properties of 3D printed baking dough as affected by different compositions. *Innovative Food Science & Emerging Technologies, 49*, 202-210.

Chapter 2

Literature review – State of the art

Parts of this review were adapted from:

Gholamipour-Shirazi, A., Kamlow, M.-A., T Norton, I., & Mills, T. (2020). How to formulate for structure and texture via medium of additive manufacturing-a review. Foods, 9(4), 497.

Azarmidokht Gholamipour-Shirazi; writing—original draft preparation, Michael-Alex Kamlow.; writing – revised manuscript, review and editing, Ian T Norton; review and editing, Tom Mills.; review and editing.

2.1 Introduction

This chapter intends to critically review the relevant literature, taking in an examination of the current state of the art in 3DP, with particular focus dedicated to research based on edible materials, which will be based on a peer-reviewed paper titled: “How to Formulate for Structure and Texture via Medium of Additive Manufacturing - A Review.” Then it considers the literature surrounding food hydrocolloid gels, especially those used in the scope of this work both as structuring materials and as release vehicles, as well as their characterisation. An overview of emulsions and emulsion gels is included, covering emulsifiers and emulsification techniques as well as of release of active molecules from emulsion gels.

2.2 3D Printing

The term additive manufacturing, which is often termed 3DP and rapid prototyping, covers several manufacturing technologies that enable the creation of objects to be fabricated on demand (Ford & Despeisse, 2016; Severini, Derossi, & Azzollini, 2016). The basic concept of 3DP is a controlled process whereby a product is built up from a digital design - usually a Computer-Aided Design (CAD) file (Dankar, Haddarah, Omar, Sepulcre, & Pujolà, 2018; Izdebska & Zolek-Tryznowska, 2016). While printing the object, the 3D model is sliced into layers, by the printer software, and then printed one at a time (layer by layer) (Rayna & Striukova, 2016). 3DP has emerged as one of the most disruptive manufacturing technologies owing to its hyper-flexible nature, potential for digital interaction with customers and point of use manufacture (Bogers, Hadar, & Bilberg, 2016). The adoption of these technologies comprises four successive stages: **Rapid prototyping** – the ability to rapidly build and change plastic models of objects (prototypes). **Rapid tooling** – using tough polymers and metals to produce customised tools and moulds. **Digital manufacturing** – a totally digital production process, using CAD to design and manufacture end-products. **Home fabrication** – consumers producing objects themselves in the home (Rayna, et al., 2016). By using a business model, it was concluded that rapid prototyping and rapid tooling had a limited impact, but direct manufacturing and home fabrication can

be highly disruptive (Rayna, et al., 2016).

The advantages of 3DP, in general, are low waste, increased precision, time-saving, and high efficiency (Chen, et al., 2019). 3DP is a platform that enables the manufacture of complex structures from digital design data immediately, without special tools and equipment, by providing new opportunities for freedom of design (Jiang, Kleer, & Piller, 2017). Rapid prototyping is one of the main benefits of 3DP (Ngo, Kashani, Imbalzano, Nguyen, & Hui, 2018). 3DP offers the capacity to build objects with any shape and dimension as well as the ability to control chemical, physical, mechanical properties, and in turn the microstructure, by modifying their composition (Poologasundarampillai & Nommeots-Nomm, 2017; Severini, Derossi, Ricci, Caporizzi, & Fiore, 2018).

3DP is a mass customisation and personalisation enabling technology. Due to limits in production speed among other technological bottlenecks, 3DP is not yet capable of mass production in all fields (Bogers, et al., 2016; Li, Aspler, Kingsland, Cormier, & Zou, 2016). 3DP enables private and commercial users to design and create their products at the point of production, removing the delays associated with centralised production, especially for low volume, highly customised, high-value products (Gebler, Schoot Uiterkamp, & Visser, 2014; Jiang, et al., 2017). 3DP can be used to produce a variety of different parts at nearly any location, potentially allowing decentralisation and localisation of production for companies (Bogers, et al., 2016).

Therefore, 3DP offers opportunities for advancement in remote areas with low economic profiles by bridging the gap between these areas and the next market, and by supplying these areas with the necessary objects to improve quality of life. The layer-by-layer nature of production, specifically the ability to lower product infill, greatly lowers resource demands and process-related waste (Gebler, et al., 2014). Conventionally, one-of-a-kind manufacturing is associated with surplus material being wasted (Jiang, et al., 2017). However, with 3DP, production of highly customised products can be made more sustainable (Ford, et al., 2016). By using 3DP, it could be possible to develop a local material recycling and manufacturing loop, which translates into reductions in landfill and emissions,

and leads to an increase in local employment through recycling centres as well as value creation (Garmulewicz, Holweg, Veldhuis, & Yang, 2018).

In its early days, 3DP was used for rapid prototyping and then tooling and these application areas continue to be used. There is an abundance of evidence that suggests 3DP will be promising in the following areas:

1. Customised healthcare products for improving health and quality of life. There are several reports on amenable 3DP technologies for pharmaceutical manufacturing which are applicable to different drug development phases (early-phase screening, testing, manufacturing, and dispensing) (Goyanes, et al., 2017; Prasad & Smyth, 2016; Rahman, et al., 2018). Human medicine, as well as veterinary medicine, can benefit from technological advances in 3DP (Hespel, Wilhite, & Hudson, 2014; Tanner, et al., 2020; Velázquez, Cavas, Bolarín, & Alió, 2020). 3DP is important to dentistry and can be used to print personalised braces for patients (Dawood, Marti, Sauret-Jackson, & Darwood, 2015).
2. In the construction industry, many experiments have been conducted to explore the full potential of 3DP as a core method, to build more sustainable and environmentally-friendly buildings, or to produce construction components (Wu, Wang, & Wang, 2016).
3. 3DP can benefit supply chain simplification to increase efficiency and responsiveness. The various 3DP technologies that enable the development of fashion products like apparel and jewellery are closely associated with low-volume manufacturing and mass customisation (Yap & Yeong, 2014).

3DP has been labelled a “disruptive technology” because it will fundamentally affect many processes in production, supply chain design, logistics, product life-cycle planning, and consumer behaviour. Due to ongoing improvements of 3DP technology, it is seeing increased usage in direct manufacturing, rather than as a technique for prototyping (Poologasundarampillai, et al., 2017). For example, 3D printers are being utilised in analytical laboratories in a wide array of applications (Gross, Lockwood, & Spence, 2017).

Moreover, the societal impact study from a technical perspective shows further research is necessary in assessing energy consumption over the 3DP lifecycle and potential occupational hazard assessment for additive manufacturing.

One of the more challenging and complex areas of 3DP are in the emerging field of gastronomy, or in other words, “3D Food printing”. The ability to selectively deposit material within a 3DP structure and, hence, tightly control the composition; offers the possibility of complex structures, with variable texture, taste, and morphology in food products. Manipulation of food microstructure will give a range of functional and novel foods.

In the past few years, several reviews have covered different aspects of 3D food printing (Godoi, Bhandari, Prakash, & Zhang, 2018). For example, there are several review articles assessing the state of the current research in printable food formulations (Jiang, et al., 2019). A review of 3DP techniques applied to design food materials (Godoi, Prakash, & Bhandari, 2016). There is a review on existing food 3D printers alongside their advantages/disadvantages (Toh, Li, Chua, & Wong, 2018). Here many of these aspects are collated.

2.2.1 3D Printing: Material and Methods

Various 3DP processes have been reported to date (Vaezi, Chianrabutra, Mellor, & Yang, 2013). The American Society of Testing and Materials (ASTM F2792-12a) have categorised the existing technologies under the following seven headings:

1. Vat photo-polymerisation
2. Material extrusion
3. Directed energy deposition
4. Powder bed fusion
5. Binder jetting
6. Material jetting
7. Sheet lamination

These can be further categorised by the printed medium (liquid-, solid-, and powder-based

materials) and by the process, used to fuse matter on a molecular scale (thermal, UV-light, laser, or electron beam) (Gebler, et al., 2014). These are described briefly in Table 2.1. To differentiate themselves, various manufacturers often use different acronyms for describing the same process, and, therefore, similar techniques might have different names (Saptarshi & Zhou, 2019). These have all been previously compared and reviewed comprehensively (Hegab, 2016; Ligon, Liska, Stampfl, Gurr, & Mülhaupt, 2017). Many of these techniques have been individually reviewed including powder-based electron beam additive manufacturing (EBAM) technology, and the Fused Filament Fabrication (FFF) process, also termed, Fused Deposition Modelling (FDM) (Gong, Anderson, & Chou, 2012; Salentijn, Oomen, Grajewski, & Verpoorte, 2017).

Materials have long been a barrier to the broader uptake of 3DP in the manufacturing industry (Chua, Yeong, & An, 2018). There are several comprehensive reviews of 3DP techniques in terms of the materials utilised (Bourell, et al., 2017; Utela, Storti, Anderson, & Ganter, 2008). The material selection depends on the process and the physical state of the material as well as the phase transitions or chemical reactions to bind the layers together (Portanguen, Tournayre, Sicard, Astruc, & Mirade, 2019). The basic materials in 3DP include a wide range of plastics including acrylonitrile butadiene styrene (ABS), polylactic acid (PLA), and nylon. A handful of other materials, for example, cellulose plus its derivatives and hydrogels are also well established in 3DP and well accepted in some manufacturing applications (Dai, et al., 2019; Li, Tan, & Li, 2018). Further progress in 3DP will require the concurrent development of pioneering 3DP methods in addition to novel feedstocks (Chang, et al., 2018).

Table 2.1: A table comparing the different types of 3DP technology based on the materials and processing BJ: Binder Jetting, CLIP: Continuous Liquid Interface Production, DLP: Direct Light Processing, DMLS: Direct Metal Laser Sintering, DOD: Drop-On-Demand, EBAM: Electron Beam Additive Manufacturing, EB: Electron Beam Melting, FDM: Fused deposition modelling, LENS: Laser Engineering Net Shape. LOM: Laminated Object Manufacturing, MJ: Material Jetting, MJF: Material Jet Fusion, NPJ: Nanoparticle Jetting, SLA: Stereolithography, SLM Selective Laser Melting, SLS: Selective Laser Sintering, SSE: Semi-Solid Extrusion, UAM: Ultrasonic Additive Manufacturing. The acronyms are taken from (Li, et al., 2016).

		Ink type	Process description	Advantage	Drawbacks
Material Jetting	DOD	Polymers	A print head deposits droplets of liquid on to a surface. These droplets set spontaneously. The most common types of DOD print heads are thermal or piezoelectric actuation.	Fast and efficient, complex structure production, high precision, easily adaptable with multiple nozzles to facilitate multi-material printing, rapid gelation enables swift layer-by-layer build-up.	High maintenance, high cost and short service life, low viscosity inks (3–12 mPa.s) only, poor thermal conductivity, small droplet volume is a restriction on any potential scale-up, printing vertical 3D structures difficult.
	NPJ	Polymers	A print head selectively deposits droplets of liquid on to a surface. They are then fused using a heat source.		
	MJ	Polymers	A print head selectively deposits droplets of liquid on to a surface. They are then cured using UV light.		
Binder Jetting	BJ	Polymers, Gypsum, Sand	In this process, the utilisation of a binder causes layers of powder to be selectively bonded. Small droplets of the binder with radii less than 50 μm are deposited in succession on to the powder bed surface.	Quick, simple and relatively inexpensive	Can only use powders, relatively weak mechanical characteristics
Powder Bed Fusion	SLS	Plastics, metals, alloys, metals with polymers and combinations of metals and ceramics	Production consists of powder deposition followed by powder solidification. After this, the build platform lowers by the thickness of one layer. This three-step cycle repeats until the final layer has sintered. The sintering process utilises a laser source.	No support structure needed, large range of material options, desirable mechanical properties, fine resolution, high quality	High power usage, size limitations, inefficient, expensive, slow throughput, highly porous
	MJF	Polymers, ceramics, metal	A fusing agent is jetted onto a heated powder bed alongside a second jet of detailing agent to improve part resolution, infra-red heaters pass over the bed, sintering the powder at the fusing agent locations.		
	DMLS/SLM	Plastic, Stainless steel, Titanium, Aluminium, Cobalt, Chrome	Parts are produced through placement a thin layer of metal powder, followed by targeted lasing to achieve the pattern designed on the computer in that section. The lasing causes the particles to melt for less than a second allowing them bind to the existing structure below.		
	EBM	Titanium, Cobalt, Chrome, Stainless steel, Aluminium, copper	The powder is melted by a 30-60 KV electron laser beam. The process occurs in a high vacuum chamber thus avoiding oxidation issues as it is intended for production of metal parts.		

VAT Polymerisation	SLA	Liquid Photopolymers (acrylic or epoxy based)	Layer-by-layer manufacture by spatially controlled photopolymerisation of a liquid resin carried out by a scanning laser.	High accuracy, high precision, high efficiency, good processing effect	Limited feedstocks, relatively costly, Lots of material used up as support structures, complex structure
	DLP	Liquid Photopolymers (acrylic or epoxy based)	Layer-by-layer manufacture by spatially controlled photopolymerisation of a liquid resin carried out by a digital light projector.		
	CLIP	Acrylates	A liquid resin undergoes continuous liquid interface production (CLIP) that uses a bottom-up building approach. It utilises a controlled oxygen inhibited dead-zone to prevent attachment of the part to a curing window that is oxygen-permeable.		
Material Extrusion	FDM	Thermoplastic filaments (ABS, Nylon, PLA), Composites, Nano-fillers, concrete	A filament is heated until it is molten or semi-molten. The softened filament passes through a nozzle, with a solid filament acting as a piston. The material is then deposited onto the print surface. The deposited material then fuses with any adjacent material that has already been deposited.	Inexpensive, uncomplicated, low maintenance, can produce relatively large constructs, room temperature processing, and high speed.	Gaps in the final product, intricate structures are difficult to produce, low accuracy, rough product surface, slow print speed, weak mechanical properties, limited materials
	SSE	Gels and pastes	Extrusion of semi-solids focusing on applications for gels and pastes		
Direct Energy Deposition	LENS	Metals, Graded/hybrid metals, Ceramics, Composites	A fabrication method where a high-powered laser is focused directly on the substrate creating a molten pool. Metal powder particles are then injected into this area to allow layer-by-layer buildup. The substrate is lowered beneath the laser beam, depositing a thin cross-section to produce the desired design. Further layers are repeatedly added to build a 3D part.	Used for structural repair, multiple axes, flexible, high resolutions (pico- to microscale), can handle small printing volumes (pico-to-nanolitre)	Limited feedstocks, post-processing could be required, high cost, complex design
	EBAM	Metals (powders/wires)	A high-energy electron beam is used as a moving heat source, to melt and fuse metal powder. Which then rapidly self-cools and produces parts layer-by-layer.		
Sheet Lamination	LOM	Plastic, Metals, Graded/hybrid materials, Paper	Using sheets of the desired material a cross-section is cut into the sheet and is then attached to the cross-section of the part being made. A laser cuts the sheet of material that is spread across a movable substrate, and a laser cuts it along the contours of the part geometry designed on the computer. The layers are fused by a hot roller compressing the sheet and activating a heat-sensitive adhesive.	High speed, low cost	Post-processing could be required, limited feedstocks
	UAM	Plastic, Metals, Graded/hybrid materials	A combination of ultrasonic metal seam welding and CNC milling in the lamination process. UAM is the only AM technique that can construct metal structures at low temperature.		

2.3 3D Food Printing

There are reports that focus on the effect of 3DP surface features on taste perception as derived from product form. For example, 3DP cups with angular surfaces increased perceived coffee and chocolate intensity ratings for bitterness and taste, but 3D-printed cups with rounded surface features cause a lower taste intensity and increase in sweetness perception (van Rompay, Finger, Saakes, & Fenko, 2017). Similar results have been reported on the effects of 3D-printed surface textures and visual design on ice-cream assessment (Van Rompay, Kramer, & Saakes, 2018). For this kind of 3DP application in the food sector, all the materials and methods in Table 2.2 are potentially viable.

However, for the focus of this section, 3D food printing is the application of 3DP in food processing. It is one of the newest developments in food design and manufacturing with the potential for further studies and applications in the industrial sector. The most common techniques used in 3D Food printing are: material extrusion, powder bed fusion (sugar only), vat polymerisation, binder jetting, and inkjet printing (Portanguen, et al., 2019; Voon, An, Wong, Zhang, & Chua, 2019). The same process principles, for 3DP in general, also apply to 3D Food printing. However, different degrees of pre-processing, such as fine-tuning of food recipes, and post-processing, such as cooking and oven drying, might be necessary for 3D food printing (Dankar, Haddarah, et al., 2018).

Some major challenges with 3D food printing include safety and labelling (Tran, 2019). For example, some 3DP samples, when stored in air, exhibited a high microbial concentration, which suggests extra consideration for hygienic process design is likely needed (Severini, Derossi, et al., 2018). The average consumer does not favour 3DP foods and typically holds a negative outlook associated with the fear of eating “alien foods” and foods that appear to have undergone a lot of processing (Lupton & Turner, 2018).

The main advantages of 3DP technology in printing edible materials comprise:

1. ***Reducing food waste, increasing the usage of existing food materials, simplification of production and streamlining the supply chain*.** The technology

prevents food waste by utilising unpreserved fruits and vegetables and low value by-products (i.e. meat off-cuts, which traditionally goes to waste) to create pleasant, wholesome food products. The company Upprinting Food uses food waste as the "ink" for 3D food printers (see https://www.upprintingfood.com/about). Ingredients like bread, fruit, and vegetables from residual food flows are blended and combined to produce a puree, which is then seasoned with herbs and spices. The puree is then 3D printed, and these prints are baked and dehydrated so that the resulting product is pleasantly crunchy, with a long shelf life. Moreover, once established, 3D food printing eliminates many of food manufacturing processes (ex. shaping, baking) (Tran, 2016). Additionally, 3D food printing can make food transport more feasible. Special food "cartridges" designed with 3DP in mind have far longer shelf lives as well as specially tailored nutritional profiles, making them especially suitable for use in developing regions (Izdebska, et al., 2016). NASA uses dry powders for 3DP with a shelf life of up to 30 years (Izdebska, et al., 2016).

2. ***Treating malnutrition by personalising/customising food.*** One solution for the malnutrition problem is to provide each person tailored nutrition. 3D food printing permits the creation of new geometries and offers original production ideas in food manufacturing with superior control over composition, structure, texture, and taste (Azam, Zhang, Bhandari, & Yang, 2018). 3D food printing could provide a solution to reconfigure a specialised supply chain intended to assist people with special dietary requirements (Derossi, Caporizzi, Ricci, & Severini, 2019). 3DP enables the creation of uniquely textured foods with superior nutritional value (Feng, Zhang, & Bhandari, 2019). Another advantage is ingredient combination during printing or use of multi-material printing to incorporate several ingredients. 3D food printing can lead to new directions in a domestic cooking or catering services (Derossi, et al., 2019).

3. ***Lowering environmental impact*****.** 3D food printing produces little waste, as only the quantity of food to be consumed, need be printed. Furthermore, due to its flexible nature, 3D food printing will promote the incorporation of low-carbon food ingredients

(algae, insects, etc.) into pioneering edible objects (Derossi, et al., 2019). 3DP seafood and meat from cells, a comprehensive review was produced by (Dick, Bhandari, & Prakash, 2019), or plant protein resources with similar taste and texture to the original leads to the development of foods at reduced environmental impact and improved quality (Severini, et al., 2016).

4. ***Alleviating issues surrounding 'food on the go' to astronauts and military personnel or 'food as pharmaceuticals' in hospitals (for humans) or veterinary clinic (for pets).*** The only necessary things to make the food will be food cartridges, food 3D printers, and energy (Tran, 2016; Tran, 2019). Cartridges loaded with customised nutrient and/or flavour profiles for each consumer can be sent, and then printed into whatever shape and size they may desire, with only the food to be eaten used. There already exists a 3D bioprinter on the international space station, meaning the required knowledge base exists for the uptake of 3DP foods.

2.3.1 Materials for 3D Food Printing

Table 2.2 summarises chronologically the reported 3D food printing material and methods currently being employed. Although there is not a universal definition for food or even edibility, the major challenge in 3D food printing is the development of edible, printable materials (Belluco, et al., 2013).

Table 2.2: A table showing the current state of literature in food 3DP, listing the materials, printing method, printer used and the major findings

Entry	Material	Printing Method	Printer	Year	Major Findings
1	Mixed hydrocolloid systems (Xanthan gum and gelatin) and flavourings	Extrusion (cold)	Fab@Home printer	2009 (Cohen, 2009)	They have shown that it is possible to create an extensive range of textures and tastes by mixing two hydrocolloids and flavour additives. However, such controlled food is typically reserved for medical and space applications.
2	Milk Chocolate	Extrusion (hot melt)	Customised extrusion system	2010 (Hao, et al., 2010)	The key parameters for chocolate 3DP were identified (the nozzle aperture diameter, the optimum nozzle height from the build bed, the extrusion, and the axis movement speed).
3	Modified turkey, scallop, celery using transglutaminase, a modified traditional cookie	Extrusion (cold)	Fab@Home printer	2010 (Lipton, et al., 2010)	To integrate 3D food printing into conventional kitchens, the printed object needs to retain its shape during post-printing processes such as cooking and frying. There are two critical methods for solving the shape stability problem: additives and recipe control, such as adding transglutaminase to the meat puree right before printing. This cross-links the proteins present in the meat and gives rise to a self-supporting structure. For the cookie, the concentration of ingredients have been changed systematically to identify a printable formulation. However, the content of some components were increased by up to 100% when compared to the traditional recipe.
4	Mashed potato, chocolate, and cream cheese	Extrusion (cold and hot melt)	RapMan 3.1	2011 (Southerland, Walters, & Huson, 2011)	Testing and comparing three methods (moulding, extrusion, and binder jetting) using a range of foodstuffs and edible products, the authors pointed out an advantage of 3DP to moulding that has rarely been addressed. Weak food structures cannot successfully be taken out of the mould.
5	Combinations of caster, icing, and silk sugars as well as blends with maltodextrin	Binder jetting	CandyFab		
6	Insect flour made more acceptable through combination with other foods including icing butter, chocolate, cream cheese, and spices	Extrusion		2014 (Soares & Forkes, 2014)	Health and preference are two main reasons to adopt customized food. Considering the high nutritional value of edible insects, the authors have 3DP visually appealing food to enhance the “preference” of a diet that may have beneficial effects on human health.
7	Mint syrup, wax, Linseed oil, carrageenan shell	Inkjet	TNO’s encapsulation printer	2015 (Godoi, Bhandari, Prakash, & Zhang, 2015)	Final products are: mint syrup core capsule with a wax shell (200 µm) and linseed oil capsule with a carrageenan shell (280 µm) Because of the use of Inkjet technology, the produced droplets are highly monodisperse. With a capacity of 100 mL/h, this method of droplet generation can compete with microfluidic-based methods.
8	Edible ink (made up of water, ethanol, glycol, and/or glycerol as solvents and an edible colourant)	Inkjet	Various	2016 (Pallottino, et al., 2016)	Inkjet printing is predominantly used for 2D graphical decorating, surface filling, or cavity depositing. It may be more appropriate to classify this as a 2D printing technique rather than a truly free form method of creating 3D edible objects.
9	Wheat dough	Extrusion (cold)	3D Printer mod. Delta 2040 (Wasp project, Italy) equipped with the Clay extruder kit 2.00 (Wasp project, Italy)	2016 (Severini, et al., 2016)	Post-printing: Cooking The effects of layer height and infill on the printing quality of cereal-based snacks with a cylinder-like shape, before and after cooking, was assessed. Many of the 3D printers, which are used in 3D food printing research studies, are intended for use with synthetic materials (such as PLA). Therefore, they might be unable to keep a good equilibrium between different printing parameters when the original ink is replaced with another material with different rheological properties.
10	Pavlova (mainly egg white) with chocolate garnish	Extrusion (cold)	Customised extrusion system	2016 (Kouzani, et al., 2016)	Post-printing: Baking The authors questioned the effect of the printing bed surface on the quality of 3DP. This subject has rarely been addressed or systematically studied in 3D food printing.
11	A formulation of low methoxylated pectin, CaCl2, bovine serum	FDM (cold)	Customised extrusion system	2017 (Vancauwenberghe, et al., 2017)	Post-treatment to solidify the pectin into a gel with Ca^{2+} ions. Pectin and sugar concentrations affect the fidelity of the printed objects by changing the viscosity of the food-ink and improving the mechanical

	albumin (BSA), edible colourant, and sugar syrup				properties. At the same time, BSA stabilises and increases the porosity of the gel.
12	Dark chocolate with the addition of magnesium stearate	Extrusion (hot melt)	PORIMY 3D chocolate printer, (China)	2017 (Mantihal, Prakash, Godoi, & Bhandari, 2017)	Magnesium stearate minimises slippage in the extruder during deposition. This yielded better printability. Furthermore, it changes the snap properties of the final product.
13	Dark chocolate	Extrusion (hot melt)	Customised syringe-based extrusion system	2017 (Lanaro, et al., 2017)	In hot melt extrusion printing of chocolate, the crucial factors are particle size, degree of crystallinity, melting behaviour, and material composition. The optimum temperature for forming the most stable crystalline chocolate melt is 32 °C.
14	A formulation of low methoxylated pectin, $CaCl_2 \cdot 2H_2O$, and red food colourant E122	FDM (cold)	Customised extrusion system equipped with a coaxial nozzle	2018 (Vancauwenberghe, Verboven, Lammertyn, & Nicolaï, 2018)	A coaxial extrusion printhead was created and used to deposit a pectin-based ink, and $CaCl_2$ cross-linking solution in the inner and outer flows, respectively. Therefore, the initial incubation or post-treatment step has been eliminated, producing more accurate control of object gelation and texture.
15	Vegemite and Marmite	Extrusion (cold)	The BioBot printer	2018 (Hamilton, Alici, & in het Panhuis, 2018)	This work, is indicative of the application of 3D food printing as an educational tool during outreach activities. These works stress the entertainment and indulgence aspect of 3D food printing to create fun designs suitable for celebratory events such as birthday parties. The flow consistency index and the flow behaviour exponent are critical parameters in determining whether a material is ideal for 3DP or not. A comprehensive rule set regarding the rheological properties of 3DP feedstocks has not yet been established.
16	Dough with varying quantities of water, sucrose, butter, flour, and eggs	Extrusion (cold)	PORIMY Co. Ltd., (China)	2018 (Yang, Zhang, Prakash, & Liu, 2018)	The authors reported that the dough formulation affects its viscoelastic properties and, thus, its printability. There is a strong link between the additives and the rheological properties of dough (and gluten), making this observation not particularly surprising.
17	Mashed potato	Extrusion (cold)	Shiyin Co. Ltd. (China)	2018 (Liu, Bhandari, Prakash, & Zhang, 2018)	These studies gave an insight into the following: (1) The link between the rheological properties of mashed potato and its printability, (2) The effect of additives (gums and starch, strawberry juice) on the rheological properties of mashed potato and its printability, and (3) Using a dual extrusion printer to print objects with alternating layers of different materials.
18	Mashed potato modified by the addition of potato starch	Extrusion (cold)	FSE2, Bolimai Co. Ltd., (China)	2018 (Liu, Bhandari, Prakash, & Zhang, 2018)	
19	Mashed potato mixed with gums of xanthan, guar, k-carrageenan, and a k-carrageenan- xanthan gum blend	Extrusion (cold)	CSE 1, Bolimai Co. Ltd., (China)	2018 (Liu, Zhang, & Bhandari, 2018)	
20	Mashed potato/strawberry juice	Dual extrusion (cold)	Shiyin Co. Ltd., Hangzhou, (China)	2018 (Liu, Zhang, & Yang, 2018)	
21	Processed cheese	Extrusion (hot melt)	Customised syringe-based extrusion	2018 (Le Tohic, et al., 2018)	This is the first report on 3DP cheese and investigating the effect of several variables on its main textural and melting properties. The authors concluded that 3DP substantially affected the properties of cheese, such as lowering its hardness and making it melt easier; most likely due to the different fat particle size distribution. They did not analyse the reproducibility of the 3DP of their samples. They also observed a colour change in the samples extruded at different speeds. The effect of 3DP on the final colour of samples is debatable and needs to be studied among different consumer preferences.
22	Starch, milk powder, cellulose nanofibre, rye bran, oat protein concentrate, and broad bean protein concentrate and their mixtures	Extrusion (cold)	VTT's micron-scale dispensing environment based	2018 (Lille, Nurmela, Nordlund, Metsä-Kortelainen, & Sozer, 2018)	Post-printing: oven drying or freeze-drying Cellulose nanofibre (CNF) improved the shape stability of the printed structures (possibly due to its shear-induced alignment properties) and decreased the hardness of the dried objects. However, the authors also reported, formulations with a high amount of CNF, clogged the nozzle, owing to some larger fibre particles remaining in the CNF after fibrillation, or shear-induced flocculation of the material when forced through the small tip of the nozzle.

23	Blend of orange concentrate with added vitamin D, wheat starch, and hydrocolloid/s (gum arabic, guar gum, k-carrageenan gum, and xanthan gum)	Extrusion (cold)	SHINNOVE-D1, Shinnove Co. Ltd., (China)	2018 (Azam, et al., 2018)	Starch is an excellent binder and is widely used as a thickening agent in the food industry. The best printability and mechanical strength have been obtained in the presence of κ-carrageenan. Possibly due to the binding of carrageenan to the double helix structure of amylose/amylose in starch.
24	A mix of hydrocolloids and three types of powdered vegetables: broccoli, spinach leaves, and carrots	Extrusion (cold)	A YL-CUBE 3D food printer YOLILO Co., Ltd., (Korea)	2018 (Kim, et al., 2018)	Xanthan gum with its high hydration ability can stop the expansion of the vegetable powder particles so that the rheological value of the gel system before and after the powder addition does not change significantly, and the difference of printability between various vegetable powders is reduced.
25	Amorphous powdered cellulose and a binder based on xanthan gum	Binder jetting	Dimatix DMP-2831 inkjet printer (FujiFilm, USA)	2018 (Holland, Foster, MacNaughtan, & Tuck, 2018)	Because of very limited feedstock of edible materials, binder jetting has been used more for demonstrative purposes. This study was on the application of binder jetting in the food sector where xanthan gum has been used as a glue to “clump” the amorphous cellulose. The aqueous ink and enough heating, recrystallize (in a semi-crystalline form) the amorphous cellulose in the printed piece but the surrounding powder remained unbound and amorphous.
26	Pectin combined with a food formula (banana, white canned beans, dried non-fat milk, lemon juice, dried mushrooms (B. Edulis) and ascorbic acid.	Extrusion (cold)	3D Printer mod. Delta 2040 (Wasp project, Italy) equipped with the Clay extruder kit 2.00 (Wasp project, Italy)	2018 (Derossi, Caporizzi, Azzollini, & Severini, 2018)	This work is studied the implementation of 3DP technology to provide innovative 3DP fruit-based snacks for children 3 to 10 years old. It is an example of the application of 3D food printing to overcome the malnutrition by getting people to consume five fruits/vegetables a day. Lemon juice and ascorbic acid, were used to prevent browning of a printable food formula consisting mainly of banana.
27	Wheat flour dough with additive (calcium caseinate) containing probiotic	Extrusion (cold)	ByFlow, (Netherlands)	2018 (Zhang, Lou, & Schutyser, 2018)	Post-printing: oven baking This report, as well as its similar report in Reference, are excellent examples of the application of 3D food printing in resolving malnutrition. The survival of a microorganism in baked food is low because of the high baking temperature. Usually, the rate of drying of the products is increased to shorten the baking time. Therefore, the product should have a high surface to volume ratio, which is very common in 3DP samples.
28	Lemon juice gel with a range of potato starch concentrations	Extrusion (cold)	Customised syringe-based extrusion	2018 (Yang, Zhang, Bhandari, & Liu, 2018)	Proposition of a mathematical formula for extrusion rate
29	Wheat dough enriched with ground yellow mealworms larvae (Tenebrio Molitor, an edible insect)	Extrusion (cold)	3D Printer mod. Delta 2040 (Wasp project, Italy) equipped with the Clay extruder kit 2.00 (Wasp project, Italy)	2018 (Severini, Azzollini, Albenzio, & Derossi, 2018)	Post-printing: oven baking See entry 6
30	Liquid chocolate	Inkjet	Customised electrostatic inkjet system	2018 (Takagishi, Suzuki, & Umezu, 2018)	The authors used electro-spraying technology (referred to as the electrostatic inkjet method), which utilised electrostatic force to print gel-like materials, with high-precision.
31	Combination of three different starches (potato, rice, and corn starch)	Extrusion (hot melt)	HE-3D printer SHINNOVE S2 (China)	2019 (Chen, Xie, Chen, & Zheng, 2019)	The extrusion process breaks the crystallinity and structure of the starch molecule. The disruption of the crystalline structure breaks the intermolecular hydrogen bonds during the gelatinization process. This is one of the parameters that lead to a formation of a continuous starch paste matrix of entangled amylose molecules with suitable viscoelastic property and shear thinning behaviour.
32	Epoxidised vegetable oils	SLA	Customised printer	2019 (Branciforti, et al., 2019)	3D food printing can help decrease food waste. It is possible to transform used cooking oil from McDonald’s into 3DP resin.
33	Mixtures of soy protein isolate, gelatin, and sodium alginate	Extrusion (hot melt)	Customised syringe-based extrusion	2019 (Chen, et al., 2019)	Soy protein isolate gel has a very high viscosity. Its rheological properties are not suitable for 3DP. Similar to entry 19, hydrocolloids were used for further tuning the viscoelastic properties.
34	A paste made out of brown rice and food additives (guar gum and xanthan gum)	Extrusion (cold)	Shiyin Co. Ltd., (China)	2019 (Huang, Zhang, & Bhandari, 2019)	See entry 19
35	A paste of beef gelatin, sucrose, egg white protein powder, and starch from corn	Extrusion (hot melt)	PORIMY3D Printing Technology Co., Ltd., (China)	2019 (Liu, Meng, Dai, Chen, & Zhu, 2019)	Studying tribological properties resulted in an improved understanding of rheological properties, and naturally 3DP formulation optimisation.

36	Heat-induced egg yolk paste	Extrusion (cold)	SHINNOVE-E1, SHIYIN Technologies Co. Ltd., Hangzhou, (China)	2019 (Xu, et al., 2020)	This study also utilised 3DP in developing protein resources. Heating egg yolk leads to a 3D protein network with a hard, cohesive, rubbery texture.
37	Cake icing, Hershey's cocoa powder, Hershey's chocolate syrup, and Nutella hazelnut chocolate spread	Extrusion (cold)	SHOTmini 200 Sx and IMAGE MASTER 350 PC Smart, Musashi Engineering Inc., (Japan)	2019 (Karyappa & Hashimoto, 2019)	This approach bypassed a significant requirement of temperature control to perform 3DP of chocolates by hot-melt extrusion. The presented technology offers an easy route to fabricate 3D structures of chocolate-based inks with liquid fillings using multiple dispensers.
38	Anthocyanin-potato starch gel Lemon juice-potato starch gel	Extrusion (cold)	SHINNOVE-D1, Shinnove Co. Ltd., Hangzhou, Zhejiang, (China)	2019 (Ghazal, Zhang, & Liu, 2019)	This is an example of moving from 3D food printing to "4D food printing". "4D printing" refers to the response of a 3DP object to stimuli from the environment, which results in physical or chemical changes in state over time. In this case, the colour of the 3DP samples is changed over time. It can be applied to prepare more visually appealing food products.
39	Sesame paste, chicken paste, and shrimp paste	Extrusion	Customised syringe-based extrusion	2019 (Hertafeld, et al., 2019)	Integrating an infrared lamp heating mechanism into the printer allows extruding and cooking food products simultaneously with high precision.
40	Potato starch	Extrusion (hot)	SHINNOVE-S2 printer Shiyin, (China)	2019 (Liu, Chen, Zheng, Xie, & Chen, 2020)	Similar to entries 18–20
41	Dark chocolate	Extrusion (hot)	Shinnove 3D printer model no. Shinnove-D1, Shiyin Co. Ltd., Hangzhou, (China)	2019 (Mantihal, Prakash, & Bhandari, 2019b)	3DP chocolates were created with varied infill patterns and percentages for textural and sensory evaluation. A comparison of a cast samples against a 100% infill printed chocolate sample showed an equal preference for both samples, which are partly influenced by their perceived texture.
42	Egg yolk and egg white with blends of rice flour	Extrusion (cold)	Delta type 3D food printer CARK - Controlled Additive-manufacturing Robotic Kit	2020 (Anukiruthika, Moses, & Anandharamakrishnan, 2020)	Rice flour (1:1 and 1:2 w/w) was used as a filler agent and has a significant effect on the stability and strength of materials printed with egg yolk and egg white.
43	A mixture of 50% native wheat starch, 40% maltodextrin, and 10% palm oil powder	SLS	EOS P380 machine	2020 (Jonkers, van Dommelen, & Geers, 2020)	Maltodextrin and palm oil were used as binding agents. A constitutive model was obtained that describes the large-strain material behaviour of 3DP starch-based foods based on experimental research.
44	Dark chocolate containing either: magnesium stearate or plant sterols	Extrusion (hot melt)	PORIMY 1.0 (PORIMY, Kunshan, China)	2020 (Mantihal, Prakash, & Bhandari, 2019a)	The star and honeycomb infill pattern produced the most stable and tough structure at 60% infill.

There exist three types of extrusion printing: screw-based extrusion, air pressure driven extrusion, and syringe-based extrusion (Chen, et al., 2019; Hamilton, et al., 2018; Jiang, et al., 2019; Liu, et al., 2018; Pérez, Nykvist, Brøgger, Larsen, & Falkeborg, 2019). In this table, screw-based extrusion in which the material is fed to the machine through a hopper, is called an extrusion system. FDM, Fused deposition modelling. SLA, stereolithography. SLS, selective laser sintering. FDM is the extrusion system where the feed is entering the nozzle via a tube, and a syringe pump drives it. Hot-melt extrusion is when the feed enters the extrusion in a temperature higher than the ambient temperature against cold extrusion where the feed is at an ambient temperature.

For 3D food printing to have an increased uptake the relationship between rheological characteristics and their connection with printing parameters must be established and standardised in order to improve the quality and reproducibility of 3DP food. There are still shortcomings in the knowledge of how to link material structure to process printing parameters to produce a desirable 3DP product (Dankar, Haddarah, et al., 2018). In previous years, two significant areas within 3D food printing have been investigated. The first, is the study of the relationship between 3D food printing and mechanical properties of food as well as rheological properties (Gholamipour-Shirazi, Norton, & Mills, 2019; Warner, Norton, & Mills, 2019). The second is the formulation and development of 3D food printing products. However, most of the time, a clear border cannot be drawn between these two areas.

In general, 3DP materials must exhibit a controllable viscoelastic response, must form stable structures capable of withstanding compressive stresses from capillary forces, and must not shrink too much when undergoing drying (the exact % varies depending on material) to avoid deformation and/or fissure formation (Dai, et al., 2019;). These materials must be able to hold their shape once deposited without slumping, spreading, or bridging. Shape fidelity is an assessment of how well the printed structure conforms to the original design (Gholamipour-Shirazi, et al., 2019). It is commonplace to classify the materials into natively printable (i.e., confectionery, dairy, hydrogels) versus non-natively printable (i.e., plants, meat). However, this cannot be accurate for several reasons:

1. There is no consensus on how to assess or predict shape fidelity, let alone printability (Ribeiro, et al., 2017).
2. Printability is affected by multiple factors (temperature, components and additives) (Kim, Bae, & Park, 2017).
3. Various ingredients (varying in flavour and nutritional value) can be printed at once by using multiple cartridges and/or printheads.
4. One material can be printable in one technique and non-printable in another technique.

Several hydrogels are popular in the field of 3DP, including alginate, gelatin, chitosan, methylcellulose, agar, and carrageenan. Often, hydrocolloids are used for fine-tuning material properties and to improve printability. Apart from the materials reported in Table 2.2, there exist other 3DP food products created by developers, companies, and designers looking to test the capabilities of the technology. Examples include an extruded pizza base topped with tomato sauce and cheese (Lipton, Cutler, Nigl, Cohen, & Lipson, 2015), rose-shaped pasta, rose-shaped chocolates, and sugar confections in geometric shapes (Lupton, et al., 2018).

As seen in Table 2.2, the extrusion method is the most widely adopted. To be used in extrusion-based printing, a material should display shear thinning behaviour. This is an indicator that the material can be extruded from a nozzle (Gholamipour-Shirazi, et al., 2019). One advantage of extrusion-based printing is the wide variety of food materials that can be extruded from a nozzle. These are then able to hold their shape and support the weight of the next layer. Currently, extrusion based 3DP is used to prepare many different types of food such as dough (Severini, et al., 2016), mashed potatoes (Dankar, Haddarah, et al., 2018), cheese (Le Tohic, et al., 2018), and meat (Dick, et al., 2019) with a variety of complex and unique structures.

In 2009, a fundamental work in 3D food printing was carried out by to create a wide range of textures (i.e., mouth feel) (Cohen, 2009). They believed the feedstock for 3D food printing must be developed in such a way that enables the 3DP of an extensive range of foods without expanding unnecessarily the size of the required materials, which was set to be kept at a manageable level. They developed two component basic hydrogel formulations of gelatin and xanthan and investigated their mouthfeel in sensory analysis. By varying the concentrations of the two gelling agents, it was possible to cover a matrix of textures ranging from weak nongranular materials simulating milk to firm nongranular (chocolate, mushroom) and solid granular materials (tomato). This method gave them many degrees of freedom in texture and flavour with a minimal number of required materials.

Therefore, they established one way to generate texture variety in products with a bread-like structure that could be the fractionation of individual bread-structuring functions into modular formulation components (e.g., viscosity, bubble-stabilisation, structure), which was followed by recombination at varying ratios (Wegrzyn, Golding, & Archer, 2012).

Based on these promising results in 2010, 3D printed cereal paste and protein pastes (meat or scallop) were created (Lipton, et al., 2010). They investigated the additives' (transglutaminase or agar) effect on shape fidelity of the produced 3DP structures before and after post-processing by cooking or deep frying. Transglutaminase allowed the meat to be directly 3DP for the first time. This work demonstrated that 3DP food could be prepared like traditional cuisine. The implementation of alternative ingredients could help alleviate a potential global food shortage. 3D food printing has been employed to design appropriate insect products as a new source of proteins to overcome the disgust of consumers by consuming whole insects. 3DP technology has been applied to formulating palatable insect protein products (Soares, et al., 2014). In 2014, they printed flour made from edible dried insects in combination with fondant to produce icing for cake decoration. They focused on creating visually appealing products that would appeal to consumers. They used shapes inspired by insects' natural form and movements, such as their wing patterns and eggs when formulating the design of these food products, attempting to make the shapes resemble jewellery rather than mimicking existing food products.

Further work was carried out by to obtain snacks from insect-enriched wheat flour dough as a new source of proteins (Severini, Azzollini, et al., 2018). The printed snacks reproduced the overall structure of the designed object, but the addition of different concentrations of the insect powder modified the printability of the dough and the morphological and microstructural properties of the final product. However, the nutritional quality was higher than that of the un-supplemented wheat dough. After baking, the size of the snacks was reported to be decreased due to water loss. Nevertheless, the enrichment of dough with insects reduced this effect. Moreover, baking conditions modified their microstructure, which induced non-enzymatic browning reactions and altered mechanical

properties and protein digestibility (Severini, Azzollini, et al., 2018).

The Netherlands Organisation for Applied Scientific Research (TNO)'s experience in inkjet printing suggested the ability to generate monodisperse droplets might be of interest to food sectors. Their research reported a printhead (500 nozzles with a capacity of 100 mL/h) that produces highly monodisperse droplets converted into highly monodisperse powders after drying. Their printing technology allowed the use of a wide range of materials (waxes and fats, polymers, aqueous (or other) solutions, emulsions, and dispersions). Core-shell microcapsules and particles were prepared to encapsulate aqueous flavour and colourant solutions. Moreover, they fabricated calcium alginate gel particles made by printing alginate drops through a screen of calcium chloride solution (Godoi, et al., 2019).

In 2018, one study designed a co-axial extrusion printhead to deposit a low methoxy pectin-based ink and Ca^{2+} cross-linking solution in the inner and outer flows, respectively (Vancauwenberghe, et al., 2018). This enabled accurate control over the textural properties and gelation of the printing object. It also eliminated the pre- and post-treatment steps. In their earlier study, food-inks were formulated by changing the low methoxy pectin, sugar syrup, or bovine serum albumin (BSA) concentration to obtain printed objects with variable textural and structural properties (Vancauwenberghe, et al., 2017). Vancauwenberghe, et al., found that pectin and sugar concentrations were affecting the build quality of the printed objects (by changing the viscosity of the food-ink) and were improving the mechanical properties while BSA was stabilizing and promoting the porosity of the gel. In another attempt to eliminate the post-processing step, an integrated infrared cooker within a 3D food printer was created enabling simultaneous extrusion and cooking (Hertafeld, et al., 2019).

Again in 2018, by using a commercially available processed cheese as the printing material, one study assessed and compared the texture and mechanical properties of untreated, melted, and printed cheese samples (Le Tohic, et al., 2018). They found that the 3DP cheese samples are different than melted and untreated samples in bulk mechanical properties. They concluded during the printing process that fat globules are disrupted during shearing and then partially coalesce during solidification, leading to the softer structure of

the 3DP samples.

For 3DP foods that do not require post-processing treatment (e.g., cooking, baking), such as mashed potato, chocolate, and cheese, most studies assess how the rheological and mechanical properties of food materials or the printing parameters (nozzle size, printing speed) affect the printability (Dankar, Pujolà, El Omar, Sepulcre, & Haddarah, 2018; Yang, et al., 2018). Few studies considered the effect of post-printing treatment on the 3DP samples. However, given the highly perishable nature of most food materials, the post-printing stability is an important consideration. In 2018, a study used cold swelling starch, milk powder, rye bran, oat, fava bean protein concentrates and cellulose nanofibre for 3DP (Lille, et al., 2018). After measuring the hardness and dry matter content, they compared the effects of oven drying (100 ˚C for 20–30 min) and freeze-drying (at −18 ˚C) on the shape fidelity of the 3DP samples. Their results showed that freeze-drying has almost no effect on the shape fidelity of the 3DP samples. In oven drying, high water binding capacity reduces the drying rate and, yields better shape fidelity after drying.

The infill pattern refers to the structure that is printed inside the 3D construct. Structural properties of the 3DP object by varying infill structure has been investigated mostly in polymer and bio-printing. In polymer printing, it has been reported that the honeycomb pattern is relatively tougher compared to rectilinear and line patterns (Fernandez-Vicente, Calle, Ferrandiz, & Conejero, 2016). In bio-printing, a well-developed inner structure in 3D tissues construction such as a cross-link pattern is essential to maintain the mechanical properties of the constructs (Williams, Thayer, Martinez, Gatenholm, & Khademhosseini, 2018). There are also some reports on designing an internal structure of 3D constructs to modify the textural properties of the printed foods. The textural and structural quality of mashed potatoes was investigated by changing infill percentages (10%, 40%, 70%, and 100%) with different infill patterns (rectilinear, honeycomb, and Hilbert curve) and printed shells (3, 5, and 7 shells) (Liu, et al., 2018). Although a direct relationship has been observed between the infill percentage and hardness, gumminess, and Young's modulus of the printed samples, no similar results have been obtained for the infill pattern. From the studies

scrutinised, even though various studies have been carried out over the last ten years, few have been linked, with little to no common design rules arising as a result.

2.4 Future of 3DP in the Food Industry

As 3DP matures as an industry, it will likely find applications in food science and technology. These niche food applications will draw from the power of the platform as a tool for producing highly customisable foods for specific groups and needs. Moreover, patentability could be another motivation for the industry to adopt 3D food printing.

Although there is still a challenge of consumer acceptance, not just of 3DP foods but the incorporation of 3D food printers into the home (Lupton, 2017). Global food companies are investing in research into 3D food printing as well as utilising it in production. Several 3D food printers are available for domestic use. One company, called Natural Machines, created the Foodini 3D printer, which can make 3DP food from fresh ingredients (Saptarshi, et al., 2019). Companies releasing 3D food printers for the home envision that they will one day be considered a standard kitchen appliance (Lupton, et al., 2018). Most studies focus on improving the appearance of the printed food rather than developing technology that will give access to large-scale production systems (Le-Bail & Maniglia, 2020).

In the food sector, there is some scepticism about the use or value of 3D food printing technologies to enrich people's lives (Schneider, Eli, Dolan, & Ulijaszek, 2018). There still exist many questions about the safety and capabilities of 3D food printing and how to address them (Lupton, 2017). At present, there are three major problems with 3D food printing that need to be solved:

1. **Scaling up of 3DP:** Compared to traditional manufacturing methods, 3DP is a slow set of technologies, often requiring hours to produce large constructs. To be used on an industrial scale, the printers would either need to be faster, or sufficiently cheap to allow for thousands of them to be run simultaneously. However, the small-scale food manufacturing industry (bakeries and chocolatiers) will benefit from the added artistry and customization through 3DP.

2. **Environmental impact:** 3D food printers are capable of positively impacting the environment by decreasing food waste and food or food-related transports as well as by producing/replacing meat. However, there is a downside as well. 3D food printing, if omnipresent, will change the agricultural practice and lead to a dramatic impact on the entire ecosystem (Tran, 2016). Plus, decentralising food production, may in fact lead to more energy input as it is less efficient to produce lots of small batches.
3. **Hygiene and sanitation:** As of right now, no-one has established proper cleaning protocols to ensure food products from 3D printers are safe to eat. One food type must not affect the quality of the next one to maintain safety and quality over the lifetime of the 3D printers.

Before any sort of full transition to 3D food printing, hybrid technologies, i.e., 3DP methods adapted to current food manufacturing processes should be trialled. Whether the technology can transition from the novelty sector will depend on the identification of a broader range of edible feedstocks, which is something that is being done in academia but will require input from both the layperson in their kitchen and from printer developers in the industry (Gorkin III & Dodds, 2013).

2.5 Food hydrocolloid gels

Hydrocolloid is the general term used to describe a series of proteins and polysaccharides with a wide range of use within myriad sectors including food (Milani & Maleki, 2012; Saha & Bhattacharya, 2010) and pharmaceuticals (Bhardwaj, Kanwar, Lal, & Gupta, 2000; Kashyap, Kumar, & Kumar, 2005) as well as other specialised uses such as catalyst research (Wang, Wang, Ye, & Song, 2019) and biotechnology (Chien, Makridakis, & Shah, 2013; Woehl, et al., 2014). Hydrocolloids contain many hydroxyl groups, which impart their affinity for water, and subsequent ability to bind water molecules (Saha, et al., 2010). Hydrocolloids are typically present in 0.1-10% concentration within a formulation and have many uses in food systems. These include rheology modification (Marcotte, Hoshahili, & Ramaswamy, 2001), fat replacement (Milani, et al., 2012), stabilising emulsions (Dickinson, 2009) and more. In

addition to thickening materials, many hydrocolloids also form viscoelastic gels. In some cases, such as alginate the gels are not thermoreversible owing to gelation occurring through the formation of covalent bonds (Martinsen, Skjåk-Bræk, & Smidsrød, 1989). Others however, are thermoreversible including gelatin, agar, gellan, κC and iota-carrageenan (ιC) and more (BeMiller, 2008).

Hydrocolloid gelation relies on various factors depending on the hydrocolloid in question, but one constant is the requirement to be above the critical minimum concentration (C_0). When hydrocolloids gel through a coil to helix mechanism; below the C_0, the coils are able to move around in the solution without interaction and this is referred to as the dilute region (Williams & Phillips, 2021). The concentration at which the polymers can begin associating is known as the critical overlap concentration (C*) (Williams, et al., 2021). Above the C*, the polymers become entangled, leading to an increase in viscosity and/or the ability to form viscoelastic gels (Genovese & Lozano, 2001). A graphical representation of the effect of the changes of hydrocolloid concentration is shown in Figure 2.1.

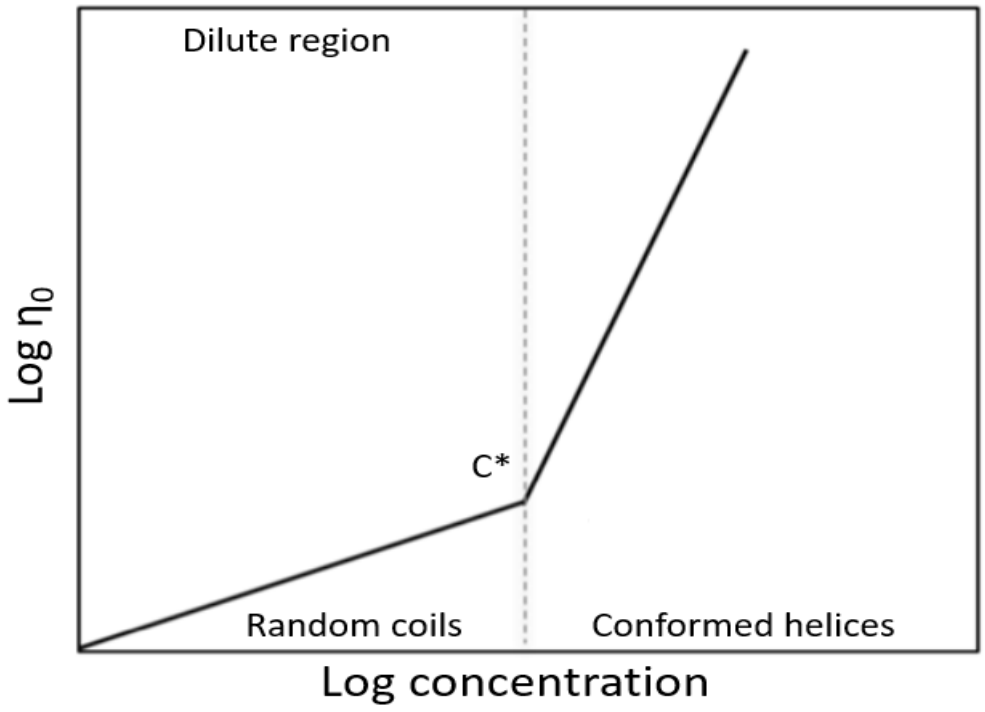

Figure 2.1: Graphical representation of log zero-shear viscosity against the log concentration. Adapted from Handbook of hydrocolloids (2009)

2.5.1 Agar

Agar consists of two fractions agarose and agaropectin and is therefore sometimes referred to as agar-agar. Of these two fractions, only agarose is responsible for the gelling properties of agar (Praiboon, Chirapart, Akakabe, Bhumibhamon, & Kajiwara, 2006). Agar has been used for hundreds of years in food production, and latterly microbial culture and medicine. Agar is generally recognised as safe according to the FDA (Phillips & Williams, 2009). The structure of agarose is shown in Figure 2.2 (Araki, 1956).

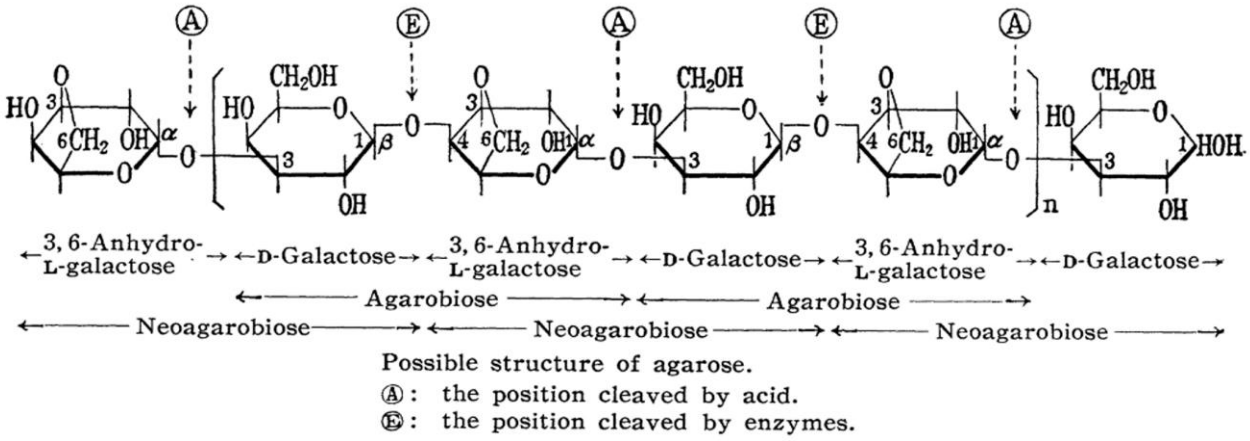

Figure 2.2: Structure of agarose taken from Araki (1956)

Being tasteless, odourless and colourless makes agar a perfect food additive. Agar cannot gel in cold water, it must be dispersed in hot water and then cooled down below its gelling temperature (Labropoulos, Niesz, Danforth, & Kevrekidis, 2002). Agar gelation occurs through a coil to helix transition upon lowering its temperature below its gelation temperature. Agar gels are typically turbid and brittle and differ from many other hydrocolloid gels for two reasons. The first is that it doesn't require any gelling cations or crosslinking agents, instead it is able to gel by hydrogen bonding with itself (Phillips, et al., 2009). The second is that agar has an extremely high melting hysteresis, with the gels melting at a far higher temperature than their gelling temperature (Armisen & Gaiatas, 2009). Gelation of agar, like all hydrocolloid gels, is concentration dependent. It is typically around 35-38 °C, while it typically melts above 80 °C

(Praiboon, et al., 2006). The gelation and melting mechanisms of agar are shown in Figure 2.3.

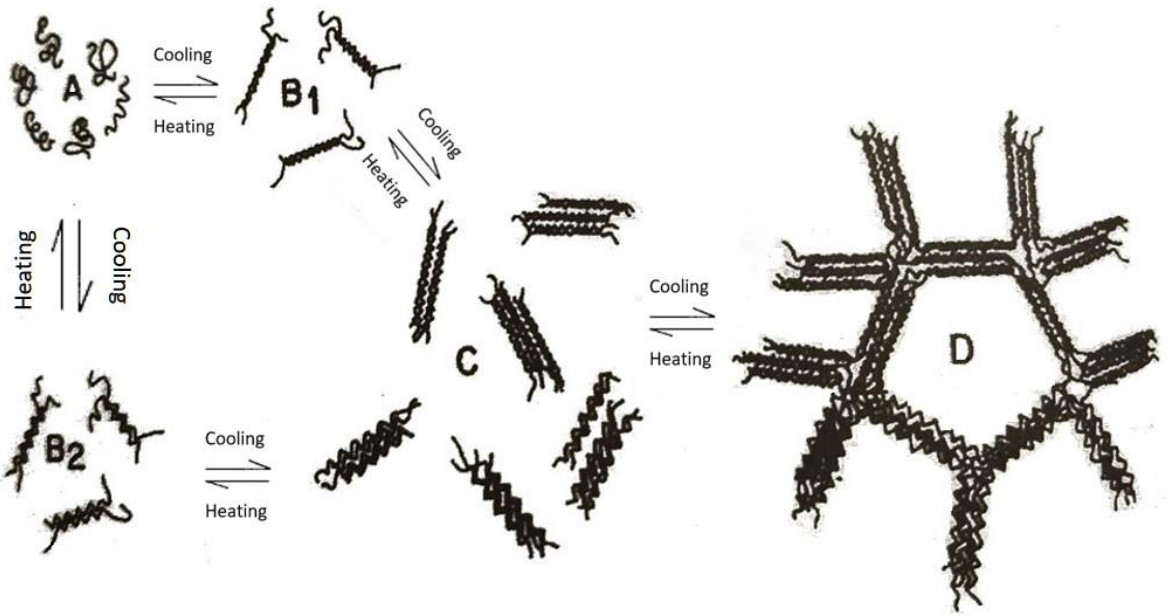

*Figure 2.3: Schematic of the gelation and melting mechanisms of agar. **A** represents random coils, **B_1** represents antisymmetric double helices, **B_2** represents symmetric double helices, **C** represents aggregated double helices and **D** represents the final macroreticulum. Both gelling processes coexist, and the cooling rate determines which is dominant, with **B_1** dominating during a fast cooling rate and **B_2** during a slower cooling rate. Adapted from Medin, A.S (1995)*

Agar's superb gel forming abilities, combined with its safety profile, abundance and reliability has led to its uptake in several areas. Agar is often used as scaffolding for cell culture work, owing to its biocompatibility (Gong, et al., 2007). It is also commonly used as a means of suspending nutrients to facilitate bacterial growth for microbiological research (Jett, Hatter, Huycke, & Gilmore, 1997). Agar is also used to cast moulds for dental work and forensic work, being stored in tubes and then melting in boiling water and then cooled to just above the gelling temperature (Armisen, et al., 2009).

Agar has seen some use as a release vehicle within literature, often as a gel-based formulation that is proposed as an alternate oral dosage form or as a film loaded with active molecules. (Desai & Bolton, 1993; Giménez, López de Lacey, Pérez-Santín, López-Caballero, & Montero, 2013). Agar gels have been shown to affect flavour molecule release based on the nature of the molecule and the concentration of the agar gel (Moritaka & Naito, 2002). Like most polymeric networks, agar releases molecules through Fickian diffusion and relaxation of the

polymer network (Kodela, et al., 2017). Agar does not cause a significant increase in the viscosity of solutions before gelation (Arakawa, 1961). This makes it useful for processes such as creating agar emulsion gels, as, provided it is kept above its gelation temperature, it can undergo emulsion processes such as high shear mixing with the agar already dispersed (Fontes-Candia, et al., 2021).

2.5.2 Kappa-carrageenan

The carrageenans are a group of anionic, sulphated polysaccharides which are extracted from an edible red seaweed called Rhodophyta. They consist of repeating galactose units and 3,6-anhydrogalactose, joined by alternating α-(1,3) and β-(1,4) glycosidic links (Imeson, 2009). The structure of several types of carrageenan are given in Figure 2.4 (Blakemore & Harpell, 2010)

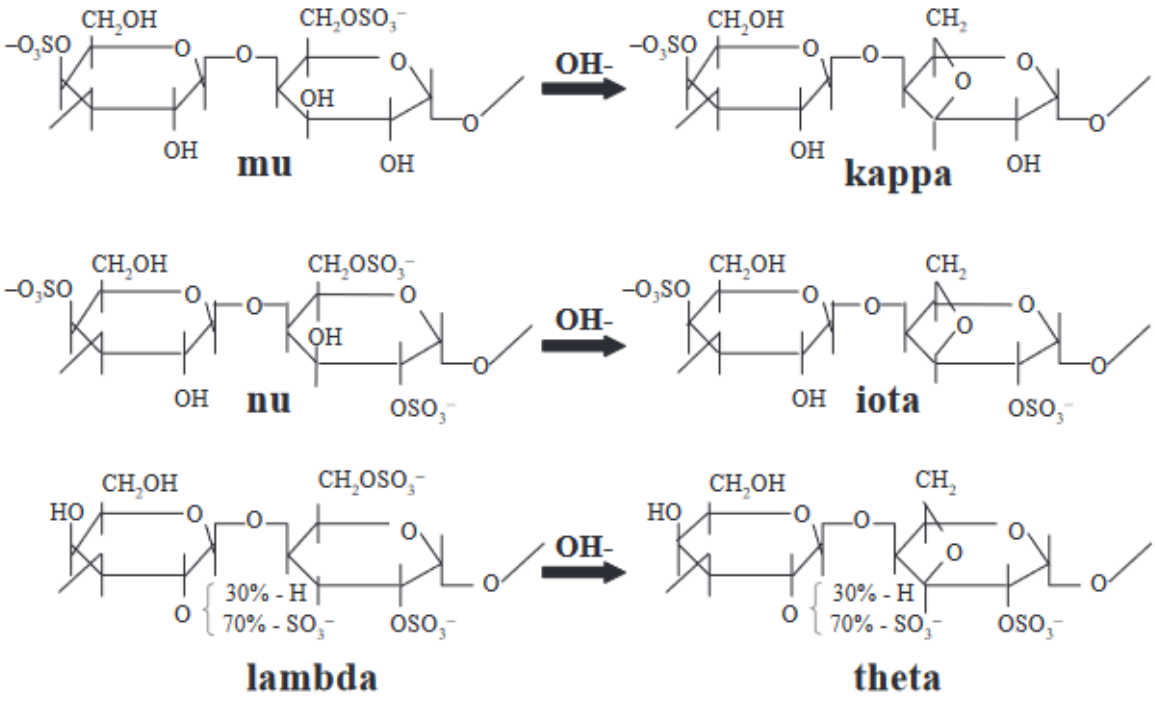

Figure 2.4: Structures of various carrageenan subtypes taken from Blakemore & Harpell (2010)

The three main carrageenans that are used, are kappa, iota and lambda (λ) (Paquin, 2009). These forms differ by the degree of sulphation, of each repeat unit. KC has one sulphate

group, ιC has two sulphate groups and λC has three sulphate groups. KC is the major focus of this work, and so from here on will be the solely discussed carrageenan.

KC, when dispersed in water and in the presence of cationic molecules, forms a strong, thermoreversible gel. It has its greatest affinity for potassium ions (Hermansson, Eriksson, & Jordansson, 1991). Once the dispersion is lowered below the gelation temperature, it undergoes a coil-helix transition, these double helices then associate to form a continuous polymer network (Norton, Morris, & Rees, 1984). This is represented in Figure 2.5 below.

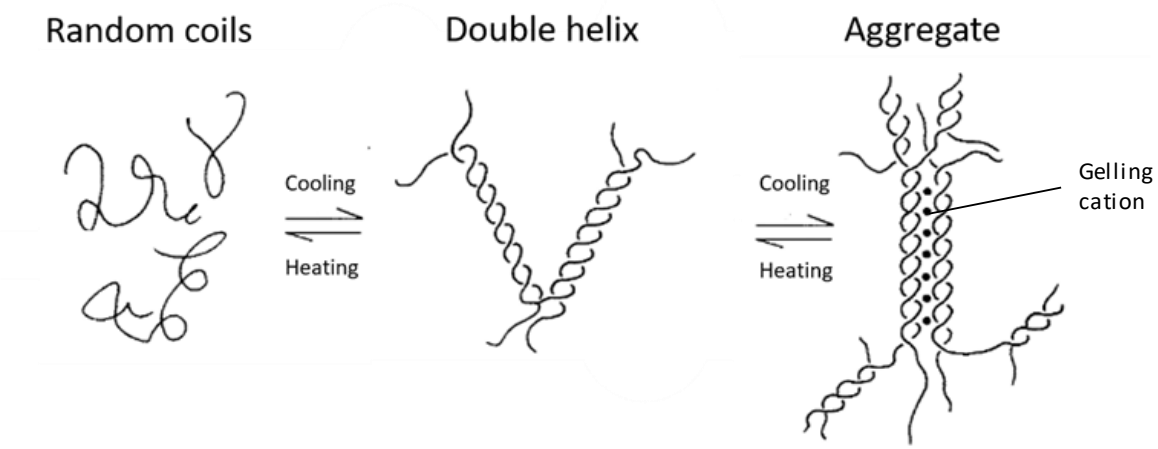

Figure 2.5: Schematic of the gelation and melting mechanisms of κC. Adapted from Robinson et al (1980)

κC has various uses within the food industry, being used as a gelling agent and a thickening agent (Saha, et al., 2010). They are used to produce gels both alone and in combination with other hydrocolloids (Astuti, Agustia, & Fkik, 2011; Athaillah, Eviana, Pudjiraharti, & Haryono, 2017). KC is known to have a highly synergistic action, at very low concentrations (up to 0.03%), with casein micelles in dairy systems, preventing bulk phase separation through adsorption to the casein micelle surfaces. This stabilises the micro-domains on the micelles, preventing them from coalescing and forming protein-enriched and depleted-phases (Spagnuolo, Dalgleish, Goff, & Morris, 2005). KC is also used in meat products as a stabiliser for injected water in products such as reduced fat sausages and meats. This helps replicate the texture and mouthfeel of the removed fat particles (Trius, Sebranek, & Lanier, 1996).

In addition to its uses in the food industry, κC has been the subject of much research as a drug delivery system owing to its biocompatibility and safety profile (Weiner, 1991). Since it entraps molecules within the gel network and releases them over time via diffusion and relaxation of the network, κC has been used as a modified release oral dose form (Picker, 1999). Other uses as a drug delivery system have been as parenteral preparations (Zhang, Tsai, Monie, Hung, & Wu, 2010) and as topical skin patches (Dalafu, Chua, & Chakraborty, 2010).

2.6 Characterisation of hydrocolloid gels

This section aims to provide an overview of the characterisation techniques utilised within this project.

2.6.1 Rheology

Rheology is the study of the flow and deformation of materials (Barnes, 2000). The viscosity is taken into account when examining material flow, and is defined as the resistance to movement (Schramm, 1994). When examining material deformation, the viscous and elastic behaviour of the material is scrutinised when the selected material is under shear. For all of the rheological characterisation within this project, a roughened (chapters 3 and 4) or serrated (chapter 4) parallel plate geometry was chosen to prevent sample slip. Parallel plate geometries confine liquid between a fixed bottom plate and top plate that rotates on an axis. The parallel plate allows variable gap sizes and is suitable for highly viscous samples. In order to prevent solvent evaporation during testing, silicone oil was spread around the edge of the parallel plate geometry. A schematic of a parallel plate geometry is shown in Figure 2.6.

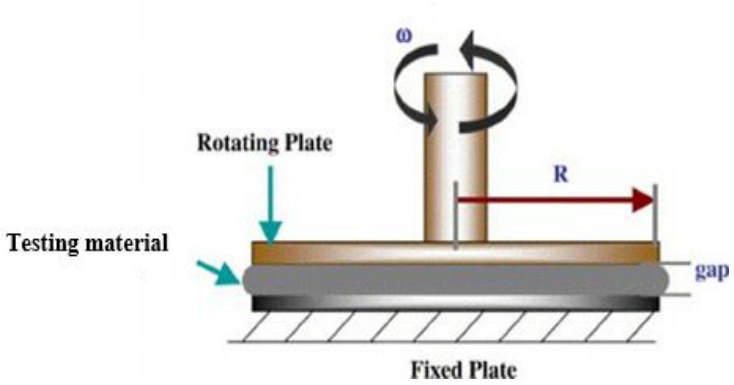

*Figure 2.6: Schematic of a parallel plate. Adapted from Nawab et al (2013). Where **ω** is angular frequency and **R** is the radius of the geometry*

Rheology has been used extensively in the characterisation of hydrocolloid gels, with literature existing for virtually all types of gel such as gelatin (Ross-Murphy, 1992), agar (Labropoulos, et al., 2002), alginate (Bonino, Samorezov, Jeon, Alsberg, & Khan, 2011), gellan (Rodrıguez-Hernández, Durand, Garnier, Tecante, & Doublier, 2003), carrageenans (Hermansson, et al., 1991; Yang, Gao, & Yang, 2020) and more as well as mixed hydrocolloid systems (Brenner, Tuvikene, Fang, Matsukawa, & Nishinari, 2015; Derkach, Ilyin, Maklakova, Kulichikhin, & Malkin, 2015; Fonkwe, Narsimhan, & Cha, 2003; Papageorgiou & Kasapis, 1995; Yano, 1986). Below is more information on the types of rheological test used within this project.

2.6.1.1 Temperature sweeps

Temperature sweeps are used to establish the T_{gel} and melting temperature (T_{melt}) of a gelling sample, along with data on the storage modulus (G′), loss modulus (G″), phase angle (δ) and more. The rheometer has the frequency and strain set to fixed values, to ensure only the temperature is responsible for any microstructural changes observed during the measurement. To obtain data for T_{gel}, the sample is loaded far above its T_{melt} (70 ˚C or 80 ˚C in chapter 3) and the temperature is lowered at a controlled rate. To obtain data for T_{melt}, the sample is loaded onto the rheometer in a sol state and allowed to gel. The rheometer temperature is then increased until the sample melts. T_{gel} and T_{melt} are determined as the temperatures of the gels where G′ and G″ cross over (Djabourov, Leblond, & Papon, 1988) An example of obtained T_{gel} data from temperature sweep data is shown in Figure 2.7.

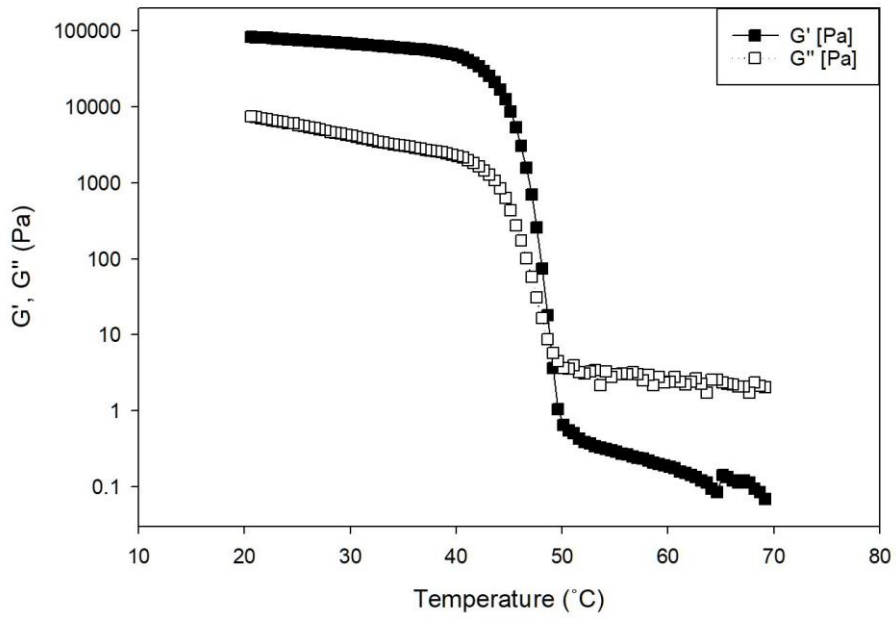

Figure 2.7: Temperature sweep data showing the gelling temperature of a 3% w/v κC and 1% w/v thiamine hydrogel. Adapted from chapter 3. T_{gel} is observed where the G' and G" values crossover.

2.6.1.2 Amplitude sweeps

Oscillatory tests were also carried out in chapter 4 to determine the linear viscoelastic region (LVER) of 3DP and cast κC-emulsion gels. Any significant difference based on the means of gel production, indicated which of casting or 3DP created a more robust gel network, determined as being more resistant to shear strain, as shown by a larger LVER. This involves fixing the frequency and temperature values and increasing the strain from 0.1% to 10%. G′, G″, δ and LVER data were all obtained from these tests. The LVER was determined as the range in which strain values showed no significant degradation (more than 5%) in G′ value. An example of LVER data is shown in Figure 2.8.

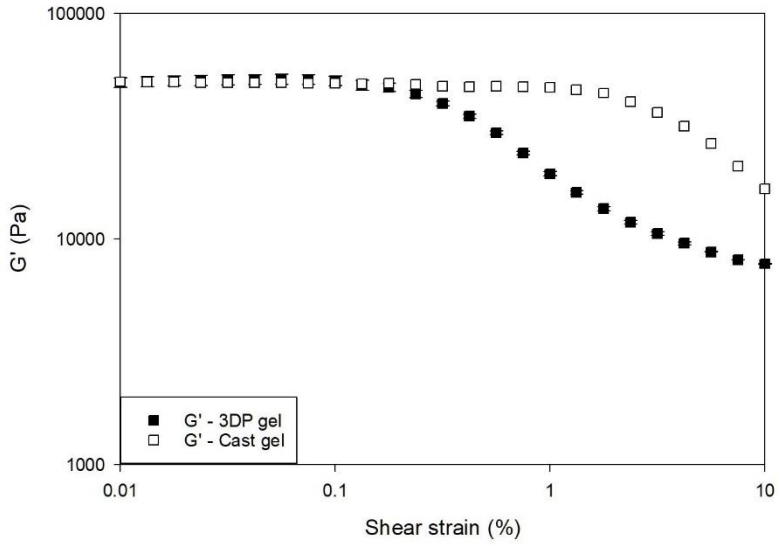

Figure 2.8: LVER data taken from chapter 4 comparing a 3DP gel to a cast gel. LVER is determined as the region before any significant degradation in G' values are observed

2.6.2 Micro differential scanning calorimetry

Micro differential scanning calorimetry (μDSC) is a method of thermal analysis that measures the difference in the heat flow rate between a known quantity of sample and a known quantity of reference as a function of temperature and time (Höhne, McNaughton, Hemminger, Flammersheim, & Flammersheim, 2003). It differs from regular DSC by utilising larger quantities of sample and a lower temperature rate (up to 1.2 ˚C min^{-1}) and as such, is more sensitive to small thermal changes in the materials (MacNaughtan & Farhat, 2008). Both the sample and the reference are loaded into the μDSC machine and are subjected to the same controlled temperature range. The aim is to determine the energy input required to sustain the same temperatures in the sample and the reference. A sample transition is indicated by an enthalpy change, which on the μDSC thermograph, is represented by a departure from the heat flow baseline (Höhne, et al., 2003). An exothermic transition such as gelation appears as a trough on a μDSC thermograph, and an endothermic transition such as melting appears as a peak. An example of μDSC is shown in Figure 2.9.

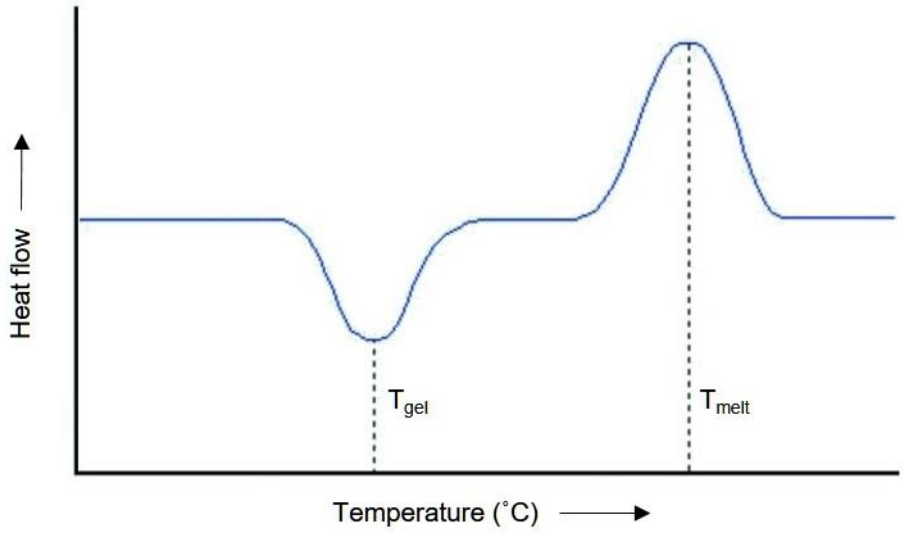

Figure 2.9: DSC thermograph showing T_{gel} and T_{melt} Adapted from PSLC (2018)

T_{gel} is taken as the lowest point on the first peak, and T_{melt} is taken as the highest point on the second peak. Enthalpy values for the values are obtained by calculating the areas of the peaks to the baseline.

Much like rheology, DSC and µDSC have been used extensively for analysis of hydrocolloid gel systems. Both alone and to confirm the data obtained from other methods of thermal analysis, including rheology. It should be noted, that there is normally a slight difference between T_{gel} and T_{melt} values reported for DSC and rheology, as they are sensitive to different parts of the gelation and melting mechanisms (Nishinari, 1997). DSC and µDSC have been used to characterise a range of hydrocolloid systems such as gelatin (Rahman, Al-Saidi, Guizani, & Abdullah, 2010), agar (Watase, Nishinari, Clark, & Ross-Murphy, 1989) gellan (Miyoshi, Takaya, & Nishinari, 1995), carrageenans (Iijima, Hatakeyama, Takahashi, & Hatakeyama, 2007; Norton, et al., 1984) and plenty more. Mixed systems have also been investigated (Garnier, et al., 2003; Singh, Aswal, & Bohidar, 2007; Wang, et al., 2015)

2.7 Emulsions and emulsion gels

2.7.1 Emulsions

Emulsions are dispersions made of two immiscible liquid phases, which are mixed using mechanical input, in the presence of an emulsifying agent (Kale & Deore, 2017). Without the emulsifying agent, the two liquid phases will be thermodynamically unstable and will rapidly phase separate (McClements & Jafari, 2018). The droplets are referred to as the dispersed, discontinuous or internal phase and the surrounding medium is the dispersing, continuous or external phase (McClements, 2007). Emulsifiers suitable for food products include low molecular weight surfactants (LMWS), proteins, polysaccharides and colloidal particles, a full review of these can be found elsewhere (McClements, et al., 2018; Nour, 2018). This work only utilises LMWS and proteins, and so only these will be discussed in more detail.

2.7.1.1 Emulsifying agents

Low molecular weight surfactants encompass molecules such as Tweens and Spans. LMWS typically have a polar head group and a non-polar tail group. The tail group can vary by the number of chains, the chain length and the degree of unsaturation. The polar head's properties vary as well, based on size and charge (anionic, cationic, zwittterionic and neutral) (Kralova & Sjöblom, 2009). If the surface of the oil droplets is fully covered by surfactant, then the emulsion will be stabilised by the repulsive forces of the surfactant (be they steric or electrostatic).

Proteins are also widely used as emulsifying agents. Proteins consist of chains of amino acids, referred to as the primary structure. The secondary structure is the regular, local structure generally consisting of α-helices and/or β-sheets, which are normally cooperative. These secondary structures orientate into structural domains, which comprise the tertiary structure. This is maintained by four types of interactions, between amino acid side chains. These include disulphide bridges, which are covalent and the strongest of the four. The other three are hydrogen bonding, hydrophobic interactions and ionic interaction between groups of opposite charge. The quaternary structure is the spatial configuration of the subunits within

the protein (Robertson & Murphy, 1997). Non-polar (hydrophobic) groups on the protein will align themselves within the oil phase and polar (hydrophilic) groups align themselves into the water phase of emulsions (Kralova, et al., 2009).

Proteins are less effective than LMWS at decreasing the interfacial tension during emulsification, since they are larger molecules and must orientate and unfold themselves at the interface (Beverung, Radke, & Blanch, 1999; Kenta, et al., 2013). Some examples of proteins commonly used as emulsifiers include whey proteins, caseins, bovine serum albumin, soy protein and many more (Lam & Nickerson, 2013). Compared to LMWS, proteins form a thicker viscoelastic layer at the interface, which enhances long term stability of protein stabilised emulsions compared to those stabilised by LMWS (Wilde, Mackie, Husband, Gunning, & Morris, 2004). Figure 2.10 shows a schematic of an oil droplet with several different emulsifiers.

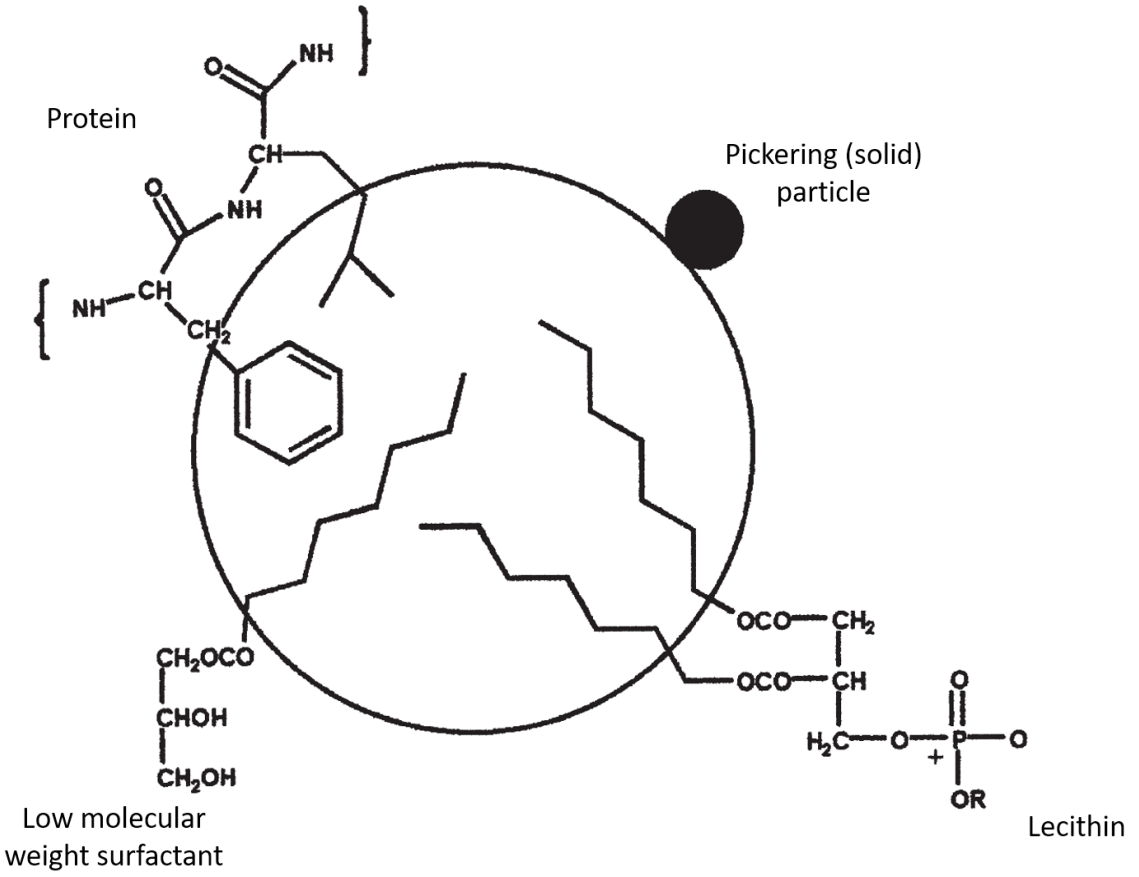

Figure 2.10: Schematic of an emulsified oil droplet, showing several emulsifier types. Adapted from Hasenhuettl (2008)

2.7.1.2 Emulsification techniques

Emulsification techniques primarily consist of rotor-stator systems such as high shear mixers, high-pressure systems such as homogenisers and microfluidisers, ultrasonic systems such as sonication probes and membrane systems (Jafari, Assadpoor, He, & Bhandari, 2008). The choice of emulsion technique generally depends on factors including volume, continuous phase viscosity, surfactant type, desired final droplet size and more.

Rotor-stator systems are generally less effective at droplet disruption owing to the larger volumes of the dispersing zones within the systems (Stang, Schuchmann, & Schubert, 2001). Essentially, the mean power density in rotor-stator systems are lower, and the mean residence time is longer compared to high-pressure devices (Jafari, et al., 2008). It has been demonstrated that droplet breakup effectiveness in turbulent flow is directly proportional to power density, and inversely proportional to droplet residence time in the dispersion zone (Floury, Legrand, & Desrumaux, 2004; Tesch & Schubert, 2002). This means they are less efficient compared to other emulsification techniques, and generally are unable to obtain a droplet size below 1 µm by themselves (Schultz, Wagner, Urban, & Ulrich, 2004).

High-pressure systems can produce droplets in the nano-scale, with a high output (McClements, 2004). They commonly require the creation of a coarse pre-emulsion as they are far more effective at reducing droplet size (McClements, 2004). Therefore, they generally require use of a rotor-stator or sonication device. High pressure homogenisers pump the pre-emulsion into a central inlet. From here, it progresses through a radial gap between the valve seat and plug. It then undergoes intense shear, cavitation and turbulent flow conditions which foster droplet breakup (Stang, et al., 2001).

2.7.2 Emulsion gels

Hydrocolloid gels typically consist of 0.1-10% w/v hydrocolloid, small amounts of salt and the rest water. This presents an issue when lipophilic molecules are required to be incorporated into the formulation. One method to overcome this issue is to formulate oil-in-water emulsions and then dispersing a gelling agent within the continuous phase and allow it to gel; in effect,

making the gel matrix the continuous phase. This enables the creation of multiphase food gels, with tuneable nutrition properties. Furthermore, the presence of an oil phase eliminates any solubility issues surrounding lipophilic molecules. Emulsion gels have also been shown to have increased stability compared to simple emulsions owing to decreased oil movement and oxygen permeation (Ma, Wan, & Yang, 2017; Sato, Moraes, & Cunha, 2014).

When creating hydrocolloid emulsion gels there are three commonly used approaches for their production. The first, and most common method involves creating a double concentrated emulsion, and a double concentrated hydrocolloid solution and then mixing them together in a 1:1 ratio. This has the advantage of straightforward emulsion and hydrocolloid gel production, with emulsion gels created with straightforward stirring under temperature (Fontes-Candia, Ström, Lopez-Sanchez, López-Rubio, & Martínez-Sanz, 2020; Soukoulis, et al., 2017). An example of this is shown in Figure 2.11.

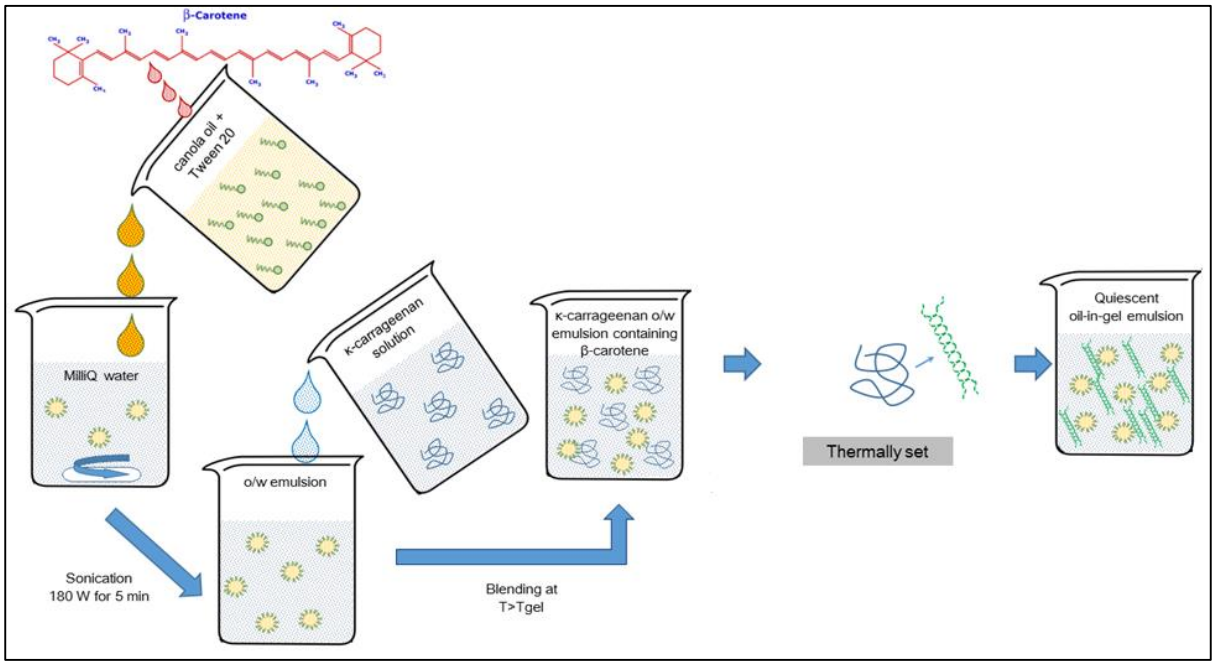

Figure 2.11: Creation of an o/w emulsion gel by creating a double concentrated o/w emulsion and a double concentrated hydrocolloid dispersion and then mixing them together in a 1:1 ratio Adapted from Soukoulis et al (2017)

The drawbacks of this method lie in the nature of the process. While creating double concentrated emulsions and hydrocolloid dispersions are feasible, it limits the ability to create high concentration final products. While other methods allow the straightforward production of

50% and above oil concentration emulsion gels, this is impossible via this method. Many hydrocolloids also have maximum concentrations at which they can be dispersed.

The second method involves dispersing the gelling agent in water, adding the oil phase and emulsifier, then carrying out the emulsification process. This can work with agar which doesn't increase the viscosity of water when added (Arakawa, 1961). For other hydrocolloids such as κC, gellan gum and alginate, which require gelling ions, the emulsification process is carried out and then the complementary crosslinker is added (Ching, Bansal, & Bhandari, 2016; Lorenzo, Zaritzky, & Califano, 2013; Yang, et al., 2020). However, this has the main drawback of requiring pure forms of these hydrocolloids, with no gelling ions present. This requires paying more money for purified forms or carrying out the purification step before use (Yang, et al., 2020). This makes it more costly, time-consuming and often both. Therefore, this process is less useful for widespread use, beyond lab-scale research. An example of this method is shown in Figure 2.12.

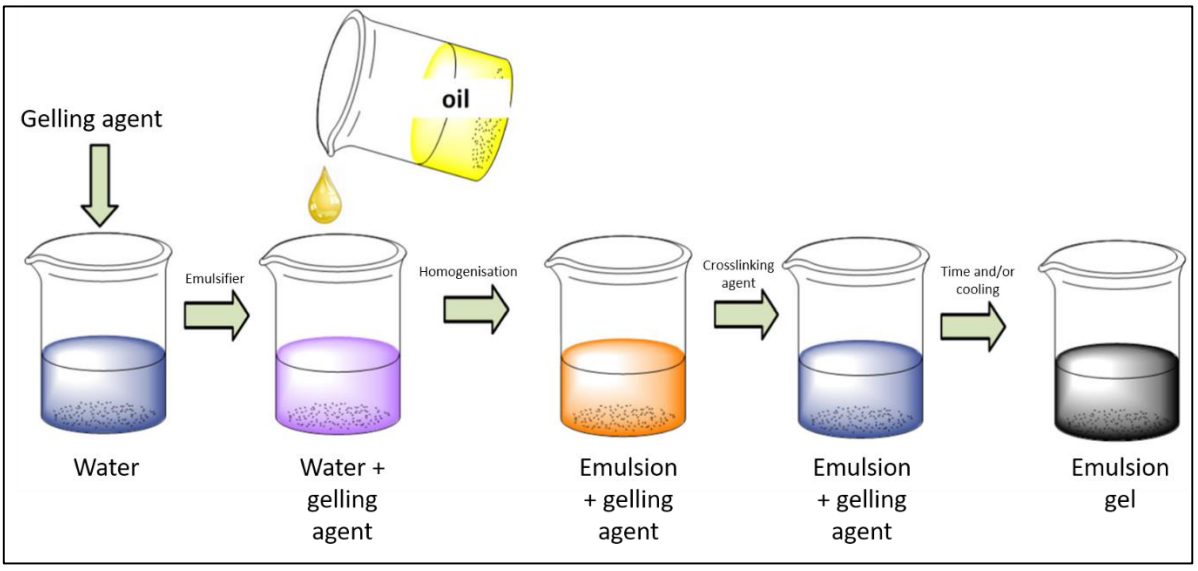

Figure 2.12: Creation of an o/w emulsion gel by dispersing a hydrocolloid within water, adding oil and an emulsifier and then carrying the emulsification process as normal. If agar is used then there is no need for the addition of a crosslinking agent, and that step can be missed out. Adapted from A. Li, Gong, Hou, Yang & Guo (2020)

The third method involves creating the emulsion at the concentration desired and then dispersing the gelling agent within it and allowing it to cool down, and undergo a sol-gel transition (Sala, de Wijk, van de Velde, & van Aken, 2008). This has the advantage of a relatively straightforward production, and the ability to create high internal phase emulsions,

unlike the first technique. It also does not require the higher cost and/or time requirement of hydrocolloids without their gelling agents the second method requires. An example of this method is shown in Figure 2.13.

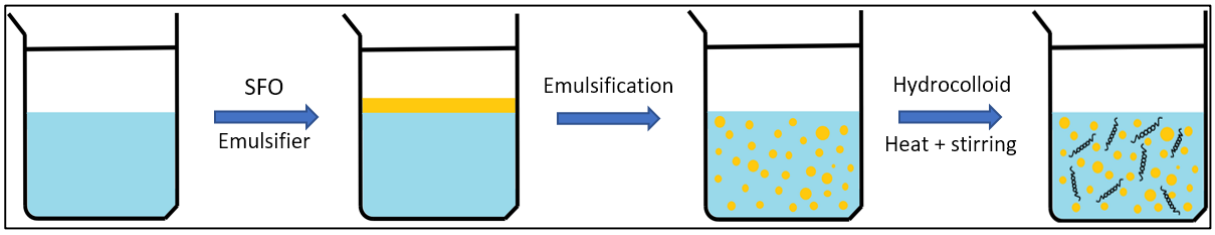

Figure 2.13: Creation of an o/w emulsion gel by creating an o/w emulsion and then dispersing a hydrocolloid within the emulsion and allowing it to gel as normal

For protein-based gels, making emulsion gels involves dispersing the protein within water, then adding oil and carrying out emulsification. This is then heated to encourage aggregation of the denatured proteins to form emulsion gels. One commonly used protein, whey protein, will be talked about in further detail (Dissanayake, Kelly, & Vasiljevic, 2010; Mcclements, Monahan, & Kinsella, 1993; Sager, Munk, Hansen, Bredie, & Ahrné, 2021; Sala, Van Aken, Stuart, & Van De Velde, 2007; Sala, van Vliet, Cohen, Stuart, Aken, & van de Velde, 2009). When whey proteins are heated to 70 ˚C and above, they unfold and denature (Dannenberg & Kessler, 1988). The changes in structure allow the proteins to interact with each other by hydrophobic bonding and thiol-disulfide exchange reactions (Sawyer, 1969; Smits & Van Brouwershaven, 1980). This means that whey protein emulsion gels can be created in a straightforward manner, similar to method 3, but using the protein as both the gelling hydrocolloid and the emulsifier.

Within the context of emulsion gels, the oil droplets can be classified as active or inactive fillers (Chen & Dickinson, 1998). Active fillers are bound to the gel network, and have been shown to contribute to the gel strength, owing to the reinforcing of the matrix by the particles coating the oil droplets, being able to interact with the gel matrix (Dickinson, 2012). Inactive fillers, on the other hand have limited, if any interaction with the gel matrix and therefore disrupt it, leading to a lowering of gel strength (Koç, et al., 2019). Only if the non-interacting droplets are

below a certain size and above a certain rigidity, will they not weaken the gel matrix (Dickinson & Chen, 1999).

The filler particles cause changes in the large deformation and fracture properties of the emulsion gels, depending on the nature of the interaction (Kokini & van Aken, 2006). The Van der Poel theory states that the determining factors for fillers in a gel matrix are the average particle size, volume fraction and spatial distribution (dispersed or flocculated) (Van der Poel, 1958). This theory has been shown to have limitations in high volume fraction systems or when flocculation occurs (Chen, et al., 1998; Houzé, Cases, Colas, & Cayot, 2005; Pal, 2002). For active filler particles, the higher the volume fraction, the higher the observed gel strength, with the opposite being observed for inactive fillers (Dickinson, et al., 1999; Sala, et al., 2009). A schematic of active and inactive filler particles is shown in Figure 2.14.

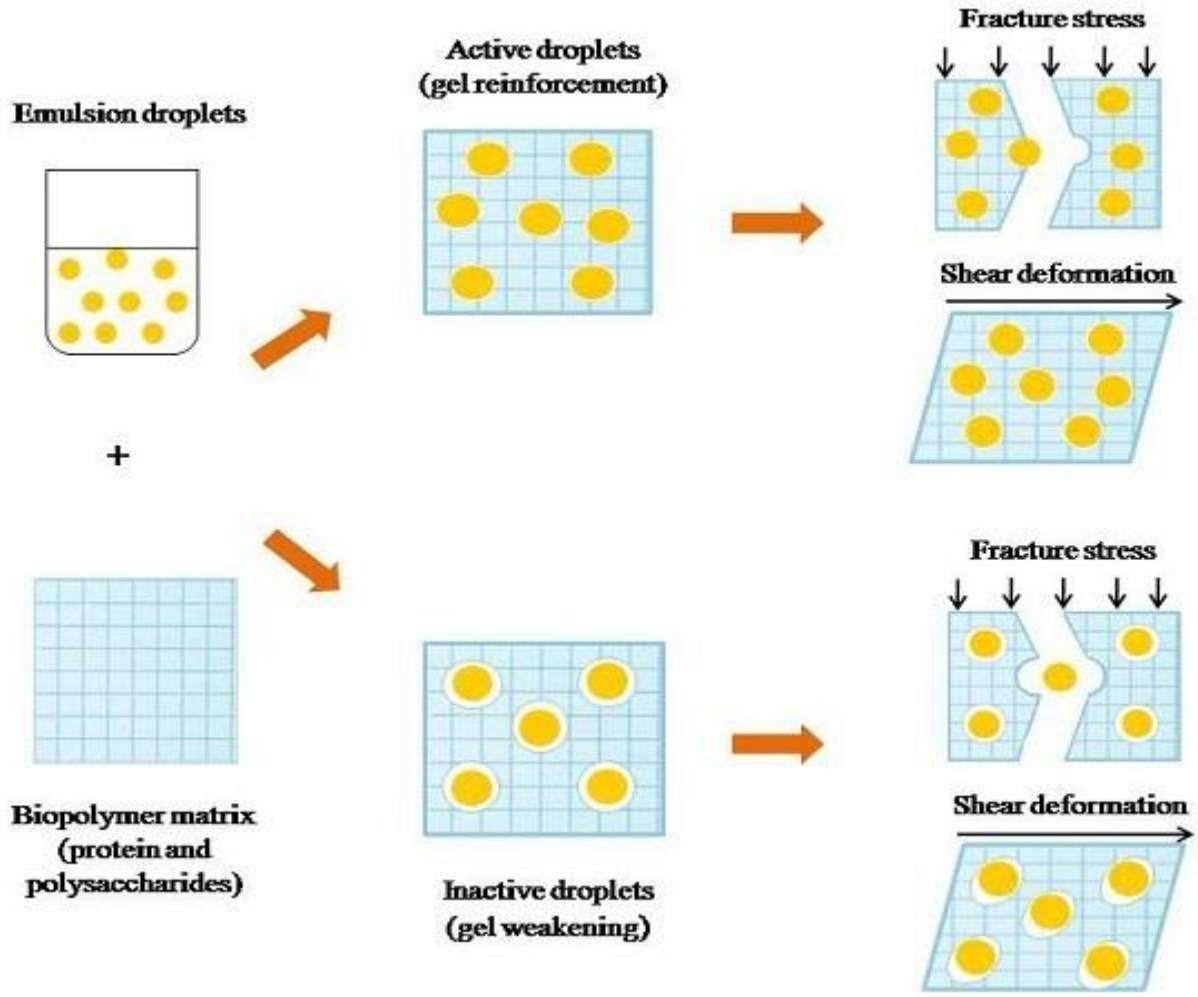

Figure 2.14: A schematic representation of the effects of fracture stress and shear deformation on emulsion gels containing active and inactive filler particles Geremias-Andrade, Souki, Moraes & Pinho (2016)

2.7.3 Agar emulsion gels

Agar has seen extensive use as the gelling agent within emulsion gels. Agar's uncharged nature, and its ability to gel in the absence of any cross-linking agents means that it is far less likely to cause stability issues with the emulsion, such as by ionic destabilisation or complexation with a charged emulsifier. Agar emulsion gels are created by the approach in Figure 2.11 (Mantelet, et al., 2019; Wang, Neves, Kobayashi, Uemura, & Nakajima, 2013) or created via the approach in Figure 2.13 (Kim, Gohtani, Matsuno, & Yamano, 1999; Malone & Appelqvist, 2003; Yamano, Kagawa, Kim, & Gohtani, 1996). The extensive use the method in Figure 2.13 is unexpected and suboptimal, as agar's lack of viscosity enhancement means that by holding the emulsions for extended periods of time at high temperatures (70 ˚C and

above), droplet coalescence is encouraged (Feng, Verstappen, Kuehne, & Sprakel, 2013). Owing to agar's uncharged nature, all emulsion gels will contain non-interacting fillers.

When agar is used to gel the continuous phase of an emulsion, flocculation of the oil droplets is seen to occur (Kim, et al., 1999; Yamano, et al., 1996). This is because the agar molecules, when in the continuous phase, cause an increase in attractive forces between the oil droplets. This occurs due to an osmotic effect related to the exclusion of colloidal particles from a slender region surrounding each droplet (Jenkins & Snowden, 1996; McClements, 2004). This is observed with LMWS (Kim, et al., 1999). However, while the same effect is suspected to occur with other emulsifiers such as Pickering emulsions, the author could find no literature that investigated this. Flocculation of oil droplets was observed however, in a Pickering emulsion dispersed within a carrageenan/agar film (Roy & Rhim, 2021). Furthermore, the only piece of literature that created agar emulsion gels stabilised with a protein, did not investigate the droplet distribution after gelation (Malone, et al., 2003). The only way to avoid the flocculation phenomenon is to use the first method of emulsion gel production, and immediately gel it, which does not give enough time for the flocculation to take place (Wang, et al., 2013).

2.7.4 Kappa-carrageenan emulsion gels

ΚC in emulsions have been the subject of several studies. Owing to its ability to act as a rheology modifier, κC is also used to stabilise o/w emulsions by increasing the viscosity of the continuous phase (Wu, et al., 2011). In terms of emulsion gels, most studies produced the emulsion gels through either the first technique of polysaccharide emulsion gel production (Sala, et al., 2008; Soukoulis, et al., 2017; Yang, et al., 2020) or the second (Fontes-Candia, et al., 2021; Fontes-Candia, et al., 2020). ΚC-emulsion gels can be created using a range of emulsifiers which can yield interacting and non-interacting fillers.

Much like agar, when κC is used as the biopolymer in an emulsion gel, flocculation is seen to occur. This has been shown for both interacting and non-interacting oil droplets (Gu, Decker, & McClements, 2005; Sala, et al., 2008; Sala, et al., 2009). This is due to the same osmotic

effect discussed earlier in the text. This has been observed for other polysaccharide gels such as gelatin showing that it isn't specifically caused by κC or its anionic nature (Sala, et al., 2009). This tends to happen when LMWS are used to stabilise the emulsions within the κC gels (Hanani & Husna, 2018). This has also been shown to occur with some Pickering emulsions (Jiang, Li, Du, Liu, & Meng, 2021). Much like agar, by making the emulsion and the κC dispersion separately, then mixing them together and gelling it the flocculation can be prevented (Fontes-Candia, et al., 2020).

The same depletion flocculation behaviour has been observed for κC-emulsion gels with protein stabilised emulsions as well, with examples for whey protein isolate (Sala, et al., 2009), caseinate (Koo, et al., 2019), bovine serum albumin (Dickinson & Pawlowsky, 1998) and soy oil bodies (Yang, et al., 2020) in current literature. It should be noted, that if the proteins are below their isoelectric point, and therefore have an overall positive charge, κC can cause bridging flocculation as well (Shimoni, Levi, Tal, & Lesmes, 2013). However, these studies used very low concentrations of κC. In chapter 4 of this study, it was shown that by using 3% w/w κC and a whey protein isolate stabilised emulsion, it was possible to create κC emulsion gels with properly dispersed oil droplets. The major difference was that previous studies used far lower concentrations of κC, meaning that before gelation the continuous phase was far less viscous, providing less resistance to flocculation (Iglauer, Wu, Shuler, Tang, & Goddard III, 2011).

2.7.5 Emulsion gels as release vehicles

Emulsions gels have been widely used as release vehicles owing to their ability to incorporate lipophilic and hydrophilic molecules in a straightforward manner and undergo a variety of release profiles. This can be burst release if the emulsion gels break down readily such as with gelatin, which tends to melt around physiological body temperature (Mhando & Wan Po, 1990). If gelatin emulsion gels are formulated for and tested in an environment that doesn't cause them to melt, they undergo modified release in a similar manner to other hydrocolloid gels, with both a Fickian diffusion and relaxation component driving release of the molecule

from the gel (Thakur, et al., 2012). Furthermore, releasing a hydrophile from a gelatin emulsion gel, has no discernible effect on the release profile compared to a hydrogel with no oil phase, despite the presence of the oil droplets (Satapathy, et al., 2015).

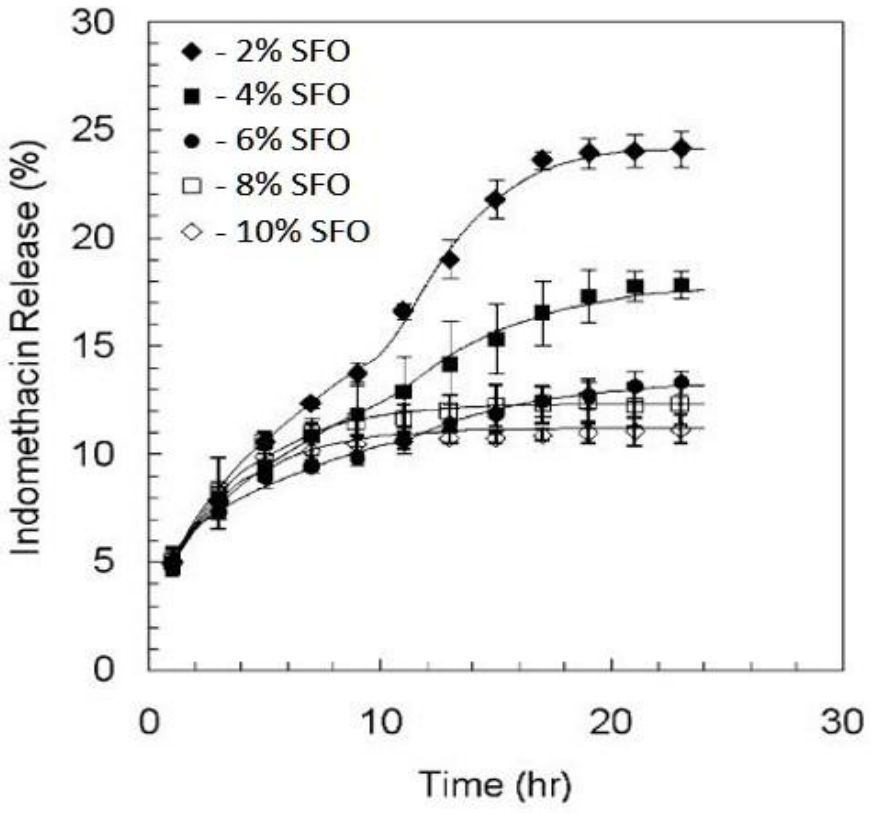

Figure 2.15: Modified release of indomethacin from a gelatin emulsion gel, with varying concentrations of sunflower oil (SFO). Adapted from Thakur, et al (2012)

Agar emulsion gels have been shown to vary in the release of flavour molecules based on the agar concentration used (Frank, et al., 2015; Malone, et al., 2003). This was associated with the gel strength, with higher concentrations yielding a more dense gel network, which slows down the diffusion of molecules, be they hydrophilic or lipophilic (Frank, et al., 2015). This is demonstrated in Figure 2.16. Agar gels have been shown to demonstrate first-order release when hydrophilic molecules are being expelled, however, when releasing lipophiles from entrapped oil droplets, this changes to zero-order release (Wanzke, Tena-Solsona, Rieß, Tebcharani, & Boekhoven, 2020). Agar gels tend to cause depletion flocculation of emulsions, and this can also affect the release rate, by increasing effective droplet size, diffusion distance and creating anisotropy (Giroux, et al., 2019; Tesch, et al., 2002; Wang, et al., 2013).

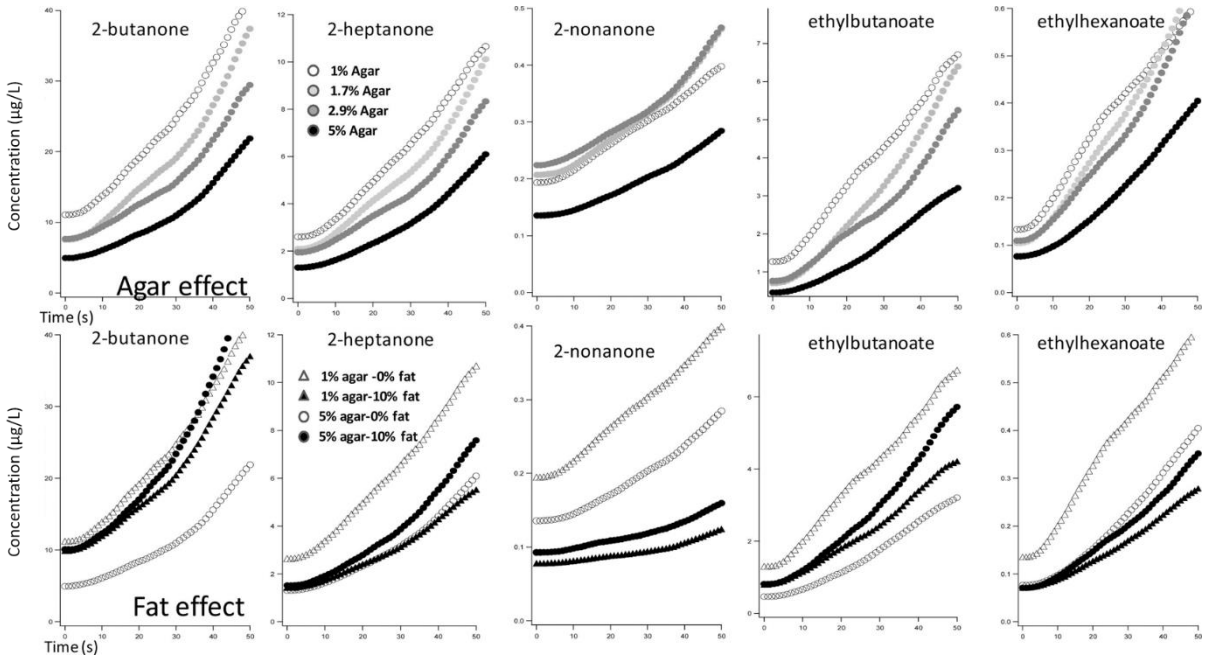

Figure 2.16: Release of hydrophilic and hydrophobic volatiles from agar hydrogels and emulsion gels, at varying concentrations of agar and oil. Taken from Frank, et al., (2015)

ΚC at lower concentrations can be formulated to undergo melting at physiological temperature, but these gels are weak and not easy to handle (Fenton, Kanyuck, Mills, & Pelan, 2021). Thus, typically when used as a release vehicle, work tends to focus on modified release formulations that don't melt in vivo. Owing to κC's ability to gel with a variety of cations (see section 2.5.2), emulsion gels with varying textural properties can be formed with κC by varying the gelling cation used. This was shown in a study assessing the bioavailability of beta-carotene from kappa-carrageenan emulsion gels based on the gelling cation and its effect on the gel strength of the gels (Soukoulis, et al., 2017). When combined with β-carotene enriched oleogels (structured, self-supporting oil systems consisting of oils and waxes), κC was found to give a firm gel network that held the well-dispersed oleogel network in place. This study rapidly gelled the κC-oleogel emulsion and so flocculation had no time to take place, thus making it unclear if use of an oleogel prevents the flocculation common with κC-emulsion gels. This study again, showed the utility of κC as a modified release vehicle, as it prevented rapid release of the embedded β-carotene (Zheng, Mao, Cui, Liu, & Gao, 2020). Another study showed that by embedding a curcumin enriched o/w emulsion into a κC gel network, the curcumin had superior storage and thermal stability. The curcumin was found to release in a controlled

manner over five hours, and the results were repeated with β-carotene as a model active (Tan, Ng, & Loo, 2021). This is shown in Figure 2.17.

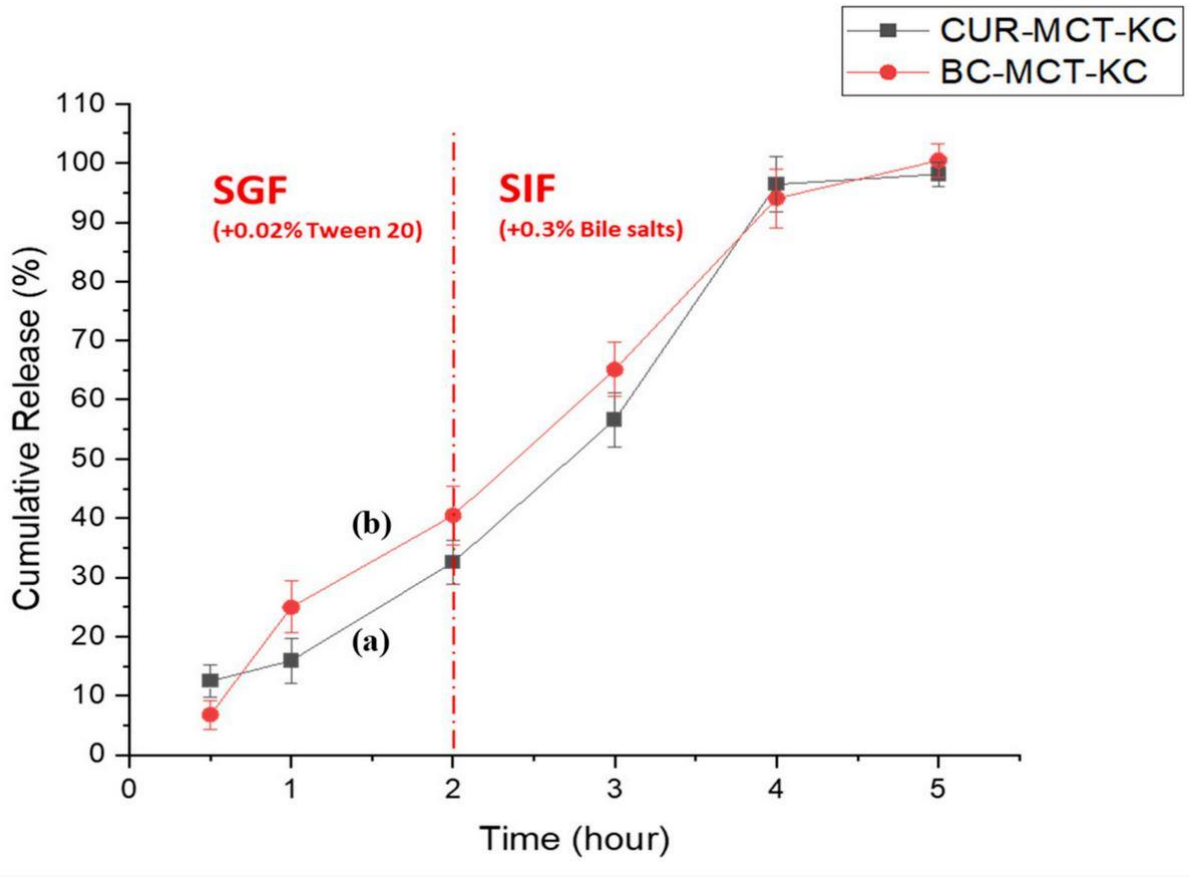

Figure 2.17: Release of hydrophobic model molecules from κC emulsion gels, initially in simulated gastric fluid (SGF) (pH 1.2) and then simulated intestinal fluid (SIF) (pH 6.8). Taken from Tan, Ng & Loo, (2021)

2.7.6 3D printing of emulsion gels

With 3DP of hydrocolloid gels still being a relatively young area of research, it follows that there exists even less research on 3DP of emulsion gels. Various types of emulsion gels have been 3DP, utilising various gelling agents and emulsifiers. This includes gelatin (Du, et al., 2021), alginate (Li, Gong, Hou, Yang, & Guo, 2020) heat-set whey proteins (Daffner, Ong, Hanssen, Gras, & Mills, 2021; Y. Liu, et al., 2019), cellulose nanofibre (Huan, Ajdary, Bai, Klar, & Rojas, 2019), casein/pectin gels (Bi, et al., 2022), rice protein and carboxymethyl cellulose (Wan, Wang, Feng, Chen, & Wang, 2021) and cod protein (Li, et al., 2020). A more comprehensive review can be found elsewhere (Li, Fan, Liu, & Li, 2021).

However, the work carried out in this project, especially chapters 4 and 5, differs in several significant ways compared to the above studies. One major difference is that this work utilises hot-extrusion 3DP with a sol-gel phase transition occurring *in-situ.* With the exception of (Daffner, et al., 2021) all of the other 3DP emulsion gel papers have no phase transition and the extruded gels act as yield stress materials. This is a different process, requiring differing approaches to formulation and processing parameters, with limits based on the pressure needed to extrude high G′ gels and syneresis issues with long term storage for some gels. Hot-extrusion 3DP negates these by using a hydrocolloid solution, which then gels upon printing. Furthermore, this work studies κC-emulsion gels, which have not been examined in the literature for 3DP emulsion gels. There is virtually no literature examining not just the effect of oil concentration in an emulsion gel, but whether the emulsifier can affect the overall structure of the 3DP emulsion gel. Nor does there exist any literature examining release of a lipophile from a 3DP emulsion gel structure or comparisons of their mechanical and microstructural; characteristics compared to traditional cast gels. The uniqueness of these aspects of the research within this work highlights the importance of this project in addressing several of these gaps within the literature, contributing knowledge to the field and helping overcome several of the issues regarding formulation, encapsulation of lipophilic and hydrophilic molecules, and how they release and printing parameters.

2.8 References

Anukiruthika, T., Moses, J. A., & Anandharamakrishnan, C. (2020). 3D printing of egg yolk and white with rice flour blends. *Journal of Food Engineering, 265*, 109691.

Arakawa, K. (1961). Rheological properties of hydrogels of agar-agar. *Bulletin of the Chemical Society of Japan, 34*(9), 1233-1235.

Araki, C. (1956). Structure of the agarose constituent of agar-agar. *Bulletin of the Chemical Society of Japan, 29*(4), 543-544.

Armisen, R., & Gaiatas, F. (2009). Agar. In *Handbook of hydrocolloids* (pp. 82-107): Elsevier.

Astuti, S. D., Agustia, F. C., & Fkik, U. (2011). Formulation and Characterization of Functional Jelly Drink as Source of Dietary Fiber and Vitamin C Consisting of Kappa Carrageenan, Konjac Glucomannan and Hibiscus sabdariffa, Linn Extract. *Jurnal Penelitian Sains Dan Teknologi, 1*(1), 1-13.

Athaillah, Z. A., Eviana, I., Pudjiraharti, S., & Haryono, A. (2017). Optimization of carrageenan-based jelly products added with nutrients for reducing osteoporosis risks. In *AIP Conference Proceedings* (Vol. 1904, pp. 020051): AIP Publishing LLC.

Azam, R. S. M., Zhang, M., Bhandari, B., & Yang, C. (2018). Effect of Different Gums on Features of 3D Printed Object Based on Vitamin-D Enriched Orange Concentrate. *Food Biophysics, 13*(3), 250-262.

Barnes, H. A. (2000). *A handbook of elementary rheology* (Vol. 1): University of Wales, Institute of Non-Newtonian Fluid Mechanics Aberystwyth.

Belluco, S., Losasso, C., Maggioletti, M., Alonzi, C. C., Paoletti, M. G., & Ricci, A. (2013). Edible Insects in a Food Safety and Nutritional Perspective: A Critical Review. *Comprehensive Reviews in Food Science and Food Safety, 12*(3), 296-313.

BeMiller, J. N. (2008). Hydrocolloids. In *Gluten-free cereal products and beverages* (pp. 203-215): Elsevier.

Beverung, C. J., Radke, C. J., & Blanch, H. W. (1999). Protein adsorption at the oil/water interface: characterization of adsorption kinetics by dynamic interfacial tension measurements. *Biophysical Chemistry, 81*(1), 59-80.

Bhardwaj, T. R., Kanwar, M., Lal, R., & Gupta, A. (2000). Natural gums and modified natural gums as sustained-release carriers. *Drug Dev Ind Pharm, 26*(10), 1025-1038.

Bi, A.-Q., Xu, X.-B., Guo, Y., Du, M., Yu, C.-P., & Wu, C. (2022). Fabrication of flavour oil high internal phase emulsions by casein/pectin hybrid particles: 3D printing performance. *Food Chemistry, 371*, 131349.

Blakemore, W. R., & Harpell, A. R. (2010). Carrageenan. *Food stabilisers, thickeners and gelling agents*, 73-94.

Bogers, M., Hadar, R., & Bilberg, A. (2016). Additive manufacturing for consumer-centric business models: Implications for supply chains in consumer goods manufacturing. *Technological Forecasting and Social Change, 102*, 225-239.

Bonino, C. A., Samorezov, J. E., Jeon, O., Alsberg, E., & Khan, S. A. (2011). Real-time in situ rheology of alginate hydrogel photocrosslinking. *Soft Matter, 7*(24), 11510-11517.

Bourell, D., Kruth, J. P., Leu, M., Levy, G., Rosen, D., Beese, A. M., & Clare, A. (2017). Materials for additive manufacturing. *CIRP Annals, 66*(2), 659-681.

Branciforti, D. S., Lazzaroni, S., Milanese, C., Castiglioni, M., Auricchio, F., Pasini, D., & Dondi, D. (2019). Visible light 3D printing with epoxidized vegetable oils. *Additive Manufacturing, 25*, 317-324.

Brenner, T., Tuvikene, R., Fang, Y., Matsukawa, S., & Nishinari, K. (2015). Rheology of highly elastic iota-carrageenan/kappa-carrageenan/xanthan/konjac glucomannan gels. *Food Hydrocolloids, 44*, 136-144.

Chang, J., He, J., Mao, M., Zhou, W., Lei, Q., Li, X., Li, D., Chua, C.-K., & Zhao, X. (2018). Advanced Material Strategies for Next-Generation Additive Manufacturing. *Materials, 11*(1).

Chen, H., Xie, F., Chen, L., & Zheng, B. (2019). Effect of rheological properties of potato, rice and corn starches on their hot-extrusion 3D printing behaviors. *Journal of Food Engineering, 244*, 150-158.

Chen, J., & Dickinson, E. (1998). Viscoelastic Properties Of Heat-Set Whey Protein Emulsion Gels. *Journal of Texture Studies, 29*(3), 285-304.

Chen, J., Mu, T., Goffin, D., Blecker, C., Richard, G., Richel, A., & Haubruge, E. (2019). Application of soy protein isolate and hydrocolloids based mixtures as promising food material in 3D food printing. *Journal of Food Engineering, 261*, 76-86.

Chien, K. B., Makridakis, E., & Shah, R. N. (2013). Three-dimensional printing of soy protein scaffolds for tissue regeneration. *Tissue Eng Part C Methods, 19*(6), 417-426.

Ching, S. H., Bansal, N., & Bhandari, B. (2016). Rheology of emulsion-filled alginate microgel suspensions. *Food Research International, 80*, 50-60.

Chua, C. K., Yeong, W. Y., & An, J. (2018). NextGen materials for 3D printing. In (Vol. 11, pp. 555): Multidisciplinary Digital Publishing Institute.

Daffner, K., Ong, L., Hanssen, E., Gras, S., & Mills, T. (2021). Characterising the influence of milk fat towards an application for extrusion-based 3D-printing of casein− whey protein suspensions via the pH− temperature-route. *Food Hydrocolloids*, 106642.

Dai, L., Cheng, T., Duan, C., Zhao, W., Zhang, W., Zou, X., Aspler, J., & Ni, Y. (2019). 3D printing using plant-derived cellulose and its derivatives: A review. *Carbohydrate Polymers, 203*, 71-86.

Dalafu, H., Chua, M. T., & Chakraborty, S. (2010). Development of κ-Carrageenan Poly (acrylic acid) Interpenetrating Network Hydrogel as Wound Dressing Patch. In *Biomaterials* (pp. 125-135): ACS Publications.

Daniel L. Cohen, J. I. L., Meredith Cutler, Deborah Coulter, Anthony Vesco, Hod Lipson. (2009). Hydrocolloid Printing - A Novel Platform for Customized Food Production.

Dankar, I., Haddarah, A., Omar, F. E. L., Sepulcre, F., & Pujolà, M. (2018). 3D printing technology: The new era for food customization and elaboration. *Trends in Food Science & Technology, 75*, 231-242.

Dankar, I., Pujolà, M., El Omar, F., Sepulcre, F., & Haddarah, A. (2018). Impact of Mechanical and Microstructural Properties of Potato Puree-Food Additive Complexes on Extrusion-Based 3D Printing. *Food and Bioprocess Technology, 11*(11), 2021-2031.

Dannenberg, F., & Kessler, H. G. (1988). Reaction kinetics of the denaturation of whey proteins in milk. *Journal of Food Science, 53*(1), 258-263.

Dawood, A., Marti, B. M., Sauret-Jackson, V., & Darwood, A. (2015). 3D printing in dentistry. *British Dental Journal, 219*(11), 521-529.

Derkach, S. R., Ilyin, S. O., Maklakova, A. A., Kulichikhin, V. G., & Malkin, A. Y. (2015). The rheology of gelatin hydrogels modified by κ-carrageenan. *LWT - Food Science and Technology, 63*(1), 612-619.

Derossi, A., Caporizzi, R., Azzollini, D., & Severini, C. (2018). Application of 3D printing for customized food. A case on the development of a fruit-based snack for children. *Journal of Food Engineering, 220*, 65-75.

Derossi, A., Caporizzi, R., Ricci, I., & Severini, C. (2019). Critical variables in 3D food printing. In *Fundamentals of 3D food printing and applications* (pp. 41-91): Elsevier.

Desai, S., & Bolton, S. (1993). A Floating Controlled-Release Drug Delivery System: In Vitro-in Vivo Evaluation. *Pharmaceutical Research, 10*(9), 1321-1325.

Dick, A., Bhandari, B., & Prakash, S. (2019). 3D printing of meat. *Meat Science, 153*, 35-44.

Dickinson, E. (2009). Hydrocolloids as emulsifiers and emulsion stabilizers. *Food Hydrocolloids, 23*(6), 1473-1482.

Dickinson, E. (2012). Emulsion gels: The structuring of soft solids with protein-stabilized oil droplets. *Food Hydrocolloids, 28*(1), 224-241.

Dickinson, E., & Chen, J. (1999). Heat-set whey protein emulsion gels: Role of active and inactive filler particles. *Journal of Dispersion Science and Technology, 20*(1-2), 197-213.

Dickinson, E., & Pawlowsky, K. (1998). Influence of κ-carrageenan on the properties of a protein-stabilized emulsion. *Food Hydrocolloids, 12*(4), 417-423.

Dissanayake, M., Kelly, A. L., & Vasiljevic, T. (2010). Gelling properties of microparticulated whey proteins. *J Agric Food Chem, 58*(11), 6825-6832.

Djabourov, M., Leblond, J., & Papon, P. (1988). Gelation of aqueous gelatin solutions. II. Rheology of the sol-gel transition. *Journal de Physique, 49*(2), 333-343.

Du, J., Dai, H., Wang, H., Yu, Y., Zhu, H., Fu, Y., Ma, L., Peng, L., Li, L., Wang, Q., & Zhang, Y. (2021). Preparation of high thermal stability gelatin emulsion and its application in 3D printing. *Food Hydrocolloids, 113*, 106536.

Feng, C., Zhang, M., & Bhandari, B. (2019). Materials Properties of Printable Edible Inks and Printing Parameters Optimization during 3D Printing: a review. *Critical Reviews in Food Science and Nutrition, 59*(19), 3074-3081.

Feng, H., Verstappen, N. A., Kuehne, A. J., & Sprakel, J. (2013). Well-defined temperature-sensitive surfactants for controlled emulsion coalescence. *Polymer Chemistry, 4*(6), 1842-1847.

Fenton, T., Kanyuck, K., Mills, T., & Pelan, E. (2021). Formulation and characterisation of kappa-carrageenan gels with non-ionic surfactant for melting-triggered controlled release. *Carbohydrate Polymer Technologies and Applications, 2*, 100060.

Fernandez-Vicente, M., Calle, W., Ferrandiz, S., & Conejero, A. (2016). Effect of infill parameters on tensile mechanical behavior in desktop 3D printing. *3D Printing and Additive Manufacturing, 3*(3), 183-192.

Floury, J., Legrand, J., & Desrumaux, A. (2004). Analysis of a new type of high pressure homogeniser. Part B. study of droplet break-up and recoalescence phenomena. *Chemical Engineering Science, 59*(6), 1285-1294.

Fonkwe, L. G., Narsimhan, G., & Cha, A. S. (2003). Characterization of gelation time and texture of gelatin and gelatin–polysaccharide mixed gels. *Food Hydrocolloids, 17*(6), 871-883.

Fontes-Candia, C., Lopez-Sanchez, P., Ström, A., Martínez, J. C., Salvador, A., Sanz, T., Trefna, H. D., López-Rubio, A., & Martínez-Sanz, M. (2021). Maximizing the oil content in polysaccharide-based emulsion gels for the development of tissue mimicking phantoms. *Carbohydrate Polymers, 256*, 117496.

Fontes-Candia, C., Ström, A., Lopez-Sanchez, P., López-Rubio, A., & Martínez-Sanz, M. (2020). Rheological and structural characterization of carrageenan emulsion gels. *Algal Research, 47*, 101873.

Ford, S., & Despeisse, M. (2016). Additive manufacturing and sustainability: an exploratory study of the advantages and challenges. *Journal of Cleaner Production, 137*, 1573-1587.

Frank, D., Eyres, G. T., Piyasiri, U., Cochet-Broch, M., Delahunty, C. M., Lundin, L., & Appelqvist, I. M. (2015). Effects of Agar Gel Strength and Fat on Oral Breakdown,

Volatile Release, and Sensory Perception Using in Vivo and in Vitro Systems. *Journal of Agricultural and Food Chemistry, 63*(41), 9093-9102.

Garmulewicz, A., Holweg, M., Veldhuis, H., & Yang, A. (2018). Disruptive Technology as an Enabler of the Circular Economy: What Potential Does 3D Printing Hold? *California Management Review, 60*(3), 112-132.

Garnier, C., Michon, C., Durand, S., Cuvelier, G., Doublier, J.-L., & Launay, B. (2003). Iota-carrageenan/casein micelles interactions: evidence at different scales. *Colloids and surfaces B: Biointerfaces, 31*(1-4), 177-184.

Gebler, M., Schoot Uiterkamp, A. J. M., & Visser, C. (2014). A global sustainability perspective on 3D printing technologies. *Energy Policy, 74*, 158-167.

Genovese, D. B., & Lozano, J. E. (2001). The effect of hydrocolloids on the stability and viscosity of cloudy apple juices. *Food Hydrocolloids, 15*(1), 1-7.

Ghazal, A. F., Zhang, M., & Liu, Z. (2019). Spontaneous Color Change of 3D Printed Healthy Food Product over Time after Printing as a Novel Application for 4D Food Printing. *Food and Bioprocess Technology, 12*(10), 1627-1645.

Gholamipour-Shirazi, A., Norton, I. T., & Mills, T. (2019). Designing hydrocolloid based food-ink formulations for extrusion 3D printing. *Food Hydrocolloids, 95*, 161-167.

Giménez, B., López de Lacey, A., Pérez-Santín, E., López-Caballero, M. E., & Montero, P. (2013). Release of active compounds from agar and agar–gelatin films with green tea extract. *Food Hydrocolloids, 30*(1), 264-271.

Giroux, H. J., Shea, R., Sabik, H., Fustier, P., Robitaille, G., & Britten, M. (2019). Effect of oil phase properties on peptide release from water-in-oil-in-water emulsions in gastrointestinal conditions. *Lwt, 109*, 429-435.

Godoi, F. C., Bhandari, B., Prakash, S., & Zhang, M. (2018). *Fundamentals of 3D food printing and applications*: Academic press.

Godoi, F. C., Bhandari, B. R., Prakash, S., & Zhang, M. (2019). An Introduction to the Principles of 3D Food Printing. In *Fundamentals of 3D Food Printing and Applications* (pp. 1-18).

Godoi, F. C., Prakash, S., & Bhandari, B. R. (2016). 3d printing technologies applied for food design: Status and prospects. *Journal of Food Engineering, 179*, 44-54.

Gong, X., Anderson, T., & Chou, K. (2012). Review on powder-based electron beam additive manufacturing technology. In *International Symposium on Flexible Automation* (Vol. 45110, pp. 507-515): American Society of Mechanical Engineers.

Gong, Y., He, L., Li, J., Zhou, Q., Ma, Z., Gao, C., & Shen, J. (2007). Hydrogel-filled polylactide porous scaffolds for cartilage tissue engineering. *Journal of Biomedical Materials Research Part B: Applied Biomaterials, 82*(1), 192-204.

Gorkin III, R., & Dodds, S. (2013). The ultimate iron chef-when 3D printers invade the kitchen.

Goyanes, A., Scarpa, M., Kamlow, M., Gaisford, S., Basit, A. W., & Orlu, M. (2017). Patient acceptability of 3D printed medicines. *Int J Pharm, 530*(1-2), 71-78.

Gross, B., Lockwood, S. Y., & Spence, D. M. (2017). Recent Advances in Analytical Chemistry by 3D Printing. *Analytical Chemistry, 89*(1), 57-70.

Gu, Y. S., Decker, E. A., & McClements, D. J. (2005). Influence of pH and carrageenan type on properties of β-lactoglobulin stabilized oil-in-water emulsions. *Food Hydrocolloids, 19*(1), 83-91.

Hamilton, C. A., Alici, G., & in het Panhuis, M. (2018). 3D printing Vegemite and Marmite: Redefining “breadboards”. *Journal of Food Engineering, 220*, 83-88.

Hao, L., Mellor, S., Seaman, O., Henderson, J., Sewell, N., & Sloan, M. (2010). Material characterisation and process development for chocolate additive layer manufacturing. *Virtual and Physical Prototyping, 5*(2), 57-64.

Hegab, H. A. (2016). Design for additive manufacturing of composite materials and potential alloys: a review. *Manufacturing Rev., 3*, 11.

Hermansson, A.-M., Eriksson, E., & Jordansson, E. (1991). Effects of potassium, sodium and calcium on the microstructure and rheological behaviour of kappa-carrageenan gels. *Carbohydrate Polymers, 16*(3), 297-320.

Hertafeld, E., Zhang, C., Jin, Z., Jakub, A., Russell, K., Lakehal, Y., Andreyeva, K., Bangalore, S. N., Mezquita, J., & Blutinger, J. (2019). Multi-material three-dimensional food

printing with simultaneous infrared cooking. *3D Printing and Additive Manufacturing, 6*(1), 13-19.

Hespel, A.-M., Wilhite, R., & Hudson, J. (2014). Invited Review-Applications For 3d Printers In Veterinary Medicine. *Veterinary Radiology & Ultrasound, 55*(4), 347-358.

Höhne, G., McNaughton, J., Hemminger, W., Flammersheim, H.-J., & Flammersheim, H.-J. (2003). *Differential scanning calorimetry*: Springer Science & Business Media.

Holland, S., Foster, T., MacNaughtan, W., & Tuck, C. (2018). Design and characterisation of food grade powders and inks for microstructure control using 3D printing. *Journal of Food Engineering, 220*, 12-19.

Houzé, G., Cases, E., Colas, B., & Cayot, P. (2005). Viscoelastic properties of acid milk gel as affected by fat nature at low level. *International Dairy Journal, 15*(10), 1006-1016.

Huan, S., Ajdary, R., Bai, L., Klar, V., & Rojas, O. J. (2019). Low Solids Emulsion Gels Based on Nanocellulose for 3D-Printing. *Biomacromolecules, 20*(2), 635-644.

Huang, M.-s., Zhang, M., & Bhandari, B. (2019). Assessing the 3D Printing Precision and Texture Properties of Brown Rice Induced by Infill Levels and Printing Variables. *Food and Bioprocess Technology, 12*(7), 1185-1196.

Iglauer, S., Wu, Y., Shuler, P., Tang, Y., & Goddard III, W. A. (2011). Dilute iota-and kappa-Carrageenan solutions with high viscosities in high salinity brines. *Journal of Petroleum science and Engineering, 75*(3-4), 304-311.

Iijima, M., Hatakeyama, T., Takahashi, M., & Hatakeyama, H. (2007). Effect of thermal history on kappa-carrageenan hydrogelation by differential scanning calorimetry. *Thermochimica Acta, 452*(1), 53-58.

Imeson, A. (2009). Carrageenan and furcellaran. In *Handbook of hydrocolloids* (pp. 164-185): Elsevier.

Izdebska, J., & Zolek-Tryznowska, Z. (2016). 3D food printing–facts and future. *Agro FOOD Industry Hi Tech, 27*(2), 33-37.

Jafari, S. M., Assadpoor, E., He, Y., & Bhandari, B. (2008). Re-coalescence of emulsion droplets during high-energy emulsification. *Food Hydrocolloids, 22*(7), 1191-1202.

Jett, B. D., Hatter, K. L., Huycke, M. M., & Gilmore, M. S. (1997). Simplified agar plate method for quantifying viable bacteria. *Biotechniques, 23*(4), 648-650.

Jiang, H., Zheng, L., Zou, Y., Tong, Z., Han, S., & Wang, S. (2019). 3D food printing: main components selection by considering rheological properties. *Critical Reviews in Food Science and Nutrition, 59*(14), 2335-2347.

Jiang, Q., Li, S., Du, L., Liu, Y., & Meng, Z. (2021). Soft κ-carrageenan microgels stabilized pickering emulsion gels: Compact interfacial layer construction and particle-dominated emulsion gelation. *Journal of Colloid and Interface Science, 602*, 822-833.

Jiang, R., Kleer, R., & Piller, F. T. (2017). Predicting the future of additive manufacturing: A Delphi study on economic and societal implications of 3D printing for 2030. *Technological Forecasting and Social Change, 117*, 84-97.

Jonkers, N., van Dommelen, J. A. W., & Geers, M. G. D. (2020). Experimental characterization and modeling of the mechanical behavior of brittle 3D printed food. *Journal of Food Engineering, 278*, 109941.

Kale, S. N., & Deore, S. L. (2017). Emulsion micro emulsion and nano emulsion: a review. *Systematic Reviews in Pharmacy, 8*(1), 39.

Karyappa, R., & Hashimoto, M. (2019). Chocolate-based Ink Three-dimensional Printing (Ci3DP). *Scientific Reports, 9*(1), 14178.

Kashyap, N., Kumar, N., & Kumar, M. N. V. R. (2005). Hydrogels for Pharmaceutical and Biomedical Applications. *Critical Reviews in Therapeutic Drug Carrier Systems, 22*(2), 107-150.

Kenta, S., Raikos, V., Vagena, A., Sevastos, D., Kapolos, J., Koliadima, A., & Karaiskakis, G. (2013). Kinetic study of aggregation of milk protein and/or surfactant-stabilized oil-in-water emulsions by Sedimentation Field-Flow Fractionation. *Journal of Chromatography A, 1305*, 221-229.

Kim, H. W., Bae, H., & Park, H. J. (2017). Classification of the printability of selected food for 3D printing: Development of an assessment method using hydrocolloids as reference material. *Journal of Food Engineering, 215*, 23-32.

Kim, H. W., Lee, J. H., Park, S. M., Lee, M. H., Lee, I. W., Doh, H. S., & Park, H. J. (2018). Effect of Hydrocolloids on Rheological Properties and Printability of Vegetable Inks for 3D Food Printing. *Journal of Food Science, 83*(12), 2923-2932.

Kim, K.-H., Gohtani, S., Matsuno, R., & Yamano, Y. (1999). Effects of oil droplet and agar concentration on gel strength and microstructure of o/w emulsion gel. *Journal of Texture Studies, 30*(3), 319-335.

Koç, H., Drake, M., Vinyard, C. J., Essick, G., van de Velde, F., & Foegeding, E. A. (2019). Emulsion filled polysaccharide gels: Filler particle effects on material properties, oral processing, and sensory texture. *Food Hydrocolloids, 94*, 311-325.

Kodela, S. P., Pandey, P. M., Nayak, S. K., Uvanesh, K., Anis, A., & Pal, K. (2017). Novel agar–stearyl alcohol oleogel-based bigels as structured delivery vehicles. *International Journal of Polymeric Materials and Polymeric Biomaterials, 66*(13), 669-678.

Kokini, J., & van Aken, G. (2006). Discussion session on food emulsions and foams. *Food Hydrocolloids, 20*(4), 438-445.

Koo, C. K. W., Chung, C., Fu, J.-T. R., Sher, A., Rousset, P., & McClements, D. J. (2019). Impact of sodium caseinate, soy lecithin and carrageenan on functionality of oil-in-water emulsions. *Food Research International, 123*, 779-789.

Kouzani, A. Z., Adams, S., Oliver, R., Nguwi, Y. Y., Hemsley, B., & Balandin, S. (2016). 3D printing of a pavlova. In *2016 IEEE Region 10 Conference (TENCON)* (pp. 2281-2285): IEEE.

Kralova, I., & Sjöblom, J. (2009). Surfactants Used in Food Industry: A Review. *Journal of Dispersion Science and Technology, 30*(9), 1363-1383.

Labropoulos, K., Niesz, D., Danforth, S., & Kevrekidis, P. (2002). Dynamic rheology of agar gels: theory and experiments. Part II: gelation behavior of agar sols and fitting of a theoretical rheological model. *Carbohydrate Polymers, 50*(4), 407-415.

Lam, R. S., & Nickerson, M. T. (2013). Food proteins: a review on their emulsifying properties using a structure–function approach. *Food Chemistry, 141*(2), 975-984.

Lanaro, M., Forrestal, D. P., Scheurer, S., Slinger, D. J., Liao, S., Powell, S. K., & Woodruff, M. A. (2017). 3D printing complex chocolate objects: Platform design, optimization and evaluation. *Journal of Food Engineering, 215*, 13-22.

Le-Bail, A., & Maniglia, B. C. (2020). PL-B. 3D printing of foods: Recent developments, future perspectives and challenges. *Curr. Opin. Food Sci, 243*, 153057.

Le Tohic, C., O'Sullivan, J. J., Drapala, K. P., Chartrin, V., Chan, T., Morrison, A. P., Kerry, J. P., & Kelly, A. L. (2018). Effect of 3D printing on the structure and textural properties of processed cheese. *Journal of Food Engineering, 220*, 56-64.

Li, A., Gong, T., Hou, Y., Yang, X., & Guo, Y. (2020). Alginate-stabilized thixotropic emulsion gels and their applications in fabrication of low-fat mayonnaise alternatives. *International Journal of Biological Macromolecules, 146*, 821-831.

Li, H., Tan, C., & Li, L. (2018). Review of 3D printable hydrogels and constructs. *Materials & Design, 159*, 20-38.

Li, T., Aspler, J., Kingsland, A., Cormier, L. M., & Zou, X. (2016). 3d printing–a review of technologies, markets, and opportunities for the forest industry. *J. Sci. Technol. For. Prod. Process, 5*(2), 30.

Li, X., Fan, L., Liu, Y., & Li, J. (2021). New insights into food O/W emulsion gels: Strategies of reinforcing mechanical properties and outlook of being applied to food 3D printing. *Critical Reviews in Food Science and Nutrition*, 1-23.

Li, X., Xu, X., Song, L., Bi, A., Wu, C., Ma, Y., Du, M., & Zhu, B. (2020). High Internal Phase Emulsion for Food-Grade 3D Printing Materials. *ACS applied materials & interfaces, 12*(40), 45493-45503.

Ligon, S. C., Liska, R., Stampfl, J., Gurr, M., & Mülhaupt, R. (2017). Polymers for 3D Printing and Customized Additive Manufacturing. *Chemical reviews, 117*(15), 10212-10290.

Lille, M., Nurmela, A., Nordlund, E., Metsä-Kortelainen, S., & Sozer, N. (2018). Applicability of protein and fiber-rich food materials in extrusion-based 3D printing. *Journal of Food Engineering, 220*, 20-27.

Lipton, J., Arnold, D., Nigl, F., Lopez, N., Cohen, D., Norén, N., & Lipson, H. (2010). Multi-material food printing with complex internal structure suitable for conventional post-processing. In *2010 International Solid Freeform Fabrication Symposium*: University of Texas at Austin.

Lipton, J. I., Cutler, M., Nigl, F., Cohen, D., & Lipson, H. (2015). Additive manufacturing for the food industry. *Trends in Food Science & Technology, 43*(1), 114-123.

Liu, L., Meng, Y., Dai, X., Chen, K., & Zhu, Y. (2019). 3D Printing Complex Egg White Protein Objects: Properties and Optimization. *Food and Bioprocess Technology, 12*(2), 267-279.

Liu, Y., Liu, D., Wei, G., Ma, Y., Bhandari, B., & Zhou, P. (2018). 3D printed milk protein food simulant: Improving the printing performance of milk protein concentration by incorporating whey protein isolate. *Innovative Food Science & Emerging Technologies, 49*, 116-126.

Liu, Y., Zhang, W., Wang, K., Bao, Y., Regenstein, J. M., & Zhou, P. (2019). Fabrication of Gel-Like Emulsions with Whey Protein Isolate Using Microfluidization: Rheological Properties and 3D Printing Performance. *Food and Bioprocess Technology, 12*(12), 1967-1979.

Liu, Z., Bhandari, B., Prakash, S., & Zhang, M. (2018). Creation of internal structure of mashed potato construct by 3D printing and its textural properties. *Food Research International, 111*, 534-543.

Liu, Z., Chen, H., Zheng, B., Xie, F., & Chen, L. (2020). Understanding the structure and rheological properties of potato starch induced by hot-extrusion 3D printing. *Food Hydrocolloids, 105*, 105812.

Lorenzo, G., Zaritzky, N., & Califano, A. (2013). Rheological analysis of emulsion-filled gels based on high acyl gellan gum. *Food Hydrocolloids, 30*(2), 672-680.

Lupton, D. (2017). 'Download to delicious': Promissory themes and sociotechnical imaginaries in coverage of 3D printed food in online news sources. *Futures, 93*, 44-53.

Lupton, D., & Turner, B. (2018). “I can’t get past the fact that it is printed”: consumer attitudes to 3D printed food. *Food, Culture & Society, 21*(3), 402-418.

Ma, L., Wan, Z., & Yang, X. (2017). Multiple water-in-oil-in-water emulsion gels based on self-assembled saponin fibrillar network for photosensitive cargo protection. *Journal of Agricultural and Food Chemistry, 65*(44), 9735-9743.

MacNaughtan, B., & Farhat, I. A. (2008). Thermal methods in the study of foods and foods ingredients. *Principles and applications of thermal analysis*, 330-402.

Malik, H. H., Darwood, A. R., Shaunak, S., Kulatilake, P., Abdulrahman, A., Mulki, O., & Baskaradas, A. (2015). Three-dimensional printing in surgery: a review of current surgical applications. *journal of surgical research, 199*(2), 512-522.

Malone, M. E., & Appelqvist, I. A. M. (2003). Gelled emulsion particles for the controlled release of lipophilic volatiles during eating. *Journal of Controlled Release, 90*(2), 227-241.

Mantelet, M., Panouillé, M., Boué, F., Bosc, V., Restagno, F., Souchon, I., & Mathieu, V. (2019). Impact of sol-gel transition on the ultrasonic properties of complex model foods: Application to agar/gelatin gels and emulsion filled gels. *Food Hydrocolloids, 87*, 506-518.

Mantihal, S., Prakash, S., & Bhandari, B. (2019a). Textural modification of 3D printed dark chocolate by varying internal infill structure. *Food Research International, 121*, 648-657.

Mantihal, S., Prakash, S., & Bhandari, B. (2019b). Texture-modified 3D printed dark chocolate: Sensory evaluation and consumer perception study. *Journal of Texture Studies, 50*(5), 386-399.

Mantihal, S., Prakash, S., Godoi, F. C., & Bhandari, B. (2017). Optimization of chocolate 3D printing by correlating thermal and flow properties with 3D structure modeling. *Innovative Food Science & Emerging Technologies, 44*, 21-29.

Marcotte, M., Hoshahili, A. R. T., & Ramaswamy, H. (2001). Rheological properties of selected hydrocolloids as a function of concentration and temperature. *Food Research International, 34*(8), 695-703.

Martinsen, A., Skjåk-Bræk, G., & Smidsrød, O. (1989). Alginate as immobilization material: I. Correlation between chemical and physical properties of alginate gel beads. *Biotechnology and bioengineering, 33*(1), 79-89.

McClements, D. J. (2004). *Food emulsions: principles, practices, and techniques*: CRC press.

McClements, D. J. (2007). Critical Review of Techniques and Methodologies for Characterization of Emulsion Stability. *Critical Reviews in Food Science and Nutrition, 47*(7), 611-649.

McClements, D. J., & Jafari, S. M. (2018). Improving emulsion formation, stability and performance using mixed emulsifiers: A review. *Advances in colloid and interface science, 251*, 55-79.

Mcclements, D. J., Monahan, F. J., & Kinsella, J. E. (1993). Effect Of Emulsion Droplets On The Rheology Of Whey Protein Isolate Gels. *Journal of Texture Studies, 24*(4), 411-422.

Mhando, J. R., & Wan Po, A. L. (1990). Two-stage release of benzocaine from sunflower oil/gelatin emulsion films. *International Journal of Pharmaceutics, 59*(2), 165-170.

Milani, J., & Maleki, G. (2012). Hydrocolloids in food industry. *Food industrial processes–Methods and equipment, 2*, 2-37.

Miyoshi, E., Takaya, T., & Nishinari, K. (1995). Effects of salts on the gel-sol transition of gellan gum by differential scanning calorimetry and thermal scanning rheology. *Thermochimica Acta, 267*, 269-287.

Moritaka, H., & Naito, S. (2002). Agar and gelatin gel flavor release. *Journal of Texture Studies, 33*(3), 201-214.

Nawab, Y., Shahid, S., Boyard, N., & Jacquemin, F. (2013). Chemical shrinkage characterization techniques for thermoset resins and associated composites. Journal of Materials Science, 48, 5387–5409

Ngo, T. D., Kashani, A., Imbalzano, G., Nguyen, K. T. Q., & Hui, D. (2018). Additive manufacturing (3D printing): A review of materials, methods, applications and challenges. *Composites Part B: Engineering, 143*, 172-196.

Nishinari, K. (1997). Rheological and DSC study of sol-gel transition in aqueous dispersions of industrially important polymers and colloids. *Colloid and Polymer Science, 275*(12), 1093-1107.

Norton, I. T., Morris, E. R., & Rees, D. A. (1984). Lyotropic effects of simple anions on the conformation and interactions of kappa-carrageenan. *Carbohydrate research, 134*(1), 89-101.

Nour, A. H. (2018). Emulsion types, stability mechanisms and rheology: A review. *International Journal of Innovative Research and Scientific Studies (IJIRSS), 1*(1).

Nur Hanani, Z. A., & Aelma Husna, A. B. (2018). Effect of different types and concentrations of emulsifier on the characteristics of kappa-carrageenan films. *International Journal of Biological Macromolecules, 114*, 710-716.

Pal, R. (2002). Complex shear modulus of concentrated suspensions of solid spherical particles. *Journal of Colloid and Interface Science, 245*(1), 171-177.

Pallottino, F., Hakola, L., Costa, C., Antonucci, F., Figorilli, S., Seisto, A., & Menesatti, P. (2016). Printing on food or food printing: a review. *Food and Bioprocess Technology, 9*(5), 725-733.

Panesar, S. S., Magnetta, M., Mukherjee, D., Abhinav, K., Branstetter, B. F., Gardner, P. A., Iv, M., & Fernandez-Miranda, J. C. (2019). Patient-specific 3-dimensionally printed models for neurosurgical planning and education. *Neurosurgical Focus FOC, 47*(6), E12.

Papageorgiou, M., & Kasapis, S. (1995). The effect of added sucrose and corn syrup on the physical properties of gellan—gelatin mixed gels. *Food Hydrocolloids, 9*(3), 211-220.

Paquin, P. (2009). *Functional and speciality beverage technology*: Elsevier.

Pérez, B., Nykvist, H., Brøgger, A. F., Larsen, M. B., & Falkeborg, M. F. (2019). Impact of macronutrients printability and 3D-printer parameters on 3D-food printing: A review. *Food Chemistry, 287*, 249-257.

Phillips, G. O., & Williams, P. A. (2009). *Handbook of hydrocolloids*: Elsevier.

Picker, K. M. (1999). Matrix tablets of carrageenans. II. Release behavior and effect of added cations. *Drug development and industrial pharmacy, 25*(3), 339-346.

Poologasundarampillai, G., & Nommeots-Nomm, A. (2017). Materials for 3D printing in medicine: Metals, polymers, ceramics, hydrogels. In *3D Printing in Medicine* (pp. 43-71): Elsevier.

Portanguen, S., Tournayre, P., Sicard, J., Astruc, T., & Mirade, P.-S. (2019). Toward the design of functional foods and biobased products by 3D printing: A review. *Trends in Food Science & Technology, 86*, 188-198.

Praiboon, J., Chirapart, A., Akakabe, Y., Bhumibhamon, O., & Kajiwara, T. (2006). Physical and Chemical Characterization of Agar Polysaccharides Extracted from the Thai and Japanese Species of Gracilaria. *ScienceAsia, 32(s1)*.

Prasad, L. K., & Smyth, H. (2016). 3D Printing technologies for drug delivery: a review. *Drug development and industrial pharmacy, 42*(7), 1019-1031.

Rahman, M. S., Al-Saidi, G., Guizani, N., & Abdullah, A. (2010). Development of state diagram of bovine gelatin by measuring thermal characteristics using differential scanning calorimetry (DSC) and cooling curve method. *Thermochimica Acta, 509*(1-2), 111-119.

Rahman, Z., Barakh Ali, S. F., Ozkan, T., Charoo, N. A., Reddy, I. K., & Khan, M. A. (2018). Additive Manufacturing with 3D Printing: Progress from Bench to Bedside. *The AAPS Journal, 20*(6), 101.

Rayna, T., & Striukova, L. (2016). From rapid prototyping to home fabrication: How 3D printing is changing business model innovation. *Technological Forecasting and Social Change, 102*, 214-224.

Ribeiro, A., Blokzijl, M. M., Levato, R., Visser, C. W., Castilho, M., Hennink, W. E., Vermonden, T., & Malda, J. (2017). Assessing bioink shape fidelity to aid material development in 3D bioprinting. *Biofabrication, 10*(1), 014102.

Robertson, A. D., & Murphy, K. P. (1997). Protein structure and the energetics of protein stability. *Chemical reviews, 97*(5), 1251-1268.

Robinson, G., Morris, E. R., & Rees, D. A. (1980). Role of double helices in carrageenan gelation: the domain model. *Journal of the Chemical Society, Chemical Communications*(4), 152-153.

Rodrıguez-Hernández, A., Durand, S., Garnier, C., Tecante, A., & Doublier, J. L. (2003). Rheology-structure properties of gellan systems: evidence of network formation at low gellan concentrations. *Food Hydrocolloids, 17*(5), 621-628.

Ross-Murphy, S. B. (1992). Structure and rheology of gelatin gels: recent progress. *Polymer, 33*(12), 2622-2627.

Roy, S., & Rhim, J.-W. (2021). Carrageenan/agar-based functional film integrated with zinc sulfide nanoparticles and Pickering emulsion of tea tree essential oil for active packaging applications. *International Journal of Biological Macromolecules, 193*, 2038-2046.

Sager, V. F., Munk, M. B., Hansen, M. S., Bredie, W. L. P., & Ahrné, L. (2021). Formulation of Heat-Induced Whey Protein Gels for Extrusion-Based 3D Printing. *Foods, 10*(1).

Saha, D., & Bhattacharya, S. (2010). Hydrocolloids as thickening and gelling agents in food: a critical review. *J Food Sci Technol, 47*(6), 587-597.

Sala, G., de Wijk, R. A., van de Velde, F., & van Aken, G. A. (2008). Matrix properties affect the sensory perception of emulsion-filled gels. *Food Hydrocolloids, 22*(3), 353-363.

Sala, G., Van Aken, G. A., Stuart, M. A. C., & Van De Velde, F. (2007). Effect of droplet–matrix interactions on large deformation properties of emulsion-filled gels. *Journal of Texture Studies, 38*(4), 511-535.

Sala, G., van Vliet, T., Cohen Stuart, M. A., Aken, G. A. v., & van de Velde, F. (2009). Deformation and fracture of emulsion-filled gels: Effect of oil content and deformation speed. *Food Hydrocolloids, 23*(5), 1381-1393.

Salentijn, G. I. J., Oomen, P. E., Grajewski, M., & Verpoorte, E. (2017). Fused Deposition Modeling 3D Printing for (Bio)analytical Device Fabrication: Procedures, Materials, and Applications. *Analytical Chemistry, 89*(13), 7053-7061.

Saptarshi, S. M., & Zhou, C. (2019). Basics of 3D printing: Engineering aspects. In *3D Printing in Orthopaedic Surgery* (pp. 17-30): Elsevier.

Satapathy, S., Singh, V. K., Sagiri, S. S., Agarwal, T., Banerjee, I., Bhattacharya, M. K., Kumar, N., & Pal, K. (2015). Development and characterization of gelatin-based hydrogels, emulsion hydrogels, and bigels: A comparative study. *Journal of Applied Polymer Science, 132*(8).

Sato, A. C. K., Moraes, K. E. F. P., & Cunha, R. L. (2014). Development of gelled emulsions with improved oxidative and pH stability. *Food Hydrocolloids, 34*, 184-192.

Sawyer, W. (1969). Complex between β-lactoglobulin and κ-casein. A review. *Journal of Dairy Science, 52*(9), 1347-1355.

Schneider, T., Eli, K., Dolan, C., & Ulijaszek, S. (2018). *Digital food activism*: Routledge London.

Schramm, G. (1994). *A practical approach to rheology and rheometry*: Haake Karlsruhe.

Schultz, S., Wagner, G., Urban, K., & Ulrich, J. (2004). High-pressure homogenization as a process for emulsion formation. *Chemical Engineering & Technology: Industrial Chemistry‐Plant Equipment‐Process Engineering‐Biotechnology, 27*(4), 361-368.

Severini, C., Azzollini, D., Albenzio, M., & Derossi, A. (2018). On printability, quality and nutritional properties of 3D printed cereal based snacks enriched with edible insects. *Food Research International, 106*, 666-676.

Severini, C., Derossi, A., & Azzollini, D. (2016). Variables affecting the printability of foods: Preliminary tests on cereal-based products. *Innovative Food Science & Emerging Technologies, 38*, 281-291.

Severini, C., Derossi, A., Ricci, I., Caporizzi, R., & Fiore, A. (2018). Printing a blend of fruit and vegetables. New advances on critical variables and shelf life of 3D edible objects. *Journal of Food Engineering, 220*, 89-100.

Shimoni, G., Levi, C. S., Tal, S. L., & Lesmes, U. (2013). Emulsions stabilization by lactoferrin nano-particles under in vitro digestion conditions. *Food Hydrocolloids, 33*(2), 264-272.

Singh, S. S., Aswal, V., & Bohidar, H. (2007). Structural studies of agar–gelatin complex coacervates by small angle neutron scattering, rheology and differential scanning calorimetry. *International Journal of Biological Macromolecules, 41*(3), 301-307.

Smits, P., & Van Brouwershaven, J. H. (1980). Heat-induced association of β-lactoglobulin and casein micelles. *Journal of Dairy Research, 47*(3), 313-325.

Soares, S., & Forkes, A. (2014). Insects Au gratin-an investigation into the experiences of developing a 3D printer that uses insect protein based flour as a building medium for the production of sustainable food. In *DS 78: Proceedings of the 16th International conference on Engineering and Product Design Education (E&PDE14), Design Education and Human Technology Relations, University of Twente, The Netherlands, 04-05.09. 2014* (pp. 426-431).

Soukoulis, C., Tsevdou, M., Andre, C. M., Cambier, S., Yonekura, L., Taoukis, P. S., & Hoffmann, L. (2017). Modulation of chemical stability and in vitro bioaccessibility of beta-carotene loaded in kappa-carrageenan oil-in-gel emulsions. *Food Chemistry, 220*, 208-218.

Southerland, D., Walters, P., & Huson, D. (2011). Edible 3D printing. In *NIP & Digital Fabrication Conference* (Vol. 2011, pp. 819-822): Society for Imaging Science and Technology.

Spagnuolo, P. A., Dalgleish, D. G., Goff, H. D., & Morris, E. R. (2005). Kappa-carrageenan interactions in systems containing casein micelles and polysaccharide stabilizers. *Food Hydrocolloids, 19*(3), 371-377.

Stang, M., Schuchmann, H., & Schubert, H. (2001). Emulsification in high-pressure homogenizers. *Engineering in Life Sciences, 1*(4), 151-157.

Takagishi, K., Suzuki, Y., & Umezu, S. (2018). The high precision drawing method of chocolate utilizing electrostatic ink-jet printer. *Journal of Food Engineering, 216*, 138-143.

Tan, K.-X., Ng, L.-L. E., & Loo, S. C. J. (2021). Formulation Development of a Food-Graded Curcumin-Loaded Medium Chain Triglycerides-Encapsulated Kappa Carrageenan (CUR-MCT-KC) Gel Bead Based Oral Delivery Formulation. *Materials, 14*(11), 2783.

Tanner, J. A., Jethwa, B., Jackson, J., Bartanuszova, M., King, T. S., Bhattacharya, A., & Sharma, R. (2020). A Three-Dimensional Print Model of the Pterygopalatine Fossa Significantly Enhances the Learning Experience. *Anatomical Sciences Education, 13*(5), 568-580.

Tesch, S., & Schubert, H. (2002). Influence of increasing viscosity of the aqueous phase on the short-term stability of protein stabilized emulsions. *Journal of Food Engineering, 52*(3), 305-312.

Thakur, G., Naqvi, M. A., Rousseau, D., Pal, K., Mitra, A., & Basak, A. (2012). Gelatin-Based Emulsion Gels for Diffusion-Controlled Release Applications. *Journal of Biomaterials Science, Polymer Edition, 23*(5), 645-661.

Toh, W. Y., Li, L., Chua, C. K., & Wong, G. (2018). Comparison of existing 3D food printers. In *Proceedings of the 3rd International Conference on Progress in Additive Manufacturing (Pro-AM 2018), Singapore* (pp. 14-17).

Tran, J. L. (2016). 3D-printed food. *Minn. JL Sci. & Tech., 17*, 855.

Tran, J. L. (2019). Safety and Labelling of 3D Printed Food. In *Fundamentals of 3D Food Printing and Applications* (pp. 355-371).

Trius, A., Sebranek, J., & Lanier, T. (1996). Carrageenans and their use in meat products. *Critical Reviews in Food Science & Nutrition, 36*(1-2), 69-85.

Utela, B., Storti, D., Anderson, R., & Ganter, M. (2008). A review of process development steps for new material systems in three dimensional printing (3DP). *Journal of Manufacturing Processes, 10*(2), 96-104.

Vaezi, M., Chianrabutra, S., Mellor, B., & Yang, S. (2013). Multiple material additive manufacturing – Part 1: a review. *Virtual and Physical Prototyping, 8*(1), 19-50.

Van der Poel, C. (1958). On the rheology of concentrated dispersions. *Rheologica Acta, 1*(2), 198-205.

van Rompay, T. J. L., Finger, F., Saakes, D., & Fenko, A. (2017). "See me, feel me": Effects of 3D-printed surface patterns on beverage evaluation. *Food Quality and Preference, 62*, 332-339.

Van Rompay, T. J. L., Kramer, L.-M., & Saakes, D. (2018). The sweetest punch: Effects of 3D-printed surface textures and graphic design on ice-cream evaluation. *Food Quality and Preference, 68*, 198-204.

Vancauwenberghe, V., Katalagarianakis, L., Wang, Z., Meerts, M., Hertog, M., Verboven, P., Moldenaers, P., Hendrickx, M. E., Lammertyn, J., & Nicolaï, B. (2017). Pectin based food-ink formulations for 3-D printing of customizable porous food simulants. *Innovative Food Science & Emerging Technologies, 42*, 138-150.

Vancauwenberghe, V., Verboven, P., Lammertyn, J., & Nicolaï, B. (2018). Development of a coaxial extrusion deposition for 3D printing of customizable pectin-based food simulant. *Journal of Food Engineering, 225*, 42-52.

Velázquez, J. S., Cavas, F., Bolarín, J. M., & Alió, J. L. (2020). 3D printed personalized corneal models as a tool for improving patient's knowledge of an asymmetric disease. *Symmetry, 12*(1), 151.

Voon, S. L., An, J., Wong, G., Zhang, Y., & Chua, C. K. (2019). 3D food printing: a categorised review of inks and their development. *Virtual and Physical Prototyping, 14*(3), 203-218.

Wan, Y., Wang, R., Feng, W., Chen, Z., & Wang, T. (2021). High internal phase Pickering emulsions stabilized by co-assembled rice proteins and carboxymethyl cellulose for food-grade 3D printing. *Carbohydrate Polymers, 273*, 118586.

Wang, H., Wang, L., Ye, S., & Song, X. (2019). Construction of Bi2WO6–TiO2/starch nanocomposite films for visible-light catalytic degradation of ethylene. *Food Hydrocolloids, 88*, 92-100.

Wang, L., Cao, Y., Zhang, K., Fang, Y., Nishinari, K., & Phillips, G. O. (2015). Hydrogen bonding enhances the electrostatic complex coacervation between κ-carrageenan and

gelatin. *Colloids and Surfaces A: Physicochemical and Engineering Aspects, 482*, 604-610.

Wang, Z., Neves, M. A., Kobayashi, I., Uemura, K., & Nakajima, M. (2013). Preparation, Characterization, and in Vitro Gastrointestinal Digestibility of Oil-in-Water Emulsion–Agar Gels. *Bioscience, biotechnology, and biochemistry*, 120659.

Wanzke, C., Tena-Solsona, M., Rieß, B., Tebcharani, L., & Boekhoven, J. (2020). Active droplets in a hydrogel release drugs with a constant and tunable rate. *Materials Horizons, 7*(5), 1397-1403.

Warner, E. L., Norton, I. T., & Mills, T. B. (2019). Comparing the viscoelastic properties of gelatin and different concentrations of kappa-carrageenan mixtures for additive manufacturing applications. *Journal of Food Engineering, 246*, 58-66.

Watase, M., Nishinari, K., Clark, A., & Ross-Murphy, S. (1989). Differential scanning calorimetry, rheology, X-ray, and NMR of very concentrated agarose gels. *Macromolecules, 22*(3), 1196-1201.

Wegrzyn, T. F., Golding, M., & Archer, R. H. (2012). Food Layered Manufacture: A new process for constructing solid foods. *Trends in Food Science & Technology, 27*(2), 66-72.

Weiner, M. L. (1991). Toxicological properties of carrageenan. *Agents and actions, 32*(1), 46-51.

Wilde, P., Mackie, A., Husband, F., Gunning, P., & Morris, V. (2004). Proteins and emulsifiers at liquid interfaces. *Advances in colloid and interface science, 108-109*, 63-71.

Williams, D., Thayer, P., Martinez, H., Gatenholm, E., & Khademhosseini, A. (2018). A perspective on the physical, mechanical and biological specifications of bioinks and the development of functional tissues in 3D bioprinting. *Bioprinting, 9*, 19-36.

Williams, P. A., & Phillips, G. O. (2021). Introduction to food hydrocolloids. In *Handbook of hydrocolloids* (pp. 3-26): Elsevier.

Woehl, M. A., Ono, L., Vidotti, I. C. R., Wypych, F., Schreiner, W. H., & Sierakowski, M. R. (2014). Bioactive nanocomposites of bacterial cellulose and natural hydrocolloids. *Journal of Materials Chemistry B, 2*(40), 7034-7044.

Wu, N.-n., Yang, X.-q., Teng, Z., Yin, S.-w., Zhu, J.-h., & Qi, J.-r. (2011). Stabilization of soybean oil body emulsions using κ, ι, λ-carrageenan at different pH values. *Food Research International, 44*(4), 1059-1068.

Wu, P., Wang, J., & Wang, X. (2016). A critical review of the use of 3-D printing in the construction industry. *Automation in Construction, 68*, 21-31.

Xu, L., Gu, L., Su, Y., Chang, C., Wang, J., Dong, S., Liu, Y., Yang, Y., & Li, J. (2020). Impact of thermal treatment on the rheological, microstructural, protein structures and extrusion 3D printing characteristics of egg yolk. *Food Hydrocolloids, 100*, 105399.

Yamano, Y., Kagawa, Y., Kim, K.-H., & Gohtani, S. (1996). Stability and uniformity of oil droplets in preparation of O/W emulsion agar gel. *Food Science and Technology International, Tokyo, 2*(1), 16-18.

Yang, D., Gao, S., & Yang, H. (2020). Effects of sucrose addition on the rheology and structure of iota-carrageenan. *Food Hydrocolloids, 99*, 105317.

Yang, F., Zhang, M., Bhandari, B., & Liu, Y. (2018). Investigation on lemon juice gel as food material for 3D printing and optimization of printing parameters. *Lwt, 87*, 67-76.

Yang, F., Zhang, M., Prakash, S., & Liu, Y. (2018). Physical properties of 3D printed baking dough as affected by different compositions. *Innovative Food Science & Emerging Technologies, 49*, 202-210.

Yang, N., Feng, Y., Su, C., Wang, Q., Zhang, Y., Wei, Y., Zhao, M., Nishinari, K., & Fang, Y. (2020). Structure and tribology of κ-carrageenan gels filled with natural oil bodies. *Food Hydrocolloids, 107*, 105945.

Yano, Y. S. a. T. (1986). Viscoelastic behavior of an agar - gelatin mixture gel as a function of its composition.

Yap, Y. L., & Yeong, W. Y. (2014). Additive manufacture of fashion and jewellery products: a mini review. *Virtual and Physical Prototyping, 9*(3), 195-201.

Zhang, L., Lou, Y., & Schutyser, M. A. I. (2018). 3D printing of cereal-based food structures containing probiotics. *Food Structure, 18*, 14-22.

Zhang, Y.-Q., Tsai, Y.-C., Monie, A., Hung, C.-F., & Wu, T.-C. (2010). Carrageenan as an adjuvant to enhance peptide-based vaccine potency. *Vaccine, 28*(32), 5212-5219.

Zheng, H., Mao, L., Cui, M., Liu, J., & Gao, Y. (2020). Development of food-grade bigels based on κ-carrageenan hydrogel and monoglyceride oleogels as carriers for β-carotene: Roles of oleogel fraction. *Food Hydrocolloids, 105*, 105855.

Zhuang, Y.-d., Zhou, M.-c., Liu, S.-c., Wu, J.-f., Wang, R., & Chen, C.-m. (2019). Effectiveness of personalized 3D printed models for patient education in degenerative lumbar disease. *Patient Education and Counseling, 102*(10), 1875-1881.

Chapter 3

3D printing of edible hydrogels containing thiamine and their comparison to cast gels

This chapter was published as

Kamlow, M.-A., Vadodaria, S., Gholamipour-Shirazi, A., Spyropoulos, F., & Mills, T. (2021). 3D printing of edible hydrogels containing thiamine and their comparison to cast gels. Food Hydrocolloids, 116, 106550.

Michael-Alex Kamlow: Conceptualization, Methodology, Formal analysis, Investigation, Writing - original draft. Saumil Vadodaria: Methodology, Software. Azarmidokht Gholamipour-Shirazi: Methodology, Software. Fotis Spyropoulos: Writing - review & editing, Supervision. Tom Mills: Writing - review & editing, Supervision, Funding acquisition.

Abstract

In this study, 3% w/v kappa-carrageenan (κC) and 2% w/v agar were assessed for their suitability for hot extrusion 3D printing (3DP) and compared to cast gels of equivalent composition. Moreover, incorporation of a model active (thiamine) at varying concentrations, was studied for both 3DP and cast microstructures. Rheology and differential scanning calorimetry showed that thiamine (via electrostatic complexation) reinforced the kappa-carrageenan gel network (up to a certain threshold concentration), whereas the agar gel was structurally unaltered by the active's presence. While the κC-thiamine formulations were printable (within a relatively narrow formulation/processing window), the agar-thiamine systems were not printable via the current set up. Texture profile analysis (TPA) showed that 3DP κC-thiamine cylinders had a hardness value of 860 g ± 11% compared to 1650 g ± 6% for cast cylinders. When compressed they delaminated due to failure between consecutive layers of material deposited during the printing process; light microscopy revealed distinct layering across the printed gel structure. Release tests at 20°C showed printed gels expelled 64% ± 2.2% of the total active compared to 59% ± 0.8% from the cast gels over six hours. At 37°C these values increased to 78% ± 2.6% and 66% ± 3.5% respectively. This difference was believed to be due to the significant swelling exhibited by the printed systems. A simple empirical model, applied to the release data, revealed that thiamine discharge from 3DP gels was solely driven by diffusion while ejection of the active from cast systems had both diffusional and relaxation contributions.

3.1 Introduction

Additive manufacturing, also known as 3D-printing (3DP), is a layer-by-layer production method that uses digital files to create parts and products. While many different areas of industry have adopted it, its uptake as a means of manufacture at the point of production has still not caught up in areas like homes, health care facilities and pharmacies. However, despite this it is still a growth industry worth billions of dollars per year (McCue, 2012). Most research and utilisation has been focused on plastic polymers (Rahim, Abdullah, & Md Akil, 2019), metal (Buchanan & Gardner, 2019), and ceramics (Chen, et al., 2019) with the emphasis being on the small scale production of highly customised items. Other areas of interest have included pharmaceuticals (Goyanes, et al., 2017), biotechnology (Singh, Singh, & Han, 2016) and prosthesis development (Koprnický, Najman, & Šafka, 2017). The plug and play nature of 3D printing is appealing because laymen are able to connect a printer, load in the printing material and then download one of many designs from the internet, modify it if they choose to and then print it. This allows customisation at the point of demand and modification without the need for additional tooling or moulding.

From the start of the last decade, food 3DP has started to rapidly develop as an area of research. This is due to various factors such as design of complex geometries without moulds, production of softer foods that mimic the appearance of normal foods for people with conditions such as dysphagia, while reducing production time and skill level of the person producing it as well as increasing repeatability (Kouzani, et al., 2017), and using 3D printing to precisely control ingredient placement and distribution (Diaz, Van Bommel, Noort, Henket, & Briër, 2018). However, development and subsequent uptake of food 3DP in homes and by industry has been inhibited by various issues. The major problem is that 3D printing is still too slow, with larger objects taking upwards of an hour to produce (Lin, 2015). Moreover, food systems are multifaceted, often consisting of several materials in varying ratios, sensory characteristics related to internal microstructure and thermal transition temperature as well as most food materials not being readily extrudable. This is why a lot of research into food 3DP

has focused on natively extrudable food such as chocolate (Lanaro, Desselle, & Woodruff, 2019), cheese (Le Tohic, et al., 2018) and dough (Fan Yang, Zhang, Prakash, & Liu, 2018). Some non-natively extrudable food materials tested for 3D printing include fish surimi gel (Wang, Zhang, Bhandari, & Yang, 2018) and fruit (Severini, Derossi, Ricci, Caporizzi, & Fiore, 2018). However, most research has been directed into finding a wider range of materials that can be utilised in food 3DP as well as trying to establish an understanding of how their various properties affect their printability.

Hydrocolloid gels (hereafter referred to as hydrogels) are an area of interest in food 3DP with a large body of work directed into investigations regarding their suitability and utility in this field (Kim, et al., 2018; Liu, Zhang, & Yang, 2018; Rutz, Hyland, Jakus, Burghardt, & Shah, 2015). They are considered ideal owing to the fact that many of them are renewable; coming from plant or bacterial sources, widely used already in foods and pharmaceuticals and are known to be biocompatible. Hydrogel printing normally involves the cold extrusion of systems that have already set, requiring little, if any, temperature control. Cold extrusion approaches to date have included mixed hydrogels (Kim, Bae, & Park, 2017), single hydrogels (Gholamipour-Shirazi, Norton, & Mills, 2019) and the use of hydrogels as an adjunctive material (Kim, et al., 2019). The second method is the hot extrusion of hydrogels in the sol state, with the sol-gel transition occurring on the printing bed rapidly after being deposited. This has the advantage of being able to print highly viscous gels far more readily, as they would still be in the sol state unlike the gelled samples; this has been highlighted for cold extrusion (Azam, Zhang, Bhandari, & Yang, 2018) which essentially is printing yield stress materials. There exist fewer examples of hot extrusion hydrogel printing such as kappa-carrageenan (κC) with gelatin (Warner, Norton, & Mills, 2019), κC by itself (Diañez, et al., 2019) and agar with gelatin (Serizawa, et al., 2014). Another type of 3DP is freeform reversible embedding of suspended hydrogels (FRESH) which involves directly printing the hydrogel into a support bath of a second hydrogel (Hinton, et al., 2015). This allows for a range of intricate structures to be produced that more accurately mimic a cast gel. This process can also be modified to include different support bath materials such as gellan fluid gels (Compaan, Song, & Huang, 2019).

This process so often focused on alginate gels loaded with cells being printed, but there is no reason why cold-set hydrogels could not be printed in this manner, with gelatin having been utilised as a support material (Jin, Compaan, Bhattacharjee, & Huang, 2016). However, this process requires the presence of the fluid gel bath, with fluid gels normally requiring equipment capable of delivering shear while controlling temperature such as a rheometer or a pin stirrer vessel (Garrec & Norton, 2012). This makes it more impractical if 3D printers were to become ubiquitous within homes and healthcare settings. Furthermore, having laymen handle more complicated tasks such as removing the remaining support fluid gel could also be a barrier to uptake of this method. Whereas hot extrusion 3DP will produce finalised products that are immediately ready for use and will not require a constant supply of fluid gel.

Owing to the fact that hot extrusion hydrogel printing requires rapid thermal gelation and a high storage modulus (Diañez, et al., 2019). κC and agar are considered suitable for hot hydrogel 3DP and have been the focus of most studies in this field. κC is a sulphated polysaccharide that is extracted from red seaweed. When added to water it has the ability to form thermo-reversible gels in the presence of complementary gelling cations (Hermansson, Eriksson, & Jordansson, 1991). Its gelation is believed to occur through the ordering of randomised coils into double helices and then the aggregation of these helices into a polymeric network (Norton, Morris, & Rees, 1984). Agar is a polysaccharide that is extracted from agarophyte seaweeds. Although like κC it is as able to form thermo-reversible hydrogels, agar does not require any crosslinkers, it forms physical gels simply through hydrogen bridges; and as such it is uncharged. Agar contains two fractions, agarose and agaropectin with only agarose responsible for gelation (Armisen & Gaiatas, 2009). Both of these polysaccharides have many uses in foods as rheology modifiers and gelling agents (Saha & Bhattacharya, 2010). Vitamin B1 also known as thiamine is a water soluble essential vitamin. It is on the WHO list of essential medications and deficiencies can lead to Wernicke-Korsakoff syndrome and may arise from alcoholism or malabsorption (Kril, 1996).

While agar and κC are widespread within the food sector, they are also used as drug delivery systems as well, in part due to the biocompatibility of these hydrogels (Nayak & Gupta, 2015; Weiner, 1991). Research has gone into modified release oral dosing (Ito & Sugihara, 1996; Picker, 1999), parenteral preparations (Santoro, et al., 2011; Zhang, Tsai, Monie, Hung, & Wu, 2010) and patches applied directly to the skin (Dalafu, Chua, & Chakraborty, 2010). One of the major issues with the centralised, large scale production of medications is that doses are decided on how many people from clinical trials saw the most benefit at that dose. This can lead to people receiving too much or too little of a medicine despite being given a clinically appropriate dose (Cohen, 1999). Hence 3DP of hydrogels is considered suitable to produce customisable delivery vehicles for medicines tailored to the individual patient at the point of delivery (Fina, et al., 2018; Long, et al., 2019). However, 3DP of hydrogels is suited best for smaller batches that require high levels of customisation, whether this is for printing medicines or implant devices (Ventola, 2014). Furthermore, there is still an issue with a limited range of materials currently available (Ngo, Kashani, Imbalzano, Nguyen, & Hui, 2018). While studies such as this one aim to address this issue, there is still some way to go. Finally, there will have to be widespread training in order to familiarise medical professionals at the point of production or delivery in the use of 3D printers (Choonara, du Toit, Kumar, Kondiah, & Pillay, 2016; Ventola, 2014).

This study aimed to evaluate the suitability of hydrogels for hot extrusion 3DP and compare and contrast the physical properties of printed gels to cast gels, before assessing them both as release vehicles. Because there exists little literature on the interactions of thiamine with agar and κC, and none looking into how thiamine might affect the microstructure of the hydrogels, the first step was to characterise the thermal characteristics of the κC-thiamine and agar-thiamine hydrogels. Rheology and differential scanning calorimetry were used to determine which formulations were suitable candidates for hot extrusion 3DP. κC and agar were chosen for printing because of their desirable gelling characteristics. Thiamine was chosen as a model molecule because it has been used in release studies before (Kevadiya, et al., 2010). After suitable thiamine containing hydrogel systems were established then 3D

printing under several parameters took place. The printed gels' physical properties were ascertained through texture profile analysis and light microscopy and then compared to cast gels. This highlighted the variances in the structures fabricated between the two production methods. Finally, the printed and cast gels underwent release tests to assess their performances as release vehicles in water. This allowed this study to examine physical differences between printed and cast hydrogels and compare the performance of 3DP hydrogels to cast gels as drug delivery vehicles.

3.2 Materials and methods

3.2.1 Materials

κC, agar and sodium chloride were purchased from Sigma-Aldrich (UK). Thiamine hydrochloride 99% (hereafter referred to as thiamine) was purchased from Alfa Aesar (UK). Sodium hydroxide 1M was purchased from Honeywell and was used for pH adjustment. Milli-Q water was used (Elix® 5 distillation apparatus, Millipore®, USA) for sample preparation. All materials were used without further purifications or modifications.

3.2.2 Hydrogel Preparation

Samples of κC hydrogels were prepared by dispersing 3% w/v of κC into deionised water. First, a hotplate was set to 80 ˚C and then the water was placed on top of it in a 250 mL beaker. A magnetic stirrer was used in order to facilitate dispersion and hydration of the κC into the water. After adding the κC powder into the water, it was left to stir for sixty minutes. Agar hydrogels were produced by placing 2% w/v agar into deionised water. This was then covered and placed in an 800 W microwave and heated for ninety seconds until the agar melted into the water. After sixty seconds the microwave was stopped and the beaker was shaken gently. After this the solution was stored on a hotplate set to 70 ˚C and stirred by a magnetic stirrer.

3.2.3 Thiamine hydrogel preparation

For agar samples containing thiamine, the same methodology used in section 3.2.2 was followed. However, thiamine at the required concentration (0.1%, 1%, 2% and 5% w/v) was added and then the pH was balanced back up to 5.5 using sodium hydroxide 1M and the solution was then held at 70 ˚C until it was ready to be used. This pH was chosen as agar did not undergo acid hydrolysis at this pH (Phillips & Williams, 2000) and the thiamine was still stable at this pH and temperature (Arnold & Dwivedi, 1971). For κC samples containing thiamine, first the thiamine was added to water and then the pH was adjusted to pH 5.5 once more to protect both the thiamine and the κC from degradation. Owing to the fact that sodium ions affect gel strength of κC hydrogels (Hermansson, et al., 1991) the exact amount of sodium hydroxide added for each concentration of thiamine was calculated from the amount of 1M sodium hydroxide added. The amount of sodium ions added to the highest concentration of thiamine was calculated to be 546 mg. Therefore, the 0%, 0.1%, 1% and 2% κC-thiamine gels had sodium chloride added to them to ensure they all contained 546 mg of sodium ions. This ensured any changes to the gel strength alone came from the thiamine and not the sodium ions.

3.2.4 Rheology

Rheological analysis of the samples was carried out using a modular compact rheometer 302 (Anton Paar, Austria), using parallel 50 mm sandblasted plates or 20 mm serrated plates. A working gap of 1 mm was used for all measurements. All samples were covered with silicone oil around the edges to minimise evaporation during testing. Temperature sweeps were carried out at a fixed frequency of 1 Hz within the linear viscoelastic region. The sweeps ran from 70 ˚C to 20 ˚C except for 5% w/v thiamine and κC which was carried out from 80 ˚C to 20 ˚C owing to the far higher gelling point of the system. This helped to prevent errors whereby the rheometer gave the initial storage modulus (G′) as higher than the initial loss modulus (G″) despite being above the sol-gel transition temperature. Temperature sweeps were carried out at a scanning rate of 1 ˚C min^{-1} to be in line with previous studies (Liu & Li, 2016; Tomšič,

Prossnigg, & Glatter, 2008). Information from the temperature sweeps gave data on G′, G″ and the phase angle (tan δ). From this information it was possible to determine the gelling (T_{gel}) and melting (T_{melt}) temperatures of the gels as the point where G′ and G″ cross over (Djabourov, Leblond, & Papon, 1988).

3.2.5 Micro differential scanning calorimetry

Micro differential scanning calorimetry (μDSC) was carried out using a Seteram MicroDSC 3 evo (Seteram, France). This involved analysis of the thermal transitions of the tested hydrogels. 0.6-0.8 g of sample was loaded into a stainless steel cell. Then the reference cell was filled with the equivalent amount of deionised water ± 0.005 g. Samples were then subjected to the following measurement conditions used in previous studies (Brenner, Wang, Achayuthakan, Nakajima, & Nishinari, 2013; Iijima, Hatakeyama, & Hatakeyama, 2014). First, they were cooled to 0 ˚C and held there for sixty minutes. Then they were heated up to 100 ˚C at a scanning rate of 1 ˚C per minute and cooled back down to 0 ˚C at the same rate. Then it was held for another sixty minutes and the cycle was repeated twice more. This gave three heating and cooling curves per run. Each different formulation was tested in triplicate in this manner, giving a total of nine cooling and heating curves per formulation (Brenner, et al., 2013; Iijima, et al., 2014). The temperature range of 0-100 ˚C was chosen because all thermal transitions in the tested systems occur within this range. Transition temperature was taken as the peak of the curve and were obtained by integrating the area below the baseline. Changes in enthalpy (ΔH) were also determined through this method (Iijima, et al., 2014).

3.2.6 3D printing

The 3D printing system was created from a commercially available printrbot simple metal printer which was retrofitted to handle a liquid feed. This involved replacing the components which originally fed the plastic filament into the hot end. The new parts were computer-aided design (CAD) 3D printed parts (1. and 6. in Figure 3.1) which facilitated the use of a 10 mL syringe (2. In Figure 3.1) Due to the fact that there was no heating system, the syringe was insulated to prevent temperature loss. This was to maintain the sol state in order to allow the

sol-gel transition to occur *in situ* (Warner, et al., 2019). The syringe was then filled with the hot liquid sample and nozzles of several different internal diameters were tested (3. In Figure 3.1). Printing was carried out at ambient temperature which was set to 20 ˚C by the climate control. Several printing parameters were adjusted depending on the sample such as infill %, print speed, flow %, and layer height. The software used to control the printer was cura software which is freeware available online. Previous works have shown that varying these parameters can have a major impact on the outcome of print fidelity in food systems (Severini, et al., 2018; Fanli Yang, Zhang, Bhandari, & Liu, 2018). This proved to be true in this case with many failed prints occurring during parameter optimisation. Printability was assessed through shape fidelity (Chimene, Lennox, Kaunas, & Gaharwar, 2016) and weight uniformity (Goyanes, Buanz, Basit, & Gaisford, 2014). If the printed shapes were close to the computer generated image and were within 5% of the average weight of the printed samples they were considered to be successful. Another risk was premature gelation on the printing bed itself, which led to the nozzle dragging through gelled material owing to the pattern of printing. Conversely, if the sol-gel transition had happened too late then the hydrogel spread across the printing bed and fail to achieve layer by layer build up (Wei, et al., 2015). Layer height has been shown to affect the final print outcome in cold extrusion hydrogel 3D printing (Carla Severini, Derossi, & Azzollini, 2016). This also held true with hot extrusion printing. If the layer height was set too high the hydrogel solution came out in drops, giving broken lines and low quality prints. If it was set too low then the nozzle dragged through the gel, yielding a low quality print. If the bed (4. In Figure 3.1) was too cold, the first layer set too quickly and then the print might fail as the nozzle might have scraped through the set material. If the bed was too hot, the print was of low quality as the first layer spread across the build plate due to a failure to set quickly enough. This led to subsequent layers being deposited incorrectly and the final product not properly resembling the CAD shape. Before each print the printer bed level was calibrated manually using a 100 µm gauge. A schematic of the printer is shown in Figure 3.1.

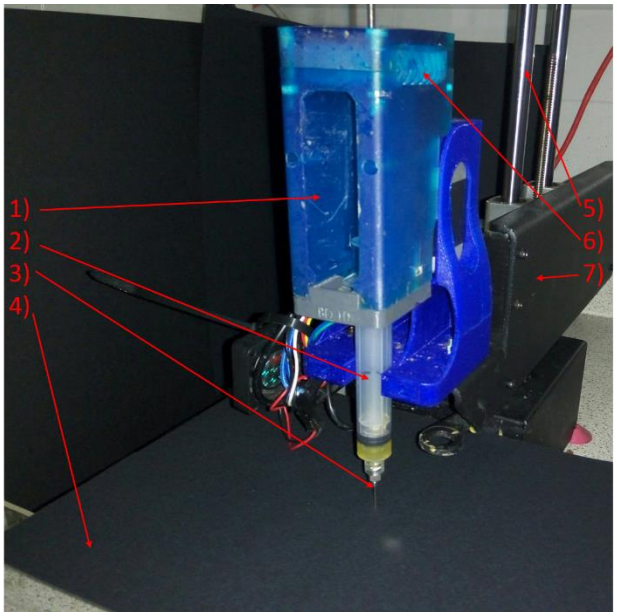

Figure 3.1: Schematic of the retrofitted printrbot simple metal printer including 1) 3DP bracket to hold syringe, 2) Syringe to hold liquid feed, 3) Nozzle for extrusion, 4) Temperature controlled printing bed, 5) Support rods enabling movement in the Z-axis 6) Syringe driver for extrusion, 7) Arm to control movement in the X and Y-axes. Printer was connected to and controlled by a computer running cura freeware.

3.2.7 Production of moulds for casting

Moulds were produced by stereolithography 3D printing using a form 2 3D printer (Formlabs, USA). A cube and a cylinder mould were designed by CAD and uploaded to the software, this was then sliced and sent to the printer digitally to print.

3.2.8 Texture Profile analysis

Texture profile analysis (TPA) of the printed samples and the cast control samples was carried out using a TA XT plus Texture Analyser (Stable Micro Systems Ltd. UK) with 30 kg load cell, 3 g trigger force, P/40 (40 mm) cylindrical aluminium probe at a constant speed of 1 mm/s to match previous studies (Garrec & Norton, 2013). 12 mm^3 cubes and cylinders of 12 mm height and diameter were printed to be used for testing (see Figure 3.5.) 12mm^3 cubes and cylinders of 12 mm height and diameter were cast and used as control samples. After printing, samples were tested immediately while, for cast samples, the hydrogel solution was poured into the mould and left to gel at ambient temperature for two minutes; this was approximately equal to the printing time. Cast samples were then immediately evaluated in the texture analyser. Each test was carried out in triplicate. 3DP samples were compressed in the orientation shown in

Figure 3.5. Through compression testing data on hardness and Young's modulus were obtained for the printed and cast samples. Hardness is defined as the peak force during the first compression cycle (Jones, Woolfson, & Brown, 1997). Young's modulus also known as elasticity, is the stiffness of the material calculated through the relationship between stress and strain of the material at low strains (Jones, et al., 1997). Therefore, it was obtained from analysis of the same samples that underwent compression that gave the hardness values.

3.2.9 Reflective light microscopy

An optical microscope (DM 2500 LED, Leica®, CH) was used to examine central cross sections of printed and cast hydrogels. The cross sections were obtained by slicing the gels thinly with a scalpel. They were then placed on a glass slide and a cover slip was placed over the top. The microscope was set to reflective bright field settings and the software included was used to optimise the image. 4 times and 10 times magnification objectives were used. Images were captured using a charge coupled device camera (DFC450 C, Leica®, CH) attached to the microscope.

3.2.10 Release studies

Release studies were carried out using UV-visible spectrophotometry to assess the release of thiamine from the printed gels and compare it to that from cast gels. The gels each contained 2% w/v thiamine. Three cylinders of 12 mm height and 12 mm diameter were printed and each one was placed into a beaker containing 100mL of deionised water. Water was used as a simple, preliminary medium. Cylinders of the same height and diameter were also cast and used as control tests. Owing to thiamine's extremely high water solubility (Pharmacopoeia, 2016) this was an acceptable phase volume to obtain sink conditions (Gibaldi & Feldman, 1967). The beakers of water were put into an Incu-Shake MIDI shaker incubator (Sciquip, UK) at 100 rpm. Release tests were carried out at 20 ˚C in order to test out room temperature for uses other than ingestion and 37 ˚C to mimic physiological temperature. Measurements were taken at 0, 5, 10, 15, 30, 60, 90, 120, 180, 240, 300 and 360 minutes and 24 and 48 hours. Determination of the concentration of thiamine within the dissolution medium were carried out

using an Orion AquaMate 8000 UV-VIS Spectrophotometer (Thermo Fisher Scientific, UK) set to 235 nm, which was the wavelength at which the thiamine was best detected by the spectrophotometer. 20 µL of dissolution medium was taken with an eppendorf pipette and added to a 1000 µL cuvette. Then 980 µL of deionised water were added to the cuvette and the solution was homogenised in a vortex shaker for 15 seconds to be in line with previous studies (Hansen & Warwick, 1978). This was then placed into the UV-VIS spectrophotometer following calibration with deionised water. This gave the concentration of thiamine within the cuvette which was then adjusted to account for the total thiamine released within the dissolution medium. The release profile was calculated from a calibration curve determined by the UV-visible spectrophotometer which had an R^2 value of 0.998. The cuvette was then discarded and 20 µL of deionised water was added into each beaker. This was corrected for when calculating the thiamine concentration following the procedure of (Singh, Kaur, & Singh, 1997). All tests were carried out in triplicate. The calibration curve can be found in Appendix 2.

3.2.11 Modelling of release data

Thiamine release data (up to 60%) were fitted to the model proposed by (Peppas & Sahlin, 1989):

$$\frac{M_t}{M_\infty} = k_1 t^m + k_2 t^{2m} \qquad \text{Eq [1.1]}$$

Where M_t/M_∞ is the fraction of active released at time t. The first term ($k_1 t^m$) relates to Fickian effects while the second term ($k_2 t^{2m}$) to relaxational contributions to the release. k_1 is the kinetic constant regarding release from the matrix by Fickian diffusion and k_2 is the kinetic constant for case-II relaxation. Lastly the coefficient m is the purely Fickian diffusion exponent which is dependent on the shape of the device (Peppas, et al., 1989); the value of the exponent concerning relaxation transport is in theory twice the Fickian exponent (2m). The same study further reported that the impact of each of the two mechanisms to the obtained release profile

can be assessed by calculating the fractional Fickian (F) and relaxational (R) contributions from:

$$F = \frac{1}{1+\frac{k_2}{k_1}t^m} \quad \text{Eq [1.2]}$$

$$R = \frac{\frac{k_2}{k_1}t^m}{1+\frac{k_2}{k_1}t^m} \quad \text{Eq [1.3]}$$

3.3 Results and discussion

3.3.1 Pre-printing thermal characterisation of the hydrogels

Before printing could occur it was important to establish the thermal characteristics of the gel systems. This was crucial as a strong understanding of these parameters is necessary in order to establish whether a material is printable or not. There exists virtually no literature on the effect thiamine has on the thermal characteristics of κC and agar gels. So investigations had to be carried out in order to establish if there were any changes to the gel networks following thiamine incorporation. The sol-gel transition temperature of the thiamine-biopolymer systems was determined using a rotational rheometer. This is in line with previous studies (Hermansson, et al., 1991; Watase & Arakawa, 1968). The results for average T_{gel} and T_{melt} for 3% κC and 2% agar with 0, 0.1, 1, 2 and 5% w/v thiamine are shown in Figure 3.2. G′ and G″ for all the examined systems are presented in Figure 3.3.

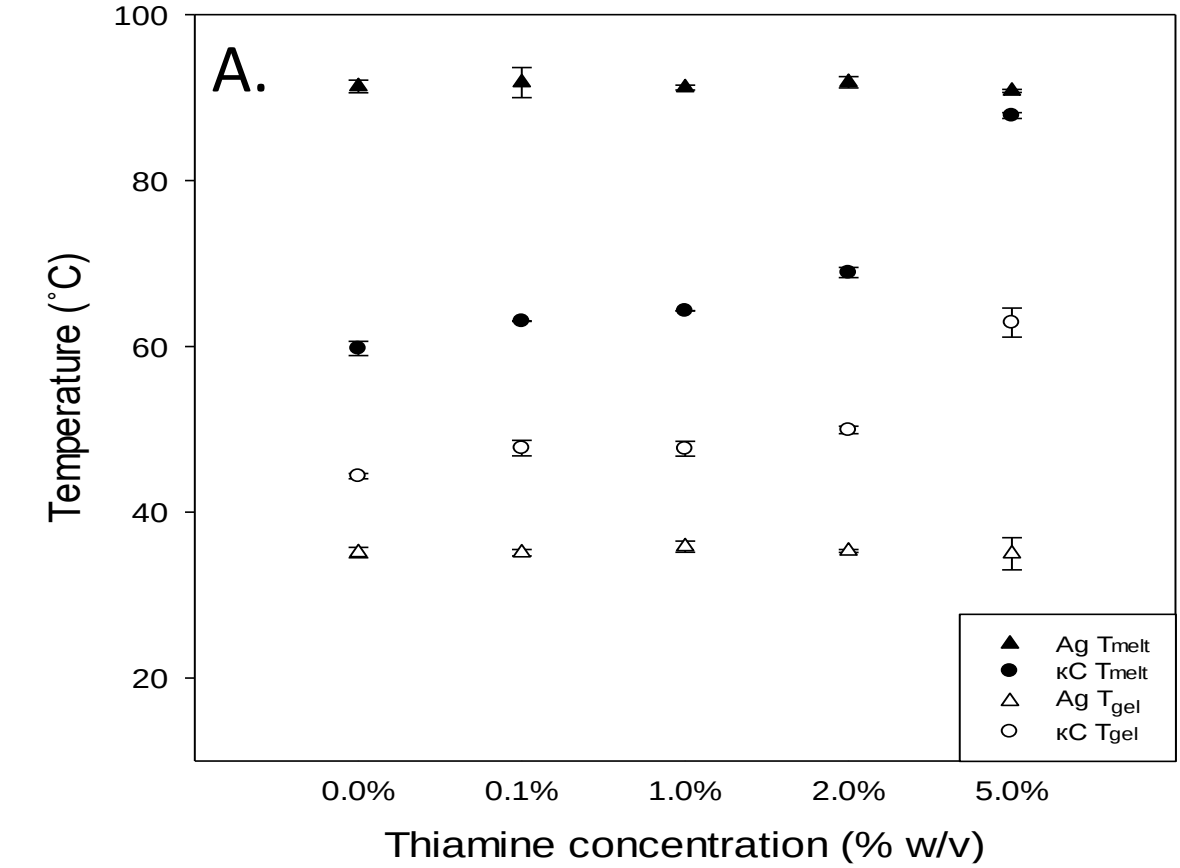

Figure 3.2: T_{gel} and T_{melt} of 0, 0.1, 1, 2 and 5% thiamine with 3% κC and 2% agar – Error bars are the standard deviation of the mean. n = 3

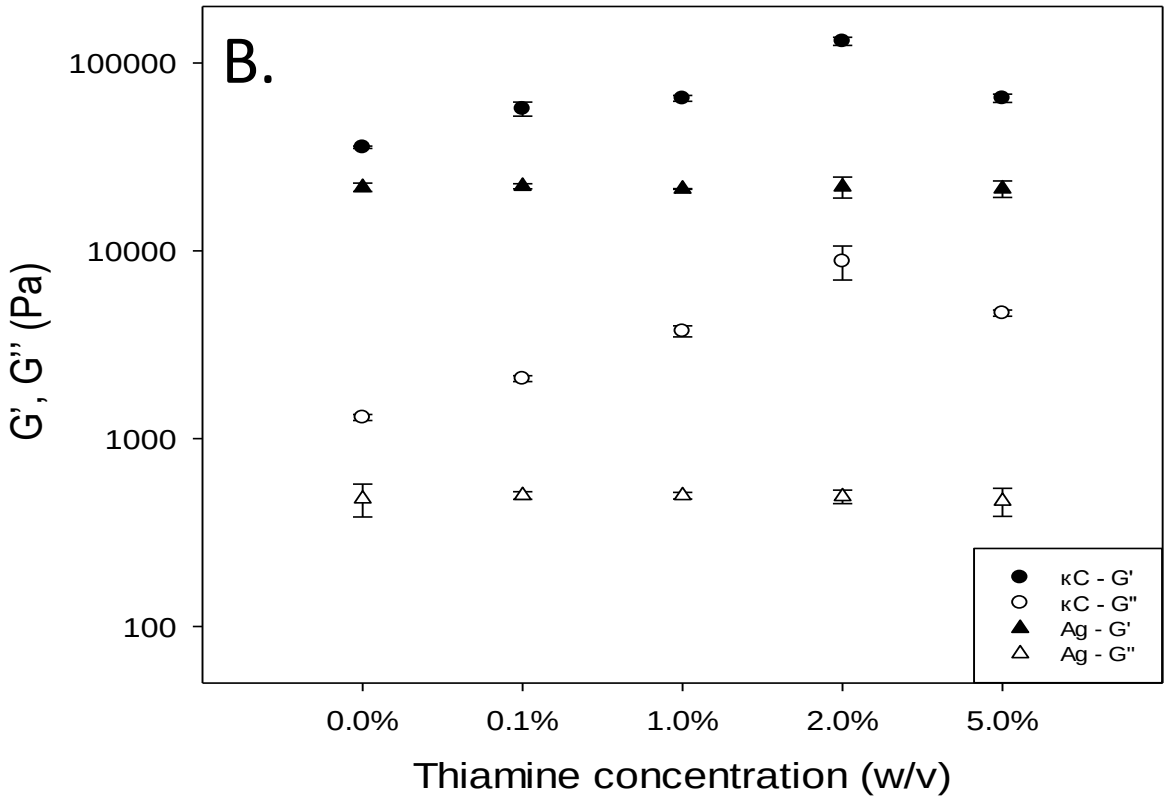

Figure 3.3: G' and G" of 0, 0.1, 1, 2 and 5% thiamine with 3% κC and 2% agar

Figures 3.2 and 3.3 show that there is no interaction between the agar and the thiamine. As an uncharged molecule, agar gels through hydrogen bonding and doesn't rely on crosslinkers (Tako & Nakamura, 1988). This is reflected in Figures 3.2 and 3.3 by the transition temperatures and the moduli of agar remaining constant regardless of thiamine concentration. However, with κC and thiamine, as the concentration of thiamine increased there was a linear increase in both T_{gel} and T_{melt}. This indicates that an interaction between thiamine and κC was occurring with the transition temperatures increasing with the concentrations of the active. After dissociating from the hydrochloride salt, thiamine is a cationic molecule and κC is an anionic molecule which relies on cationic ions for gelation (Hermansson, et al., 1991). Therefore the results from the T_{gel} and T_{melt} suggest that the thiamine is complexing with the κC and reinforcing the gel network. This phenomenon has been observed with κC and other cationic molecules such as surfactants (Grządka, 2015). However, Figure 3.3 shows that the reinforcement of the gel network through increasing thiamine concentration, peaks at 2% w/v thiamine. At 5% thiamine a decrease in G′ and G″ were observed despite increasing T_{gel} and T_{melt}. This was probably due to the κC becoming saturated with the thiamine, which is a less effective gelling agent than ions such as potassium and sodium. This led to a decrease in the aggregation of double helices which are essential to normal κC gelation. The formation of these thiamine-κC complexes caused charge cancellation and therefore hydrophobic domains which will increase the transition temperatures and inhibit gelation. This has been shown before with cationic compounds reducing gelation of κC and even preventing it when they are solely present (Norton, et al., 1984).

However, rheological results alone are not enough to conclusively show that the complexation of κC and thiamine is occurring. The same systems were tested using a μDSC as well. This reaffirmed the transition temperatures and gave information on the gelling and melting enthalpies of the systems as well. Figure 3.4A shows the T_{gel} and T_{melt} for the thiamine biopolymer systems. Figures 3.4B and C show the gelling and melting enthalpies.

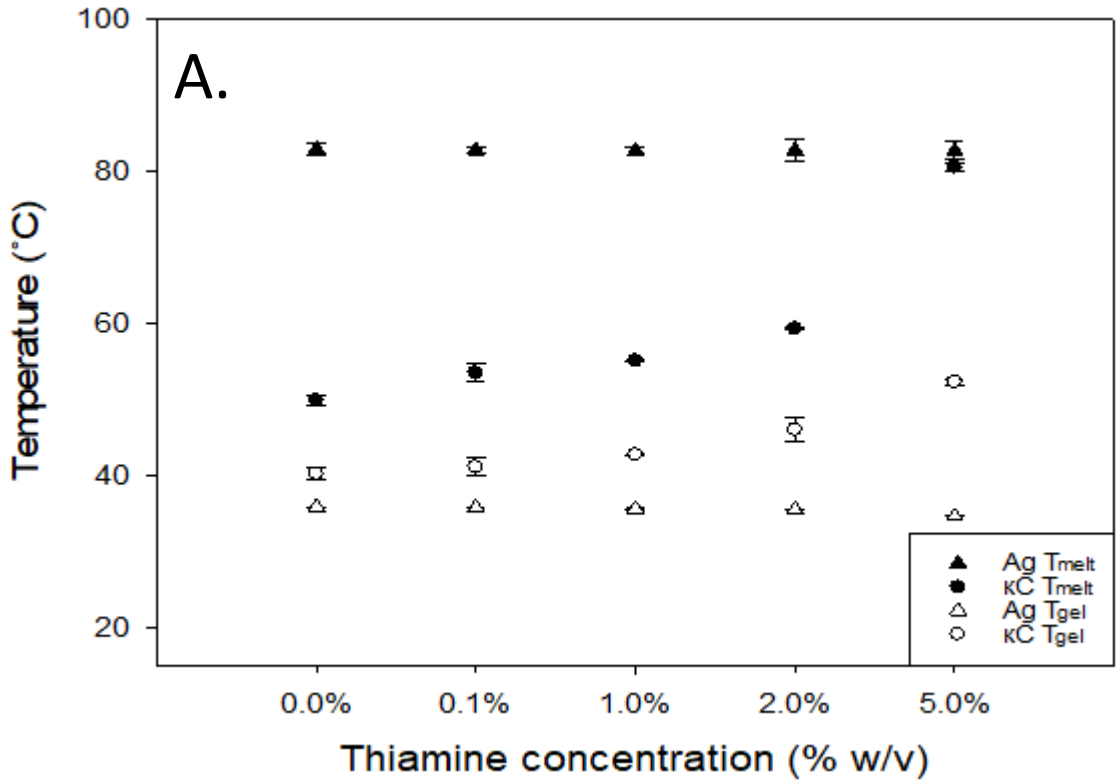
A.
Temperature (°C)
100
80
60
40
20
0.0%
0.1%
1.0%
2.0%
5.0%
Thiamine concentration (% w/v)
Ag Tmelt
KC Tmelt
Ag Tgel
KC Tgel

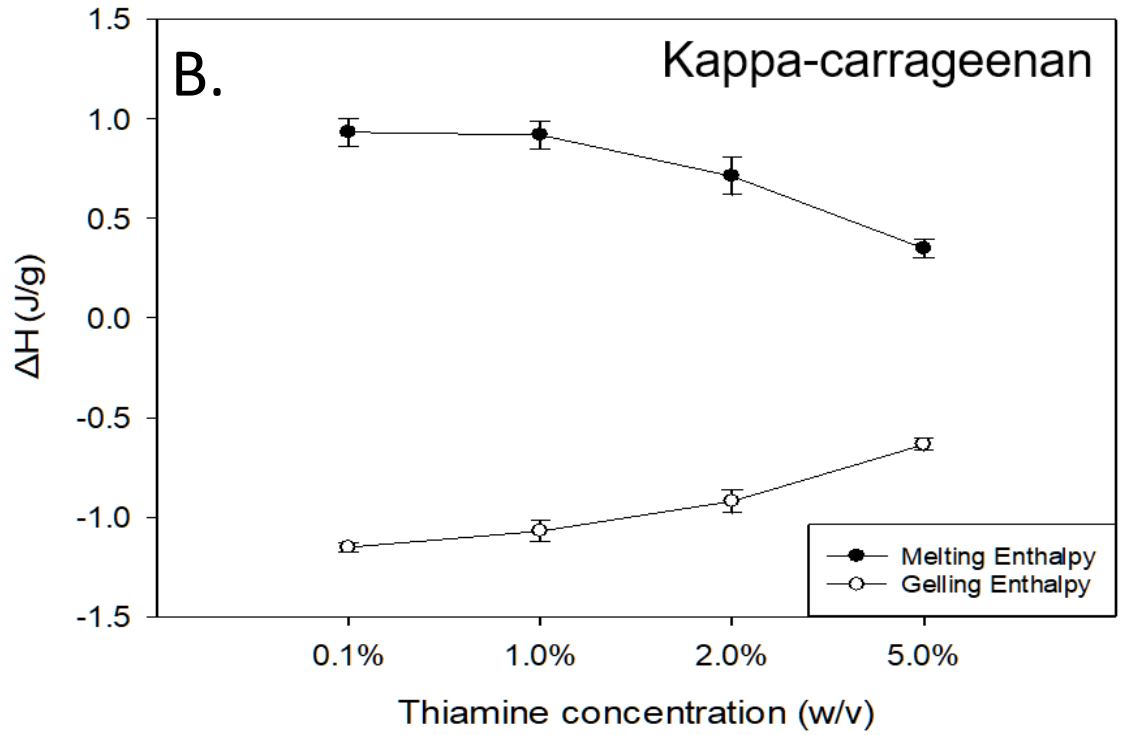
B.
Kappa-carrageenan
ΔH (J/g)
1.5
1.0
0.5
0.0
-0.5
-1.0
-1.5
0.1%
1.0%
2.0%
5.0%
Thiamine concentration (w/v)
Melting Enthalpy
Gelling Enthalpy

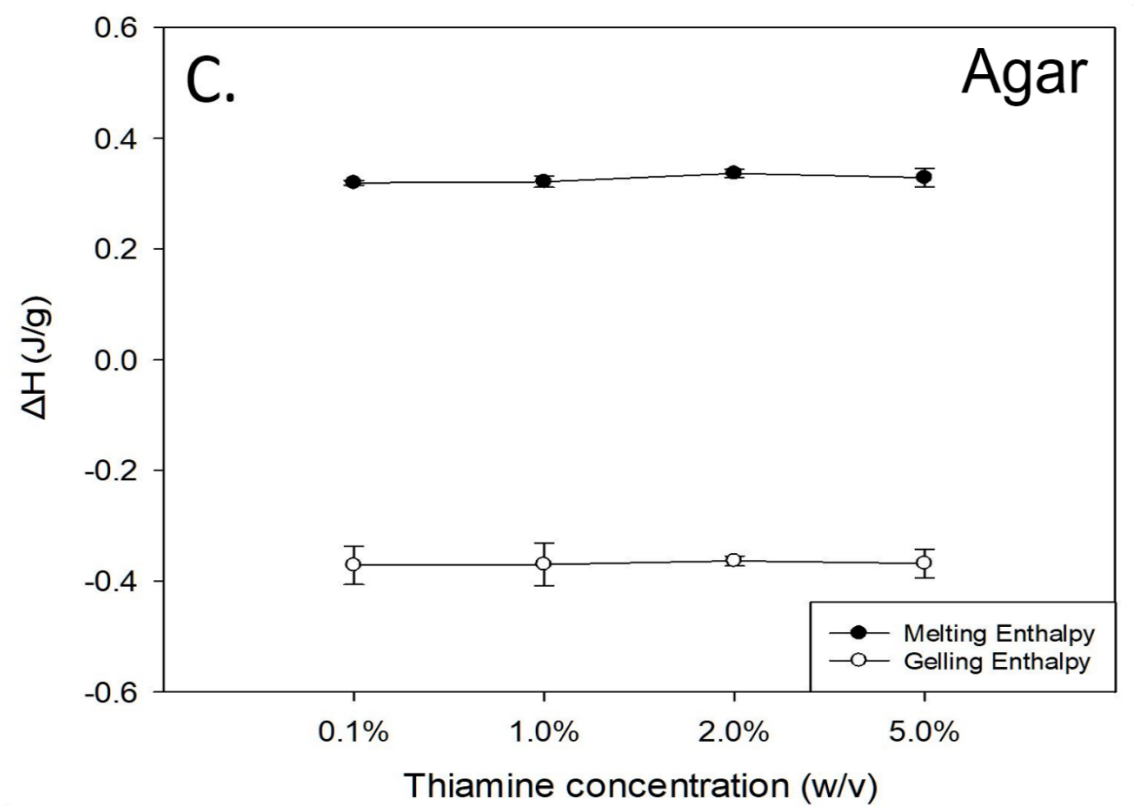

Figure 3.4: DSC data for (A) the average thermal transition temperature of κC- and agar-thiamine gels, and the gelling and melting enthalpies of (B) κC-thiamine and (C) agar-thiamine gels.

The T_{gel} and T_{melt} for the thiamine-biopolymer systems were in agreement with the results from the rotational rheometer. While they do return somewhat different results, this is to be expected owing to the different ways in which they assess the coil to helix transition and vice versa. The rheometer and the DSC are sensitive to different parts of the gelation process of the hydrogels and the results are therefore not obtained from the same segment of the gelling mechanism (Nishinari, 1997). Again, the μDSC results for the thiamine-agar systems confirmed that no interaction is taking place between the agar and the thiamine, with constant transition temperatures and enthalpies recorded regardless of thiamine concentration. However, with the κC, the thiamine concentration had a negative correlation with the gelling and melting enthalpies. The decrease in enthalpy values indicated that there was a reduction in the amount of free sulphate groups on the backbone available for formation of electrostatic bridges with gelling cations (Rosas-Durazo, et al., 2011). Oversaturation with K^+ ions has been shown to lead to the disruption of κC cross-linking and prevention of the aggregation of double

helices (Thrimawithana, Young, Dunstan, & Alany, 2010), and this phenomenon is believed to occur within these systems. The thiamine-κC hydrogels also became visually more turbid with increasing thiamine concentrations, suggesting the formation of larger complexes which were able to scatter light.

3.3.2 Hydrogel printing

The samples chosen for printing were those that had a higher storage modulus and exhibited rapid solidification (Li, Li, Qi, Jun, & Zuo, 2014). A higher storage modulus has been shown to produce printed products with better shape retention (Costakis, Rueschhoff, Diaz-Cano, Youngblood, & Trice, 2016). The thermal characterisation identified that hydrogels with a 2% thiamine concentration were best suited for 3DP, as it gave the highest storage modulus and gelled rapidly for the κC. The agar was the same regardless of the thiamine concentration so 2% was also used. The parameters tested for the 3D printing of κC-thiamine hydrogels are shown in Table 3.1 below.

Table 3.1: A table showing the different parameters tested in the hydrogel 3D printing process

NS	H_L (mm)	Flow (%)	T_{PB} (°C)	v_p (mm/s)	T_H (°C)	3D Outcome and Comments
18G	1.4	50	40	30	80	Under extrusion – Set too slowly
18G	1.4	60	45	30	75	Under extrusion – Set too quickly
18G	1.4	70	45	20	75	Over extrusion – Set too slowly
20G	1	35	40	20	75	Slight under extrusion – Set properly – nozzle dragged through shape
20G	1	40	40	20	75	Sufficient extrusion – Set properly – nozzle dragged through shape
20G	1.2	35	40	20	75	Slight under extrusion – Set properly
20G	1.2	35	40	20	80	Slight over extrusion – Set properly
20G	1.2	40	40	20	70	Slight under extrusion – Set properly
20G	1.2	40	40	20	75	Sufficient extrusion – Set properly
20G	1.2	40	40	20	80	Over extrusion – Set properly
20G	1.2	45	40	20	75	Slight over extrusion – Set properly
20G	1.2	50	40	20	75	Over extrusion – Set too slowly
20G	1.4	35	40	20	75	Under extrusion – Set properly
20G	1.4	40	40	20	75	Under extrusion – Set properly
20G	1.4	45	40	30	75	Over extrusion – Set properly – nozzle dragged through shape
20G	1.4	50	45	20	80	Over extrusion – Set too slowly
22G	1.4	30	40	20	60	Under extrusion – Set too quickly
22G	1.4	40	45	30	75	Under extrusion – Set too slowly
22G	1.4	50	50	40	80	Over extrusion – Set too slowly

NS: Nozzle size

H_L: Layer height (mm)

Flow: Flow percentage (%)

T_{PB}: Printer bed temperature (°C)

v_p: Print speed (mm/s)

T_H: Hold temperature (°C)

The printing parameters from table 3.1 that yielded the highest quality and most repeatable prints for thiamine-κC hydrogels were a 20 gauge nozzle, layer height 1.2 mm, flow percentage

of 40%, printer bed temperature 40 ˚C, print speed of 20 mm/s and a hold temperature of 75 ˚C.

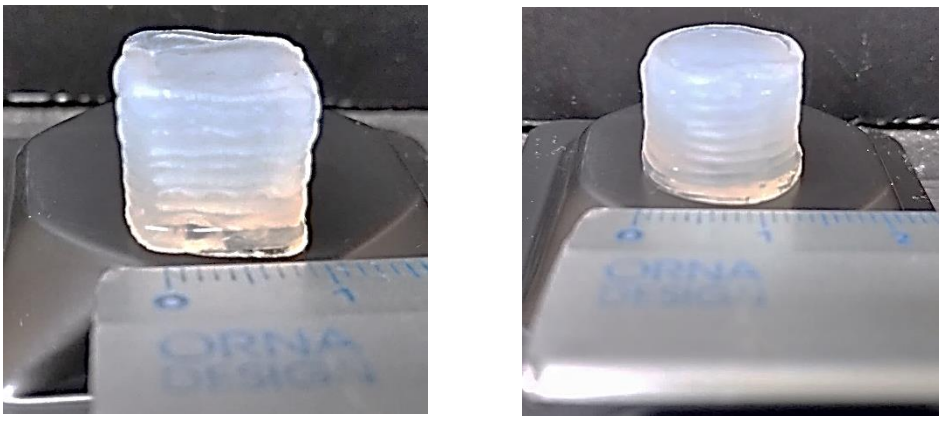

Figure 3.5: 3D printed 12 mm cube (A) and 12 mm height and diameter cylinder (B) printed using 3% κC and 2% thiamine hydrogel

The agar was unable to successfully print under all tested conditions. This was believed to be because the agar-thiamine hydrogels with their far lower G′ of 30,000 Pascals had poorer shape retention compared to the κC-thiamine hydrogels which had a G′ of around 120,000 Pascals. Agar's lower T_{gel} of around 37 ˚C might also have been a contributing factor as well. This meant that there was less of a temperature differential between the T_{gel} and printing temperature. This led to a slower gelation time and poorer shape fidelity, with the shape unable to hold the weight of subsequent layers. Too much spreading also meant that the nozzle dragged through the hydrogel solution, distorting the shape. The reasons for failure might also have been due to limitations with the printer hardware, as a lack of temperature control on the syringe meant that the hydrogel solution could not be held just above its T_{gel}. Other modifications such as a cooling fan might also have yielded improved results. Finally changes to the formulation such as increasing the concentration of the agar or addition of an adjunct such as sucrose to increase gel strength and temperature could be successful in future (Normand, 2003). Therefore going forward only thiamine-κC gels were used.

3.3.3 Post-printing texture profile analysis of the hydrogels

TPA of gels is often used to assess their microstructure performance and how this affects specific functionality, including their ability to deliver therapeutic molecules (Özcan, et al.,

2009). With the layer by layer nature of 3D printing, the 3D printed structures have a different internal structure compared to a cast/moulded structures (Padzi, Bazin, & Muhamad, 2017). However, there is not much literature that compares 3DP hydrogels to their cast equivalent, and thus TPA was used to begin understanding and characterising some of the internal differences. Figure 3.6 shows the data obtained for the hardness and Young's modulus of printed and cast cubes and cylinders.

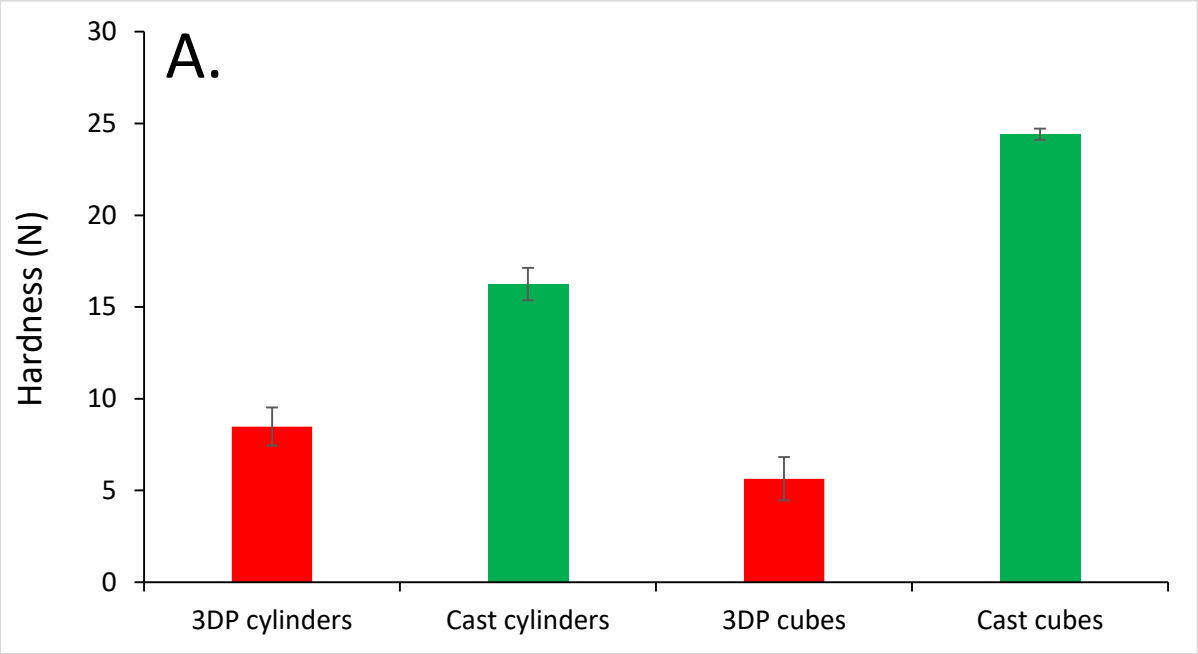

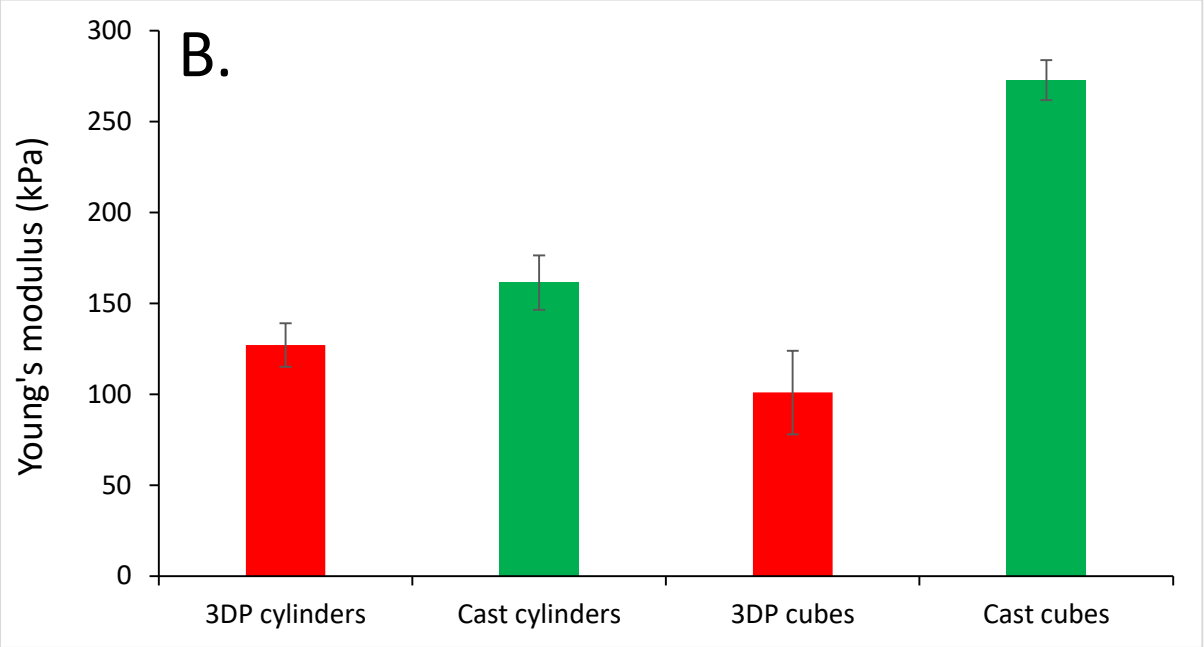

Figure 3.6: Hardness (A) and Young's modulus (B) of the printed and cast cubes and cylinders

The results obtained from the TPA are much higher than those observed in literature (Artignan, Corrieu, & Lacroix, 1997; Garrec, et al., 2013) which is due to both the higher concentration of κC used and the addition of the Na^+ ions and the thiamine reinforcing the gel network as discussed. The TPA data highlights the differences in the bulk structure of a printed gel compared to a cast gel. The higher hardness value shows that the continuous cast gel network is much more robust. The TPA showed that the cast samples were stiffer than the printed samples when undergoing compression. It was also noted that cubes were harder and less elastic than the cylinders for the cast samples. The cubes had a cross-sectional surface area of 144 mm^2 and a volume of 1728 mm^3. The cylinders had a cross-sectional surface area of approximately 113 mm^2 and a volume of 1357 mm^3. There exists almost no literature comparing cubes to cylinders of the same material subjected to compression tests, within the range of materials studied, however it has been shown that variations in surface area can affect results obtained from TPA, owing to the amount of material in contact with the probe (Rosenthal, 2010). Since gels printed in this manner are in effect a discontinuous network, with several small networks only semi fused, the TPA showed they are less resistant to the

external damage owing to the differences in the structure. Figure 3.7 shows a cube that has undergone compression testing. The printed shapes delaminated rather than fracturing like a cast gel. Since this was occurring rather than a fracture, the bonds holding the layers together must have been weaker than the gel network itself. Since the cast gels were one continuous network, they therefore could resist greater amounts of force as shown by the TPA results.

Figure 3.7: A printed 12 mm κC-thiamine hydrogel cube that has delaminated after undergoing compression testing. Each square on the grid shown is 10 mm^2

3.3.4 Post-printing light microscopy of the hydrogels

While the separate printed layers could clearly be seen when observing the printed shapes with the naked eye, when cutting a central cross-section they were no longer discernible. It was important to establish whether the shapes had undergone layer fusion or whether the printed shapes were a series of individual gel networks held together by physical bonds. FDM printed plastics have been shown to have gaps running through the structure as a consequence of the manufacturing technique (Sood, Ohdar, & Mahapatra, 2010). The presence of these gaps running through the printed shapes could affect the final release profile of the thiamine by creating a shorter diffusion path. It also helped to confirm the findings from the TPA as the internal structure differed from that of a cast gel network. The differences in internal structure were responsible for overall different bulk structure. Figure 3.8A and B show the outside of a cast cube and a printed cube respectively. The ridges observed in 8B are due

to the printing process and show a clearly different external structure to the cast cube. Figure 3.8C and D show a central cross-section from a cast cube and a printed cube. This highlights the stark differences in the structures created by 3DP and casting when it comes to hydrogel production. Figure 3.8D presented that 3DP produced hydrogels have visible layering running through them as indicated by the lines visible in the image. Figure 3.8C showed cast gels with a homogenous, continuous structure as was expected. This layering is believed to affect the physical characteristics of the gel as determined in the TPA.

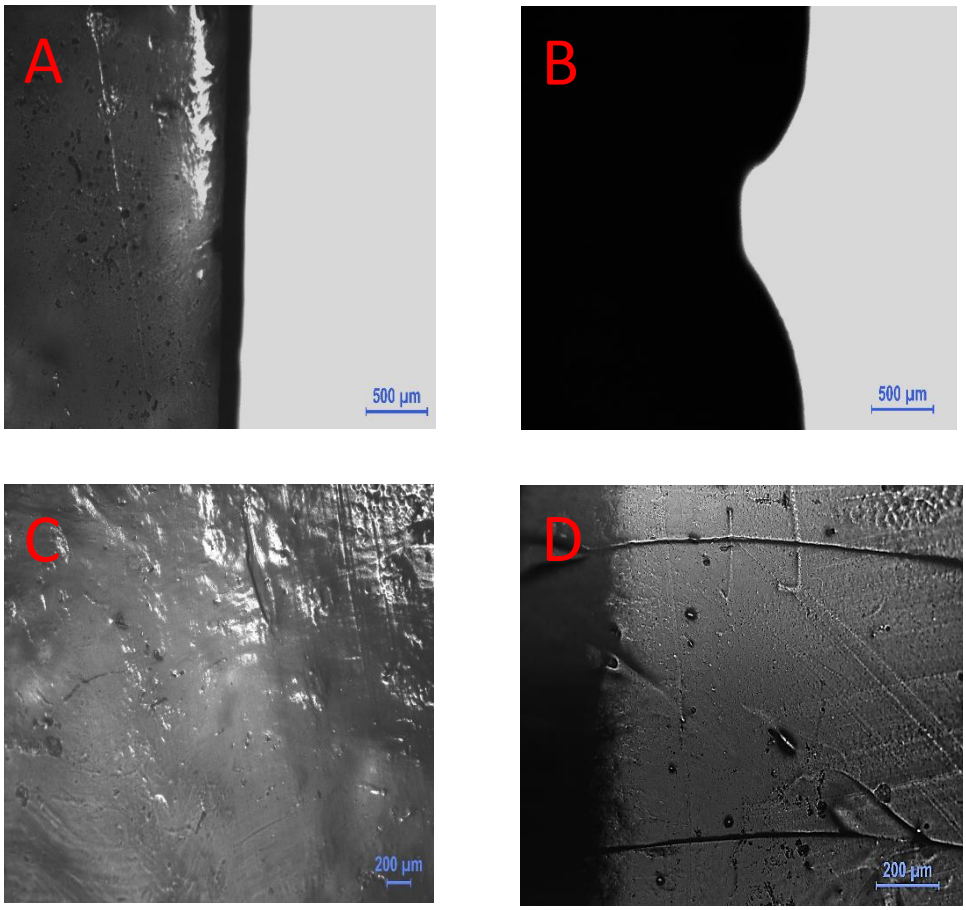

Figure 3.8: Microscope images of cast (A) and printed (B) κC-thiamine hydrogels from the outside layer, and cross-sections of cast (C) and printed (D) κC-thiamine hydrogels

3.3.5 Hydrogel release studies

There exists very little literature comparing the release rate from 3DP and traditionally manufactured structures. 3DP capsules have been shown to release dye at the same rate as injection moulded capsules (Melocchi, et al., 2015). However, these were only 0.3 mm in width and hollow, so this might not be applicable to the shapes studied which were far thicker and

solid throughout. The amount of thiamine released from the printed and cast cylinders was assessed at 20 ˚C and 37 ˚C and the obtained release profiles are shown in Figures 3.9A and 3.9B respectively. Cubes were not selected for release testing as the chosen model for analysis does not account for this shape (Peppas, et al., 1989). All of the cylinders both printed and cast weighed 1.45 g ± 5%. Release of the active increased from 20 ˚C to 37 ˚C due to increased energy in the system facilitating a greater rate of release by diffusion (Vrentas & Vrentas, 1992). However, diffusion might not be the only factor in effect. Release of an active from a polymer matrix can also be dependent on relaxation of the polymer matrix as well as Fickian diffusion (Peppas, et al., 1989). The release data also showed a difference in the release rates between the printed and the cast gels. At both temperatures the printed gels showed an increase in initial release rate over the first fifteen minutes as shown by Figure 3.9C when compared to the cast gels. Moreover, the release data showed that there was a greater amount of thiamine released from the printed cylinders after 360 minutes compared to the cast ones.

Figures 3.9A and 3.9B showed that the cast cylinders released less thiamine over six hours at both of the tested temperatures compared to the 3D printed cylinders. Figure 3.9C highlighted the differences in release rates over the first 15 minutes, cast gels releasing far less thiamine compared to 3DP gels. Therefore, structural and mechanical differences between the two types of gel system must also contribute to the different release rates. In hydrogels, the physical characteristics determined from TPA such as hardness have been shown to affect molecular release (Jones, Woolfson, Djokic, & Coulter, 1996). This was observed to occur in this study as well with the printed samples having lower values for hardness compared to the cast samples. Also, the elasticity seemed to have no effect on the release in their study with the elasticity values for the highest and lowest releasing systems being within 0.04 of each other on average. This indicates that while the TPA data might go some way in explaining the differences in release rate, it is not absolute. The layers running throughout the printed shapes lead to a decrease in the diffusion path as water is able to pass into the printed cylinders at a quicker rate than the cast cylinders owing to the differences in

the bulk structure. This led to an increase in the release rate as shown by (Liang, et al., 2006). Furthermore, after the release tests the cast and printed cylinders had the surface water removed by drying and were weighed out, with the printed cylinders having increased on average more in weight than the cast cylinders. This further supports the notion that water was able to pass into the 3DP cylinders at a faster rate.

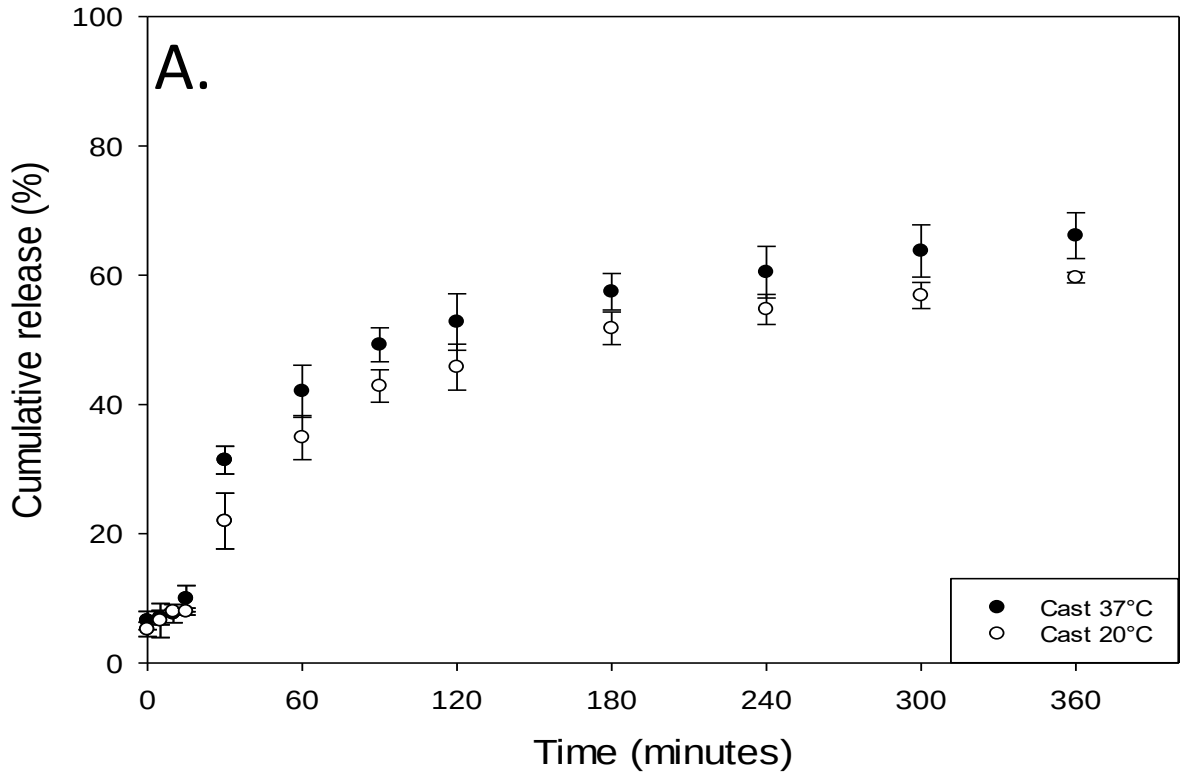

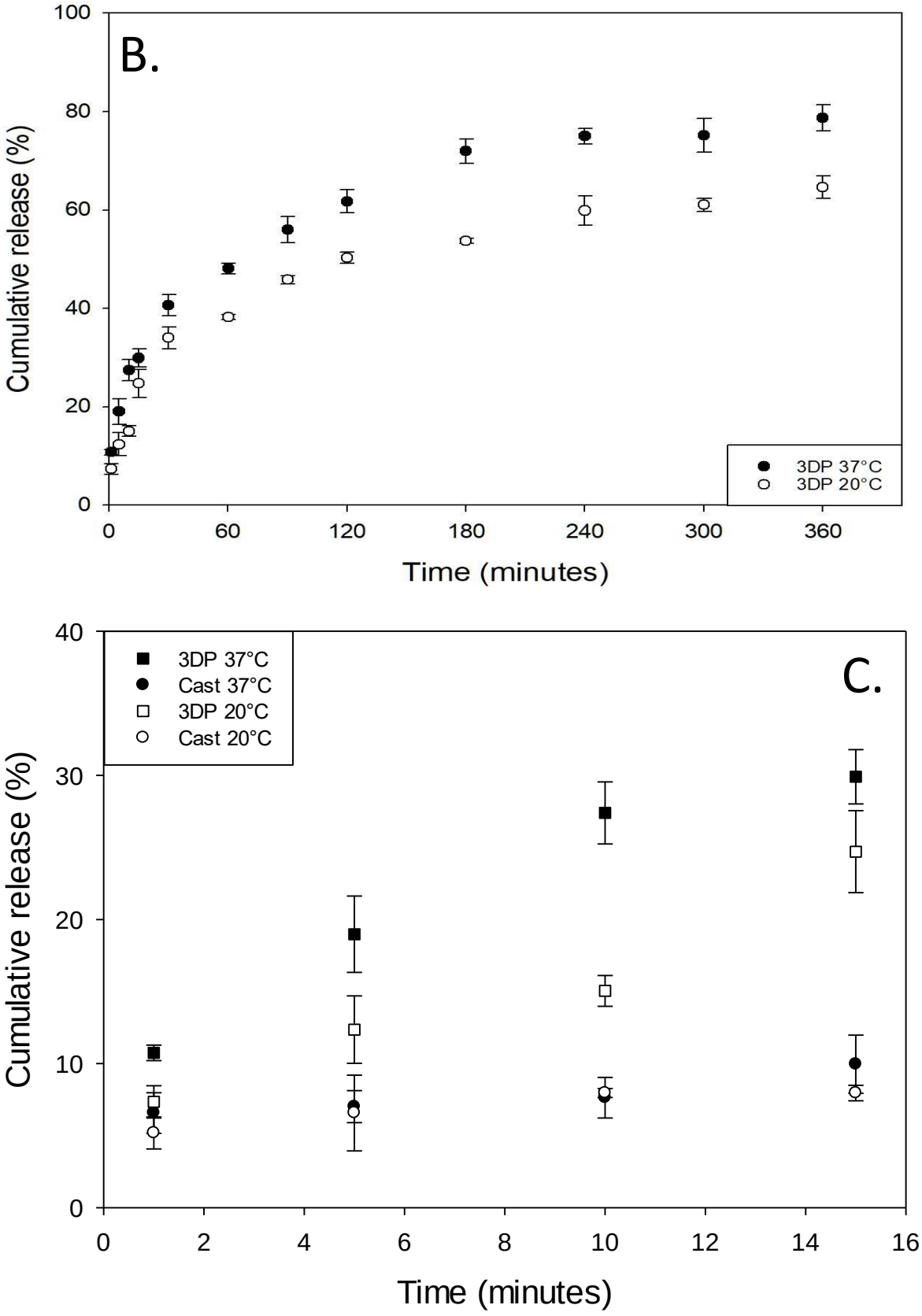

Figure 3.9: A comparison of cumulative release rates of thiamine from printed (A) and cast (B) and both for the first 15 minutes (C) κC 3% and thiamine 2% hydrogels.

The drug release profiles for the printed and cast gels at both temperatures were fitted to the Peppas-Sahlin equation. The kinetic constants for Fickian diffusion and case-II relaxational contribution were calculated through plotting the first 60% of the release data to equation 1. This made it possible to calculate F and R to the release of thiamine from the printed and cast hydrogels. The data is shown in Figure 3.10, with the information on k_1, k_2 *and* m available in Table 3.2.

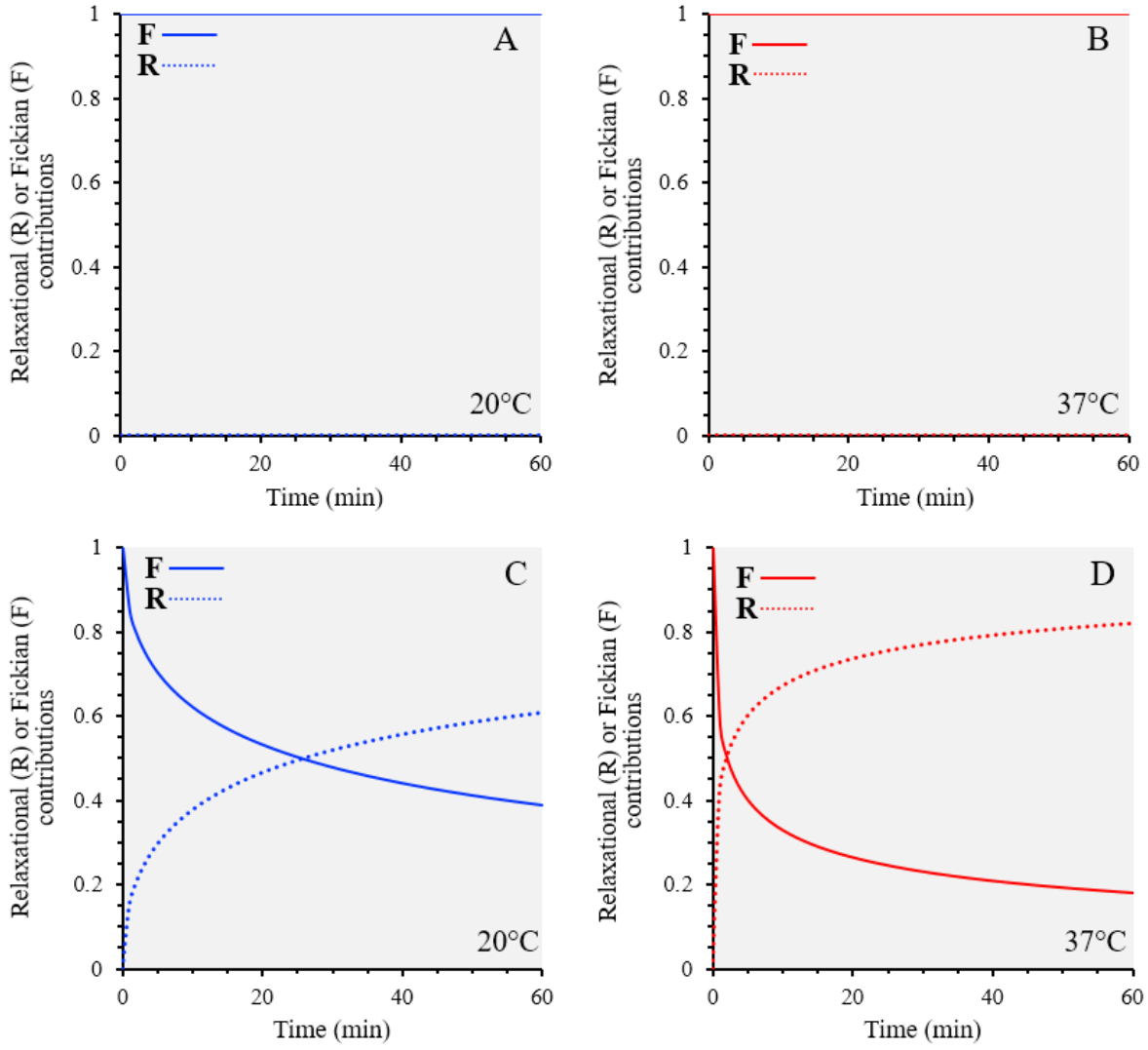

Figure 3.10: Data showing the percentage thiamine release due to Fickian diffusion and relaxation for printed cylinders at 37 ˚C (A) and 20 ˚C (B) and cast cylinders at 37 ˚C (C) and 20 ˚C (D)

Table 3.2: The constant values used in the calculation for F and R for the release tests of the cast and printed cylinders at both temperatures

	37 ˚C printed	37 ˚C cast	20 ˚C printed	20 ˚C cast
k_1	11.46	1.266	6.902	1.586
k_2	$8.37E^{-14}$	0.9282	$2.91E^{-9}$	0.2867
m	0.3572	0.4459	0.4321	0.5267

Figures 3.10A and 3.10B showed that with the 3DP shapes the diffusion contribution was essentially 100% for the printed shapes at both temperatures, with F being practically equal to 1 throughout the test. Whereas Figures 3.10C and 3.10D show that there is a relaxation contribution to the thiamine release from the cast cylinders. Both of the cast temperatures started out with diffusion being the dominant contribution. However, as the tests progressed the relaxation contribution started to exert more influence eventually becoming the dominant mechanism of release. This can be observed where the dotted line crosses the solid line. This happened more quickly at 37 ˚C compared to 20 ˚C due to there being more energy in the system. This led to a faster relaxation of the polymer chains (Watase, et al., 1968). This showed that the cast systems behaved in a manner seen in previous reports (Baggi & Kilaru, 2016) and (Lupo, Maestro, Gutiérrez, & González, 2015). However, for the 3DP cylinders it is believed that the different internal structure allowed water to penetrate faster into the shapes and so diffusion had been encouraged to such an extent as to make the relaxation contribution negligible (Falk, Garramone, & Shivkumar, 2004).

Figure 3.11A and B show the TPA data for the printed cylinders had a greater decrease in hardness and elasticity compared to the cast cylinders. By absorbing more water, essentially the concentration of the κC and the thiamine within the gel decreased more compared to the cast gels. This caused there to be a less dense polymer network and could have contributed to an increase in release rate (Wu, Joseph, & Aluru, 2009). Also swelling would have increased the pore size of the hydrogel (Ganji, Vasheghani, & Vasheghani, 2010), which could also have increased the release rate in this case if the pore size was a rate limiting factor (Meena, Prasad, & Siddhanta, 2007). If it was not then the swelling would not have affected the release

rate (Varghese, Chellappa, & Fathima, 2014). However, even after 48 hours, neither formulation had released 100% of the thiamine into the dissolution medium. This might be because with such a high G′ value, the gel network was simply so dense that not all of the thiamine was able to diffuse out despite the swelling that occurred (Patil, Dordick, & Rethwisch, 1996). However, it could also be due to the use of an incubator shaker rather than the use of a USP paddle apparatus as is usually used in release studies. Finally, the electrostatic complexation of the κC and the thiamine might also have been responsible for the failure to reach 100% release (Daniel-da-Silva, Ferreira, Gil, & Trindade, 2011). Future study needs to go into this area as well as studying different pH levels in the release media.

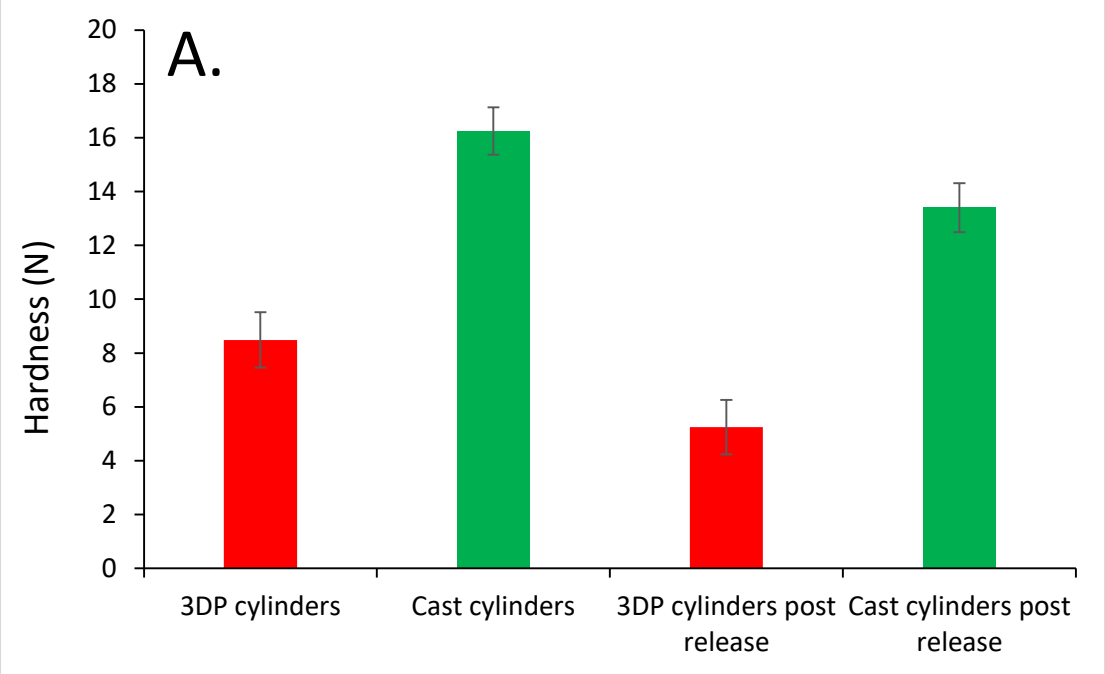

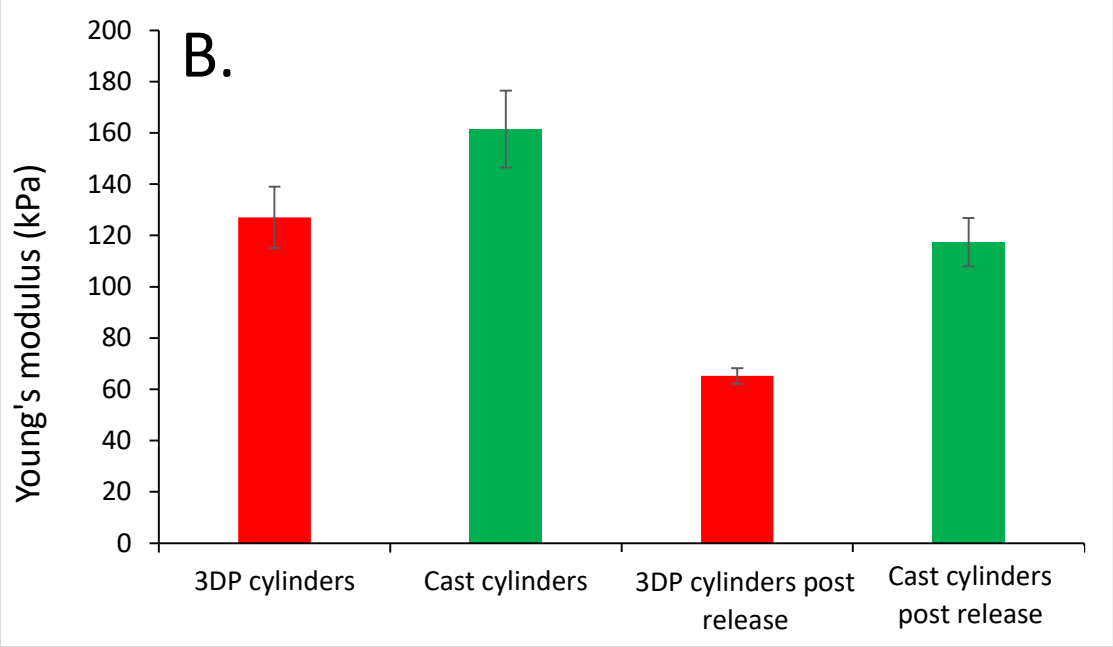

Figure 3.11: Post-release study texture analysis of printed and cast gels assessing hardness (A) and Young's modulus (B)

3.4 Conclusions

In this study, κC and agar thiamine-loaded hydrogels were assessed for their suitability for 3D printing. Rheological analysis showed that while thiamine does not interact with agar, it can form electrostatic complexes with κC that lead to gel structure reinforcement (up to a point). Beyond this, thiamine addition caused a marked decrease in G′ while both T_{gel} and T_{melt} continued to increase. μDSC confirmed the same trends and further revealed that the gelling and melting enthalpies for κC-thiamine systems were shown to decline with increasing thiamine concentration.

2% agar was unable to print due to a lower G′ and T_{gel}, but 3% κC-2% thiamine hydrogels were printable, and cubes and cylinders could be formed with reproducible weights and dimensions. The printed gels' physical properties were then compared to traditionally produced cast gels of the same dimensions and weight within a margin of ± 5%. TPA, microscopy and release studies were used to show that 3D printing facilitated the creation of gels with different physical properties without having to chemically modify the gel ingredients. In terms of release, printed cylinders released a higher fraction of enclosed active than the cast cylinders. They also exhibited a faster rate of release over the first 15 minutes of testing.

This was due to differences in the physical structure of the printed cylinders compared to the cast cylinders, which meant that printed cylinders were more prone to swelling.

Modelling showed that while thiamine release from the cast cylinders was driven by both Fickian and relaxation phenomena, printed cylinders allowed the delivery of the active solely via diffusion. Although agar was not shown to be suitable for printing under the current formulation/processing conditions, printability might still be realised at higher hydrocolloid concentrations or through the use of adjunctive materials to increase its gelation rate and G′ value. Similarly, although κC hydrogels could be successfully printed, they were unable to release the entirety of enclosed thiamine, thus further flexibility in terms of active delivery could be achieved for non-interacting actives. Nonetheless, the current study does clearly highlight the promise of hydrogel utility for formation of food-related structures via 3D-printing, capable of performing differently to cast gels of the same material.

Acknowledgements

This work was supported by the Engineering and Physical Sciences Research Council [grant number EP/N024818/1].

3.5 References

Armisen, R., & Gaiatas, F. (2009). Agar. In *Handbook of hydrocolloids* (pp. 82-107): Elsevier.

Arnold, R. G., & Dwivedi, B. K. (1971). Hydrogen sulfide from heat degradation of thiamine. *Journal of Agricultural and Food Chemistry, 19*(5), 923-926.

Artignan, J.-M., Corrieu, G., & Lacroix, C. (1997). Rheology of pure and mixed kappa-carrageenan gels in lactic acid fermentation conditions. *Journal of Texture Studies, 28*(1), 47-70.

Azam, R. S. M., Zhang, M., Bhandari, B., & Yang, C. (2018). Effect of Different Gums on Features of 3D Printed Object Based on Vitamin-D Enriched Orange Concentrate. *Food Biophysics, 13*(3), 250-262.

Baggi, R. B., & Kilaru, N. B. (2016). Calculation of predominant drug release mechanism using Peppas-Sahlin model, Part-I (substitution method): A linear regression approach. *Asian Journal of Pharmacy and Technology, 6*(4), 223-230.

Brenner, T., Wang, Z., Achayuthakan, P., Nakajima, T., & Nishinari, K. (2013). Rheology and synergy of κ-carrageenan/locust bean gum/konjac glucomannan gels. *Carbohydrate Polymers, 98*(1), 754-760.

Buchanan, C., & Gardner, L. (2019). Metal 3D printing in construction: A review of methods, research, applications, opportunities and challenges. *Engineering Structures, 180*, 332-348.

Chen, Z., Li, Z., Li, J., Liu, C., Lao, C., Fu, Y., Liu, C., Li, Y., Wang, P., & He, Y. (2019). 3D printing of ceramics: A review. *Journal of the European Ceramic Society, 39*(4), 661-687.

Chimene, D., Lennox, K. K., Kaunas, R. R., & Gaharwar, A. K. (2016). Advanced Bioinks for 3D Printing: A Materials Science Perspective. *Ann Biomed Eng, 44*(6), 2090-2102.

Choonara, Y. E., du Toit, L. C., Kumar, P., Kondiah, P. P. D., & Pillay, V. (2016). 3D-printing and the effect on medical costs: a new era? *Expert Review of Pharmacoeconomics & Outcomes Research, 16*(1), 23-32.

Cohen, J. S. (1999). Ways to minimize adverse drug reactions: individualized doses and common sense are key. *Postgraduate medicine, 106*(3), 163-172.

Compaan, A. M., Song, K., & Huang, Y. (2019). Gellan Fluid Gel as a Versatile Support Bath Material for Fluid Extrusion Bioprinting. *ACS applied materials & interfaces, 11*(6), 5714-5726.

Costakis, W. J., Rueschhoff, L. M., Diaz-Cano, A. I., Youngblood, J. P., & Trice, R. W. (2016). Additive manufacturing of boron carbide via continuous filament direct ink writing of aqueous ceramic suspensions. *Journal of the European Ceramic Society, 36*(14), 3249-3256.

Dalafu, H., Chua, M. T., & Chakraborty, S. (2010). Development of κ-Carrageenan Poly (acrylic acid) Interpenetrating Network Hydrogel as Wound Dressing Patch. In *Biomaterials* (pp. 125-135): ACS Publications.

Daniel-da-Silva, A. L., Ferreira, L., Gil, A. M., & Trindade, T. (2011). Synthesis and swelling behavior of temperature responsive kappa-carrageenan nanogels. *J Colloid Interface Sci, 355*(2), 512-517.

Diañez, I., Gallegos, C., Brito-de la Fuente, E., Martínez, I., Valencia, C., Sánchez, M. C., Diaz, M. J., & Franco, J. M. (2019). 3D printing in situ gelification of κ-carrageenan solutions: Effect of printing variables on the rheological response. *Food Hydrocolloids, 87*, 321-330.

Diaz, J. V., Van Bommel, K. J. C., Noort, M. W.-J., Henket, J., & Briër, P. (2018). Method for the production of edible objects using sls and food products. In: Google Patents.

Djabourov, M., Leblond, J., & Papon, P. (1988). Gelation of aqueous gelatin solutions. II. Rheology of the sol-gel transition. *Journal de Physique, 49*(2), 333-343.

Falk, B., Garramone, S., & Shivkumar, S. (2004). Diffusion coefficient of paracetamol in a chitosan hydrogel. *Materials Letters, 58*(26), 3261-3265.

Fina, F., Goyanes, A., Madla, C. M., Awad, A., Trenfield, S. J., Kuek, J. M., Patel, P., Gaisford, S., & Basit, A. W. (2018). 3D printing of drug-loaded gyroid lattices using selective laser sintering. *International journal of pharmaceutics, 547*(1-2), 44-52.

Ganji, F., Vasheghani, S., & Vasheghani, E. (2010). Theoretical description of hydrogel swelling: A review. *Iranian Polymer Journal (English), 19*(5 (119)), 375-398.

Garrec, D. A., & Norton, I. T. (2012). Understanding fluid gel formation and properties. *Journal of Food Engineering, 112*(3), 175-182.

Garrec, D. A., & Norton, I. T. (2013). Kappa carrageenan fluid gel material properties. Part 2: Tribology. *Food Hydrocolloids, 33*(1), 160-167.

Gholamipour-Shirazi, A., Norton, I. T., & Mills, T. (2019). Designing hydrocolloid based food-ink formulations for extrusion 3D printing. *Food Hydrocolloids, 95*, 161-167.

Gibaldi, M., & Feldman, S. (1967). Establishment of sink conditions in dissolution rate determinations. Theoretical considerations and application to nondisintegrating dosage forms. *Journal of pharmaceutical sciences, 56*(10), 1238-1242.

Goyanes, Buanz, A. B., Basit, A. W., & Gaisford, S. (2014). Fused-filament 3D printing (3DP) for fabrication of tablets. *International journal of pharmaceutics, 476*(1-2), 88-92.

Goyanes, A., Scarpa, M., Kamlow, M., Gaisford, S., Basit, A. W., & Orlu, M. (2017). Patient acceptability of 3D printed medicines. *Int J Pharm, 530*(1-2), 71-78.

Grządka, E. (2015). Interactions between kappa-carrageenan and some surfactants in the bulk solution and at the surface of alumina. *Carbohydrate Polymers, 123*, 1-7.

Hansen, L. G., & Warwick, W. J. (1978). An improved assay method for serum vitamins A and E using fluorometry. *American Journal of Clinical Pathology, 70*(6), 922-923.

Hermansson, A.-M., Eriksson, E., & Jordansson, E. (1991). Effects of potassium, sodium and calcium on the microstructure and rheological behaviour of kappa-carrageenan gels. *Carbohydrate Polymers, 16*(3), 297-320.

Hinton, T. J., Jallerat, Q., Palchesko, R. N., Park, J. H., Grodzicki, M. S., Shue, H.-J., Ramadan, M. H., Hudson, A. R., & Feinberg, A. W. (2015). Three-dimensional printing of complex biological structures by freeform reversible embedding of suspended hydrogels. *Science advances, 1*(9), e1500758.

Iijima, M., Hatakeyama, T., & Hatakeyama, H. (2014). Gel–sol–gel transition of kappa-carrageenan and methylcellulose binary systems studied by differential scanning calorimetry. *Thermochimica Acta, 596*, 63-69.

Ito, A., & Sugihara, M. (1996). Development of oral dosage form for elderly patient: use of agar as base of rapidly disintegrating oral tablets. *Chemical and pharmaceutical bulletin, 44*(11), 2132-2136.

Jin, Y., Compaan, A., Bhattacharjee, T., & Huang, Y. (2016). Granular gel support-enabled extrusion of three-dimensional alginate and cellular structures. *Biofabrication, 8*(2), 025016.

Jones, D. S., Woolfson, A. D., & Brown, A. F. (1997). Textural, viscoelastic and mucoadhesive properties of pharmaceutical gels composed of cellulose polymers. *International journal of pharmaceutics, 151*(2), 223-233.

Jones, D. S., Woolfson, A. D., Djokic, J., & Coulter, W. (1996). Development and mechanical characterization of bioadhesive semi-solid, polymeric systems containing tetracycline for the treatment of periodontal diseases. *Pharmaceutical research, 13*(11), 1734-1738.

Kevadiya, B. D., Joshi, G. V., Patel, H. A., Ingole, P. G., Mody, H. M., & Bajaj, H. C. (2010). Montmorillonite-alginate nanocomposites as a drug delivery system: intercalation and in vitro release of vitamin B1 and vitamin B6. *Journal of biomaterials applications, 25*(2), 161-177.

Kim, H. W., Bae, H., & Park, H. J. (2017). Classification of the printability of selected food for 3D printing: Development of an assessment method using hydrocolloids as reference material. *Journal of Food Engineering, 215*, 23-32.

Kim, H. W., Lee, I. J., Park, S. M., Lee, J. H., Nguyen, M.-H., & Park, H. J. (2019). Effect of hydrocolloid addition on dimensional stability in post-processing of 3D printable cookie dough. *Lwt, 101*, 69-75.

Kim, H. W., Lee, J. H., Park, S. M., Lee, M. H., Lee, I. W., Doh, H. S., & Park, H. J. (2018). Effect of hydrocolloids on rheological properties and printability of vegetable inks for 3D food Printing. *Journal of food science, 83*(12), 2923-2932.

Koprnický, J., Najman, P., & Šafka, J. (2017). 3D printed bionic prosthetic hands. In *2017 IEEE International Workshop of Electronics, Control, Measurement, Signals and their Application to Mechatronics (ECMSM)* (pp. 1-6).

Kouzani, A. Z., Adams, S., J. Whyte, D., Oliver, R., Hemsley, B., Palmer, S., & Balandin, S. (2017). 3D Printing of Food for People with Swallowing Difficulties. *KnE Engineering, 2*(2).

Kril, J. J. (1996). Neuropathology of thiamine deficiency disorders. *Metabolic brain disease, 11*(1), 9-17.

Lanaro, M., Desselle, M. R., & Woodruff, M. A. (2019). 3D Printing Chocolate. In *Fundamentals of 3D Food Printing and Applications* (pp. 151-173).

Le Tohic, C., O'Sullivan, J. J., Drapala, K. P., Chartrin, V., Chan, T., Morrison, A. P., Kerry, J. P., & Kelly, A. L. (2018). Effect of 3D printing on the structure and textural properties of processed cheese. *Journal of Food Engineering, 220*, 56-64.

Li, H.-p., Li, H.-j., Qi, L.-h., Jun, L., & Zuo, H.-s. (2014). Simulation on deposition and solidification processes of 7075 Al alloy droplets in 3D printing technology. *Transactions of Nonferrous Metals Society of China, 24*(6), 1836-1843.

Liang, S., Xu, J., Weng, L., Dai, H., Zhang, X., & Zhang, L. (2006). Protein diffusion in agarose hydrogel in situ measured by improved refractive index method. *Journal of controlled release, 115*(2), 189-196.

Lin, C. (2015). 3D Food Printing: A Taste of the Future. *14*(3), 86-87.

Liu, S., & Li, L. (2016). Thermoreversible gelation and scaling behavior of Ca 2+ -induced κ-carrageenan hydrogels. *Food Hydrocolloids, 61*, 793-800.

Liu, Z., Zhang, M., & Yang, C.-h. (2018). Dual extrusion 3D printing of mashed potatoes/strawberry juice gel. *Lwt, 96*, 589-596.

Long, J., Etxeberria, A. E., Nand, A. V., Bunt, C. R., Ray, S., & Seyfoddin, A. (2019). A 3D printed chitosan-pectin hydrogel wound dressing for lidocaine hydrochloride delivery. *Materials Science and Engineering: C, 104*, 109873.

Lupo, B., Maestro, A., Gutiérrez, J. M., & González, C. (2015). Characterization of alginate beads with encapsulated cocoa extract to prepare functional food: comparison of two gelation mechanisms. *Food Hydrocolloids, 49*, 25-34.

McCue, T. (2012). 3D printing industry will reach $3.1 billion worldwide by 2016. *Retrieved, 3*(02), 2015.

Meena, R., Prasad, K., & Siddhanta, A. K. (2007). Effect of genipin, a naturally occurring crosslinker on the properties of kappa-carrageenan. *Int J Biol Macromol, 41*(1), 94-101.

Melocchi, A., Parietti, F., Loreti, G., Maroni, A., Gazzaniga, A., & Zema, L. (2015). 3D printing by fused deposition modeling (FDM) of a swellable/erodible capsular device for oral pulsatile release of drugs. *Journal of Drug Delivery Science and Technology, 30*, 360-367.

Nayak, K. K., & Gupta, P. (2015). In vitro biocompatibility study of keratin/agar scaffold for tissue engineering. *International journal of biological macromolecules, 81*, 1-10.

Ngo, T. D., Kashani, A., Imbalzano, G., Nguyen, K. T. Q., & Hui, D. (2018). Additive manufacturing (3D printing): A review of materials, methods, applications and challenges. *Composites Part B: Engineering, 143*, 172-196.

Nishinari, K. (1997). Rheological and DSC study of sol-gel transition in aqueous dispersions of industrially important polymers and colloids. *Colloid and Polymer Science, 275*(12), 1093.

Normand, V. (2003). Effect of sucrose on agarose gels mechanical behaviour. *Carbohydrate Polymers, 54*(1), 83-95.

Norton, I. T., Morris, E. R., & Rees, D. A. (1984). Lyotropic effects of simple anions on the conformation and interactions of kappa-carrageenan. *Carbohydrate research, 134*(1), 89-101.

Özcan, İ., Abacı, Ö., Uztan, A. H., Aksu, B., Boyacıoğlu, H., Güneri, T., & Özer, Ö. (2009). Enhanced topical delivery of terbinafine hydrochloride with chitosan hydrogels. *AAPS PharmSciTech, 10*(3), 1024.

Padzi, M., Bazin, M. M., & Muhamad, W. (2017). Fatigue Characteristics of 3D Printed Acrylonitrile Butadiene Styrene (ABS). In *Materials Science and Engineering Conference Series* (Vol. 269, pp. 012060).

Patil, N. S., Dordick, J. S., & Rethwisch, D. G. (1996). Macroporous poly (sucrose acrylate) hydrogel for controlled release of macromolecules. *Biomaterials, 17*(24), 2343-2350.

Peppas, N. A., & Sahlin, J. J. (1989). A simple equation for the description of solute release. III. Coupling of diffusion and relaxation. *International journal of pharmaceutics, 57*(2), 169-172.

Pharmacopoeia, B. (2016). *British pharmacopoeia.*

Phillips, G. O., & Williams, P. A. (2000). *Handbook of hydrocolloids*: CRC press Boca Raton, FL.

Picker, K. M. (1999). Matrix tablets of carrageenans. II. Release behavior and effect of added cations. *Drug development and industrial pharmacy, 25*(3), 339-346.

Rahim, T. N. A. T., Abdullah, A. M., & Md Akil, H. (2019). Recent Developments in Fused Deposition Modeling-Based 3D Printing of Polymers and Their Composites. *Polymer Reviews, 59*(4), 589-624.

Rosas-Durazo, A., Hernández, J., Lizardi, J., Higuera-Ciapara, I., Goycoolea, F. M., & Argüelles-Monal, W. (2011). Gelation processes in the non-stoichiometric polylectrolyte–surfactant complex between κ-carrageenan and dodecyltrimethylammonium chloride in KCl. *Soft Matter, 7*(5), 2103-2112.

Rosenthal, A. J. (2010). Texture profile analysis–how important are the parameters? *Journal of Texture Studies, 41*(5), 672-684.

Rutz, A. L., Hyland, K. E., Jakus, A. E., Burghardt, W. R., & Shah, R. N. (2015). A multimaterial bioink method for 3D printing tunable, cell-compatible hydrogels. *Advanced Materials, 27*(9), 1607-1614.

Saha, D., & Bhattacharya, S. (2010). Hydrocolloids as thickening and gelling agents in food: a critical review. *J Food Sci Technol, 47*(6), 587-597.

Santoro, M., Marchetti, P., Rossi, F., Perale, G., Castiglione, F., Mele, A., & Masi, M. (2011). Smart Approach To Evaluate Drug Diffusivity in Injectable Agar−Carbomer Hydrogels for Drug Delivery. *The Journal of Physical Chemistry B, 115*(11), 2503-2510.

Serizawa, R., Shitara, M., Gong, J., Makino, M., Kabir, M. H., & Furukawa, H. (2014). *3D jet printer of edible gels for food creation* (Vol. 9058): SPIE.

Severini, C., Derossi, A., & Azzollini, D. (2016). Variables affecting the printability of foods: Preliminary tests on cereal-based products. *Innovative Food Science & Emerging Technologies, 38*, 281-291.

Severini, C., Derossi, A., Ricci, I., Caporizzi, R., & Fiore, A. (2018). Printing a blend of fruit and vegetables. New advances on critical variables and shelf life of 3D edible objects. *Journal of Food Engineering, 220*, 89-100.

Singh, B., Kaur, T., & Singh, S. (1997). Correction of raw dissolution data for loss of drug and volume during sampling. *Indian journal of pharmaceutical sciences, 59*(4), 196.

Singh, D., Singh, D., & Han, S. S. (2016). 3D Printing of Scaffold for Cells Delivery: Advances in Skin Tissue Engineering. *Polymers (Basel), 8*(1).

Sood, A. K., Ohdar, R. K., & Mahapatra, S. S. (2010). Parametric appraisal of mechanical property of fused deposition modelling processed parts. *Materials & design, 31*(1), 287-295.

Tako, M., & Nakamura, S. (1988). Gelation mechanism of agarose. *Carbohydrate research, 180*(2), 277-284.

Thrimawithana, T. R., Young, S., Dunstan, D. E., & Alany, R. G. (2010). Texture and rheological characterization of kappa and iota carrageenan in the presence of counter ions. *Carbohydrate Polymers, 82*(1), 69-77.

Tomšič, M., Prossnigg, F., & Glatter, O. (2008). A thermoreversible double gel: Characterization of a methylcellulose and κ-carrageenan mixed system in water by SAXS, DSC and rheology. *Journal of Colloid and Interface Science, 322*(1), 41-50.

Varghese, J. S., Chellappa, N., & Fathima, N. N. (2014). Gelatin–carrageenan hydrogels: role of pore size distribution on drug delivery process. *Colloids and Surfaces B: Biointerfaces, 113*, 346-351.

Ventola, C. L. (2014). Medical Applications for 3D Printing: Current and Projected Uses. *P & T : a peer-reviewed journal for formulary management, 39*(10), 704-711.

Vrentas, J., & Vrentas, C. M. (1992). Fickian diffusion in glassy polymer-solvent systems. *Journal of Polymer Science Part B: Polymer Physics, 30*(9), 1005-1011.

Wang, L., Zhang, M., Bhandari, B., & Yang, C. (2018). Investigation on fish surimi gel as promising food material for 3D printing. *Journal of Food Engineering, 220*, 101-108.

Warner, E. L., Norton, I. T., & Mills, T. B. (2019). Comparing the viscoelastic properties of gelatin and different concentrations of kappa-carrageenan mixtures for additive manufacturing applications. *Journal of Food Engineering, 246*, 58-66.

Watase, M., & Arakawa, K. (1968). Rheological properties of hydrogels of agar-agar. III. Stress relaxation of agarose gels. *Bulletin of the Chemical Society of Japan, 41*(8), 1830-1834.

Wei, J., Wang, J., Su, S., Wang, S., Qiu, J., Zhang, Z., Christopher, G., Ning, F., & Cong, W. (2015). 3D printing of an extremely tough hydrogel. *RSC Advances, 5*(99), 81324-81329.

Weiner, M. L. (1991). Toxicological properties of carrageenan. *Agents and actions, 32*(1-2), 46-51.

Wu, Y., Joseph, S., & Aluru, N. R. (2009). Effect of cross-linking on the diffusion of water, ions, and small molecules in hydrogels. *The Journal of Physical Chemistry B, 113*(11), 3512-3520.

Yang, F., Zhang, M., Bhandari, B., & Liu, Y. (2018). Investigation on lemon juice gel as food material for 3D printing and optimization of printing parameters. *Lwt, 87*, 67-76.

Yang, F., Zhang, M., Prakash, S., & Liu, Y. (2018). Physical properties of 3D printed baking dough as affected by different compositions. *Innovative Food Science & Emerging Technologies, 49*, 202-210.

Zhang, Y.-Q., Tsai, Y.-C., Monie, A., Hung, C.-F., & Wu, T.-C. (2010). Carrageenan as an adjuvant to enhance peptide-based vaccine potency. *Vaccine, 28*(32), 5212-5219.

Chapter 4

3D printing of kappa-carrageenan emulsion gels

This chapter was published as

Kamlow, M.-A., Spyropoulos, F., & Mills, T. (2021). 3D printing of kappa-carrageenan emulsion gels. Food Hydrocolloids for Health, 1, 100044

Michael-Alex Kamlow: Conceptualization, Methodology, Formal analysis, Investigation, Writing - original draft; Fotis Spyropoulos: Writing - review & editing, Supervision; Tom Mills: Writing - review & editing, Supervision, Funding acquisition.

Abstract

The interest in personalised food through 3D printing has led to an increased demand for more complex foodstuffs suitable for 3D printing rather than just simple water-based systems. 3% w/w Kappa-carrageenan (κC) emulsion gels were created containing 5-40% w/w sunflower oil (SFO); using two different emulsifiers, Tween 20 (T20) and Whey protein isolate (WPI). Differential scanning calorimetry showed that both T20 and WPI stabilised emulsions had only minor effects on the gelling and melting enthalpies of the κC, and had the same gelling temperatures. All tested formulations were printable under the same printing parameters, provided the feed rate was increased with SFO concentration. Confocal microscopy showed the presence of layering throughout the printed gels and that T20-stabilised emulsion gels had flocculated. Texture profile analysis was used to compare printed and cast 20x20x9.6 mm cuboids. For cast cuboids, as the SFO concentration increased, the hardness values decreased from 75 N ± 4 N to 18 N ± 1.5 N. For printed cuboids the hardness values were constant at 13 N ± 2 N. Upon compression, printed cuboids delaminated at the areas between the printed layers. Oscillatory rheology showed that cast gels were more resistant to shear strain compared to the printed gels and this was again believed to occur due to delamination between the semi-fused printed layers. This work demonstrates that 3D printed κC emulsion gels maintain their mechanical performance regardless of SFO concentration up to 40%.

4.1 Introduction

Since hydrogels are generally formed using approximately 0.1-10% w/v hydrocolloid, small quantities of salts and the rest water, issues exist when it comes to the incorporation of hydrophobic molecules within such constructs. One approach to address this is to create oil-in-water (o/w) emulsions by dispersing oil within a continuous water phase and then allowing this to gel (as it would normally) to create emulsion gels, with the gel matrix acting as the continuous phase. This allows the creation of more complex structures and the incorporation of an oil phase enables straightforward encapsulation of lipophilic molecules within the gel matrix. Emulsion gels have been researched for a long time (Hemker, 1981) and their uses include modification of food texture (Matsumura, Kang, Sakamoto, Motoki, & Mori, 1993), delivery of lipophilic drugs (Thakur, et al., 2012) and dual delivery of lipo- and hydrophilic drugs (Singla, Saini, Joshi, & Rana, 2012).

Since 3DP of food materials allows for customisation of food structures through ingredient placement (Diaz, Noort, & Van Bommel, 2017), it makes sense that the creation of more complex emulsion gels, as opposed to hydrogels should be an area of interest for researchers. This will allow highly customised food items that could still retain the desirable creamy mouth feel of fat-based foods, but through use of an emulsion gel could reduce the overall fat content of the food itself (Sala, de Wijk, van de Velde, & van Aken, 2008). ΚC emulsion gels have had some research dedicated to them (Fontes-Candia, Ström, Lopez-Sanchez, López-Rubio, & Martínez-Sanz, 2020; Sala, et al., 2008), however, to the authors' knowledge there exists little if any literature on the 3DP of κC emulsion gels despite its usefulness as both a food additive and 3DP biopolymer ink. Most studies into 3DP of emulsion gels appear to be based on cold-extrusion techniques (Du, et al., 2021; Y. Liu, Y. Yu, et al., 2019; Sager, Munk, Hansen, Bredie, & Ahrné, 2021), with none assessing whether varying oil concentrations or emulsifiers could affect printability within hot-extrusion 3DP.

This study formulated 3% w/w κC emulsion gels containing a range of sunflower oil concentrations (5-40% w/w). Once simple o/w emulsions were produced, the droplet size was

tested via laser diffraction and emulsion stability was assessed via zeta-potential measurements. The emulsion was then examined under a light microscope in order to ascertain whether flocculation had occurred or not. After this, emulsion gels were created by dispersing the κC powder into the simple o/w emulsions. The κC emulsion gels were assessed based on the oil concentration and its effects on 3DP κC emulsion gels. Two emulsifiers with different stabilisation mechanisms, were compared since it was hypothesised that the differences in their structures and charge could lead to variation in their interactions with the gel structure. They were evaluated by micro differential scanning calorimetry (μDSC) in order to ascertain their T_{gel} and melting temperature (T_{melt}), as well as their gelling and melting enthalpies. Following this, 3D printing took place, testing several parameters to optimise print quality. After suitable and consistent 3DP emulsion gels could be fabricated the gels' mechanical properties were ascertained through texture profile analysis (TPA) and oscillatory rheology comparing printed gels to cast gels over a range of oil concentrations. Finally, the emulsion gels were imaged using confocal laser scanning microscopy (CLSM) in order to visualise any difference between 3DP and cast emulsion gels as well as emulsion gels stabilised by T20 and WPI.

4.2 Materials and methods

4.2.1 Materials

κC and T20 and were purchased from Sigma-Aldrich (UK). Nile red was purchased from Fischer Scientific (UK). WPI was obtained from Sachsenmilch Milk & Whey Ingredients (Sachsenmilch Leppersdorf GmbH, Wachau, Germany). According to the manufacturer it contained 93.74% w/w protein in dry matter, 0.23% w/w fat, 0.61% w/w lactose and 3.16% w/w ash. Sunflower oil was purchased from the supermarket Spar (UK). Milli-Q water was used (Elix® 5 distillation apparatus, Millipore®, USA) for sample preparation. All materials were used as received with no further modification or purification.

4.2.2 Preparation of κC solutions containing emulsifiers

κC solutions containing the emulsifiers were produced to be used as 0% w/w sunflower oil gels. This was to ensure any changes observed were caused by the presence of the sunflower oil and not just the emulsifying agent. κC solutions containing T20 were produced by adding 3% w/w κC to 192 mL of deionised water which had been placed on top of a hotplate-stirrer set to 80 °C. A magnetic stir bar was used to aid with dispersion of the κC into the water. This was left to stir for two hours. After the κC had dispersed 1% w/w T20 was added to the heated κC solution and this was stirred at a lower speed for another 30 minutes following the method set out in previous studies (Fenton, Kanyuck, Mills, & Pelan, 2021). κC solutions containing WPI were produced by first dispersing 2% w/w WPI in deionised water and stirring at 40 °C for five hours. This WPI stock solution was then stored in the fridge overnight to allow for full hydration. 100g of the 2% w/w WPI solution was then diluted by adding to 94 g of deionised water. This was then heated and the κC powder dispersed as above. This gave a final solution of 1% w/w WPI and 3% w/w κC.

4.2.3 Emulsion preparation

Simple emulsions containing no κC were produced in for particle size analysis and zeta-potential measurements. This was because these tests cannot be carried out in a straightforward manner on gelled samples. Sunflower O/W emulsions stabilised with T20 were produced by first measuring out the required amount of water and then adding 1% w/w of T20 to the water. This was stirred gently with a magnetic stirrer for 10 minutes. Then, the required percentage of oil was added and premixed on a Silverson L5M for 3 minutes at 6000 rpm with a fine emulsor screen. The formed pre-emulsion was then passed through a high-pressure homogeniser at 25 bar. O/W emulsions stabilised with WPI were made by using the WPI stock solution described in 4.2.2, which was added to the required amount of oil and processed as described for the T20 emulsions.

4.2.4 κC-Emulsion solution preparation

T20 and WPI stabilised O/W emulsions (as described in section 4.2.3) were used for the preparation of κC-emulsion solutions. Emulsions were first placed on a hotplate-stirrer set to 80°C for 30 min. Then, κC was added and left to stir for two hours to ensure that all κC had been dispersed. Because of the varying amount of oil (dispersed) phase in the emulsions, the amount of κC added to each system was kept constant at 3% w/w with reference to (in each case) the aqueous (continuous) phase fraction. In this way the amount of κC in the aqueous phase of all O/W emulsions (regardless of their oil content) was the same. The 3% w/w κC concentration was chosen as this was previously reported to give optimal printing outcomes (Kamlow, Vadodaria, Gholamipour-Shirazi, Spyropoulos, & Mills, 2021). Finally, O/W emulsion gels were formed by cooling the systems, either via 3D printing as described in section 4.2.8 or casting in moulds as described in section 4.2.9.

4.2.5 Particle size analysis

The emulsion droplet size was obtained using a Malvern Mastersizer MS 2000 (Malvern Panalytical, UK), utilising a Hydro SM manual small volume sample dispersion unit. The values for refractive index were input into the software and were 1.33 for water and 1.467 for the sunflower oil. The sample was dispersed in distilled water at 1300 rpm until an obscuration value of 4.2-4.6% was achieved. This gave values for the volume mean droplet diameter ($d_{4,3}$) and unless stated otherwise, droplet size refers to this parameter. Samples were prepared and tested in triplicate and droplet size values were the average of at least three measurements. Droplet size values were obtained immediately after preparation.

4.2.6 Zeta-potential measurement

The zeta potential (ζ-potential) was determined using a Zetasizer (Malvern Panalytical, UK) in order to assess the stability of the emulsions created. Samples were diluted 100 times with deionised water (Y. Wu, et al., 2016). This was to reduce the absorbance of laser light and multiple scattering. All ζ-potential measurements were carried out at room temperature.

Samples were prepared and tested in triplicate, and the zeta-potential values were the average of at least three measurements.

4.2.7 Micro differential scanning calorimetry

Micro Differential Scanning Calorimetry (μDSC) was carried out using a Seteram MicroDSC3 evo (Seteram, France). Experiments were performed over a range of temperatures for the hydrogels and the emulsion gels following the same procedure as that previously described by (Kamlow, et al., 2021). The tested temperature range was 0-70 °C, and tests were carried out at a scan rate of 1 °C per minute for both cooling and heating. The samples were first cooled to 0 °C and held for 60 min and then heated to 70 °C and cooled back down to 0 °C. This was repeated three times per sample. This temperature range was chosen since all thermal transitions occurred within this range. Each different formulation was tested in triplicate in this manner, giving a total of nine cooling and heating curves per formulation.

4.2.8 3D printing

The 3D printer was supplied by the Institute of Food Science and Biotechnology at the University of Hohenheim (Germany). A Fabbster 3D printer was modified in order to handle a liquid feed. This modification involved retrofitting several hoses onto the printer containing inner pipes where the material flows through and a surrounding water environment i to maintain the temperature of the gel to keep it in the sol state. These were connected to two water baths. These pipes carry water to and from the printer by counter-flow. One set was responsible for the gel solution being kept above its T_{gel} from the syringe to the nozzle (1. and 2. in Figure 4.1A) and the other set ensured that the temperature within the final length of pipe including the nozzle can be controlled (3. and 4. in Figure 4.1A). This enabled maintenance of the sol state, which would then enable the sol-gel transition to occur *in situ* as with previous studies (Kamlow, et al., 2021; Warner, et al., 2019). This prevented any pre-gelation before the feed material reached the nozzle. To further control the rate at which the phase transition could occur, there was a heated bed, with a removable section (6. and 7. in Figure 4.1A). The temperature was controlled by a third water bath connected by insulated pipes (5. in Figure

4.1A). The syringe pump (8. in Figure 4.1A) was equipped with a 60 mL syringe wrapped with a heating pad (9. and 10. in Figure 4.1A). This prevented the feed material in the syringe from undergoing premature gelation. The heating pad was powered with a computer power supply unit and controlled with an Arduino Uno, to control the heating pad temperature (11. and 12. in Figure 4.1A). Several temperature probes were placed at various points on the printer and monitored with a data logger (13 in Figure 4.1A). The printer was controlled by a laptop connected to a controller (14. and 15. in Figure 4.1A). This allowed to the printer to move in the XYZ axis via the arms and motors that form the frame of the printer (16. and 17. in Figure 4.1A). Figure 4.1B shows the nozzle itself. The outer pipe (4. in Figure 4.1B) was copper and inside contained a smaller brass pipe where the feed material flowed through. It was held in place using a stainless-steel mount made by the technical workshop of the University of Hohenheim. This was surrounded by water flowing in a counter current to the flow of the feed material. There were two 3D printed parts (3. and 7. in Figure 4.1B) which allowed connection of the pipes and formed the nozzle from which the gels were extruded onto the printing bed. Thermocouples monitoring the temperature of the feed material were placed at the top and the bottom of the copper pipe (2. and 6. in Figure 4.1B). Several parameters for the printing itself were tested. Some were controlled by the printer software (Netfabb for Fabbster, Fabbster, Germany), such as layer height, print speed and fill spacing. These parameters have been shown to have a major effect on print fidelity in food systems before (Severini, Derossi, Ricci, Caporizzi, & Fiore, 2018; Fanli Yang, Zhang, Bhandari, & Liu, 2018). The nature of this printer's operation meant that the syringe driver rate was responsible for the amount of material extruded and so this had to be tested and controlled. Print success was judged according to weight consistency and final shape fidelity (Chimene, Lennox, Kaunas, & Gaharwar, 2016).

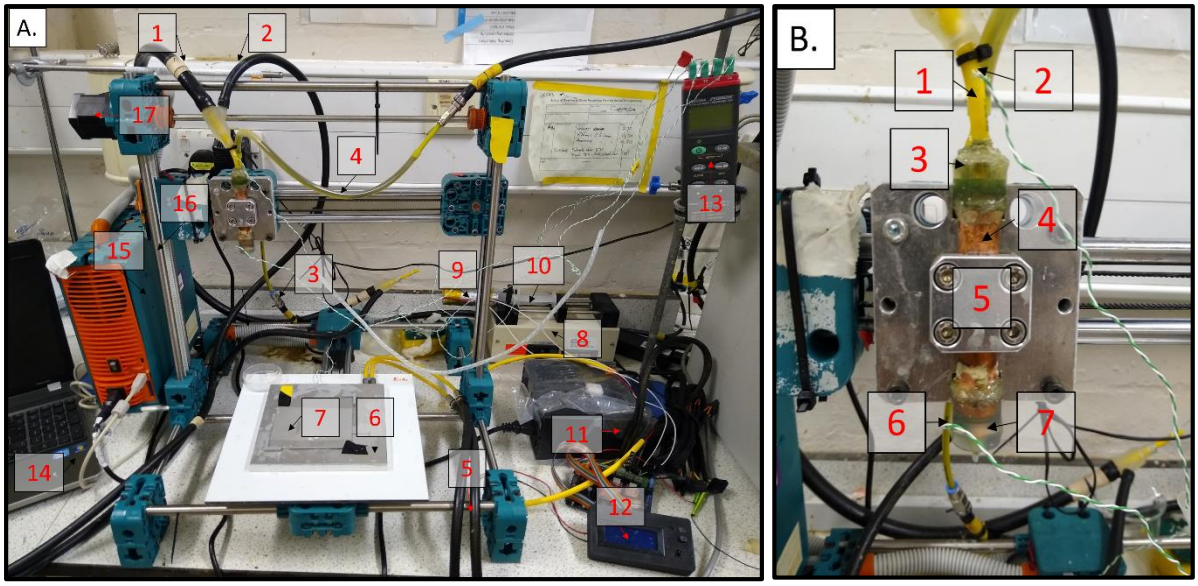

*Figure 4.1: Schematic of the retrofitted Fabbster printer (**A**) including 1) Jacketed pipe from the syringe to the nozzle, 2) Jacketed pipe from the nozzle to the water bath, 3) Jacketed pipe from a water bath to the bottom of the nozzle, 4) Pipe from the top of the nozzle to the water bath, 5) Jacketed pipes to and from a water bath to the temperature controlled bed, 6) Temperature controlled printing bed 7) Removable section of the printing bed 8) Syringe driver, 9) Heating jacket, 10) 60 mL syringe, 11) Power supply unit, 12) Controller for heating jacket, 13) Data logger, 14) Laptop to control printer, 15) Controller unit for the printer, 16) Support rods for the printer, 17) Support rods and motor for the printer. (**B**) Schematic of the printer nozzle including 1) Feed pipe into the nozzle, 2) Thermocouple to monitor temperature of feed material as it enters the nozzle, 3) 3D printed part to connect feed pipe to the copper pipe, 4) Copper outer pipe containing brass inner pipe, 5) Bracket to hold copper pipe in place, 6) Thermocouple to monitor temperature of feed material as it enters the die, 7) 3D Printed nozzle. The printer was connected to and controlled by a computer running Netfabb for Fabbster software.*

4.2.9 Production of moulds for casting

A cuboid shaped mould was produced by stereolithography 3D printing using a form 2 3D printer (Formlabs, USA). The mould was designed by CAD and uploaded to the software, this was then sliced and sent to the printer digitally to print. This mould would allow the production of hydrogel and emulsion gel cuboids with dimensions of 20x20x9.6 mm by casting. These were then used for comparative mechanical testing as a control, cast sample to compare to the 3D printed cuboids produced in 4.2.8.

4.2.10 Texture profile analysis

Texture profile analysis (TPA) was carried out using a TA XT plus Texture Analyser as described in previous studies (Kamlow, et al., 2021). Printed and cast cuboids of dimensions 20×20×9.6 mm were tested; the cast cuboids were given 3 minutes 30 seconds to set, mimicking the time taken to print their respective counterparts. Tests were carried out using a

P/40 cylindrical aluminium probe set to a constant speed of 1 mm/s, alongside a 30 kg load cell and 3 g of trigger force. Through compression testing, data for hardness and Young's modulus was acquired for printed and cast cuboids. Hardness is calculated from the peak force during the initial compression cycle, while Young's modulus is the stiffness of the material calculated through the stress/strain relationship of the material at low strains (Jones, Woolfson, & Brown, 1997). All tests were carried out in triplicate, and the hardness and Young's modulus values were the average of at least three measurements.

4.2.11 Rheological testing

Rheological tests were performed using a modular compact rheometer 302 (Anton Paar, Austria) using a parallel 25 mm serrated plate. For cast gels, the rheometer was heated to 60 °C and then the sample was loaded on. Then a working gap of 1mm was used and the excess trimmed off. The temperature was then lowered to 20 °C and each sample was left to equilibrate for ten minutes. Then amplitude sweeps were performed at a fixed frequency of 1 Hz and the strain amplitude was varied from 0.1-10%. This matched previous studies where gel brittleness made testing above that level of strain unnecessary (Jong, 2020; Loizou, et al., 2006). For 3DP samples a disc 1 mm high and 30 mm in diameter was printed. Owing to the inability to reliably remove the single layer disc from the printing bed, the printing bed was removed and placed on the rheometer. The printing bed was 1 mm thick, so the rheometer was set to use a 2.015 mm working gap owing to the placement of foil on the bottom plate of the rheometer to prevent it being scratched by the printing bed. This allowed for reliable data to be obtained and the printed sample was given eight minutes to equilibrate at 20 °C. This allowed for the 40 second print time and the approximate one minute needed to transfer the print bed containing the sample to the rheometer. This gave data for the linear viscoelastic region (LVER), storage modulus (G′), loss modulus (G″) and G′ as the function of shear strain. Samples were prepared and tested in triplicate, and the values were the average of at least three measurements.

4.2.12 Confocal laser scanning microscopy

Emulsion gel samples were produced for CLSM by the addition of nile red to the oil phase before emulsification. A Leica DM2500 confocal microscope (Leica®, CH) was used for the imaging. Three different objective lenses were used 10 times, 40 times and 63 times, with immersion oil being used for the 63 times objective. A 532 nm laser at 100% intensity was used to excite the dye and emissions at the range of 550-700 nm wavelength were detected for imaging in line with previous studies (Vadodaria, He, Mills, & Wildman, 2020). Stained, gelled samples were placed onto glass slides. For 3DP samples discs 500 μm high and 18 mm in diameter were printed directly onto a glass slide and a glass cover slip was placed over the top.

4.2.13 Statistics

The average droplet size, hardness and Young's modulus values were compared using the two-sample T-test in the Analysis ToolPack for Microsoft Excel. Confidence levels were set at 95%. Therefore, if $P < 0.05$, the two sets of data have different means, otherwise the two means have no significant difference.

4.3 Results and discussion

4.3.1 Droplet size analysis and zeta-potential measurements

The droplet sizes of O/W emulsions stabilised by either T20 or WPI and containing varying amounts of sunflower oil (dispersed phase) were measured; the droplet size data is presented in Figure 4.2A, with the distributions presented in Figures 4.2B and 4.2C. To minimise the risk of phase inversion in the system, the sunflower oil content in the emulsions was kept below 50%. The emulsifier concentration (T20 or WPI) was fixed at 1% w/w which was sufficient to enable emulsion stabilisation. Stability in this instance, was determined by no separation, coarsening or flocculation being observed during production and testing of the simple emulsion systems at any SFO concentration.

Statistical analysis showed no significant difference between the SFO concentrations' effect on droplet sizes. Another point of note is that increasing the amount of dispersed phase can have a negative impact on the longer term stability of emulsions containing emulsifier concentrations used in this study (Dapčević Hadnađev, Dokić, Krstonošić, & Hadnađev, 2013). However, this was not an issue in this case as shortly after the formation of these emulsions they were to be 3D printed into κC-emulsion gels. The data in Figure 4.2A also shows that on average the emulsions stabilised by T20 had smaller droplet sizes than those stabilised by WPI, ranging from around 11-13 μm and 18-22 μm respectively, which was a statistically significant difference ($P < 0.05$). This is due to low molecular weight surfactants (LMWS), owing to their smaller size and molecular weight, being able to position themselves at the interface quicker than proteins, which take longer to orientate and unfold themselves at the interface (Kenta, et al., 2013). Furthermore, LMWS such as T20 decrease interfacial tension more than proteins, and this further enhances droplet breakup (Beverung, Radke, & Blanch, 1999).

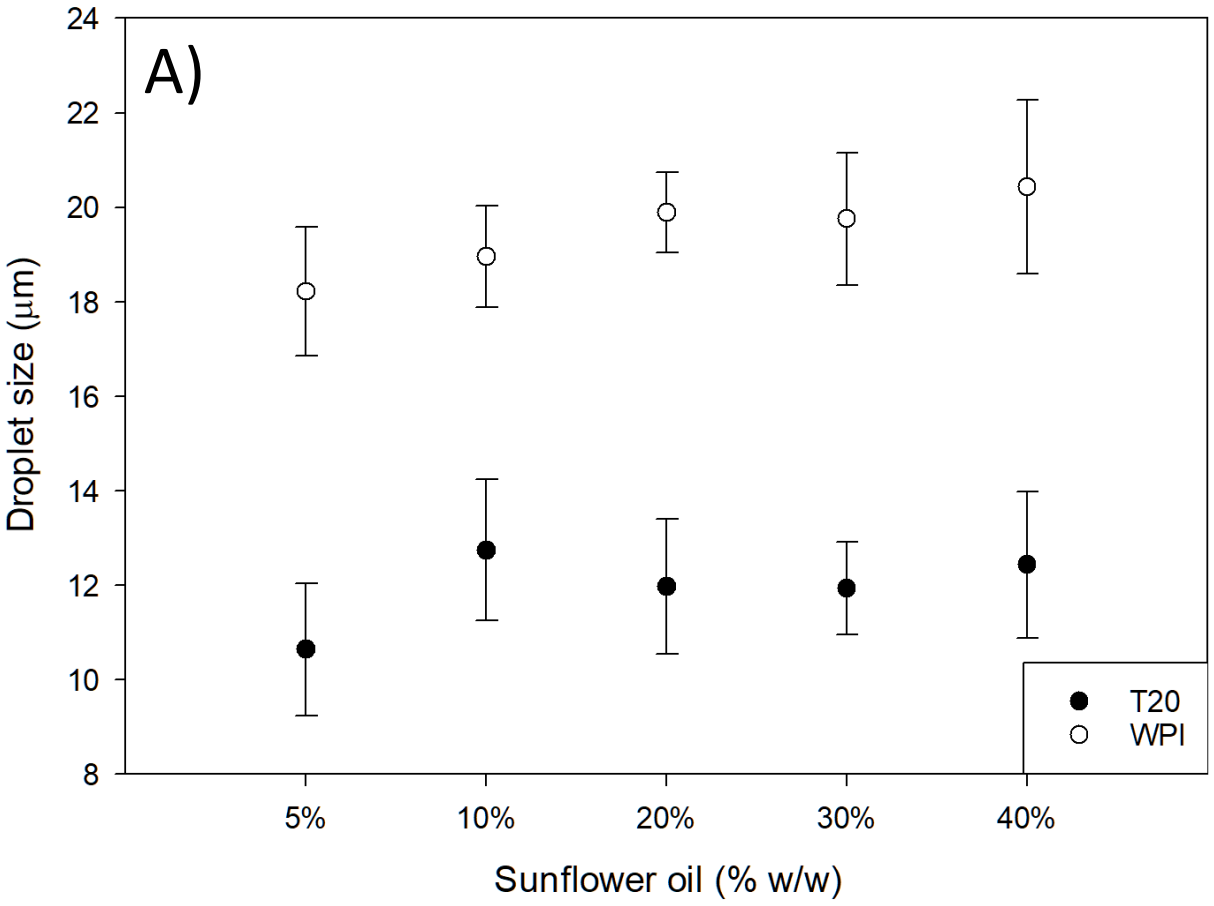
A)
Droplet size (μm)
24
22
20
18
16
14
12
10
8
5%
10%
20%
30%
40%
Sunflower oil (% w/w)
T20
WPI

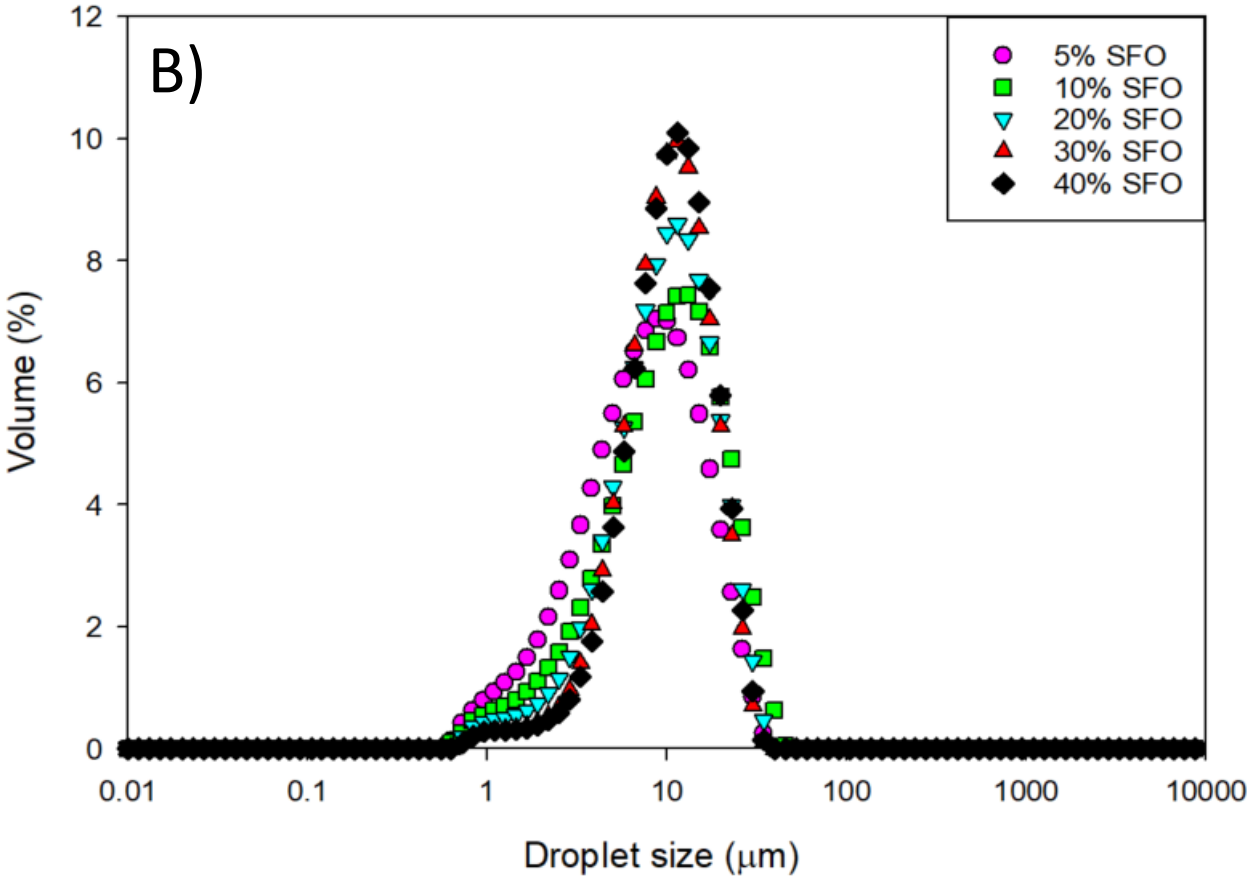
B)
Volume (%)
12
10
8
6
4
2
0
0.01
0.1
1
10
100
1000
10000
Droplet size (μm)
5% SFO
10% SFO
20% SFO
30% SFO
40% SFO

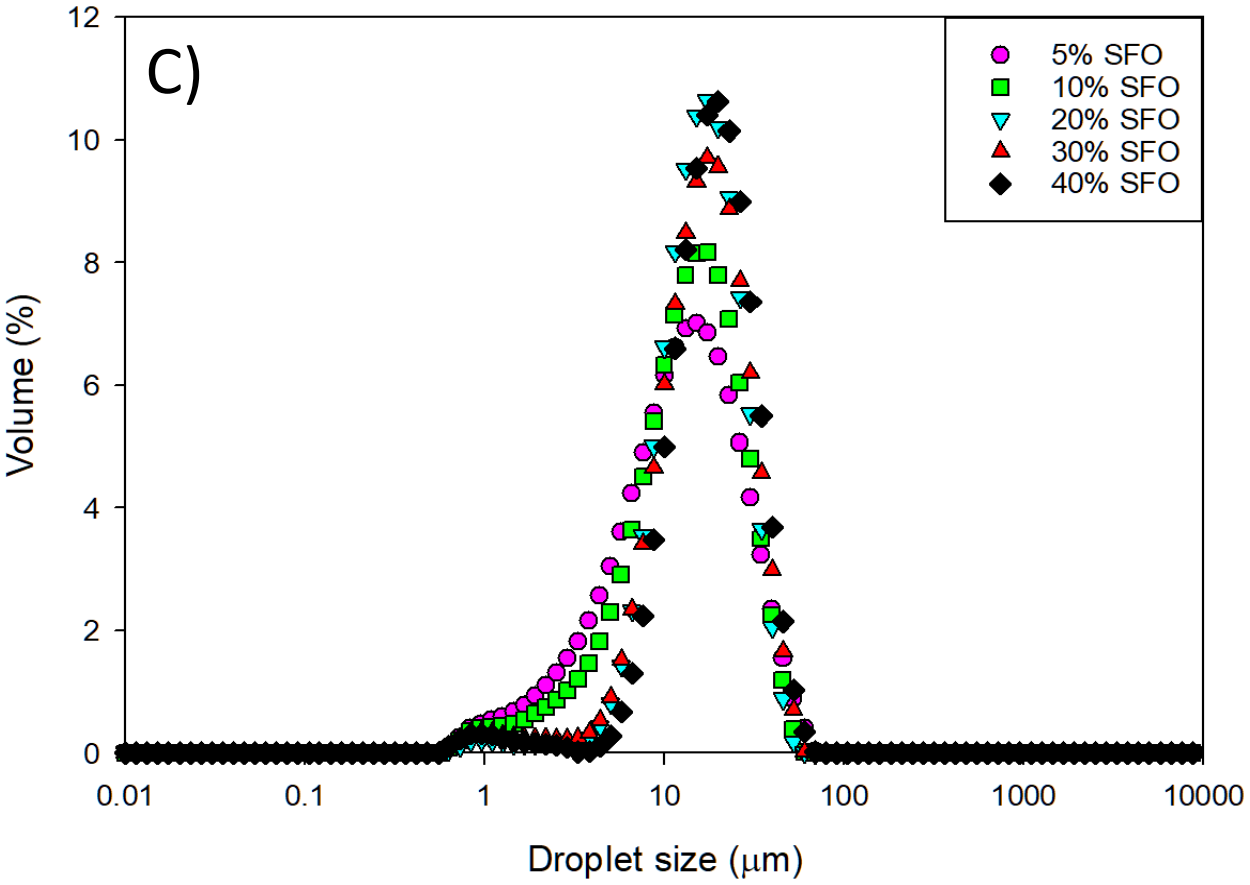

Figure 4.2: A) Comparison of the average droplet size of emulsions produced using a range of sunflower oil concentrations and 1% T20 or 1% WPI, B) Droplet size distribution for T20 stabilised emulsions and C) Droplet size distribution for WPI stabilised emulsions.

After producing the emulsions, they were then tested for their ζ-potential to assess the surface charge on the oil droplets. The results for the ζ-potential measurements are shown in Figure 4.3. The ζ-potential values for the emulsions stabilised by T20, show that T20 does not carry much surface charge giving values of -6mV to -8mV. This is typical for non-ionic emulsifiers, since they do not rely on surface charge to stabilise emulsions but instead do it through steric repulsion (Teo, et al., 2016). However, even though non-ionic surfactants would not expect to present with any surface charge, it has been shown before that ionised surface-active impurities like free fatty acids can lead to some charge being detectable in emulsions stabilised by non-ionic surfactants (M.-H. Wu, Yan, Chen, & He, 2017). Whereas because the emulsions were all at neutral pH, the emulsions stabilised by WPI had a negative charge. This is because neutral pH is above the isoelectric point of the WPI which, is around 4-6 (Chanamai & McClements, 2002), giving the protein molecules a negative surface charge. This explains

why the WPI emulsions had ζ-potential values of around -34mv to -37mv with the small differences being within the error values of each other.

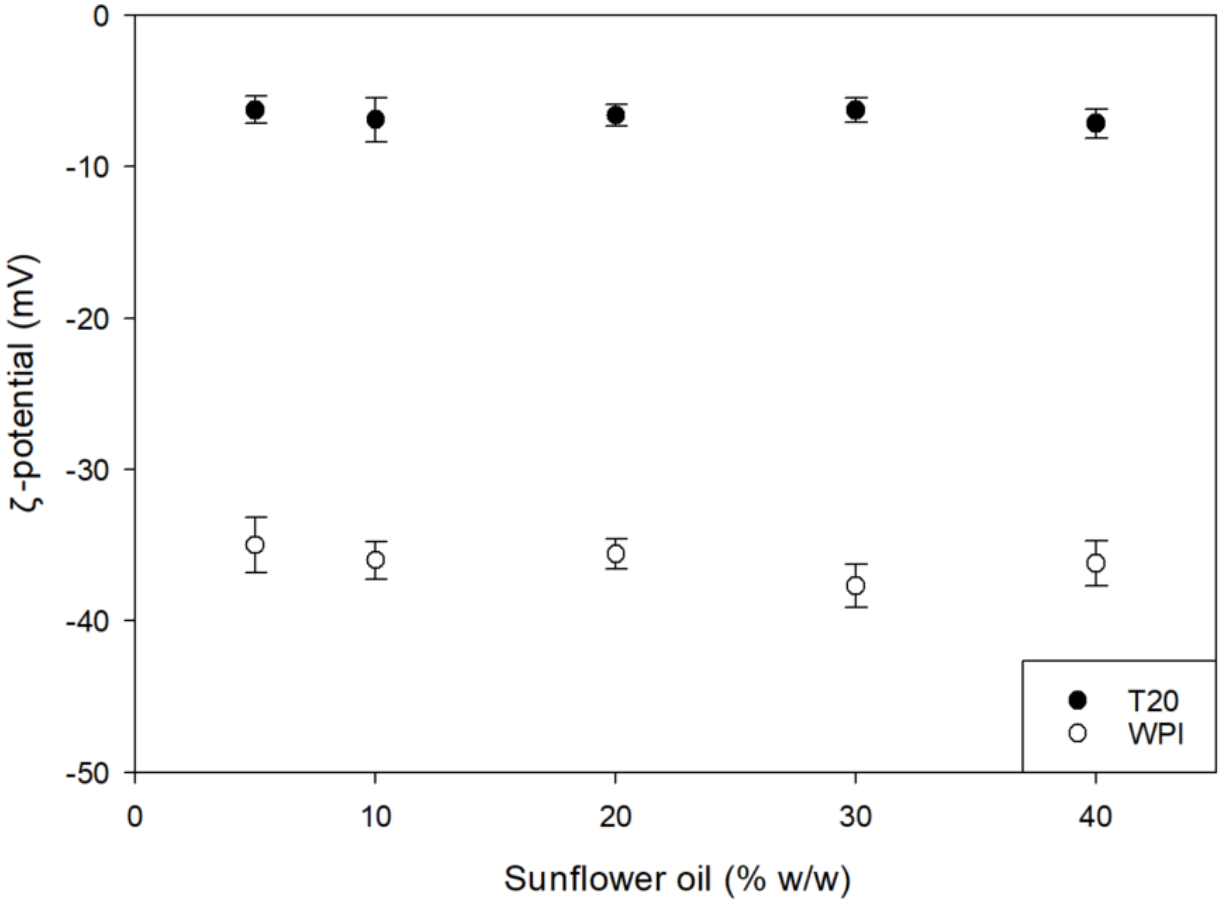

Figure 4.3: ζ-potential of O/W emulsions stabilised by either T20 or WPI as a function of sunflower oil (dispersed phase) content.

4.3.2 Pre-printing μDSC analysis of emulsion gels

It was first important to establish the thermal characteristics of the κC gels, as this is necessary in designing printable formulations for hot-extrusion printing. After they were established, then κC emulsion gels could be characterised and assessed for their suitability in 3DP. Previous studies reported that increasing the concentration of oil led to an increase in gel strength, T_{gel} and T_{melt} values. However, this was due to the total concentration of κC remaining constant in the formulations, leading to an effective increase in κC concentration in the water phase as the oil concentration increased (Fontes-Candia, et al., 2020). So, it was important to assess the effects of varying oil concentration on the T_{gel} and T_{melt} of κC-emulsion gels while

maintaining the same concentration of κC in the water phase. The sol-gel transition temperatures of the emulsion gel systems were determined using a micro differential scanning calorimeter (Iijima, Hatakeyama, Takahashi, & Hatakeyama, 2007; Snoeren & Payens, 1976; Williams, Clegg, Langdon, Nishinari, & Piculell, 1993). The results for mean T_{gel} and T_{melt} for 3% κC emulsion gels with 0, 5, 10, 20, 30 and 40% w/w sunflower oil are shown in Figure 4.4A. Gelling and melting enthalpies for the assessed systems are found in Figure 4.4B. Figures 4.5A and 4.5B show the DSC micrographs for gelation and melting respectively.

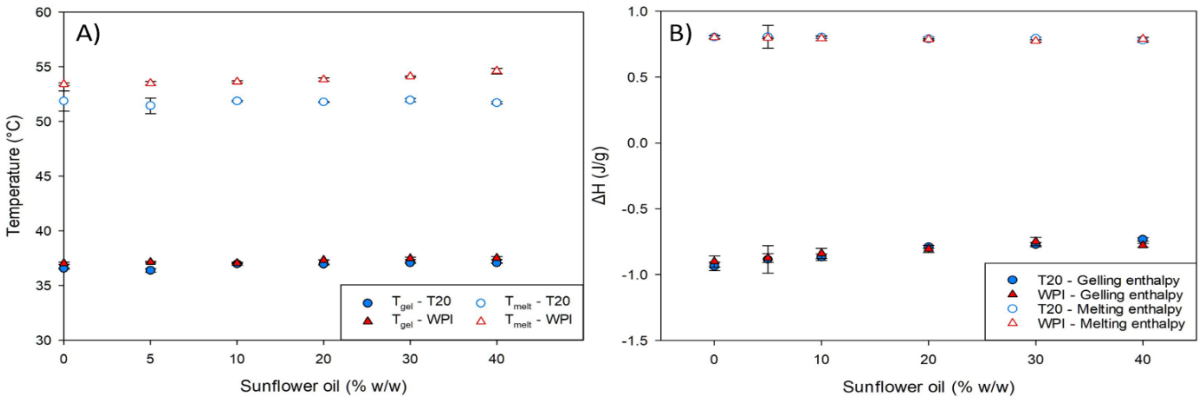

Figure 4.4: DSC data for (A) the average thermal transition temperatures (Tgel and Tmelt) and (B) the gelling and melting enthalpies of κC emulsion gels with varying sunflower oil concentrations, stabilised by Tween 20 and WPI

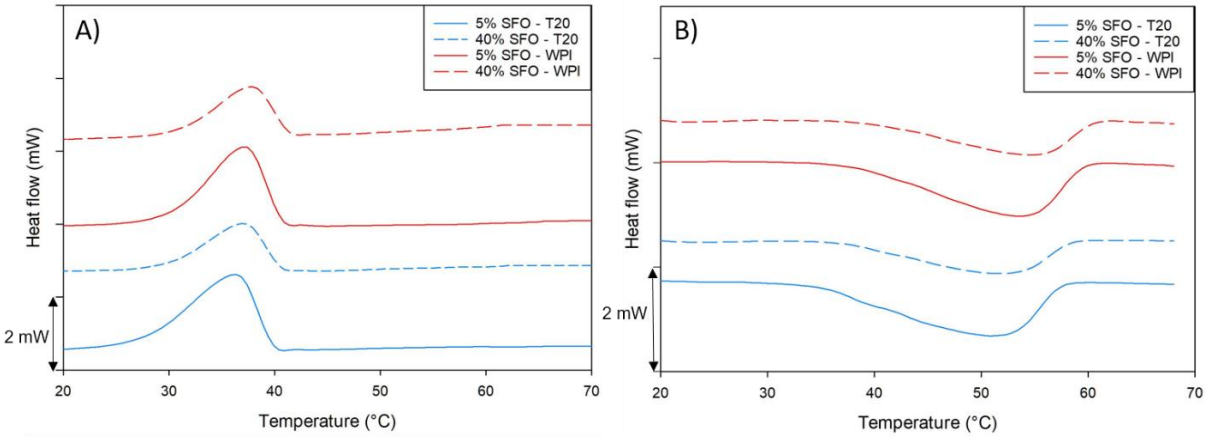

Figure 4.5: DSC micrograph data for (A) the gelling and (B) melting enthalpies of κC emulsion gels, stabilised by Tween 20 and whey protein isolate, with 5% and 40% w/w concentrations of sunflower oil

Figure 4.4A shows that if the concentration of κC is kept constant in the water phase of emulsion gels, the T_{gel} and T_{melt} of the systems stay approximately constant. This was important, because if the concentration of the κC was not adjusted to remain at 3% w/w in the water phase, then the effective concentration would have kept increasing and each

concentration of SFO would have required different printing parameters, adding an additional layer of complexity during production. Furthermore, as far as the data for T_{gel} in Figure 4.4A shows, both emulsifiers had the same T_{gel} values, of 36-37 °C. This meant that they could be printed at the same temperatures. However, the T_{melt} data showed that there was a statistically significant disparity of 1-2 °C between the emulsion gels stabilised by T20 and those stabilised by WPI. As stated in 2.2.1 the WPI was assessed to contain 3.16% ash. Milk-based ash is known to contain cations such as potassium and calcium (Aaltonen, Kytö, Ylisjunttila-Huusko, & Outinen, 2020). Cations are known to cause the reinforcement of κC gel networks (Hermansson, et al., 1991) and so would cause an increase in the melting temperature. However, another explanation could have been that the WPI was interacting with the κC. Though this was unlikely as the WPI was at pH 7, which is above its isoelectric point and therefore its overall net charge would be negative. Since κC in anionic, it cannot electrostatically interact with another anionic molecule such as negatively charged WPI. However, the enthalpy data in Figure 4.4B suggests that there was no interaction between WPI and κC as the enthalpy values for both types of emulsion gels are approximately equal. This implies that there were no new bonds being formed, which would indicate that the differences seen in Figure 4.4A were down to the presence of cations with the WPI, reinforcing the κC gel network.

The data in Figure 4.4B shows that once normalised to a constant κC concentration, the gelling and melting enthalpies remain practically consistent, with a slight decrease seen in the gelling enthalpies. This shows that addition of the oil has little, if any impact on the gel network itself. This is in contrast with what has been observed with emulsion gel studies before (Dun, et al., 2020; Liu, Zhang, et al., 2019). These studies did not appear to normalise their data to κC concentration per 100 g of water, which since adding more oil would lead to less κC per 100g, led to an apparent decrease in enthalpy values. Since the emulsion droplets were coated in either a non-ionic surfactant (T20) or a negatively charged protein they were non-interacting filler particles. Therefore they did not enhance the gel network, unlike an interacting filler (Mcclements, Monahan, & Kinsella, 1993)

4.3.3 Hydrogel and emulsion gel printing

All printed emulsion gel samples contained 3% w/w κC in the water phase, 1% w/w emulsifier and between 0-40% w/w sunflower oil. Since the μDSC data had shown the emulsion gels to have T_{gel} values of 36-37 °C, the temperature probe (16. in Figure 4.1B) was used to monitor the feed material and ensure that it would be exiting the nozzle around 9-11 °C higher than the gelling temperature. This has been shown to give optimal printing in previous studies (Warner, et al., 2019). The printing temperature was determined indirectly by the water baths attached to the printer, hence why the temperature probes were used to monitor the feed material temperature. The parameters tested for the 3D printing are shown in Table 4.1.

Table 4.1: A table showing the different parameters tested in the gel 3D printing process as well as failed prints showing a cube that the nozzle had dragged through, an over-extruded cube with excess material and an under-extruded cube with voids. Underneath are examples of failed prints

S_R (mL/min)	T_{PB} (°C)	v_p (mm/s)	Fill (mm)	T_{HWB} (°C)	T_{NWB} (°C)	3D Outcome and Comments
1.2	20	20	0.5	60	58	Over extruded – very poor shape fidelity
0.8	20	20	0.5	60	58	Over extruded – shape recognisable
0.6	20	20	0.5	60	58	Under extruded – voids in the print
0.7	20	20	0.5	60	58	No voids but poor bottom layer ruined print
0.7	40	20	0.5	60	58	Print bed too hot, shape couldn't be built up
0.7	35	20	0.5	60	58	Shape fidelity acceptable – layers not fused
0.7	35	20	0.5	66	66	Nozzle dragged through printed material
0.65	35	20	0.5	66	66	Nozzle dragged through printed material
0.65	35	20	0.75	66	66	First few layers fine, but top layers poor
0.65	35	20	1	66	66	Fidelity good, but voids present
0.7	35	20	1.25	66	66	Shape resembled CAD file, but layers still not well fused
0.7	35	20	1.25	72	72	Shape resembled CAD file; layers do not separate when handling
0.7	35	20	1.25	80	80	Shape resembled CAD file; layers do not separate upon handling – however, part of the printer deformed and broke at this temperature; so, it was not used any further
0.7	35	25	1.25	72	72	Shape resembled CAD file, even at higher speed; layers do not separate when handling
0.7	35	30	1.25	72	72	Shape resembled CAD file, even at higher speed; layers do not separate when handling
0.7	35	35	1.25	72	72	Shape fidelity less repeatable – speed to be kept at 30 mm/s

***S**R*: Syringe driver rate (mL/min)
***T**PB*: Printer bed temperature (°C)
***v**p*: Print speed (mm/s)
Fill: Fill space (mm)
***T**HWB*: Water bath temperature on the feed pipes (°C)
***T**NWB*: Water bath temperature on the nozzle (°C)

Apart from the parameters defined in Table 4.1, other parameters which were variable existed. These were layer height, nozzle size and nozzle height. The layer height was left as 1.2 mm because this was suggested in our previous study (Kamlow, et al., 2021) to be the optimal layer height for κC hydrogels; and this was confirmed to hold true in this study as well. The nozzle for the printer (7. in Figure 4.1B) was a 3DP part and had to be sealed with glue and silicone to prevent water leakage. Therefore, it was not practical to test and change various nozzle sizes, and therefore the same optimal nozzle size (20G/0.8mm) from the previous work was again used as the standard. Finally, the nozzle height was kept at a constant at 0.5 mm as these yielded prints with no issues and, unless stated otherwise, was the height used for all prints. The print settings from Table 4.1 that gave the best shape fidelity and reproducibility were: S_R of 0.7mL/min, T_{PB} of 35 ˚C, V_P of 30 mm/s, a Fill of 1.25 mm, T_{HWB} of 72 ˚C and T_{NWB} of 72 ˚C. The quality of the prints shown in Figure 4.5 demonstrate that the chosen parameters were appropriate for the printed κC gels.

Table 4.2: Table showing variances required in syringe driver rate in order to achieve successful printing based on SFO concentration

Sunflower oil concentration (% w/w)	Syringe driver rate (mL/min)
0	0.7
5	0.7
10	0.72
20	0.76
30	0.80
40	0.84

While the above settings were viable for 0% w/w SFO and 5% w/w SFO, voids were seen in higher oil concentrations under the same printing conditions as seen in Figure 4.6. These failed prints were believed to be due to the increasing concentration of sunflower oil in the κC-emulsion solutions. This led to an increase in the viscosity of the κC-emulsion solution, since the oil droplets are more densely packed (Pal & Rhodes, 1989). This meant that maintaining the S_R for higher oil concentrations led to a decrease in the amount of feed material being extruded. This problem can be overcome by increasing the extrusion rate to prevent the formation of voids (Dick, Bhandari, & Prakash, 2019). The nature of the printing setup used meant that this was achieved through increasing the S_R. The S_R values for acquiring high quality print outcomes are shown in Table 4.2. Once the optimal syringe driver rates for each sunflower oil concentration were determined it was possible to print complex geometries using any of the concentrations tested. Various prints from the printer are shown in Figure 4.6.

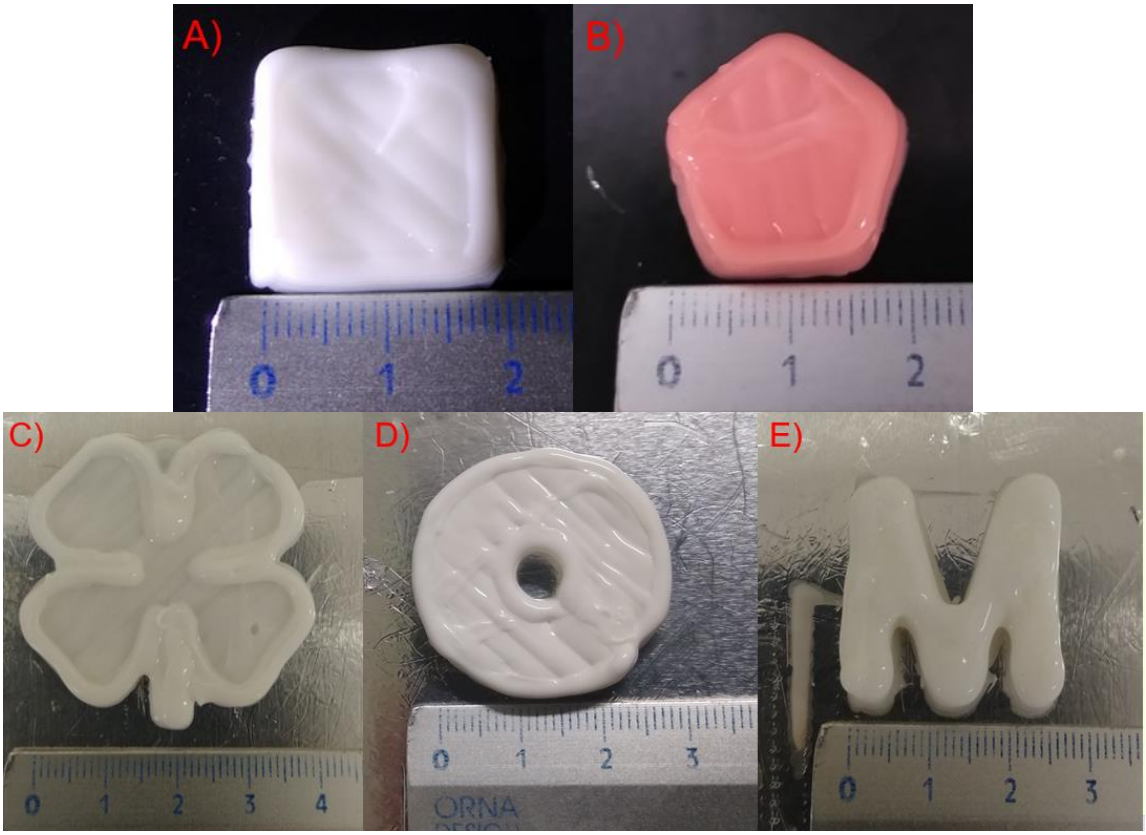

Figure 4.6: Examples of successful prints A) 5% SFO 20x20x9.6mm cuboid, B) Pentagon containing 10% SFO and 0.4% red food colouring, C) Four leaf clover printed with 20% SFO, D) Torus printed with 30% SFO and E) 'M' printed with 40% SFO.

4.3.4 Emulsion gel imaging

While the non-printed samples could be positioned onto a hot microscope slide and then a cover slip placed over them before they gelled, this was not feasible for the 3DP samples. The printer was unable to print a thin enough layer for light to pass through the gel. Furthermore, compression of samples with a cover slip has been shown to be problematic in terms of yielding a representative sample (Gibson & Lanni, 1991). Therefore, CLSM was used for both cast and 3DP emulsion gels; the sunflower oil dispersed phases of both printed and cast gels were stained with nile red. Confocal images in Figure 4.7 show the distribution of oil droplets in both cast and 3DP samples for emulsion gels stabilised by either T20 or WPI.

Representative confocal images show the distribution of the SFO droplets within the set κC matrices. As evidenced by Figure 4.7A, κC emulsion gels stabilised by T20 exhibited clear signs of flocculation between oil droplets. Whereas Figure 4.7B shows that the emulsion gels stabilised by WPI are well distributed throughout the gel network. The addition of low

concentrations of κC has been shown to cause extensive flocculation of emulsions by depletion effects. More specifically, when the κC is able to electrostatically interact with the molecules stabilising the emulsion droplets, bridging flocculation can take place (Gu, Decker, & McClements, 2005), such as when a protein below its isoelectric point is present. Otherwise, when the κC can't complex with the emulsifying agent, depletion flocculation is observed (Singh, Tamehana, Hemar, & Munro, 2003).

During the emulsion gel production, as the κC powder was dispersed, its concentration increased quickly, but the low concentrations that can cause depletion flocculation were still present for a certain time leading to flocculation effects. However, emulsions stabilised by T20, were created separately to κC hydrogel solutions and when combined together, immediately flocculated which means that at any κC concentration up to 3% w/w in the water phase, flocculation is observed in the emulsion gel systems. However, the WPI stabilised emulsion gels were still dispersed throughout the gel networks. It is believed that the thicker viscoelastic layer formed at the interface by the WPI particles compared to the T20 (Wilde, Mackie, Husband, Gunning, & Morris, 2004) before the addition of the κC gave these emulsions greater resistance to the depletion effects. Then, as the viscosity of the continuous phase increased with the κC (Iglauer, Wu, Shuler, Tang, & Goddard III, 2011) this slowed down the flocculation to a large extent, leading to presentation of dispersed emulsion gels. Another factor, shown in Figure 4.3 is the differences in ζ-potential between the T20 and WPI stabilised emulsion gels. Since WPI has a far higher level of negative charge on the oil droplets, they will repel each other more than the uncharged T20 droplets. This gives it more resistance to the flocculation effects.

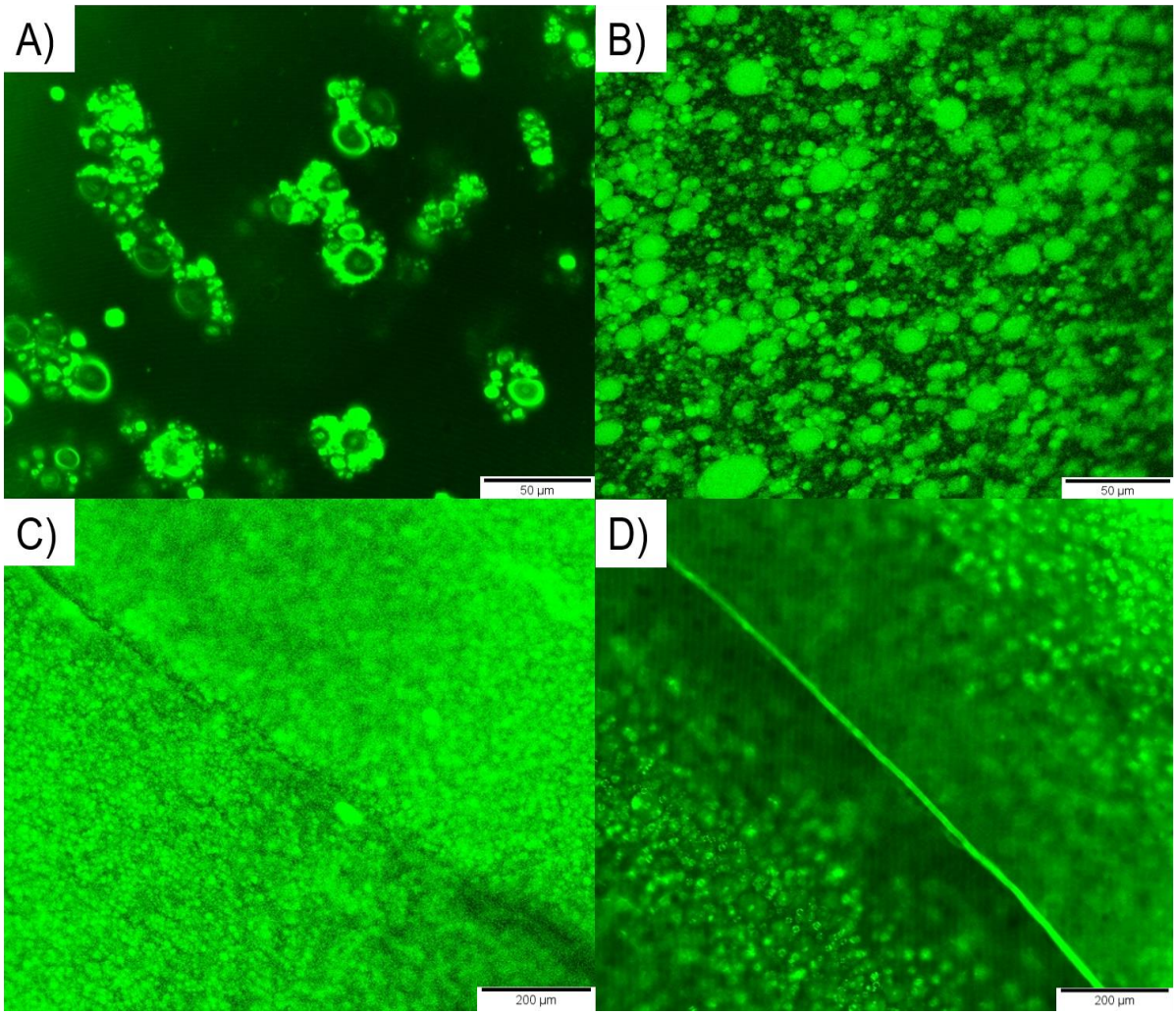

Figure 4.7: Confocal microscopy images of 10% w/w SFO A) cast κC-emulsion gel stabilised by T20, B) cast κC emulsion gel stabilised by WPI, C) 3DP κC emulsion gel stabilised by T20 and D) 3DP κC emulsion gel stabilised by WPI. The lines observed in C) and D) are lines of the printing observed at the same height. For more information see full text.

Figure 4.7C and 4.7D highlight the differences in the bulk structures produced by 3DP compared to those of traditional cast gels. The distinct layering that exists throughout the emulsion gels in Figure 4.7C and 4.7D due to printing is absent from the continuous networks seen in Figure 4.7A and 4.7B. It is created by the discontinuous network produced by the 3DP process, specifically the movement of the nozzle in the x- and y-axes. Variances in the planes of focus around the printed lines, indicate there are differences in depth around the lines themselves. This can be seen by the inability to focus and visualise all the oil droplets in the 3DP confocal images. This shows how the 3DP process gives a different surface to traditional casting. This can be imaged using a z-stack in which several planes of focus are put into a composite video or image.

4.3.5 Post-printing texture profile analysis

Texture profile analysis of gels is an established technique for testing the performance of their microstructure and whether this affects functionality. In the past, this has generally focused on the release of molecules, such as flavour (Boland, Delahunty, & van Ruth, 2006) and therapeutic molecules (Özcan, et al., 2009). 3D printing is known to fabricate structures with differing internal structure to their casted equivalents (Padzi, Bazin, & Muhamad, 2017) and previous works have demonstrated this to be true for hydrogels (Kamlow, et al., 2021). While there have been studies assessing the performance of emulsion gels by TPA (Sala, Van Aken, Stuart & van De Velde, 2007; Sala, van Vliet, Cohen Stuart, Aken, & van de Velde, 2009), there exists little literature examining TPA of 3DP emulsion gels. First typical stress/strain curves were obtained and these were analysed in order to calculate hardness and Young's modulus values of 3DP and cast cuboids containing varying concentrations of SFO.

The data from the TPA shows that as the concentration of the SFO increases, a decrease in both the hardness and Young's modulus values are observed for both types of cast emulsion gels. This is a known phenomenon whereby non-interacting filler particles disrupt the formation of the gel network, leading to weaker gels (Mcclements, et al., 1993).

Statistical analysis of the TPA data in Figure 4.8, again showed that there were no significant differences between the emulsion gels stabilised by WPI and T20 for hardness or Young's modulus. This was despite the salts present with the WPI reinforcing the κC network slightly as shown in Figure 4.4 as well as the flocculation of the T20 emulsion gels leading to larger effective droplet sizes within the network, which has been shown to weaken emulsion gels before (Kim, Gohtani, Matsuno, & Yamano, 1999). Another study into the large deformation properties of κC gels containing emulsions stabilised by WPI or T20 also found no significant difference between their Young's modulus, fracture stress and fracture strain values (Sala, et al., 2007). However, this study used a κC concentration of 0.75% w/w compared to the 3% w/w tested here. Furthermore, the oil droplets in the tested gels were around 1 µm compared to the 8-14 µm droplets in the emulsion gels tested in this study. This shows that there still

exists a conflict within the literature, owing to the various interlinked parameters that impact on the structural response of emulsion gels.

However, for the 3DP emulsion gels, the same approximate values for hardness and Young's modulus were observed regardless of oil concentration, with the values being constantly lower than those of the cast cuboids and unaffected by the increasing SFO concentration. A recent study by (Kamlow, et al., 2021) demonstrated that compression of 3DP gels leads to delamination rather than fracture, clearly suggesting that the weakest points of the discontinuous 3DP gel networks were the semi-fused sites between the printed layers. This demonstrates that 3DP produces gels that will behave the same regardless of SFO concentration up to 40%. The fact that all the printed gels could only withstand a peak force of around 10 N shows the relative weakness of the 3DP network. The lowest value recorded for the cast gels was around 16 N for 40% SFO stabilised emulsion gels. The effects of delamination could be lessened by printing at higher temperatures to promote greater layer fusion, although this could also lead to poorer shape fidelity as the printed solutions might not gel in time to hold their shape.

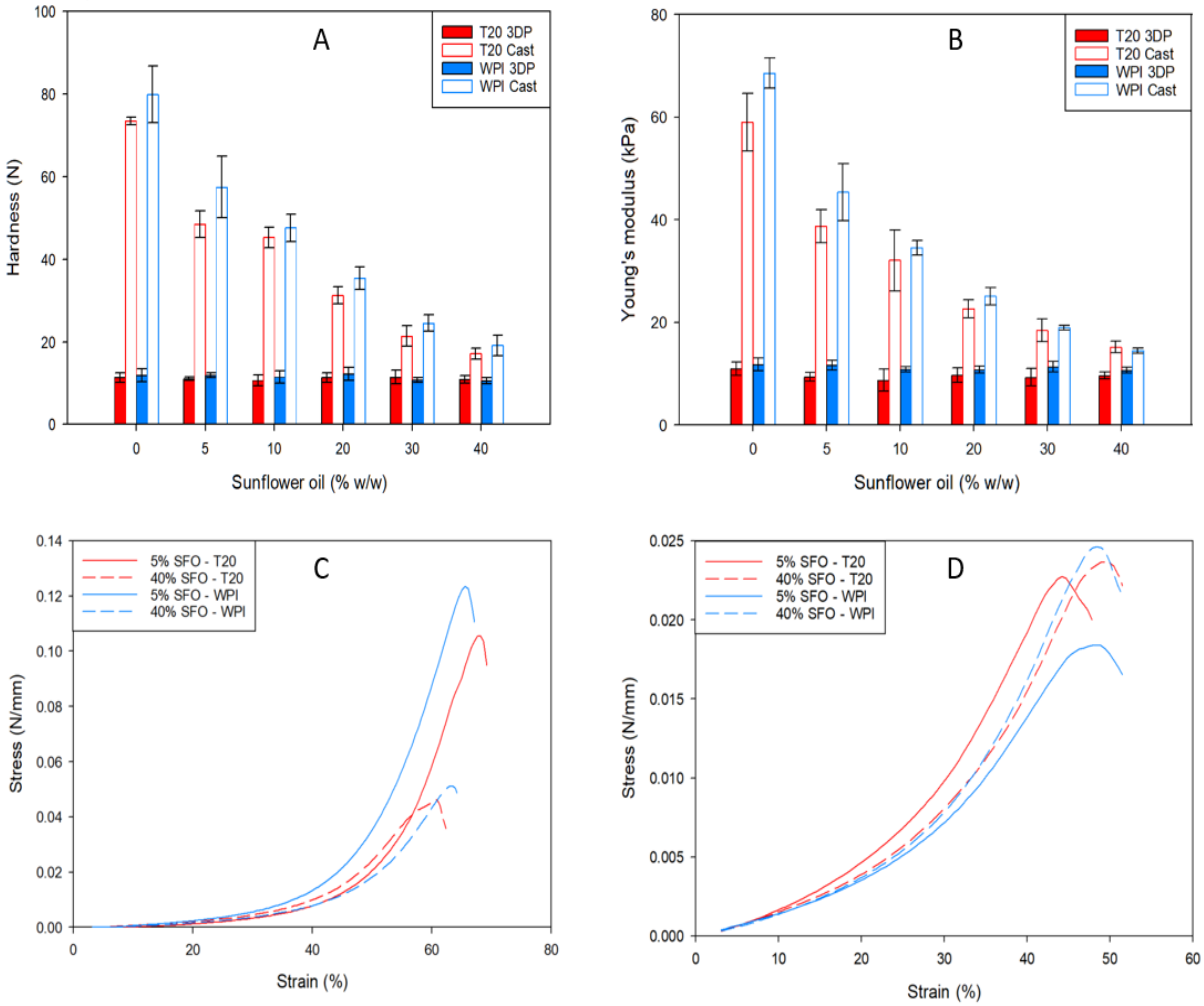

Figure 4.8: Hardness (A) and Young's modulus (B) of the printed and cast κC emulsion gel cuboids containing emulsions stabilised by T20 and WPI and stress-strain curves of cast (C) and 3DP (D) cuboids

4.3.6 Post-printing oscillatory rheology

Oscillatory rheology also reinforced the trends observed in the TPA data, with 3DP κC emulsion gels displaying different microstructural characteristics to cast gels. Data from the amplitude sweeps, from which the LVER is determined is shown in Figure 4.9.

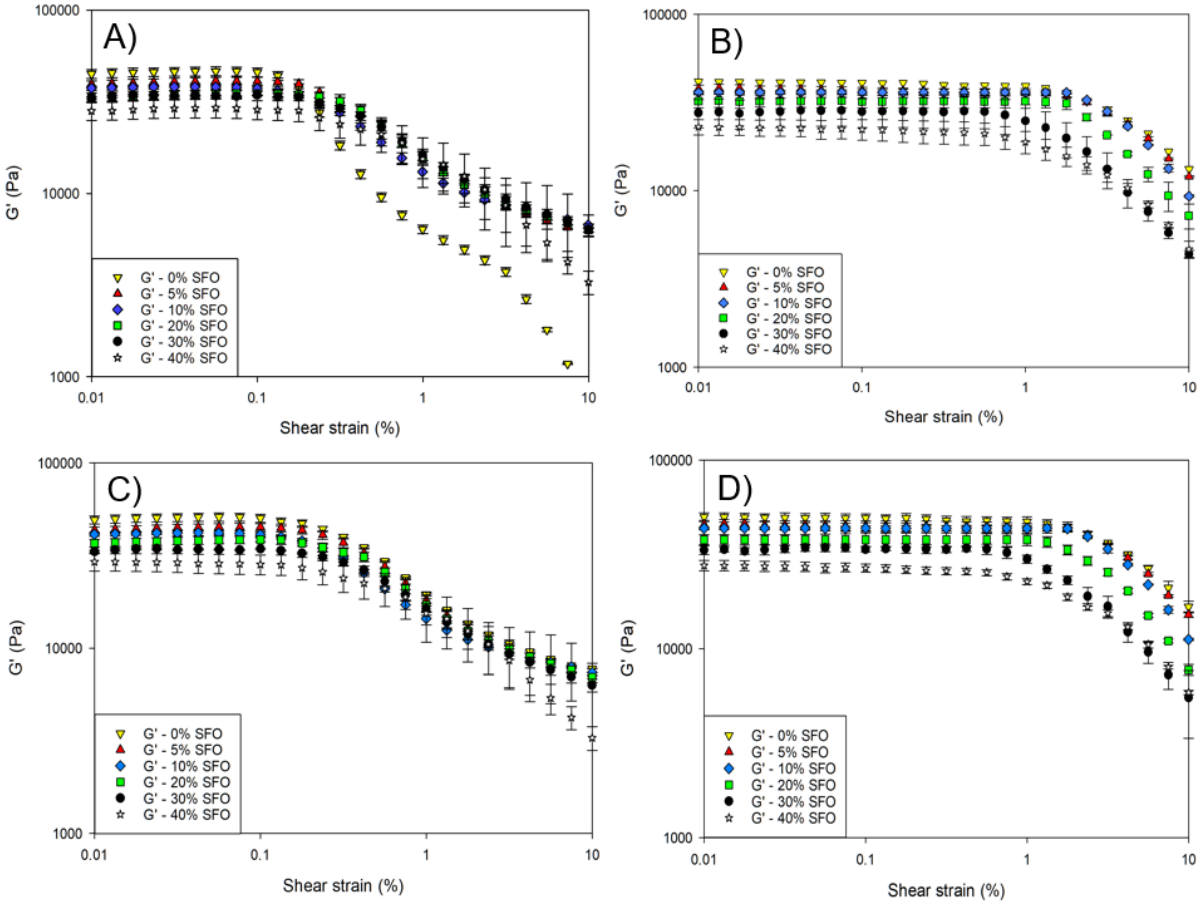

Figure 4.9: Amplitude sweep results for κC emulsion gels stabilised by T20 A) 3DP and B) cast, as well as κC emulsion gels stabilised by WPI C) 3DP and D) cast

The decreasing values for G′ as SFO concentration increased in the emulsion gels in both the 3DP and cast samples was in accordance with previous studies, whereby non-interacting filler particles reported lower G′ values (Farjami & Madadlou, 2019). This trend held true across the 3DP and cast gels regardless of which emulsifier was present. At all tested strain rates and SFO concentrations, WPI stabilised κC-emulsion gels were found to have a slightly higher G′, than those stabilised with T20, most probably owing to their reinforcement by the presence of salts. This is opposed to the TPA data from Figure 4.8, which showed no statistically significant differences between hardness and Young's modulus for the two systems. This highlights the importance of multiple analysis techniques when it comes to complex systems such as emulsion gels. While T20 has been shown to also reinforce κC gel networks, this was observed at higher concentrations (3% and above) (Fenton, et al., 2021). However, another possible reason for the slight difference in G′ was that, as shown by the CLSM images in Figure 4.7, WPI stabilised κC emulsion gels were not flocculated and therefore, while the data

in Figure 4.2 showed them to have a slightly larger droplet size, the fact that they remained dispersed meant that within the emulsion gels they would have had a smaller average droplet size (Chanamai & McClements, 2001). It has been shown that smaller oil droplet sizes give higher gel strength values in emulsion gels even when they're not bound to the gel matrix (Mcclements, et al., 1993; Sala, et al., 2009).

Furthermore, Figure 4.9A and 4.9C reveal that the 3DP emulsion gels had a far smaller LVER (0.2-0.4% shear strain) compared to the cast gels (0.8-1.1%) and thus could be considered less resistant to shear strain. The oscillatory rheology data shows that the 3DP gels will break down faster than the cast gels. Based on this data and the data from the TPA we hypothesise that is once again due to delamination of the 3DP gels. However, unlike the TPA under the amplitude strain put out by the rheometer, the printed samples did not come close to matching the values observed for the cast gels at any concentration of SFO. The post-printing analysis by TPA oscillatory rheology shows that the WPI-stabilised κC 3DP emulsion gels form a slightly more robust network than the T20-stabilised ones. This is again suspected to be linked to either the differences in the effective oil droplet sizes caused by the flocculation in the T20 stabilised emulsion gel systems or the cations inherently present in the WPI.

4.4 Conclusions

This study shows that it is possible to produce emulsions with varying SFO concentrations, disperse 3% w/w κC in the water phase and print them to create emulsion gels. It has been shown that the emulsifying agent chosen can affect the emulsion gel structure, and can in turn, be affected by the gelling agent; with T20 emulsions gels flocculating, unlike emulsion gels stabilised with WPI. Several complex geometries were produced with a final print quality that was independent of the concentration of SFO, which was demonstrated by the μDSC data. While the SFO concentration affected the cast gels' mechanical properties, it has no appreciable effect on the 3DP gels. The current study therefore highlights the ability of 3DP to produce more complex food systems with multiple phases that can be tuned depending on

the needs of the user. Future uses could involve release of lipophilic molecules or the addition of a dietarily relevant concentration of protein, to create a customisable total food source.

Acknowledgements

The authors would like to thank Dr. Stefan Nöbel from the Max Rubner-Institute in Germany for kindly sending us the printer used and liaising with us on the setup of the printer. We would like to thank Dr. Kilian Daffner for arranging the use of the printer and helping us set it up. We would also like to thank Benjamin Seifert for providing us with the CAD files used to modify the printer. Finally, we would like to thank Professor Eddie Pelan for his useful discussions. This work was supported by the Engineering and Physical Sciences Research Council [grant number EP/N024818/1].

4.5 References

Aaltonen, T., Kytö, E., Ylisjunttila-Huusko, S., & Outinen, M. (2020). Effect of the milk-based ash-protein ratio on the quality and acceptance of chocolate with a reduced sugar content. *International Dairy Journal, 105*, 104663.

Beverung, C. J., Radke, C. J., & Blanch, H. W. (1999). Protein adsorption at the oil/water interface: characterization of adsorption kinetics by dynamic interfacial tension measurements. *Biophysical Chemistry, 81*(1), 59-80.

Boland, A. B., Delahunty, C. M., & van Ruth, S. M. (2006). Influence of the texture of gelatin gels and pectin gels on strawberry flavour release and perception. *Food Chemistry, 96*(3), 452-460.

Chanamai, R., & McClements, D. J. (2001). Depletion Flocculation of Beverage Emulsions by Gum Arabic and Modified Starch. *Journal of Food Science, 66*(3), 457-463.

Chanamai, R., & McClements, D. J. (2002). Comparison of Gum Arabic, Modified Starch, and Whey Protein Isolate as Emulsifiers: Influence of pH, CaCl2 and Temperature. *Journal of Food Science, 67*(1), 120-125.

Chimene, D., Lennox, K. K., Kaunas, R. R., & Gaharwar, A. K. (2016). Advanced bioinks for 3D printing: a materials science perspective. *Annals of biomedical engineering, 44*(6), 2090-2102.

Dapčević Hadnađev, T., Dokić, P., Krstonošić, V., & Hadnađev, M. (2013). Influence of oil phase concentration on droplet size distribution and stability of oil-in-water emulsions. *European Journal of Lipid Science and Technology, 115*(3), 313-321.

Diañez, I., Gallegos, C., Brito-de la Fuente, E., Martínez, I., Valencia, C., Sánchez, M. C., Diaz, M. J., & Franco, J. M. (2019). 3D printing in situ gelification of κ-carrageenan solutions: Effect of printing variables on the rheological response. *Food Hydrocolloids, 87*, 321-330.

Diaz, J. V., Noort, M. W.-J., & Van Bommel, K. J. C. (2017). Method for the production of an edible object by powder bed (3d) printing and food products obtainable therewith. In: Google Patents.

Dick, A., Bhandari, B., & Prakash, S. (2019). 3D printing of meat. *Meat Science, 153*, 35-44.

Du, J., Dai, H., Wang, H., Yu, Y., Zhu, H., Fu, Y., Ma, L., Peng, L., Li, L., Wang, Q., & Zhang, Y. (2021). Preparation of high thermal stability gelatin emulsion and its application in 3D printing. *Food Hydrocolloids, 113*, 106536.

Dun, H., Liang, H., Zhan, F., Wei, X., Chen, Y., Wan, J., Ren, Y., Hu, L., & Li, B. (2020). Influence of O/W emulsion on gelatinization and retrogradation properties of rice starch. *Food Hydrocolloids, 103*, 105652.

Farjami, T., & Madadlou, A. (2019). An overview on preparation of emulsion-filled gels and emulsion particulate gels. *Trends in Food Science & Technology, 86*, 85-94.

Fenton, T., Kanyuck, K., Mills, T., & Pelan, E. (2021). Formulation and characterisation of kappa-carrageenan gels with non-ionic surfactant for melting-triggered controlled release. *Carbohydrate Polymer Technologies and Applications, 2*, 100060.

Fontes-Candia, C., Ström, A., Lopez-Sanchez, P., López-Rubio, A., & Martínez-Sanz, M. (2020). Rheological and structural characterization of carrageenan emulsion gels. *Algal Research, 47*, 101873.

Gholamipour-Shirazi, A., Norton, I. T., & Mills, T. (2019). Designing hydrocolloid based food-ink formulations for extrusion 3D printing. *Food Hydrocolloids, 95*, 161-167.

Gibson, S. F., & Lanni, F. (1991). Experimental test of an analytical model of aberration in an oil-immersion objective lens used in three-dimensional light microscopy. *JOSA A, 8*(10), 1601-1613.

Gu, Y. S., Decker, E. A., & McClements, D. J. (2005). Influence of pH and carrageenan type on properties of β-lactoglobulin stabilized oil-in-water emulsions. *Food Hydrocolloids, 19*(1), 83-91.

Hemker, W. (1981). Associative structures of polyglycerol esters in food emulsions. *Journal of the American Oil Chemists' Society, 58*(2), 114-119.

Hermansson, A.-M., Eriksson, E., & Jordansson, E. (1991). Effects of potassium, sodium and calcium on the microstructure and rheological behaviour of kappa-carrageenan gels. *Carbohydrate Polymers, 16*(3), 297-320.

Iglauer, S., Wu, Y., Shuler, P., Tang, Y., & Goddard III, W. A. (2011). Dilute iota-and kappa-Carrageenan solutions with high viscosities in high salinity brines. *Journal of Petroleum science and Engineering, 75*(3-4), 304-311.

Iijima, M., Hatakeyama, T., Takahashi, M., & Hatakeyama, H. (2007). Effect of thermal history on kappa-carrageenan hydrogelation by differential scanning calorimetry. *Thermochimica Acta, 452*(1), 53-58.

Jones, D. S., Woolfson, A. D., & Brown, A. F. (1997). Textural, viscoelastic and mucoadhesive properties of pharmaceutical gels composed of cellulose polymers. *International Journal of Pharmaceutics, 151*(2), 223-233.

Jong, L. (2020). Poly(acrylic acid) grafted soy carbohydrate as thickener for waterborne paints. *Materials Today Communications, 23*, 100882.

Kamlow, M.-A., Vadodaria, S., Gholamipour-Shirazi, A., Spyropoulos, F., & Mills, T. (2021). 3D printing of edible hydrogels containing thiamine and their comparison to cast gels. *Food Hydrocolloids, 116*, 106550.

Kenta, S., Raikos, V., Vagena, A., Sevastos, D., Kapolos, J., Koliadima, A., & Karaiskakis, G. (2013). Kinetic study of aggregation of milk protein and/or surfactant-stabilized oil-in-water emulsions by Sedimentation Field-Flow Fractionation. *Journal of Chromatography A, 1305*, 221-229.

Kim, K.-H., Gohtani, S., Matsuno, R., & Yamano, Y. (1999). Effects of oil droplet and agar concentration on gel strength and microstructure of o/w emulsion gel. *Journal of Texture Studies, 30*(3), 319-335.

Liu, Y., Yu, Y., Liu, C., Regenstein, J. M., Liu, X., & Zhou, P. (2019). Rheological and mechanical behavior of milk protein composite gel for extrusion-based 3D food printing. *Lwt, 102*, 338-346.

Liu, Y., Zhang, W., Wang, K., Bao, Y., Regenstein, J. M., & Zhou, P. (2019). Fabrication of Gel-Like Emulsions with Whey Protein Isolate Using Microfluidization: Rheological Properties and 3D Printing Performance. *Food and Bioprocess Technology, 12*(12), 1967-1979.

Liu, Z., Bhandari, B., Prakash, S., Mantihal, S., & Zhang, M. (2019). Linking rheology and printability of a multicomponent gel system of carrageenan-xanthan-starch in extrusion based additive manufacturing. *Food Hydrocolloids, 87*, 413-424.

Loizou, E., Weisser, J. T., Dundigalla, A., Porcar, L., Schmidt, G., & Wilker, J. J. (2006). Structural effects of crosslinking a biopolymer hydrogel derived from marine mussel adhesive protein. *Macromolecular bioscience, 6*(9), 711-718.

Matsumura, Y., Kang, I.-J., Sakamoto, H., Motoki, M., & Mori, T. (1993). Filler effects of oil droplets on the viscoelastic properties of emulsion gels. *Food Hydrocolloids, 7*(3), 227-240.

Mcclements, D. J., Monahan, F. J., & Kinsella, J. E. (1993). Effect Of Emulsion Droplets On The Rheology Of Whey Protein Isolate Gels. *Journal of Texture Studies, 24*(4), 411-422.

Özcan, İ., Abacı, Ö., Uztan, A. H., Aksu, B., Boyacıoğlu, H., Güneri, T., & Özer, Ö. (2009). Enhanced topical delivery of terbinafine hydrochloride with chitosan hydrogels. *Aaps Pharmscitech, 10*(3), 1024-1031.

Padzi, M., Bazin, M. M., & Muhamad, W. (2017). Fatigue characteristics of 3D printed acrylonitrile butadiene styrene (ABS). In *IOP Conference Series: Materials Science and Engineering* (Vol. 269, pp. 012060): IOP Publishing.

Pal, R., & Rhodes, E. (1989). Viscosity/concentration relationships for emulsions. *Journal of Rheology, 33*(7), 1021-1045.

Sager, V. F., Munk, M. B., Hansen, M. S., Bredie, W. L. P., & Ahrné, L. (2021). Formulation of Heat-Induced Whey Protein Gels for Extrusion-Based 3D Printing. *Foods, 10*(1).

Sala, G., de Wijk, R. A., van de Velde, F., & van Aken, G. A. (2008). Matrix properties affect the sensory perception of emulsion-filled gels. *Food Hydrocolloids, 22*(3), 353-363.

Sala, G., Van Aken, G. A., Stuart, M. A. C., & Van De Velde, F. (2007). Effect of droplet–matrix interactions on large deformation properties of emulsion-filled gels. *Journal of Texture Studies, 38*(4), 511-535.

Sala, G., van Vliet, T., Cohen Stuart, M. A., Aken, G. A. v., & van de Velde, F. (2009). Deformation and fracture of emulsion-filled gels: Effect of oil content and deformation speed. *Food Hydrocolloids, 23*(5), 1381-1393.

Severini, C., Derossi, A., Ricci, I., Caporizzi, R., & Fiore, A. (2018). Printing a blend of fruit and vegetables. New advances on critical variables and shelf life of 3D edible objects. *Journal of Food Engineering, 220*, 89-100.

Singh, H., Tamehana, M., Hemar, Y., & Munro, P. A. (2003). Interfacial compositions, microstructure and stability of oil-in-water emulsions formed with mixtures of milk proteins and κ-carrageenan: 2. Whey protein isolate (WPI). *Food Hydrocolloids, 17*(4), 549-561.

Singla, V., Saini, S., Joshi, B., & Rana, A. (2012). Emulgel: A new platform for topical drug delivery. *International Journal of Pharma and Bio Sciences, 3*(1), 485-498.

Snoeren, T. H. M., & Payens, T. A. J. (1976). On the sol-gel transition in solutions of Kappa-carrageenan. *Biochimica et Biophysica Acta (BBA) - General Subjects, 437*(1), 264-272.

Teo, A., Goh, K. K. T., Wen, J., Oey, I., Ko, S., Kwak, H.-S., & Lee, S. J. (2016). Physicochemical properties of whey protein, lactoferrin and Tween 20 stabilised nanoemulsions: Effect of temperature, pH and salt. *Food Chemistry, 197*, 297-306.

Thakur, G., Naqvi, M. A., Rousseau, D., Pal, K., Mitra, A., & Basak, A. (2012). Gelatin-Based Emulsion Gels for Diffusion-Controlled Release Applications. *Journal of Biomaterials Science, Polymer Edition, 23*(5), 645-661.

Vadodaria, S. S., He, Y., Mills, T., & Wildman, R. (2020). Fabrication of surfactant-polyelectrolyte complex using valvejet 3D printing-aided colloidal self assembly. *Colloids and Surfaces A: Physicochemical and Engineering Aspects, 600*, 124914.

Warner, E. L., Norton, I. T., & Mills, T. B. (2019). Comparing the viscoelastic properties of gelatin and different concentrations of kappa-carrageenan mixtures for additive manufacturing applications. *Journal of Food Engineering, 246*, 58-66.

Wilde, P., Mackie, A., Husband, F., Gunning, P., & Morris, V. (2004). Proteins and emulsifiers at liquid interfaces. *Advances in colloid and interface science, 108-109*, 63-71.

Williams, P., Clegg, S., Langdon, M., Nishinari, K., & Piculell, L. (1993). Investigation of the gelation mechanism in. kappa.-carrageenan/konjac mannan mixtures using differential scanning calorimetry and electron spin resonance spectroscopy. *Macromolecules, 26*(20), 5441-5446.

Wu, M.-H., Yan, H. H., Chen, Z.-Q., & He, M. (2017). Effects of emulsifier type and environmental stress on the stability of curcumin emulsion. *Journal of Dispersion Science and Technology, 38*(10), 1375-1380.

Wu, Y., Petrochenko, P., Chen, L., Wong, S. Y., Absar, M., Choi, S., & Zheng, J. (2016). Core size determination and structural characterization of intravenous iron complexes by cryogenic transmission electron microscopy. *International Journal of Pharmaceutics, 505*(1), 167-174.

Yang, F., Zhang, M., Bhandari, B., & Liu, Y. (2018). Investigation on lemon juice gel as food material for 3D printing and optimization of printing parameters. *Lwt, 87*, 67-76.

Yang, F., Zhang, M., Prakash, S., & Liu, Y. (2018). Physical properties of 3D printed baking dough as affected by different compositions. *Innovative Food Science & Emerging Technologies, 49*, 202-210.

Chapter 5

Release and co-release of model hydrophobic and hydrophilic actives from 3D printed kappa-carrageenan emulsion gels

This chapter was published as

Kamlow, M.-A., Holt, T., Spyropoulos, F., & Mills, T. (2022). Release and co-release of model hydrophobic and hydrophilic actives from 3D printed kappa-carrageenan emulsion gels. Food Hydrocolloids, 132, 107852

Michael-Alex Kamlow: Conceptualization, Methodology, Formal analysis, Investigation, Writing - original draft; Thomas Holt: Methodology; Fotis Spyropoulos: Writing - review & editing, Supervision; Tom Mills: Writing - review & editing, Supervision, Funding acquisition.

Abstract

This study formulated and compared 3D printed (3DP) and cast kappa-carrageenan (κC) emulsion gels for the co-release of model lipophilic (cinnamaldehyde) and hydrophilic (erioglaucine disodium salt (EDS)) molecules. Tween 20 (T20) or whey protein isolate (WPI) were used as the emulsifier. Both 3DP and cast emulsion gels maintained their oil droplet size over 8 weeks owing to the set gel matrix. Penetration texture analysis revealed 3DP and cast 5% oil emulsion gels, required more force to break compared to 40% oil gels (3 N against 0.4-0.5 N). This was because the oil droplets, disrupted the gel matrix; thereby weakening it. 3DP gels required less force to break than cast gels, owing to failure between the printed layers. Release tests in various media showed no significant difference in the final % cinnamaldehyde released between 3DP gels and cast gels. Release tests carried out in 0.1M hydrochloric acid saw an increase in cinnamaldehyde release compared to other media, owing to cinnamaldehyde's increased solubility in acidic media. Addition of EDS into the gel matrix facilitated co-release studies, with EDS release having no effect on the cinnamaldehyde release, indicating EDS release was driven by liberation from the gel network and cinnamaldehyde release by its expulsion from the oil droplets. Simple modelling showed that diffusion rather than polymeric relaxation was more dominant for active release in 3DP gels compared to cast gels. This work shows that 3DP can be used to produce customisable κC-emulsion gels, with multiple actives; suitable for use as modified release vehicles.

5.1 Introduction

There is currently an increasing interest in the formulation of multi-dose medicines and nutritionally fortified foods (McClements, 2018; Nagula & Wairkar, 2019). Therefore, emulsion gels are an obvious area for research in the sphere of functional 3DP foods, owing to their biphasic nature, and ability to manipulate energy levels through oil content. However, despite this, no previous studies have assessed the release of a model lipophile (cinnamaldehyde) with and without a model hydrophile (Erioglaucine disodium salt) from a 3DP emulsion gel and compared it to the cast equivalent. Previous studies have shown that by moving from cast to 3DP bulk structures, you can affect a change in release rates, while providing a far greater degree in flexibility with respect to dosage size, shape and appearance (Kamlow, Vadodaria, Gholamipour-Shirazi, Spyropoulos, & Mills, 2021).

Cinnamaldehyde, is a molecule with several reported properties that means it is of interest in the food and pharmaceutical sectors. Cinnamaldehyde is an essential oil extracted from the bark of cinnamon trees. It has antibacterial and antifungal properties (Gill & Holley, 2004; Siddiqua, Anusha, Ashwini, & Negi, 2015) as well as antioxidant activity (Gowder & Devaraj, 2006). Cinnamaldehyde has a log P of 1.82. logP is the ratio of concentrations of a compound in a mixture of two immiscible solvents at equilibrium. A logP of 1.82, means cinnamaldehyde has very limited water solubility, but retains enough to be able to track the release over time from a lipophilic environment to a hydrophilic one (Ben Arfa, Preziosi-Belloy, Chalier, & Gontard, 2007). Cinnamaldehyde has been utilised in release studies before, and is an optimal model lipophile owing to its ability to partition from an oil phase into a water phase, pleasant aroma and safety profile, being generally recognised as safe by the food and drug administration (Govindaraj, Subramanian, & Raghavachari, 2021). Erioglaucine disodium salt (EDS) is a water-soluble dye that once dissolved gives a blue colour and is often used in release studies as a model hydrophilic molecule (Andrews, et al., 2009; Jeong, et al., 2021; Lu, Tarn, Pamme, & Georgiou, 2018)

The present study aims to evaluate the release of model lipophilic with and without hydrophilic small molecular weight species from hot extrusion 3DP κC-emulsion gels, and assess their performance compared to the equivalent cast gels, in order to assess the performance of both as possible solid dosage forms or implants. This involved formulating 3% w/w κC-emulsion gels containing either 5% or 40% w/w sunflower oil (SFO), representing the two extremes of the oil concentrations tested in chapter 4, and stabilised with Tween 20 (T20) or whey protein isolate (WPI). After production of simple o/w emulsions with and without cinnamaldehyde, with a monomodal or bimodal distribution, droplet size was tested through laser diffraction and emulsion stability was scrutinised via zeta-potential measurements. κC-emulsion solutions were created by dispersing κC powder into the simple emulsions while heating. Following this, κC-emulsion gels were created either by 3DP or casting in moulds. 3DP and cast κC-emulsion gels had their stability tested through droplet size measurements utilising time domain nuclear magnetic resonance (NMR) spectroscopy and through syneresis measurements. The gels' mechanical properties were also scrutinised through texture profile analysis, namely penetration tests, comparing 3DP and cast gels. Finally, the printed and cast gels underwent release tests to assess their performance as release vehicles in various release media, with cinnamaldehyde release examined. After this EDS was loaded into the gels as a model molecule to test hydrophilic release and co-release studies were carried out.

5.2 Materials and methods

5.2.1 Materials

κC, T20, cinnamaldehyde, potassium chloride (KCl), and EDS were purchased from Sigma-Aldrich (UK). HPLC grade pentane and 32% w/v hydrochloric acid (HCl) were purchased from Honeywell, (UK). Phosphate Buffer Solution (PBS) tablets were obtained from Oxoid (UK). WPI was obtained from Sachsenmilch Milk & Whey Ingredients (Sachsenmilch Leppersdorf GmbH, Wachau, Germany). According to the manufacturer it contained 93.74% w/w protein in dry matter, 0.23% w/w fat, 0.61% w/w lactose and 3.16% w/w ash. SFO was purchased from the supermarket Spar (UK). Milli-Q water was used (Elix® 5 distillation apparatus,

Millipore®, USA) for sample preparation. All materials were used as received with no further modification or purification.

5.2.2 Emulsion preparation

Simple emulsions containing no κC were produced for particle size analysis before gelation and zeta-potential measurements. Production of the emulsions followed the same procedure as that previously described by (Kamlow, et al., 2021b). Emulsions stabilised with T20 had 1% w/w T20 added to the required amount of water and SFO. Emulsions stabilised with WPI had a 2% w/w stock solution of WPI diluted to 1% w/w WPI by adding deionised water and SFO. These mixtures where then premixed on a Silverson L5M for 3 minutes at 6000 rpm with a fine emulsor screen. The formed pre-emulsions were then passed through a high-pressure homogeniser at 25 bar to produce smaller scale emulsions with a droplet size of approximately 1 µm and 1000 bar to produce larger-scale emulsions with a droplet size of approximately 8-18 µm. Emulsions containing cinnamaldehyde had 0.7% w/w of the SFO fraction replaced with cinnamaldehyde and these were stirred together using a magnetic stirrer for ten minutes to ensure complete mixing. To create bimodal droplet size distribution emulsions, with a potential for customised release rates; micron and sub-micron emulsions were created and then mixed 50/50 by stirring with a magnetic stirrer for five minutes.

5.2.3 κC-Emulsion solution preparation

T20 and WPI stabilised O/W emulsions (as described in section 5.2.2) with and without cinnamaldehyde were used for the preparation of κC-emulsion solutions as described by (Kamlow, et al., 2021b). Emulsions were heated for 30 minutes on a hot-plate stirrer set to 80 °C. Then κC was added and left to stir for two hours to ensure that all κC had dispersed. 3% w/w κC in the water phase was chosen as this has been reported to give optimal printing outcomes (Kamlow, et al., 2021b; Kamlow, et al., 2021a). Finally, O/W emulsion gels were formed by cooling the systems, either via 3D printing as described in section 5.2.8 or casting in moulds as described in section 5.2.9.

5.2.4 κC-EDS-emulsion solution preparation

For the co-release tests, κC-emulsions solutions containing EDS were prepared to test the release of EDS by itself. Emulsions were produced as in section 5.2.3, but with 7.04g of water removed. Then after κC-emulsion production, 7.04g of EDS 2% w/w solution was added to the hot κC-emulsion solution and stirred for a further 30 minutes. This solution could then be gelled via 3D printing as in section 5.2.8 or casting in moulds as in section 5.2.9.

5.2.5 κC-EDS-emulsion with cinnamaldehyde solution preparation

For the co-release tests, κC-EDS-emulsion solutions containing cinnamaldehyde were produced by following the method in 5.2.4 but utilising an emulsion that had 0.7% w/w of the SFO fraction replaced with cinnamaldehyde.

5.2.6 Simple emulsion droplet size analysis

The emulsion droplet size was obtained using a Malvern Mastersizer MS 2000 (Malvern Panalytical, UK), utilising a Hydro SM manual small volume sample dispersion unit. The values for refractive index were input into the software and were 1.33 for water and 1.467 for the sunflower oil. For the SFO mixed with cinnamaldehyde, a refractometer (J357 Automatic refractometer, Rudolph research) was used to calculate the refractive index of the mixture. Cinnamaldehyde was found to have a refractive index of 1.62, and the mixture of cinnamaldehyde and sunflower oil was found to be 1.468. Samples were dispersed in distilled water at 1300 rpm to give an obscuration value of 4.2-4.6%. Samples were prepared and tested in triplicate and droplet size values were the average of at least three measurements. Surface weighted mean ($D_{3,2}$) and volume weighted mean ($D_{4,3}$) droplet size values were obtained immediately after preparation.

5.2.7 Zeta-potential measurement

The zeta potential (ζ-potential) was determined using a Zetasizer (Malvern Panalytical, UK) in order to assess the stability of the emulsions created and to assess if replacing part of the SFO fraction with cinnamaldehyde affected stability. Samples were diluted 100 times with

deionised water (Wu, et al., 2016). This was to reduce the absorbance of laser light and multiple scattering. All ζ-potential measurements were carried out at room temperature.

5.2.8 3D printing

The 3D printer was supplied by the Institute of Food Science and Biotechnology at the University of Hohenheim (Germany). A Fabbster 3D printer was modified in order to handle a liquid feed. Full detail of the printer's setup and function can be found in a previous study (Kamlow, et al., 2021b). After production of κC-emulsion solutions as in sections 5.2.3-5.2.5, these were fed into the printer, with the temperature being maintained indirectly via double walled pipes containing heated water in counterflow. The syringe was also wrapped in a heated jacket to prevent pre-gelation. The computer would then slice the desired 3D printed shape into layers and send this information to the printer which would then move in the X, Y and Z axes to produce the 3D shape. The material flowed via a syringe driver with a controllable flow rate, which was important as 5% w/w SFO and 40% w/w SFO emulsion solutions had different viscosities, necessitating two different flow rates (Pal & Rhodes, 1989). The printing parameters for these emulsion gels were determined in a previous study (Kamlow, et al., 2021b). The replacement of 0.7% of the SFO with cinnamaldehyde, as well as the addition of 0.1408% w/w EDS in the water phase had no effect on the printability of the gels which were printed at the optimal parameters previously defined. These were a printer bed temperature of 35 °C, print speed of 30 mm/s, fill space of 1.25 mm, a water bath temperature on the feed pipes of 72 °C, a water bath temperature on the nozzle of 72 °C, layer height of 1.2 mm, nozzle size of 20G/0.8mm and nozzle height of 0.5 mm. The syringe driver rate was 0.7 mL/min for 5% SFO κC-emulsion gels and 0.84 mL/min for 40% SFO κC-emulsion gels. This was used to produce 20 x 20 x 9 mm cuboids for texture profile analysis and syneresis testing, 15 x 15 x 30 mm cuboids for droplet size testing and 15mm height and 12 mm diameter cylinders for release tests. These are shown in Figure 5.1.

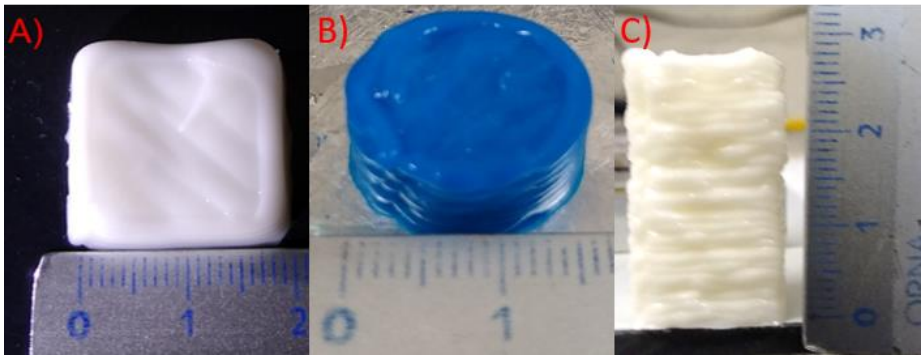

Figure 5.1: 3DP (A) 20 x 20 x 9.6 mm cuboid, (B) Cylinder containing EDS and (C) 15 x 15 x 30 mm cuboid

5.2.9 Production of moulds for casting

Cylinder and cuboid shaped moulds were produced using a form 2 stereolithography 3D printer (Formlabs, USA). The moulds were designed by computer aided design and uploaded to the software, digitally sliced into layers, then transmitted to the printer digitally to print. The cube mould facilitated the production of emulsion gel cuboids with dimensions of 20 x 20 x 9.6 mm by casting. These were then used for comparative penetration testing as a control, cast sample to compare to the 3D printed cuboids produced in 2.8. The cylinder mould was used to produce cast, control samples for release tests of cinnamaldehyde, EDS or both at the same time, to compare to the 3D printed cylinders produced in 2.8.

5.2.10 Syneresis testing

KC emulsion gel cuboids containing 5% or 40% SFO with dimensions of 20 x 20 x 9.6 mm were produced by 3D printing or casting and stored in an airtight container at 5 ˚C. Syneresis measurements were carried out by measuring the amount of water released by the emulsion gels after several time intervals as described in a previous study (Ako, 2015). The syneresis ratio (R_s) was determined using equation 5.1.

$$R_s = \frac{w_e}{w_g} x\ 100 \quad Eq\ [5.1]$$

Where w_e is the weight of water released by the gel, and w_g is the weight of the initial gel. Since 40% SFO emulsion gels contain considerably less water per 100g compared to 5% SFO emulsion gels, the values were normalised to a constant water concentration.

5.2.11 Time-Domain nuclear magnetic resonance spectroscopy

Droplet size measurements of the emulsion gels were performed using a nuclear magnetic resonance (NMR) device (Bruker Minispec NMR, Bruker Optics, UK), equipped with a gradient unit. Measurements were performed on three different samples, in triplicate. Droplet size calculations were performed using the Minispec software, which fits the data to a log-normal curve. Measurements were taken to assess the stability of the emulsion gels over 8 weeks, with samples tested at 0, 1, 2, 3, 4 and 8 weeks. Cast gels were tested by adding hot κC-emulsion gel solution to the NMR tubes. 3DP gels were tested by printing a cuboid measuring 15 x 15 x 30 mm and then using a cork borer, the same size as the internal diameter (Ø 10mm) of the NMR tubes to cut out a cylinder and place that into the NMR tube. $D_{3,2}$ values from the mastersizer were converted to the volume-weighted geometric mean diameter ($D_{3,3}$) values to be used as a comparison to see if oil droplet sizes changed during gelation, using equation 5.2.

$$D_{3,3} = \frac{D_{3,2}}{e^{-\sigma^2 \div 2}} \quad \text{Eq [5.2]}$$

Where D3,3 is the geometric weighted mean diameter, D3,2 is the surface weighted mean diameter and σ is the standard deviation of the logarithm of the droplet diameter.

5.2.12 Texture Profile Analysis

Texture profile analysis (TPA) was carried out using a TA XT plus Texture Analyser. Printed and cast cuboids of dimensions 20 × 20 × 9.6 mm were tested; the cast cuboids were given 3 minutes 30 seconds to set, mimicking the time taken to print their respective counterparts. Penetration testing was carried out using a P/6 cylindrical aluminium probe set to a constant speed of 0.5 mm/s, over a distance of 6 mm, alongside a 30 kg load cell and 3 g of trigger force. Through penetration testing, data for the force at breaking, firmness and gel strength were acquired for printed and cast cuboids. Force at breaking, in g, is defined as the first significant discontinuity produced in the curve during penetration (Fiszman, Lluch, & Salvador, 1999). Firmness, in g/mm, is the initial slope of the penetration curve within the first 2 seconds

(Fiszman & Salvador, 1999). Gel strength, in g x mm, is the multiplication of the penetration force by the distance of the penetration where failure occurs (Liu, Nie, & Chen, 2014). All tests were carried out in triplicate.

5.2.13 Release studies

Release studies were carried out using UV-visible spectrophotometry to assess the release of cinnamaldehyde from the printed and cast κC-emulsion gels. All studied gel systems were of a consistent weight; 1700 mg ± 5%. Oil droplets were tested at both the micron and sub-micron scale. Three cast and three printed κC-emulsion gels were each placed inside semipermeable cellulose dialysis membrane (approx. 80 mm x 40 mm), which had been soaked for 24 hours in deionised water. The molecular weight cut-off for the membrane was stated to be 14,000 Daltons. This was far below the molecular weight of the κC, ensuring none would interfere with the absorbance readings (Phillips & Williams, 2009). The gel-containing membranes were placed within 150 mL of various media (deionised water, PBS, 0.1 M HCl and 1 M KCl). 100% release of the cinnamaldehyde within the gels would equate to approximately 4 mg/L. Since this is significantly lower than the maximum solubility within water, this equates to sink conditions. The release tests were carried out within an Incu-Shake MIDI shaker incubator (Sciquip, UK) at 150 rpm. Release tests were carried out at 37 ˚C for *in vitro* testing. Measurements were taken at various time points up to and including 360 minutes. Determination of the cinnamaldehyde release was carried out using a Jenway Genova Bio life science spectrophotometer (Cole-Parmer, UK), set to 290 nm, the maximum absorbance for cinnamaldehyde in the various release media. 0.9 mL of dissolution medium was taken with an Eppendorf pipette and tested at the times stated above. This was placed into the UV-Vis spectrophotometer which had been blanked using fresh release media. The release profile was calculated from a calibration curve determined by the UV-Vis spectrophotometer, which had an R^2 value of 0.999. The contents of the cuvette were then discarded and 0.9 mL of fresh medium added into each beaker. This was corrected when determining the cinnamaldehyde release percentage following the procedure of (Singh, Kaur, & Singh, 1997). All tests were

carried out in triplicate. The calibration curve for cinnamaldehyde in water can be found in Appendix 5.

5.2.14 Co-release studies

Co-release studies were carried out in water using a modified version of the protocol in 5.2.13. ΚC-EDS-emulsion gels with cinnamaldehyde were cast and printed, placed within semipermeable cellulose dialysis membrane, then placed into beakers containing 150 mL water. 100% release of the EDS would equate to approximately 8 mg/L, which meant that it was being released into sink conditions. 1.8 mL aliquots were taken at the various release points. 0.9 mL was taken and tested for EDS release at 629 nm on the UV-vis spectrophotometer, which had been blanked against deionised water. The release profile was calculated from a calibration curve for the EDS which had an R^2 value of 0.999. Then a solvent extraction protocol was carried out on the remaining 0.9 mL. 0.9 mL of pentane was added to the remaining 0.9 mL of the aliquot and they were shaken together. The cinnamaldehyde was far more soluble in the pentane than the water, but the EDS is insoluble in the pentane (Balaguer, et al., 2013). This prevented any interference from the EDS when measuring the absorbance of the cinnamaldehyde in the pentane. This was tested within the UV-vis spectrophotometer at 280 nm, as being within pentane caused a shift in the maximum absorbance peak, compared to being dissolved within water. Blank pentane that had been shaken through deionised water was used to blank the instrument. A separate calibration curve was created for cinnamaldehyde in pentane which had an R^2 value of 0.990. The calibration curve for cinnamaldehyde in pentane can be found in Appendix 6 and for EDS in water, Appendix 7.

5.2.15 Modelling of release data

Cinnamaldehyde and EDS release data (up to 60%) were fitted to the following model (Ritger & Peppas, 1987)

$$\frac{M_t}{M_\infty} = k_1 t^m + k_2 t^{2m} \qquad \text{Eq [5.3]}$$

This modelling yielded values between 0.5 and 1. The closer to 0.5, the greater the contribution of Fickian diffusion to the release of the molecules. The closer to 1.0, the greater the contribution of polymeric relaxation to molecular release.

5.2.16 Statistics

The average droplet size, ζ-potential, R_s, force at break, gel strength, firmness and cumulative release % were compared using the two-sample T-test in the Analysis ToolPack for Microsoft Excel. Confidence levels were set at 95%. Therefore, if $P < 0.05$, the two sets of data have different means, otherwise the two means have no significant statistical difference.

5.3 Results and discussion

5.3.1 Droplet size analysis and zeta-potential measurements

The o/w emulsions containing 5% or 40% w/w SFO (dispersed phase) and stabilised by either T20 or WPI, were studied both in the presence and absence of included cinnamaldehyde; comprising 0.7% of the total oil fraction in each system. Emulsifier concentration was fixed at 1% w/w, which was sufficient to stabilise the emulsions. It was important to characterise the simple emulsions before conversion to emulsion gels, for printing, in order to establish a baseline for later stability testing (see section 5.3.3). These systems were all formed in dimensions that were able to undergo printing through the 0.8 mm nozzle, practically undisturbed. They were also determined to be stable during the heating step described in section 5.2.3, and thus are not expected to change from production to printing. We were able to deliver systems with controlled variations to droplet length scale, emulsifier type, dispersed phase content as well as droplet surface charge. Establishment of this level of customisation is important for proving the use of 3DP κC-emulsion gels as flexible delivery systems for targeted molecules. $D_{4,3}$ droplet size data is presented in Figure 5.2A for larger scale and Figure 5.2B for smaller scale emulsions.

Statistical analysis showed no significant difference in the droplet sizes produced by varying the SFO concentration or by replacing 0.7% of the oil fraction with cinnamaldehyde, in either length scale. However, there is a statistically significant difference between the emulsions

stabilised by T20 compared to those stabilised by WPI. This is due to T20 being a low molecular weight surfactant (LMWS), meaning it can position itself faster at the interface (Kenta, et al., 2013). Furthermore, LMWS are superior at decreasing the water/oil interfacial tension compared to proteins, further aiding droplet breakup (Beverung, Radke, & Blanch, 1999).

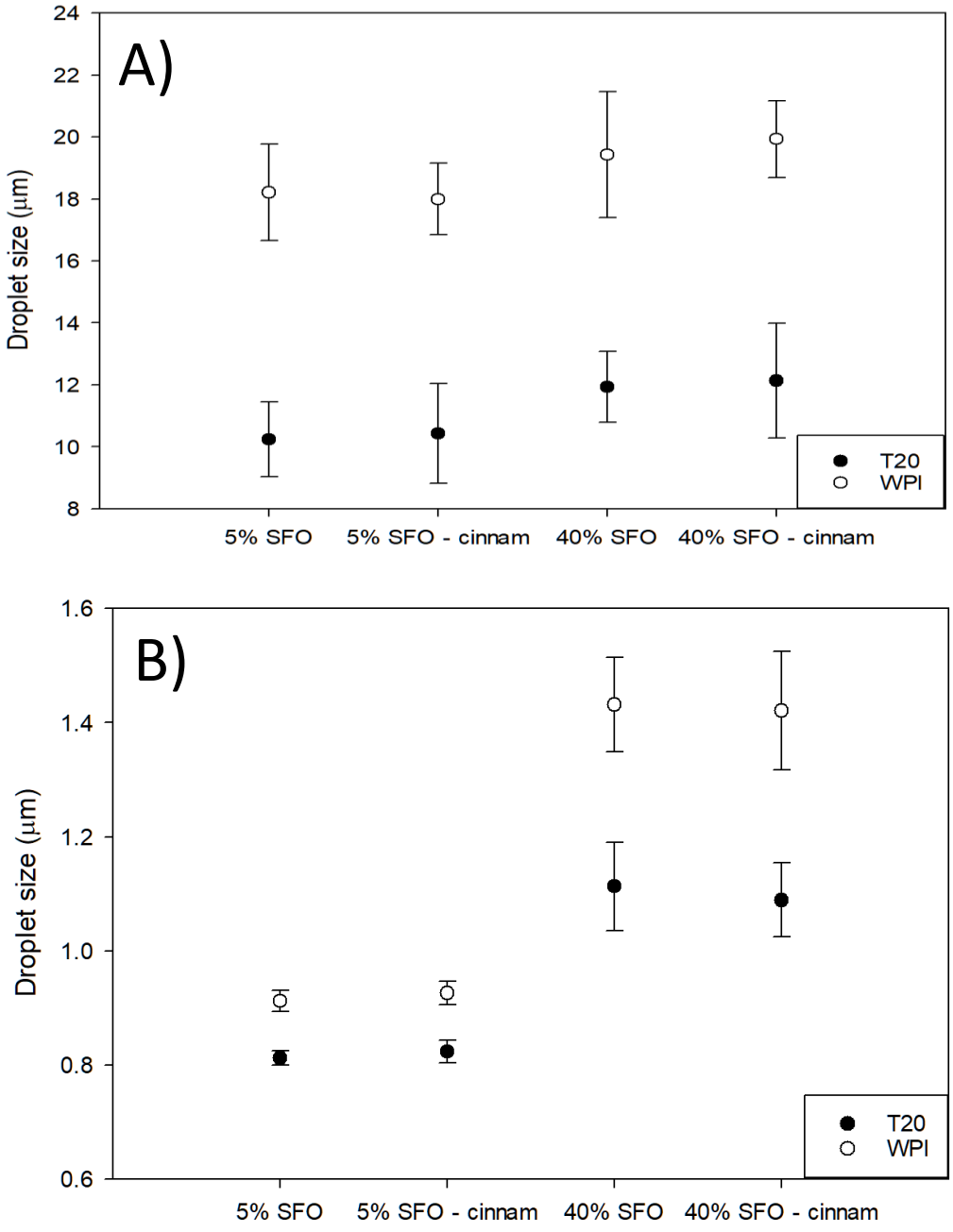

Figure 5.2: Comparison of the average droplet size of emulsions with and without cinnamaldehyde containing 5% or 40% SFO and 1% w/w T20 or WPI in the larger (A) or smaller (B) scale.

Bimodal distributions were also created to be used for stability testing (see section 5.3.3), with larger and smaller scale emulsions mixed in a 1:1 ratio. Because release studies were to be carried out, the possibility of custom release profiles created by mixing different droplet sizes in varying ratios, meant that purpose made bimodal droplet distributions were investigated as well. However, since the $D_{4,3}$ values from the mastersizer are calculated for monomodal distributions, it is far more practical to show the droplet distribution graphs, which are given in Figure 5.3, including the distributions of the individual size scale systems. This is because a single, average droplet size value does not fully represent the equally mixed droplet populations for the mixed size scale systems.

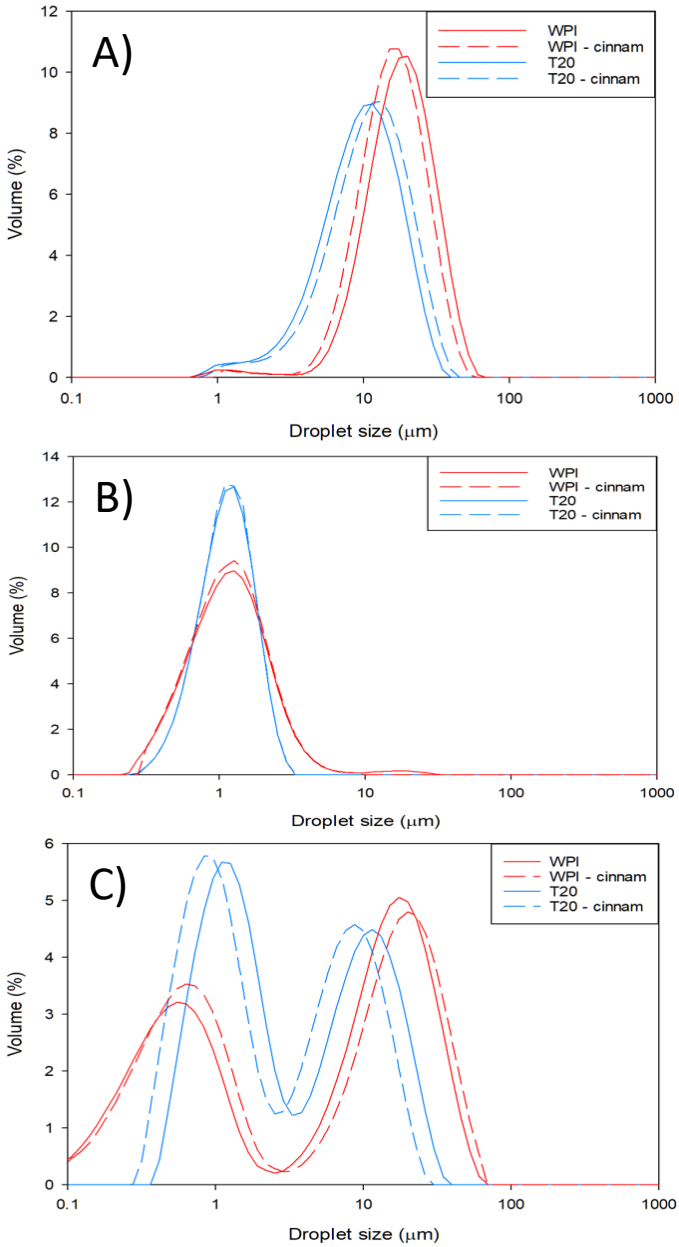

Figure 5.3: $D_{4,3}$ distribution of 40% SFO (A) larger scale emulsions, (B) smaller scale emulsions and (C) mixed scale emulsion systems stabilised with either T20 or WPI

The distributions in Figure 5.3 showed that there was no significant difference when replacing 0.7% of the oil fraction with cinnamaldehyde. Furthermore, the mixing of the larger and smaller scale emulsions created bimodal distributions, which reflected the two constituent monomodal distributions of which they were comprised.

The emulsions were also tested for their ζ-potential, to assess whether the different emulsifiers, the changes in length-scale of the emulsion droplets, or the addition of the cinnamaldehyde fraction has an effect on surface charge (Figure 5.4). The ζ-potential values

for T20 reflect that it is a non-ionic surfactant, which stabilises emulsions through steric repulsion, rather than surface charge (Teo, et al., 2016). The WPI stabilised emulsions had a strong negative charge, owing to being above their isoelectric point, giving a ζ-potential value of around -34 mV to -37mV for larger-scale emulsions and a statistically significant difference of -29mV to -32 mV for the smaller-scale emulsions. This is fairly typical with smaller droplet sizes having been shown to present with a lower ζ-potential value (Wiącek & Chibowski, 1999; Wiącek & Chibowski, 2002). Replacing 0.7% of the SFO fraction with cinnamaldehyde did not have a statistically significant difference on the ζ-potential of the emulsions.

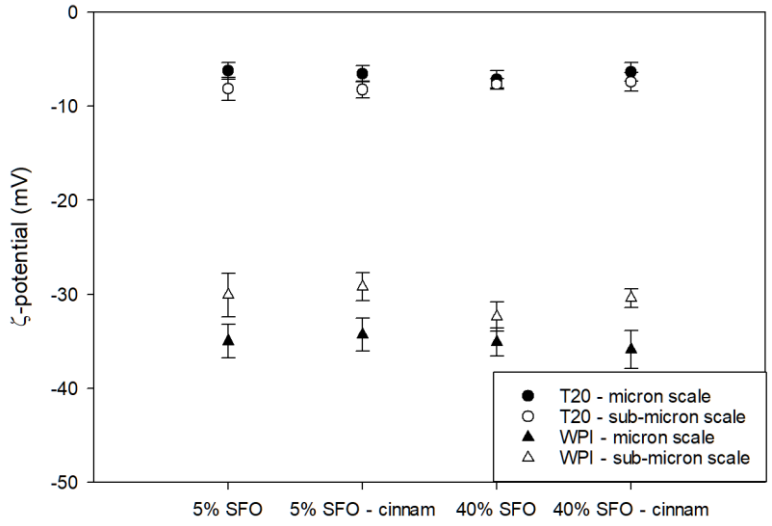

Figure 5.4: ζ-potential of O/W emulsions with and without cinnamaldehyde, stabilised by either T20 or WPI in the micron and sub-micron scale

5.3.2 Syneresis testing

During emulsion gel formation, while most water is retained within the gel network overtime, some is expelled during contraction over time as the polymer helices aggregate further (Thrimawithana, Young, Dunstan, & Alany, 2010). Syneresis is considered to be unfavourable when it comes to the use of biopolymer gels as molecular delivery vehicles, as any loss of water could lower the availability of any hydrophilic molecules within the water phase of the gels. Figure 5.5 shows the results of syneresis testing over 28 days for cast and 3DP κC-emulsion gel cuboids containing 5% or 40% SFO stabilised by either T20 or WPI. The values have been normalised for the total water content.

As the gels continued to contract over time, water is expelled from within the gel matrix. The syneresis of the emulsion gels followed the same pattern, regardless of whether they were stabilised by T20 or WPI. Previous studies have shown that an increase in SFO concentration within emulsion gels reduces the water loss from syneresis; however, this study did not fix the biopolymer concentration to the water content (Chen, Lu, Yuan, Gao, & Mao, 2021). Therefore as the oil fraction increased, there was an effective increase of the biopolymer concentration within the aqueous phase of the emulsion gels. Furthermore, while the data presented in Figure 5.5 went to 40% w/w SFO, the previous study only assessed emulsion gels up to 20% SFO, making comparisons more difficult with previous reported results in literature. Here, there was no statistically significant difference between 5% and 40% SFO κC-emulsion in terms of water loss before 28 days had passed, then a statically significant difference was observed. One explanation for this could be the far higher oil concentration within the 40% SFO emulsion gels, causing greater disruption the network structure, leading to a decrease in gel elasticity (Mcclements, Monahan, & Kinsella, 1993). A decrease in elasticity of κC-emulsion gels has been shown to increase the rate of syneresis (Rostami, Nikoo, Rajabzadeh, Niknia, & Salehi, 2018). The 3DP κC-emulsion gels lost more water than their cast equivalents, and this was believed to be due to the layering that runs through the 3DP κC-emulsion gels, as a consequence of the 3DP process, which can allow water a shorter route to exit the gels (Kamlow, et al., 2021a).

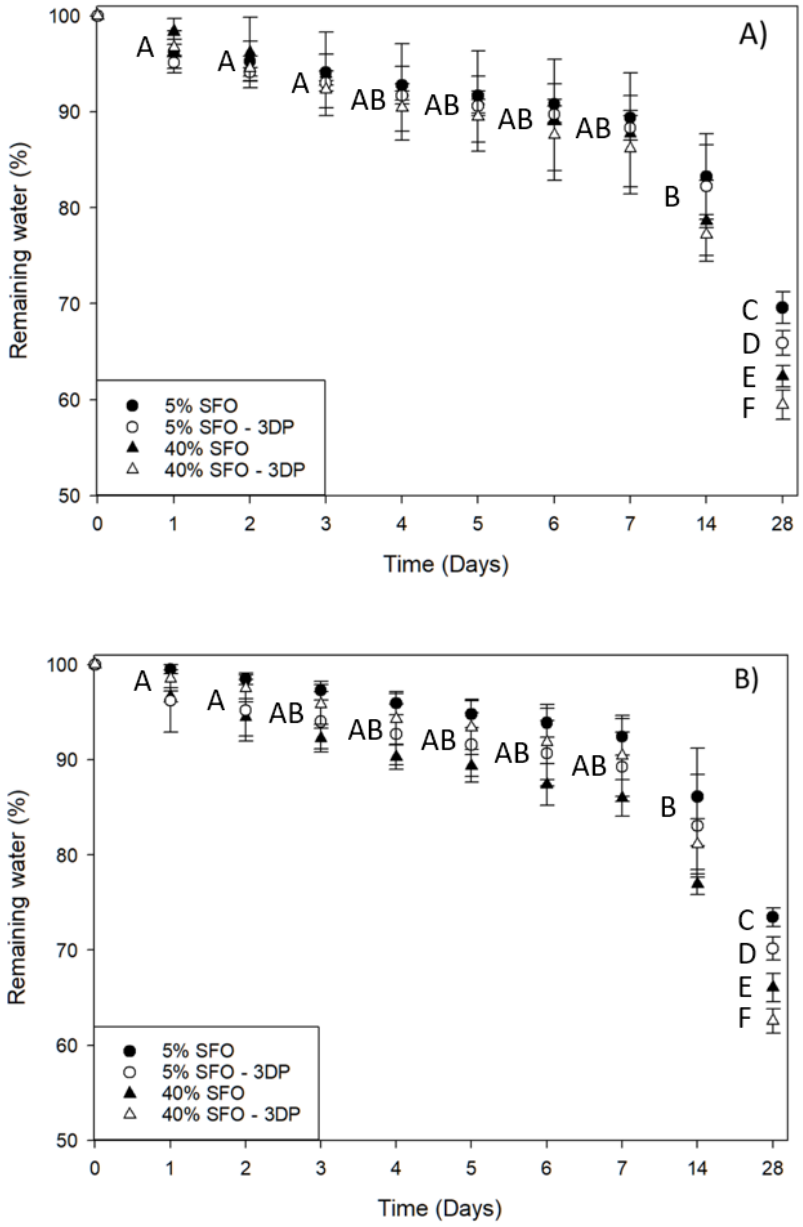

Figure 5.5: Syneresis of the κC-emulsion gels with different oil fractions for 3DP and cast κC-emulsion gels stabilised by (A) T20 and (B) WPI. Letters represent statistical significance (P<0.05)

5.3.3 TD-NMR stability testing

Time Domain-NMR (TD-NMR) was used to evaluate the droplet size within κC-emulsion gel samples containing monomodal and bimodal droplet distribution systems in both the micron and sub-micron scale. This was to assess whether the 3DP process, causes aggregation or flocculation of the emulsion systems, once gelled. TD-NMR has the advantage of being able to evaluate droplet size distributions within solid systems, unlike dynamic light scattering techniques and without the time-consuming nature of microscopy. Figure 5.6. Shows the data

for emulsion gels over 8 weeks for micron and sub-micron, monomodally distributed κC-emulsion gel samples.

Figure 5.6 showed that despite the simple emulsions being heated and stirred for two and a half hours during emulsion gel production, there was no significant coalescence of the oil droplets observed. Furthermore, the 3D printing process also appeared to have no significant effect on the oil droplet size within the κC-emulsion gels. The differences observed between the T20 and the WPI follow trends observed from section 5.3.1. While the droplet sizes appear to have stayed constant for both emulsifiers, the nature of TD-NMR means that it does not detect flocculation of oil droplets, as the restriction of self-diffusion of oil by the walls of the droplets, won't be affected by the flocculation (Goudappel, van Duynhoven, & Mooren, 2001). However, previous studies have shown that κC-emulsion gels flocculate when stabilised by T20 (Kamlow, et al., 2021b; Singh, Tamehana, Hemar, & Munro, 2003). This doesn't occur with the WPI stabilised κC-emulsion gels, and is linked to the higher surface charge on the oil droplets stabilised by WPI (see Figure 5.4). This highlights the need to examine complex systems such as emulsion gels through various techniques. There was no change seen over 8 weeks, which is due to the solid continuous phase restricting any movement of the oil droplets within the network.

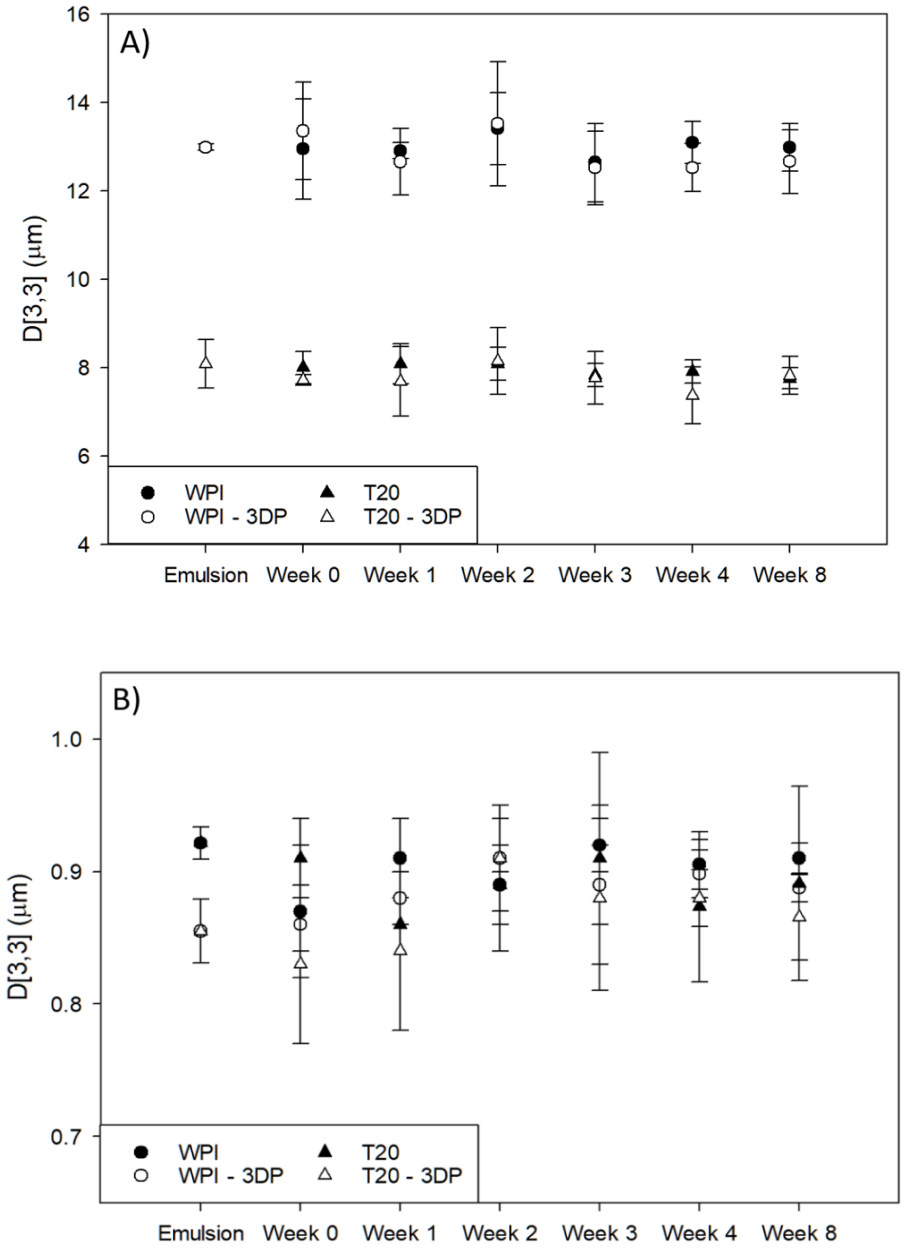

Figure 5.6: TD-NMR over 8 weeks showing $D_{3,3}$ values for cast and 3DP κC-emulsion gels in the micron (A) and sub-micron (B) scales

Separately sub-micron and micron scale emulsions were created and mixed by stirring for five minutes and then gelled as above, in order to test droplet stability in an inherently unstable system. These were also stored for 8 weeks and the droplet sizes examined. Appendix 8 shows that despite intentionally creating a bimodal emulsion distribution, the emulsion gels maintained their stability over 8 weeks. This is despite the fact that bimodal emulsions are less stable, and more prone to Ostwald ripening and coalescence (van der Ven, Gruppen, de Bont, & Voragen, 2001). The addition of cinnamaldehyde caused no significant change to the droplet

sizes. Since $D_{3,3}$ is calculated based on monomodal distributions, these values alone are not fully representative of the droplet size distributions present within these systems (Juslin, Antikainen, Merkku, & Yliruusi, 1995). It also appears that the tween emulsion gel systems appear to have eliminated the flocculation observed in the simple emulsion systems. The distribution values over 8 weeks are presented in Table 5.1.

Table 5.1 shows that the emulsion gels for the mixed-scale systems maintained the same distributions and σ values after production and storage for 8 weeks. The σ value corresponds to the standard deviation of the logarithm of the droplet diameter. The κC-emulsion gels stabilised with T20 had a narrower droplet size distribution compared to those stabilised by WPI, which is reflected in the smaller σ value. The demonstrated ability of κC-emulsion gels to maintain emulsion stability over time, coupled with their thermoreversible nature means that they could potentially be used to store poorly stable emulsions as emulsion gels, and then heat them to undergo a gel-sol transition and consume them as a liquid form if needed.

Table 1: Data on droplet size distributions of mixed scale κC-emulsion gels following production and after 8 weeks. A higher σ value indicates a wider droplet size distribution

	Droplet size after 0 weeks				Droplet size after 8 weeks			
	WPI	T20	WPI with cinnamal dehyde	T20 with cinnamal dehyde	WPI	T20	WPI with cinnamal dehyde	T20 with cinnamal dehyde
Diameter 2.5% (μm)	0.31 ± 0.05	0.25 ± 0.04	0.30 ± 0.04	0.23 ± 0.02	0.28 ± 0.07	0.25 ± 0.02	0.24 ± 0.05	0.24 ± 0.01
Diameter 50% (μm)	5.80 ± 0.23	2.89 ± 0.15	5.79 ± 0.30	3.03 ± 0.09	5.83 ± 0.33	2.96 ± 0.02	5.72 ± 0.40	3.00 ± 0.04
Diameter 97.5% (μm)	81.88 ± 4.21	47.27 ± 2.23	77.61 ± 2.14	47.66 ± 3.19	79.37 ± 3.86	48.46 ± 1.69	77.45 ± 3.61	46.34 ± 1.82
σ	2.54 ± 0.06	1.53 ± 0.08	2.55 ± 0.10	1.64 ± 0.12	2.61 ± 0.09	1.42 ± 0.36	2.59 ± 0.10	1.51 ± 0.09

5.3.4 Texture profile analysis

Texture profile analysis (TPA) of gels is an important technique for characterising the gel microstructure. In the past TPA has been used to assess how gels perform when it comes to the release of molecules from within their matrices. More rigid, and less elastic gels tend to release molecules slower, owing to a more dense gel network retarding molecular release (Boland, Delahunty, & van Ruth, 2006; Özcan, et al., 2009). While previous studies have carried out TPA on 3DP gels, there exists little, if any, literature that utilises penetration testing, with all the existing work focusing on compression testing (Kamlow, et al., 2021b; Kamlow, et al., 2021a; Strother, Moss, & McSweeney, 2020; Yang, Zhang, Bhandari, & Liu, 2018).

Since penetration testing measures force as a function of penetration depth, it is much more sensitive to local variances in the gel architecture. Whereas, compression tests are determined by the average material property for the whole sample (Lee & Chung, 1989). Penetration testing data for both the 3DP and cast κC-emulsion gels studied here are shown in Figure 5.7. Cast κC-emulsion gels display a typical shaped TPA curve, with one failure point (Figure 5.7A), whereas 3DP gels had several peaks and troughs, with each of these roughly corresponding to a penetration depth of 1.2 mm (Figure 5.7B); this is also compatible with the printed layer height. The data in Figure 5.7 also shows (for both cast and 3DP κC-emulsion gels) that as the concentration of SFO increases, the amount of force required to penetrate the gels decreased. Literature suggests this behaviour to be a result of the oil droplets within the network acting as non-interacting filler particles, with therefore further increases to their population (higher SFO content) resulting in a more pronounced disruption in the formation of the gel network around them, and thus weaker gels (Mcclements, et al., 1993).

A previous study by the present authors (Kamlow, et al., 2021b) revealed no statistically significant difference in the performance of 3DP κC-emulsion gels when undergoing compression tests, regardless of SFO concentration. It was observed that under compression, 3DP gels undergo delamination, breaking down at the semi-fused sites that follow the lines of the printing, as opposed to cast gels which are one continuous network. However, the data for

the penetration testing in Figure 5.7 highlights that penetration testing can demonstrate a difference in performance for 3DP gels; not only was a difference observed with SFO concentration, but also as a function of the emulsifier chosen. The disparity in the results between compression and penetration testing is due to how failure propagates when gels are subjected to the two different types of force. While compression testing evaluates the cohesiveness of the gels, that is to say their overall binding, penetration testing assesses the degree of compactness in the gels, that is to say, their density (Lee, et al., 1989).

From the force-distance graphs in Figure 5.7A and 5.7B, data for force at break, in g, firmness, in g/mm, and gel strength, in g x mm, could be determined and these are shown in Figure 5.7C-E. The 5% SFO cast gels had far higher values for force at break and gel strength because they lacked the extensive network disruption caused by either a high concentration of SFO or the discontinuous nature of a 3DP bulk structure. This was responsible for the far higher values observed in Figure 5.7C and 5.7D for 5% SFO cast gels. In terms of force at break and gel strength (Figure 5.7C and 5.7D), there was a statistically significant difference between the emulsion gels stabilised by either T20 or WPI, except for the cast 5% SFO gels. WPI contains 3.16%, milk-based ash contains cations such as potassium and calcium which are known to reinforce κC gels (Hermansson, et al., 1991). It is believed that this was a contributing factor, to the WPI-stabilised emulsion gels requiring more force before failure. The firmness data (Figure 5.7E) saw the 5% SFO gels having no significant difference between them, regardless of emulsifier. For the 40% SFO cast gels, there was no significant difference between the cast gels stabilised by WPI, and the 5% SFO gels. While the 40% SFO cast gels stabilised by T20 were statistically significantly different from the 5% SFO gels, but not the 40% SFO cast gel stabilised by WPI. Between the 40% SFO 3DP gels there was no statistically significant difference, nor was there one with the 40% SFO cast emulsion gel stabilised by T20, but there was for the 40% SFO cast gel stabilised by WPI. The lower firmness values of the 40% SFO gels, both cast and 3DP, suggest that these systems deformed more easily and tended to flow more before breaking, when compared to the 5% SFO gels (Pang, Deeth, Sopade, Sharma, & Bansal, 2014).

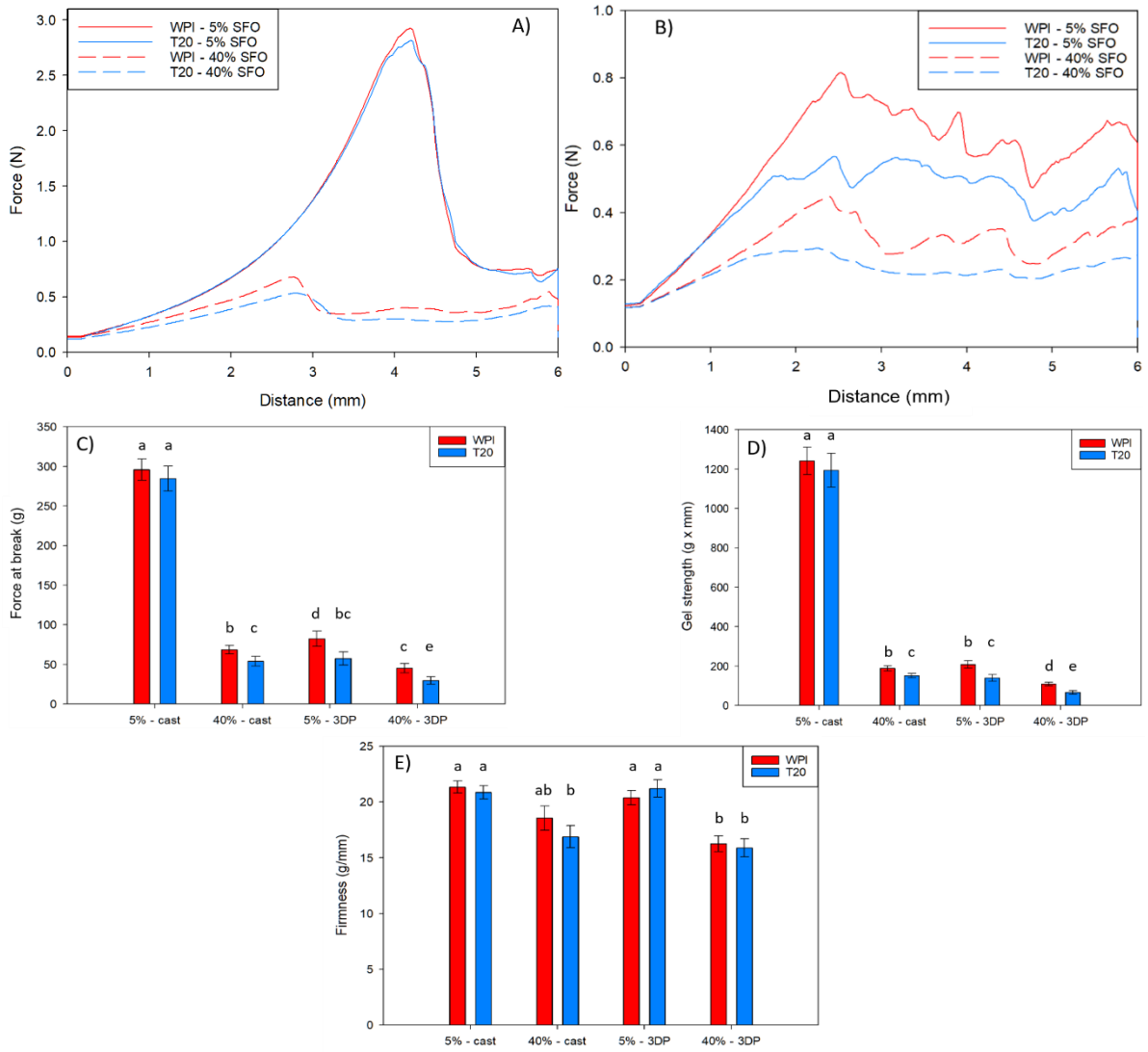

Figure 5.7: Force-time graphs for (A) cast and (B) 3DP κC-emulsion gels stabilised by T20 and WPI. (C) Force at break, (D) Gel strength and (E) Firmness of the 3DP and cast κC emulsion gel cuboids containing emulsions stabilised by T20 and WPI. Letters represent statistical significance (P<0.05)

5.3.5 Release studies

The amount of cinnamaldehyde released from 3DP and cast κC-emulsion gels was measured at 37 °C and 20 °C in water as a simple release medium and PBS and 0.1M HCl as they are more physiologically relevant release media. Control cinnamaldehyde release performance from non-gelled emulsions and a pure sunflower oil phase (both) in water at 37 °C, was also assessed. The release data acquired are all presented in Figure 5.8 and Appendix 9.

The release data showed no major difference in the amount of cinnamaldehyde being released from emulsion gels, regardless of whether they were 3DP or cast. This differed from our previous study which found that 3DP gels released a greater proportion of their active in the same timeframe compared to cast gels (Kamlow, et al., 2021a). However, the previous study

was for a hydrophilic active directly encased within the gel network, while the present work studies the release of cinnamaldehyde (which is lipophilic) from emulsion gels. This appears to suggest that in the current study, overall cinnamaldehyde release from both the 3DP and cast κC-emulsion gels is predominantly dictated by the active's liberation from the oil droplets rather than by its subsequent discharge from the surrounding gel network. One difference between 3DP and cast gels is observed in Figure 5.8A to 5.8F. Here, there is a divergence in the release performance between the 3DP and cast κC-emulsion gels that is exhibited around the 60-120 mins time frame. Placing the gels into the acceptor medium, creates an osmotic gradient for the transfer of cations from the gel into the aqueous sink; this is controlled by diffusion. This took place at a faster rate in the 3DP (than in the cast) gels, as their inherent layered structure facilitates the migration of the cations into the acceptor phase (Kamlow, et al., 2021a). However, when eventually the gel network of the cast assemblies is also lost, cinnamaldehyde release from these systems is seen to once again coincide with that from their 3DP counterparts. This divergence takes place at later stages in the release experiments utilising PBS as the acceptor phase, owing to the greater concentration of ions (compared to deionised water) present in this case.

In order to confirm that the loss of gelling cations via diffusion causes the collapse of the gels, the data for cinnamaldehyde release in 1M KCl was scrutinised (Appendix 9D). Furthermore cinnamaldehyde release at 20 ˚C (Appendix 9A-C) was carried out to assess the effect of temperature. In both cases, the previously observed divergence between 3DP and cast κC-emulsion gels was absent, either because the concentration gradient led to the gels taking up salt (1M KCl) or because the lower temperature (20 ˚C) has slowed down the diffusional transfer of salts out of the gel network (Vrentas & Vrentas, 1992). This led to release rates being lower in PBS as seen in Figure 5.8C-D compared to 5.8A-B. In 0.1M HCl (Figure 5.8E and 8F), a statistically significant increase in the percentage release of cinnamaldehyde was observed. This was due to the free carbonyl group present on cinnamaldehyde, facilitating the formation of Schiff base adducts with an increased aqueous solubility (Friedman, 2017; Wei, Xiong, Jiang, Zhang, & Wen, 2011). In terms of cinnamaldehyde release in an acidic

environment (0.1M HCl), WPI stabilised emulsion gel systems behaved differently to those stabilised by T20. As the pH in this case is below the isoelectric point of WPI, the protein has an overall positive charge (Chanamai & McClements, 2002), and thus can associate with κC, effectively acting as a gelling cation (de Kruif, Weinbreck, & de Vries, 2004; Stone & Nickerson, 2012). This meant that the cast and 3DP gels remained solid, despite any potential loss of gelling cations such as K^+ and Na^+ to the acceptor phase. This yielded the different release behaviour compared to the remaining release studies at 37 ˚C. The enhanced aqueous solubility of cinnamaldehyde within an acidic environment can be seen through comparison of Figure 5.8E and 5.8F with Figure 5.8A-D, with the release in 0.1M HCl yielding a statistically significant increased amount of cinnamaldehyde compared to release in other media; this trend persists at 20 ˚C as well as seen in Appendix 9. This shows that simply by controlling the emulsifier used to stabilise the κC-emulsion gels, the release rate of active molecules can be manipulated based on the release medium. The enhanced solubility and release of cinnamaldehyde in 0.1M HCl compared to water, was also observed when the active was simply delivered by dissolution in a pure SFO phase, as seen in Appendix 9F. Here there was again, a statistically significant difference in release based on the release medium tested (0.1M HCl or water).

Another observation was that there was no significant difference in the trends for final release concentrations observed between the micron and sub-micron scale emulsions gels, and this held true even for the simple emulsion systems in Appendix 9E. Even though a smaller average droplet size yields an increased surface (interfacial) area, that should accelerate release out of the oil globules, literature in this area includes a number of conflicting results (Li & McClements, 2010). Some studies have reported that such a droplet size reduction yields an increase in percentage release of lipophilic molecules (Charles, Lambert, Brondeur, Courthaudon, & Guichard, 2000; Lee & McClements, 2010), whereas others suggest that droplet size variations have no significant difference (Ahmed, Li, McClements, & Xiao, 2012). Additionally, the use of dialysis tubing has been shown to act as a rate limiting step for the release of lipophiles from emulsion systems, and this may have contributed in not observing

a statistically significant difference between the micron and sub-micron scale systems (Magalhaes, Cave, Seiller, & Benita, 1991). Finally, the possibility exists that κC and cinnamaldehyde interactions via hydrogen bonding could have impeded the release of the active from the gels (Yamada & Shizuma, 2021). The final cinnamaldehyde release values for the release data are presented in Table 5.2.

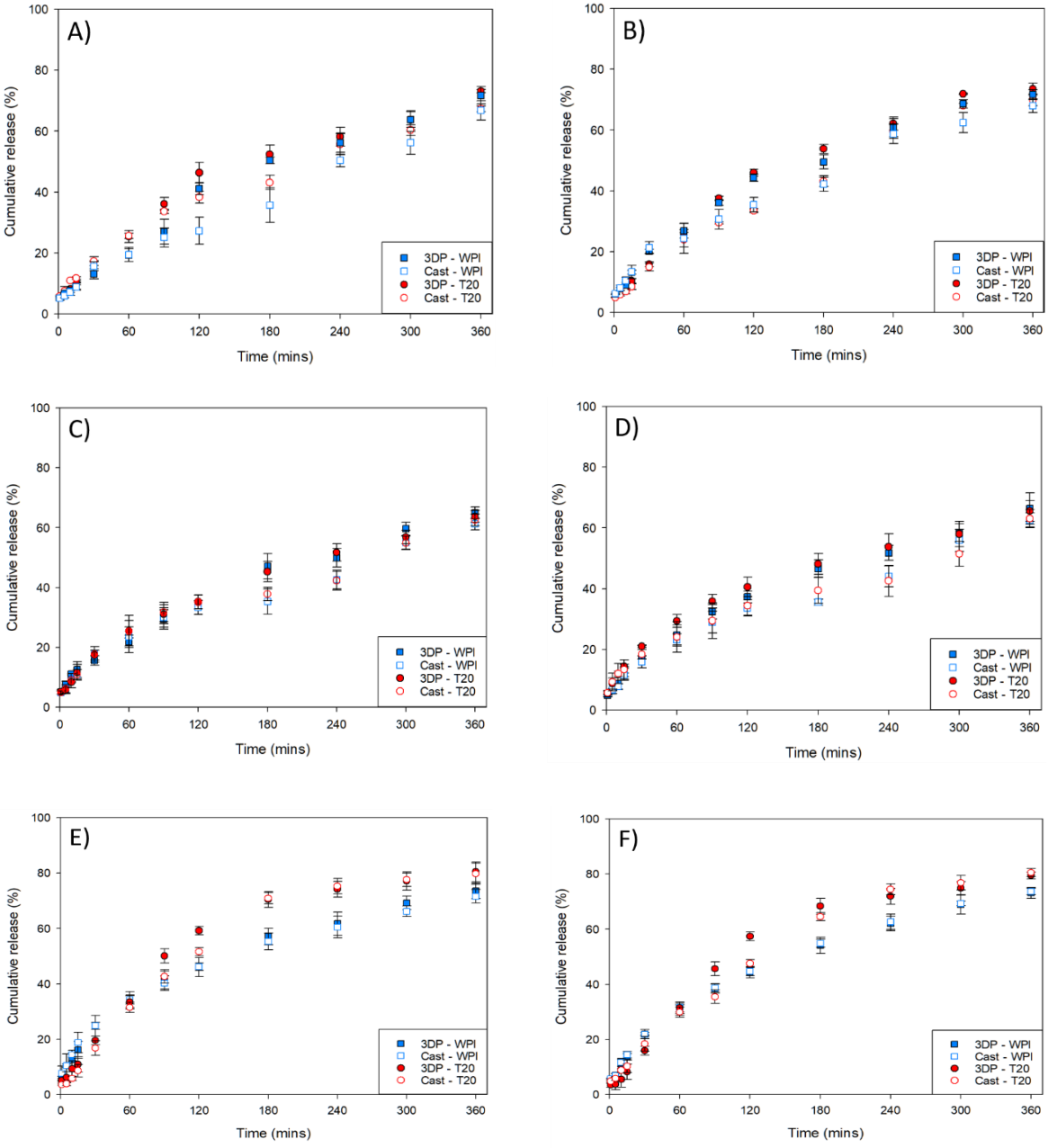

Figure 5.8: A comparison of cumulative release rates of cinnamaldehyde from 3DP and cast κC-emulsion gels at 37 ˚C in water stabilised by T20 and WPI in the (A) micron and (B) sub-micron scale and the same order is followed for the remaining figures with (C-D) in PBS, (E-F) in 0.1M HCl

Table 5.2: Final cinnamaldehyde release values as a %. Superscript letters indicate statistical significance (P<0.05)

Cinnamaldehyde-carrying system	Acceptor Phase	Temp (ºC)	Cinnamaldehyde cumulative release (%) after 6 hours							
pure SFO phase	Water	37	82.9[a]							
	0.1M HCl	37	89.3[b]							
			Micron				**Sub-micron**			
			T20		**WPI**		**T20**		**WPI**	
O/W emulsion	Water	37	76.8[c]		76.3[c]		77.7[c]		77.8[c]	
			3DP	**Cast**	**3DP**	**Cast**	**3DP**	**Cast**	**3DP**	**Cast**
O/W emulsion gel	Water	37	71.2[d]	68.4[d]	71.4[d]	68.8[d]	71.5[d]	69.9[d]	71.7[d]	69.0[d]
		20	55.6[e]	58.3[e]	56.2[e]	60.1[e]	-	-	-	-
	PBS	37	63.7[f]	62.6[f]	65.0[f]	61.2[f]	64.6[f]	63.1[f]	64.4[f]	62.6[f]
		20	53.1[g]	53.5[g]	51.9[g]	52.2[g]	-	-	-	-
	0.1M HCl	37	80.5[h]	79.8[h]	74.6[l]	74.6[l]	79.5[h]	80.5[h]	74.2[l]	74.7[l]
		20	66.4[f]	69.4[df]	66.0[f]	66.2[f]	-	-	-	-
	1M KCl	37	65.1[f]	67.5[f]	63.6[f]	64.5[f]	-	-	-	-
*O/W emulsion gel**	Water	37	69.3[d]	69.1[d]	68.8[d]	68.7[d]	-	-	-	-

*****This system was used for the co-release of cinnamaldehyde (cinn; enclosed within the oil droplets of the O/W emulsion gels) and erioglaucine disodium salt (EDS; entrapped within the gel network of the O/W emulsion gels)

The co-release profiles for cinnamaldehyde and EDS from both the printed and cast κC-emulsion gels and for all release media, were fitted to Ritger-Peppas model shown in Eq [5.3] in order to assess the contributions of diffusion and relaxation to the release of the active molecules (Ritger, et al., 1987). The exponent m values resulting from the fits are given in Table 5.3. The data suggests cinnamaldehyde release from 3DP cylinders is driven primarily by Fickian diffusion as opposed to relaxation of the polymer chains. This is believed to be due to the differences in the internal bulk structures of the 3DP cylinders allowing water to penetrate faster into the 3DP shapes compared to cast gel structures. This leads to a greater diffusion contribution to release compared to the relaxational contribution (Falk, Garramone, & Shivkumar, 2004; Kamlow, et al., 2021a). This is demonstrated by the cast gels having m values further away from 0.5, indicating that the relaxational contribution is amplified. This supports the notion that water was unable to penetrate into the cast cylinders as quickly as the 3DP cylinders, meaning that the relaxation of the polymer chains played a bigger part in the release of the actives.

This modelling data further supports some of the previous conclusions made about differences in release of cinnamaldehyde from micron and sub-micron scale oil droplets. The different droplet length scales did not see a significant difference in cinnamaldehyde release with regards to diffusion and relaxational contributions. The release tests carried in 0.1M HCl, showed that the WPI had a larger relaxational contribution, most likely due to the fact that the network remained intact owing to the WPI molecules stabilising the κC-gel network. The release tests carried out at 20 ˚C had larger m values owing to the decreased energy in the system, slowing the diffusion contribution, and this meant that there was as delay as relaxation had to come into effect to drive more of the release. In terms of the co-release experiments, the presence of the EDS releasing had no effect on the observed release phenomena of the cinnamaldehyde. This provides further evidence that their release occurred through two different mechanisms. The m values for EDS release were higher for the cast gels, compared to the 3DP gels. While our previous study highlighted a much starker difference between 3DP and cast gels for release of a hydrophilic molecule, there were differences such as the lack of dialysis tubing and the previous active, vitamin B1 being cationic, meaning it complexed with the κC which would have affected its release rate (Kamlow, et al., 2021a). 1M KCl did not have a significant effect on the m value compared to the other release media, showing that the gels turning to liquid did not necessarily affect the contributions of diffusion and relaxation to the release. This is highlighted by the similar values observed with the simple emulsions. This further supports the release of the cinnamaldehyde primarily occurring because of expulsion from the oil droplets, rather than the gel network itself.

Table 5.3: Data on the exponent m, which indicates the balance between the relaxational and diffusional contribution to the release of cinnamaldehyde and EDS.

Active-carrying system	Acceptor Phase	Temp (ºC)	Exponent *m*±SD (R^2)							
			Micron				Submicron			
			T20		WPI		T20		WPI	
O/W emulsion	Water	37	0.55±0.04 (0.99)		0.57±0.04 (0.99)		0.52±0.05 (0.97)		0.51±0.04 (0.98)	
			3DP	Cast	3DP	Cast	3DP	Cast	3DP	Cast
O/W emulsion gel	Water	37	0.58±0.03 (0.98)	0.66±0.03 (0.99)	0.58±0.06 (0.98)	0.69±0.03 (0.98)	0.55±0.04 (0.99)	0.65±0.04 (0.99)	0.53±0.03 (0.99)	0.67±0.04 (0.97)
		20	0.65±0.02 (0.99)	0.78±0.02 (0.99)	0.66±0.02 (0.99)	0.72±0.02 (0.99)	-	-	-	-
	PBS	37	0.53±0.02 (0.99)	0.67±0.03 (0.98)	0.55±0.03 (0.99)	0.69±0.03 (0.98)	0.55±0.03 (0.99)	0.67±0.03 (0.98)	0.62±0.01 (0.99)	0.62±0.03 (0.98)
		20	0.72±0.01 (0.99)	0.74±0.02 (0.99)	0.70±0.01 (0.99)	0.73±0.02 (0.99)	-	-	-	-
	0.1M HCl	37	0.58±0.04 (0.99)	0.61±0.04 (0.99)	0.63±0.01 0.99)	0.66±0.01 (0.99)	0.51±0.01 (0.99)	0.59±0.04 (0.99)	0.63±0.02 (0.99)	0.66±0.02 (0.99)
		20	0.62±0.02 (0.99)	0.65±0.02 (0.99)	0.71±0.01 (0.99)	0.75±0.02 (0.99)	-	-	-	-
	1M KCl	37	0.59±0.02 (0.99)	0.68±0.02 (0.99)	0.58±0.02 (0.99)	0.64±0.02 (0.99)	-	-	-	-
*O/W emulsion gel**	Water (cinn.)	37	0.56±0.02 (0.98)	0.69±0.03 (0.98)	0.56±0.03 (0.98)	0.67±0.04 (0.97)	-	-	-	-
	Water (EDS)	37	0.55±0.02 (0.96)	0.62±0.02 (0.98)	0.52±0.03 (0.98)	0.59±0.03 (0.98)	-	-	-	-

*****This system was used for the co-release of cinnamaldehyde (cinn; enclosed within the oil droplets of the O/W emulsion gels) and erioglaucine disodium salt (EDS; entrapped within the gel network of the O/W emulsion gels)

5.3.6 Co-release study

Co-release from κC-emulsion gels were also evaluated. Two actives were introduced within the κC-emulsion gels, with cinnamaldehyde being present within the lipid phase (oil droplets) of the emulsion gels, and EDS entrapped within the aqueous gel phase. This was carried out to assess whether co-release of actives placed within separate compartments of the κC-emulsion gel microstructure can effectively be utilised to enable their independent co-delivery. This approach is certainly unique in the 3DP emulsion gel literature, and thus extends the current capabilities of these systems to also provide opportunities for the design of novel and/or customisable co-release profiles of both hydrophilic and hydrophobic actives. As co-

morbidities increase in society, people taking many medications benefit from combined doses (Gadde, et al., 2011). The release behaviour of the κC-EDS-cinnamaldehyde emulsion gels in water at 37 ˚C were studied and the obtained data is shown in Figure 5.9.

The release profiles showed no significant difference between T20 and WPI stabilised κC-emulsion gels for the co-release of cinnamaldehyde and EDS. Furthermore, there was once again no significant difference in the final release percentages for the cinnamaldehyde, and the divergence and subsequent convergence could be once more be observed. With the EDS however, there was a statistically significant difference between its release between cast and 3DP gels after 6 hours. This indicates that the release profiles of the two model actives are independently controlled; cinnamaldehyde release is principally controlled by expulsion from the entrapped oil droplets, while EDS release is dictated by the rate of its liberation from the gel network. This is in agreement with previous studies comparing 3DP to cast κC gels when releasing a hydrophilic molecule (Kamlow, et al., 2021a). It should be noted, however, that after 24h 100% of the EDS had been released from the gel matrices for both cast and 3DP gels. Compared to the 'mono'-release of cinnamaldehyde in water at 37 ˚C, the presence of EDS in the co-release formulation did not have any significant effect on the release of the former active from the κC-emulsion gels. Overall, the data presented here offer clear confirmation that both 3DP and cast κC-emulsion gels can indeed facilitate the independent co-release of one model lipophilic active (cinnamaldehyde) and one model hydrophilic active (EDS). What is further highlighted here is that the desirable individual co-release profiles can be designed separately and then effectively assembled into one 3DP emulsion gel microstructure, without loss of individual release identity/performance, while utilising 3DP's ability to readily alter the size and shape of the desired product, delivering flexible dosing, without the need of additional moulds or tooling that would be required with cast samples.

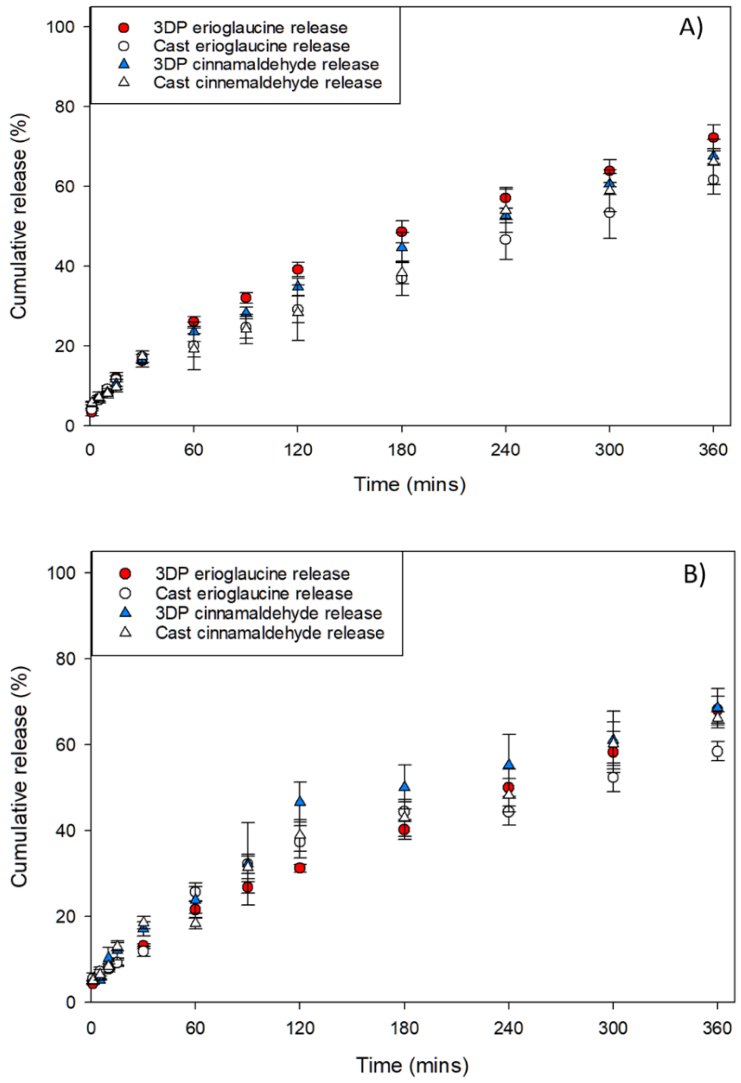

Figure 5.9: Co-release profiles for cinnamaldehyde and EDS from κC-emulsion gels stabilised by (A) T20 and (B) WPI in water at 37 ˚C

5.4 Conclusions

This study provides further insight into the stability, mechanical and performance characteristics of κC-emulsion gels. 3DP κC-emulsion gels lose slightly more water over time than cast gels, but the 3DP process has no effect on droplet size stability during production or storage of κC-emulsion gels. This study has for the first time highlighted differences between 3DP gels based on their SFO concentration and emulsifier type through penetration testing, with lower SFO concentration and the use of WPI as an emulsifier yielding more resistant gels. This study has shown for the first time in release testing, that the release medium has been shown to affect the release rate of lipophilic molecules from cast and 3DP κC- emulsion gels.

However, droplet size and production process had no effect on the release rate, although the use of dialysis tubing might have affected this. Finally, co-release of EDS and cinnamaldehyde was carried out, for the first time from a 3DP bulk structure. This shows that 3DP can be used to create customisable κC gels containing hydrophilic and/or lipophilic active molecules, with desired properties tuneable through variances in SFO concentration, shape, emulsifier type and size. Future studies could focus on the addition of a dietarily appropriate protein and carbohydrate concentrations, to give a total food source that can be fortified with active molecules.

Acknowledgements

This work was supported by the Engineering and Physical Sciences Research Council [grant number EP/N024818/1].

5.5 References

Ahmed, K., Li, Y., McClements, D. J., & Xiao, H. (2012). Nanoemulsion- and emulsion-based delivery systems for curcumin: Encapsulation and release properties. *Food Chemistry, 132*(2), 799-807.

Ako, K. (2015). Influence of elasticity on the syneresis properties of κ-carrageenan gels. *Carbohydrate Polymers, 115*, 408-414.

Andrews, G. P., Donnelly, L., Jones, D. S., Curran, R. M., Morrow, R. J., Woolfson, A. D., & Malcolm, R. K. (2009). Characterization of the Rheological, Mucoadhesive, and Drug Release Properties of Highly Structured Gel Platforms for Intravaginal Drug Delivery. *Biomacromolecules, 10*(9), 2427-2435.

Balaguer, M. P., Borne, M., Chalier, P., Gontard, N., Morel, M.-H., Peyron, S., Gavara, R., & Hernandez-Munoz, P. (2013). Retention and Release of Cinnamaldehyde from Wheat Protein Matrices. *Biomacromolecules, 14*(5), 1493-1502.

Ben Arfa, A., Preziosi-Belloy, L., Chalier, P., & Gontard, N. (2007). Antimicrobial Paper Based on a Soy Protein Isolate or Modified Starch Coating Including Carvacrol and Cinnamaldehyde. *Journal of Agricultural and Food Chemistry, 55*(6), 2155-2162.

Beverung, C. J., Radke, C. J., & Blanch, H. W. (1999). Protein adsorption at the oil/water interface: characterization of adsorption kinetics by dynamic interfacial tension measurements. *Biophysical Chemistry, 81*(1), 59-80.

Boland, A. B., Delahunty, C. M., & van Ruth, S. M. (2006). Influence of the texture of gelatin gels and pectin gels on strawberry flavour release and perception. *Food Chemistry, 96*(3), 452-460.

Chanamai, R., & McClements, D. J. (2002). Comparison of Gum Arabic, Modified Starch, and Whey Protein Isolate as Emulsifiers: Influence of pH, CaCl2 and Temperature. *Journal of Food Science, 67*(1), 120-125.

Charles, M., Lambert, S., Brondeur, P., Courthaudon, J.-L., & Guichard, E. (2000). Influence of Formulation and Structure of an Oil-in-Water Emulsion on Flavor Release. In *Flavor Release* (Vol. 763, pp. 342-354): American Chemical Society.

Chen, H., Lu, Y., Yuan, F., Gao, Y., & Mao, L. (2021). Effect of interfacial compositions on the physical properties of alginate-based emulsion gels and chemical stability of co-encapsulated bioactives. *Food Hydrocolloids, 111*, 106389.

de Kruif, C. G., Weinbreck, F., & de Vries, R. (2004). Complex coacervation of proteins and anionic polysaccharides. *Current Opinion in Colloid & Interface Science, 9*(5), 340-349.

Falk, B., Garramone, S., & Shivkumar, S. (2004). Diffusion coefficient of paracetamol in a chitosan hydrogel. *Materials Letters, 58*(26), 3261-3265.

Fiszman, S. M., Lluch, M. A., & Salvador, A. (1999). Effect of addition of gelatin on microstructure of acidic milk gels and yoghurt and on their rheological properties. *International Dairy Journal, 9*(12), 895-901.

Fiszman, S. M., & Salvador, A. (1999). Effect of gelatine on the texture of yoghurt and of acid-heat-induced milk gels. *Zeitschrift für Lebensmitteluntersuchung und -Forschung A, 208*(2), 100-105.

Friedman, M. (2017). Chemistry, Antimicrobial Mechanisms, and Antibiotic Activities of Cinnamaldehyde against Pathogenic Bacteria in Animal Feeds and Human Foods. *Journal of Agricultural and Food Chemistry, 65*(48), 10406-10423.

Gadde, K. M., Allison, D. B., Ryan, D. H., Peterson, C. A., Troupin, B., Schwiers, M. L., & Day, W. W. (2011). Effects of low-dose, controlled-release, phentermine plus topiramate combination on weight and associated comorbidities in overweight and obese adults (CONQUER): a randomised, placebo-controlled, phase 3 trial. *The Lancet, 377*(9774), 1341-1352.

Gill, A. O., & Holley, R. A. (2004). Mechanisms of bactericidal action of cinnamaldehyde against Listeria monocytogenes and of eugenol against L. monocytogenes and Lactobacillus sakei. *Applied and environmental microbiology, 70*(10), 5750-5755.

Goudappel, G. J. W., van Duynhoven, J. P. M., & Mooren, M. M. W. (2001). Measurement of Oil Droplet Size Distributions in Food Oil/Water Emulsions by Time Domain Pulsed Field Gradient NMR. *Journal of Colloid and Interface Science, 239*(2), 535-542.

Govindaraj, P., Subramanian, S., & Raghavachari, D. (2021). Preparation of gels of chitosan through a hydrothermal reaction in the presence of malonic acid and cinnamaldehyde: characterization and antibacterial activity. *New Journal of Chemistry, 45*(47), 22101-22112.

Gowder, S. J., & Devaraj, H. (2006). Effect of the food flavour cinnamaldehyde on the antioxidant status of rat kidney. *Basic & clinical pharmacology & toxicology, 99*(5), 379-382.

Hermansson, A.-M., Eriksson, E., & Jordansson, E. (1991). Effects of potassium, sodium and calcium on the microstructure and rheological behaviour of kappa-carrageenan gels. *Carbohydrate Polymers, 16*(3), 297-320.

Jeong, H.-S., Kim, E., Nam, C., Choi, Y., Lee, Y.-J., Weitz, D. A., Lee, H., & Choi, C.-H. (2021). Hydrogel Microcapsules with a Thin Oil Layer: Smart Triggered Release via Diverse Stimuli. *Advanced Functional Materials, 31*(18), 2009553.

Juslin, L., Antikainen, O., Merkku, P., & Yliruusi, J. (1995). Droplet size measurement: I. Effect of three independent variables on droplet size distribution and spray angle from a pneumatic nozzle. *International Journal of Pharmaceutics, 123*(2), 247-256.

Kamlow, M.-A., Spyropoulos, F., & Mills, T. (2021). 3D printing of kappa-carrageenan emulsion gels. *Food Hydrocolloids for Health*, 100044.

Kamlow, M.-A., Vadodaria, S., Gholamipour-Shirazi, A., Spyropoulos, F., & Mills, T. (2021). 3D printing of edible hydrogels containing thiamine and their comparison to cast gels. *Food Hydrocolloids, 116*, 106550.

Kenta, S., Raikos, V., Vagena, A., Sevastos, D., Kapolos, J., Koliadima, A., & Karaiskakis, G. (2013). Kinetic study of aggregation of milk protein and/or surfactant-stabilized oil-in-water emulsions by Sedimentation Field-Flow Fractionation. *Journal of Chromatography A, 1305*, 221-229.

Lee, C. M., & Chung, K. H. (1989). Analysis of surimi gel properties by compression and penetration tests. *Journal of Texture Studies, 20*(3), 363-377.

Lee, S. J., & McClements, D. J. (2010). Fabrication of protein-stabilized nanoemulsions using a combined homogenization and amphiphilic solvent dissolution/evaporation approach. *Food Hydrocolloids, 24*(6), 560-569.

Li, Y., & McClements, D. J. (2010). New Mathematical Model for Interpreting pH-Stat Digestion Profiles: Impact of Lipid Droplet Characteristics on in Vitro Digestibility. *Journal of Agricultural and Food Chemistry, 58*(13), 8085-8092.

Liu, H., Nie, Y., & Chen, H. (2014). Effect of Different Starches on Colors and Textural Properties of Surimi-Starch Gels. *International Journal of Food Properties, 17*(7), 1439-1448.

Lu, B., Tarn, M. D., Pamme, N., & Georgiou, T. K. (2018). Fabrication of tailorable pH responsive cationic amphiphilic microgels on a microfluidic device for drug release. *Journal of Polymer Science Part A: Polymer Chemistry, 56*(1), 59-66.

Magalhaes, N. S. S., Cave, G., Seiller, M., & Benita, S. (1991). The stability and in vitro release kinetics of a clofibride emulsion. *International Journal of Pharmaceutics, 76*(3), 225-237.

McClements, D. J. (2018). Enhanced delivery of lipophilic bioactives using emulsions: a review of major factors affecting vitamin, nutraceutical, and lipid bioaccessibility. *Food & function, 9*(1), 22-41.

Mcclements, D. J., Monahan, F. J., & Kinsella, J. E. (1993). Effect Of Emulsion Droplets On The Rheology Of Whey Protein Isolate Gels. *Journal of Texture Studies, 24*(4), 411-422.

Nagula, R. L., & Wairkar, S. (2019). Recent advances in topical delivery of flavonoids: A review. *Journal of Controlled Release, 296*, 190-201.

Özcan, İ., Abacı, Ö., Uztan, A. H., Aksu, B., Boyacıoğlu, H., Güneri, T., & Özer, Ö. (2009). Enhanced topical delivery of terbinafine hydrochloride with chitosan hydrogels. *Aaps Pharmscitech, 10*(3), 1024-1031.

Pal, R., & Rhodes, E. (1989). Viscosity/concentration relationships for emulsions. *Journal of Rheology, 33*(7), 1021-1045.

Pang, Z., Deeth, H., Sopade, P., Sharma, R., & Bansal, N. (2014). Rheology, texture and microstructure of gelatin gels with and without milk proteins. *Food Hydrocolloids, 35*, 484-493.

Phillips, G. O., & Williams, P. A. (2009). *Handbook of hydrocolloids*: Elsevier.

Ritger, P. L., & Peppas, N. A. (1987). A simple equation for description of solute release I. Fickian and non-fickian release from non-swellable devices in the form of slabs, spheres, cylinders or discs. *Journal of Controlled Release, 5*(1), 23-36.

Rostami, H., Nikoo, A. M., Rajabzadeh, G., Niknia, N., & Salehi, S. (2018). Development of cumin essential oil nanoemulsions and its emulsion filled hydrogels. *Food Bioscience, 26*, 126-132.

Serizawa, R., Shitara, M., Gong, J., Makino, M., Kabir, M. H., & Furukawa, H. (2014). 3D jet printer of edible gels for food creation. In *Behavior and Mechanics of Multifunctional*

Materials and Composites 2014 (Vol. 9058, pp. 90580A): International Society for Optics and Photonics.

Siddiqua, S., Anusha, B., Ashwini, L., & Negi, P. (2015). Antibacterial activity of cinnamaldehyde and clove oil: effect on selected foodborne pathogens in model food systems and watermelon juice. *Journal of food science and technology, 52*(9), 5834-5841.

Singh, B., Kaur, T., & Singh, S. (1997). Correction of raw dissolution data for loss of drug and volume during sampling. *Indian journal of pharmaceutical sciences, 59*(4), 196.

Singh, H., Tamehana, M., Hemar, Y., & Munro, P. A. (2003). Interfacial compositions, microstructure and stability of oil-in-water emulsions formed with mixtures of milk proteins and κ-carrageenan: 2. Whey protein isolate (WPI). *Food Hydrocolloids, 17*(4), 549-561.

Stone, A. K., & Nickerson, M. T. (2012). Formation and functionality of whey protein isolate–(kappa-, iota-, and lambda-type) carrageenan electrostatic complexes. *Food Hydrocolloids, 27*(2), 271-277.

Strother, H., Moss, R., & McSweeney, M. B. (2020). Comparison of 3D printed and molded carrots produced with gelatin, guar gum and xanthan gum. *Journal of Texture Studies, 51*(6), 852-860.

Teo, A., Goh, K. K. T., Wen, J., Oey, I., Ko, S., Kwak, H.-S., & Lee, S. J. (2016). Physicochemical properties of whey protein, lactoferrin and Tween 20 stabilised nanoemulsions: Effect of temperature, pH and salt. *Food Chemistry, 197*, 297-306.

Thrimawithana, T. R., Young, S., Dunstan, D. E., & Alany, R. G. (2010). Texture and rheological characterization of kappa and iota carrageenan in the presence of counter ions. *Carbohydrate Polymers, 82*(1), 69-77.

van der Ven, C., Gruppen, H., de Bont, D. B. A., & Voragen, A. G. J. (2001). Emulsion Properties of Casein and Whey Protein Hydrolysates and the Relation with Other Hydrolysate Characteristics. *Journal of Agricultural and Food Chemistry, 49*(10), 5005-5012.

Vrentas, J., & Vrentas, C. (1992). Fickian diffusion in glassy polymer-solvent systems. *Journal of Polymer Science Part B: Polymer Physics, 30*(9), 1005-1011.

Wei, Q.-Y., Xiong, J.-J., Jiang, H., Zhang, C., & Wen, Y. (2011). The antimicrobial activities of the cinnamaldehyde adducts with amino acids. *International Journal of Food Microbiology, 150*(2), 164-170.

Wiącek, A., & Chibowski, E. (1999). Zeta potential, effective diameter and multimodal size distribution in oil/water emulsion. *Colloids and Surfaces A: Physicochemical and Engineering Aspects, 159*(2), 253-261.

Wiącek, A. E., & Chibowski, E. (2002). Zeta potential and droplet size of n-tetradecane/ethanol (protein) emulsions. *Colloids and Surfaces B: Biointerfaces, 25*(1), 55-67.

Wu, Y., Petrochenko, P., Chen, L., Wong, S. Y., Absar, M., Choi, S., & Zheng, J. (2016). Core size determination and structural characterization of intravenous iron complexes by cryogenic transmission electron microscopy. *International Journal of Pharmaceutics, 505*(1), 167-174.

Yamada, Y., & Shizuma, M. (2021). Study on release suppression of cinnamaldehyde from κ-carrageenan gel by HR-MASNMR and pulsed field gradient NMR (PFG-NMR). *Food Hydrocolloids, 110*, 106130.

Yang, F., Zhang, M., Bhandari, B., & Liu, Y. (2018). Investigation on lemon juice gel as food material for 3D printing and optimization of printing parameters. *Lwt, 87*, 67-76.

Yang, F., Zhang, M., Prakash, S., & Liu, Y. (2018). Physical properties of 3D printed baking dough as affected by different compositions. *Innovative Food Science & Emerging Technologies, 49*, 202-210.

Chapter 6

Conclusions and future work

6.1 Conclusions

This research intended to assess the printability of hydrocolloid gel systems and analyse their mechanical characteristics and performance as release vehicles compared to the equivalent cast systems. More complex systems were designed containing an oil phase to increase the functionality of the 3DP systems. Rheological and DSC data were applied to scrutinise the systems before printing and in depth characterisation was carried out after printing to evaluate textural characteristics and performance in release and stability.

The study intended to establish some parameters for the characterised systems that could be transferred between different printer systems. It also aimed to quantify the differences in microstructure and bulk structure between 3DP and cast gel systems. In depth conclusions can be found at the end of each of the result chapters within the thesis. The proceeding sections contain highlighted conclusions established over the course of this work.

6.1.1 Development of hydrocolloid feeds suitable for hot-extrusion 3DP

Most of the current literature pertaining to the 3DP of hydrocolloid gels focuses on cold-extrusion of already set gels. These maintain their shape after printing owing to a yield stress. Whereas the work set out in this thesis developed formulations which underwent a sol-gel transition within the printer itself. Hydrocolloids that rapidly gel below their T_{gel} were targeted, in this case κC and agar. Several printing parameters were tested but agar was not found to be printable under the circumstances at the time, although it was believed that it would be printable through increasing the hydrocolloid concentration or using an adjunct. Therefore, κC was the main focus of the work within this study as it was found to be readily printable within a narrow range of parameters, even after embedding vitamin B1 within it as a model molecule. The parameters determined from this were used in the subsequent chapters to produce 3DP κC-gels in various shapes and sizes. These were translatable between two different printing setups with varying temperature control, software and dimensions. Therefore, from this it's likely that these parameters will translate to other 3D printers, for other researchers looking to 3D print κC gels.

6.1.2 Addition of an oil phase to create emulsion gels does not affect printability

It was found to be possible to disperse SFO into an emulsion using 1% w/w T20 or WPI as an emulsifier and create printable systems ranging from 0-40% w/w SFO. This required the concentration of κC to be fixed at 3% w/w within the aqueous phase of the emulsion system. These emulsion gels provide far more flexibility as a food system with their straightforward ability to incorporate lipophilic molecules and controllable energy content. The low molecular weight surfactant T20 stabilised emulsions underwent flocculation when the κC was introduced into the emulsion system, but the WPI-stabilised emulsions remained well dispersed. Droplet size analysis of the emulsion gel systems showed that the droplet sizes remained stable over 8 weeks. This was believed to be because the solid continuous gel phase did not allow movement of the oil droplets within the gels. Since most research focuses on simple hydrogel systems, the ability to produce emulsion gels provides far more scope to utilise 3D printing in the production of food. Fat-soluble flavours and molecules can be incorporated in a straightforward manner and the creamy mouthfeel fats impart will go a long way to making these foods more palatable and help to overcome consumer reticence, while being an emulsion means that the fat level is still far lower than an oleogel.

6.1.3 There is a clear distinction between the mechanical characteristics of 3DP and cast gels

Texture profile analysis of 3DP gels showed that when subjected to compression forces, 3DP gels fail at the semi-fused sites between layers. Whereas continuous cast gel networks fracture upon failure. This is because the semi-fused sites are weaker than the gel network. With the addition of the oil phase, this trend held true. Even though increasing the oil concentration weakened the cast gel network, there was no significant difference for the 3DP gels regardless of the oil concentration as the semi-fused sites were still the weakest points of the gel. This trend held true for amplitude sweeps carried out on printed and cast discs. The

cast discs were far more resistant to shear strain and therefore had a larger LVER compared to the printed discs which broke down faster along the semi-fused sites of the printing. With penetration testing the cast gels were still stronger than the printed gels but owing to the test examining local variations around the probe head, it showed a difference between 3DP based on oil concentrations. 5% w/w SFO 3DP emulsion gels required more force to rupture the surface compared to 40% w/w SFO 3DP emulsion gels, which wasn't observed with compression testing or oscillatory rheology. The fact that these gels require less force to break down than the equivalent cast gels, means that they will be suitable for patients with swallowing difficulties, as they are softer. The same holds true for people who are unwilling or unable to swallow tablets. The use of a chewable dosage form is recommended in these situations. Liquid dosage forms often have issues with having to be shaken, often leading to uneven doses. The solid gel network prevents aggregation or sedimentation of dissolved molecules.

6.1.4 Performance of 3DP and cast gel systems as release vehicles

When placed into water it was found that the 3DP gels released more of the vitamin B1 than the cast gels in the same period. Light microscopy showed that there was layering throughout the bulk structure of the 3DP gels. It was believed that this allowed water to penetrate faster into the gels and facilitated the faster release of hydrophilic molecules that were held within the aqueous gelled phase. Simple mathematical modelling supported this hypothesis further, showing that diffusion was entirely responsible for the release of vitamin B1 from the κC hydrogels. This suggested that the 3DP gels had encouraged diffusion to such an extent as to make the relaxational contribution to release essentially zero. With the addition of the oil phase, cinnamaldehyde, a lipophilic molecule, was added to the oil phase and its release was examined. Unlike the hydrophilic vitamin B1, there was no significant difference in the cinnamaldehyde released for cast and 3DP gels. This indicated that the release of the lipophile was controlled by its rate of expulsion from the oil droplets rather than liberation from the gel network which controlled the release of the hydrophilic molecules.

6.1.5 Co-release of lipophilic and hydrophilic molecules

Chapter 5 of this work demonstrated that in addition to being able to release a lipophilic molecule from within the entrapped oil droplets, a hydrophile could be entrapped within the gel network to facilitate co-release of two molecules from the emulsion gels. The addition of the EDS did not lead to any change in the release profile of the cinnamaldehyde. This means that these gels can be formulated with at least two separate active molecules and these can be released with simultaneously without effecting each other. 3D printing's inherent flexibility allowing the easy production of various shapes and sizes, plus the ability to modulate the release rates through formulation (i.e. different emulsifiers, hydrocolloids, oil concentration); means that multiple actives can be loaded into gels alongside colours and flavours and this can be used to create innovative and palatable medical dosage forms. Furthermore, the biocompatible nature of these hydrocolloids would permit the use of these 3DP gels to create implants tailored for specific areas and patient size requirements, with changes in size and shape being a simple matter of changing a shape on a computer.

6.2 Future work

6.2.1 Investigating different hydrocolloid systems

Having found a formulation this was printable between different printing setups; this work was able to carry out in-depth analysis of 3DP gels and quantify how they compare to cast gels. However, this work focused almost entirely on κC, so one area for future work would be to examine other hydrocolloid systems such as gelatin, gellan and agar. The appeal of gelatin would be the production of a gel system that would give rapid, melt-triggered release of an active molecule. However, there may well exist other hydrocolloids or hydrocolloid combinations that melt at physiological pH without the slow gelling issues of gelatin.

6.2.2 Rheological investigation into viscosity

Almost all the rheological investigation contained within this project was focused on the transition temperatures and the gel characteristics. The assumption that hydrocolloid

solutions would extrude in a straightforward manner, held true across all the experimental work. The only focus on the sol state was in chapter 4, when it was observed that increased SFO concentrations required a greater syringe driver rate to extrude the same amount of material. Therefore, in future especially when creating emulsion gels, it would be prudent to test viscosity of the solutions at the printing temperatures, to ensure that they will print without issue as opposed to the trial and error approach taken in chapter 4.

6.2.3 Examining the effects of cationic and Pickering emulsifiers

Another area to consider in future projects is the κC-emulsion gel systems. Two emulsifiers were utilised within this project. WPI was negatively charged and T20 is non-ionic. So, one area to examine would be a protein below its isoelectric point or a cationic surfactant such as lauric arginate. The oil droplets with a positive surface charge would interact with the κC gel network and reinforce it. Another possibility would be stabilising an emulsion using Pickering particles. It would be interesting to examine the textural properties of these gels systems, as well as assessing whether they undergo flocculation in a similar manner to the T20 stabilised emulsion gel systems.

6.2.4 Further experiments examining co-release of multiple actives

Having carried out release testing of both hydrophilic and lipophilic molecules separately and together, future work could assess the release of multiple hydrophiles and lipophiles within the same gel network. Either by entrapping multiple hydrophiles within the gel network or by dispersing multiple lipophiles into oil and then mixing them together. It would be interesting to see if they started interfering with each other's release. Another interesting avenue would be mixing cationic and anionic hydrophiles to see if their interaction or lack thereof with the anionic κC backbone affects the release of these molecules. Another exciting avenue would be the use of Pickering particles as mentioned above, that consist of molecular complexes that can entrap a molecule. In effect allowing for triple release from three different pathways.

6.2.5 3D printing of a total food source

The addition of the oil allowed for the creation of emulsion gels in Chapter 4 as a more complex foodstuff. In future this could be taken further with the addition of dietarily relevant quantities of carbohydrates and proteins. This would require either a hydrocolloid system that requires holding at a lower temperature to prevent WPI denaturation and aggregation or the use of a protein that doesn't aggregate when heated to around 50 ˚C and held for around two hours. This work has shown that up to 40% w/w SFO can be incorporated into κC-gel systems without affecting printability. If a formulation could be created with 15% w/w each of oil, protein and carbohydrate you could then have a food source that can be customised for a certain need with each of the three being adjustable. Then small amounts of flavour and colour molecules could be added, as well as nutrients such as vitamins and minerals, although chapter 3 showed that even small amounts of these can have a pronounced effect on the nature of the gel network, so this would have to be taken into account. Since 3DP already facilitates easily adjustable sizes and shapes of printed items, this highly customisable system can be used to facilitate the dissemination of customisable nutrition for speciality groups.

Appendices

Appendix 1

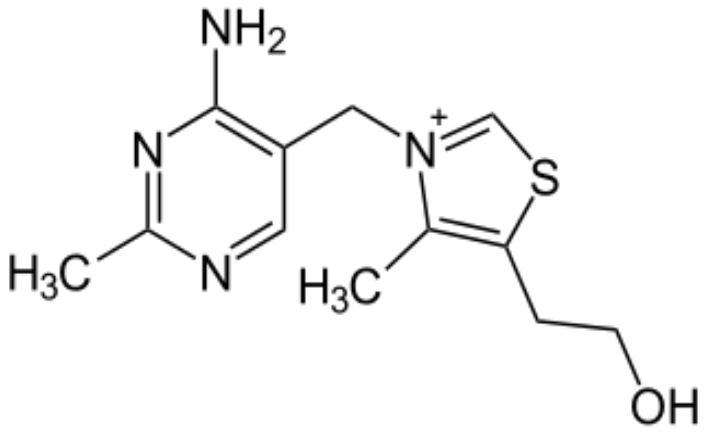

Appendix 1: Chemical structure of thiamine (vitamin B1)

Appendix 2

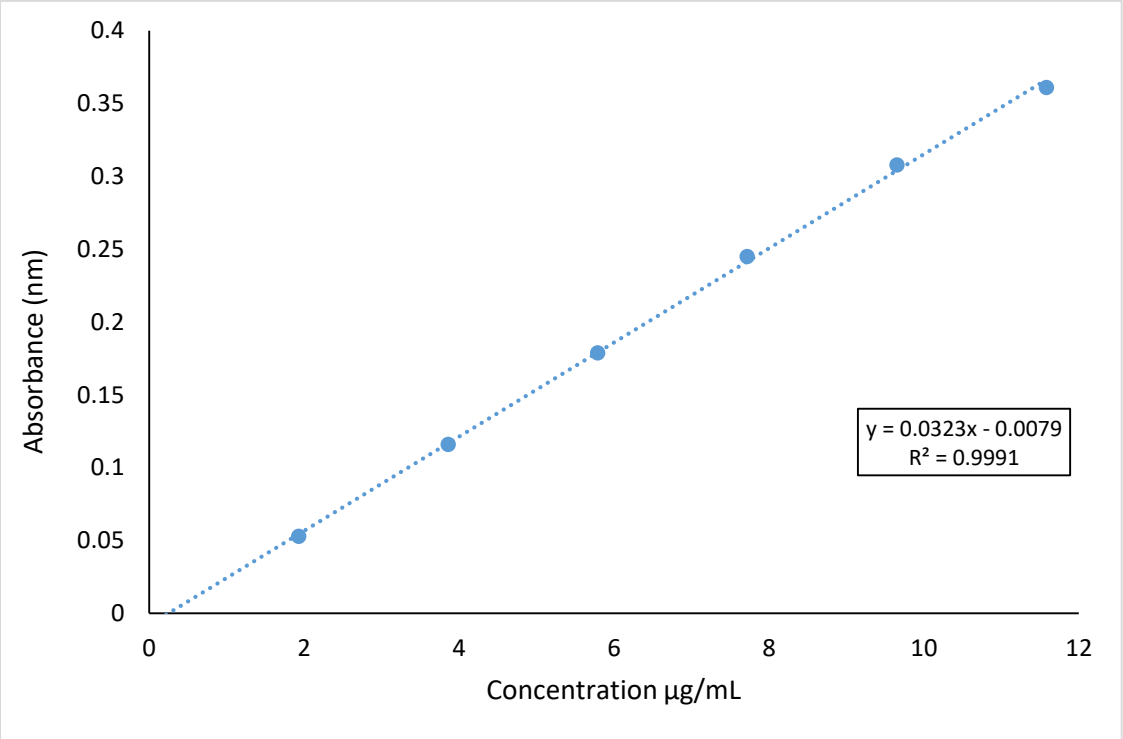

Appendix 2: Calibration curve for thiamine hydrochloride in water

Appendix 3

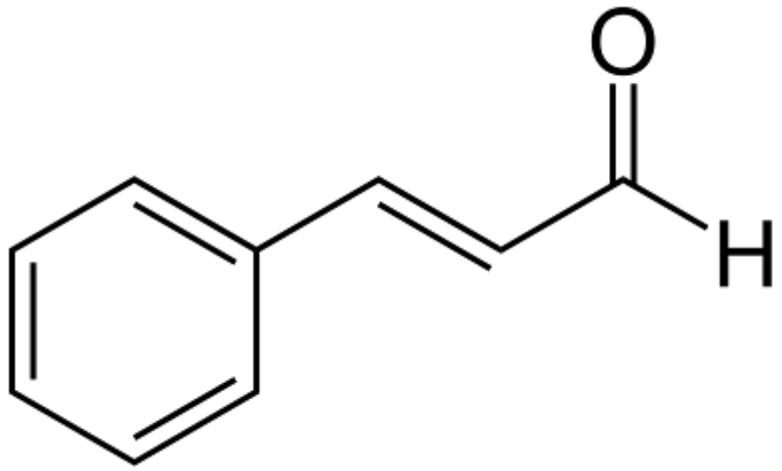

Appendix 3: Chemical structure of cinnamaldehyde

Appendix 4

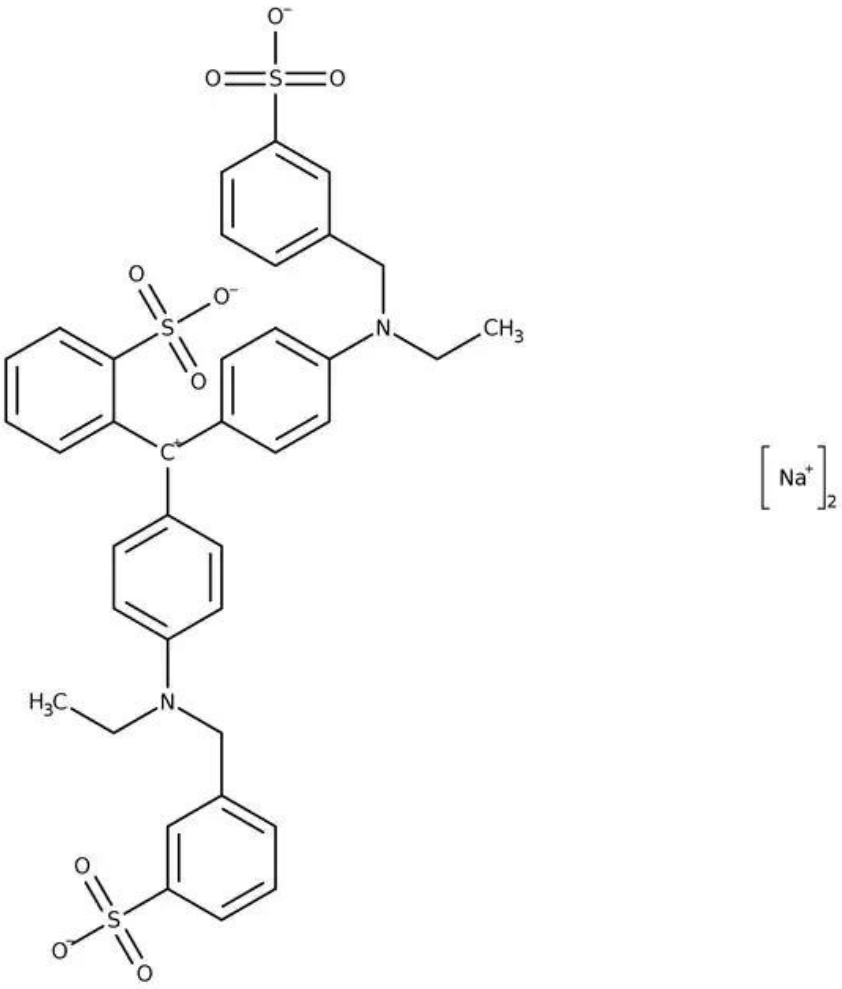

Appendix 4: Chemical structure of erioglaucine disodium salt

Appendix 5

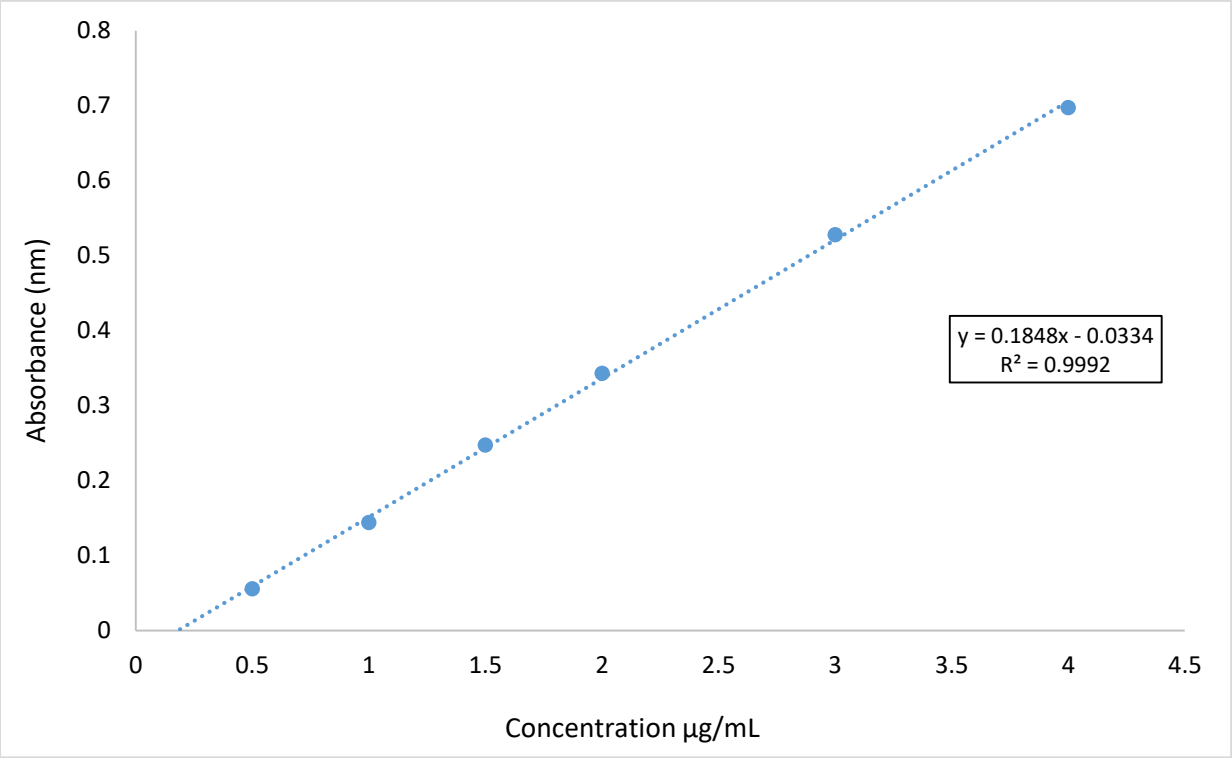

Appendix 5: Calibration curve for cinnamaldehyde in water

Appendix 6

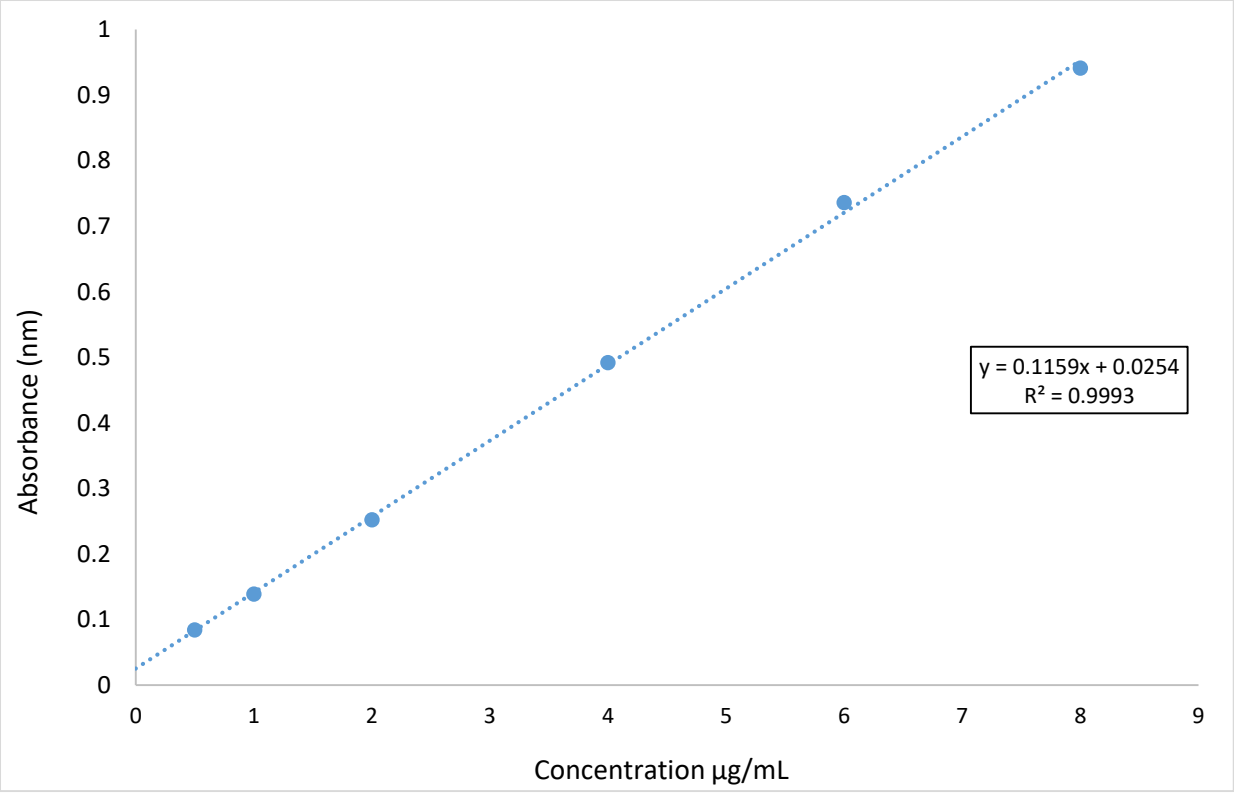

Appendix 6: Calibration curve for EDS in water

Appendix 7

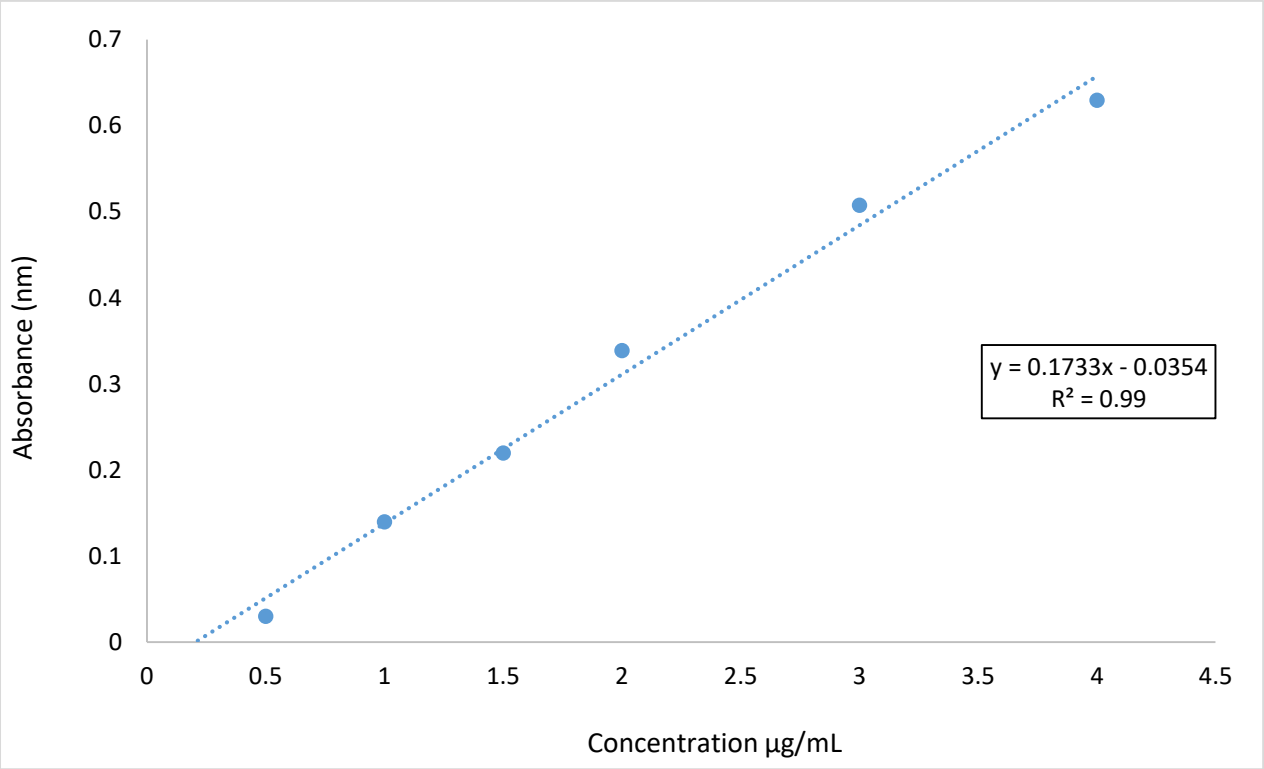

Appendix 7: Calibration curve for cinnamaldehyde in pentane following two-phase extraction from water

Appendix 8

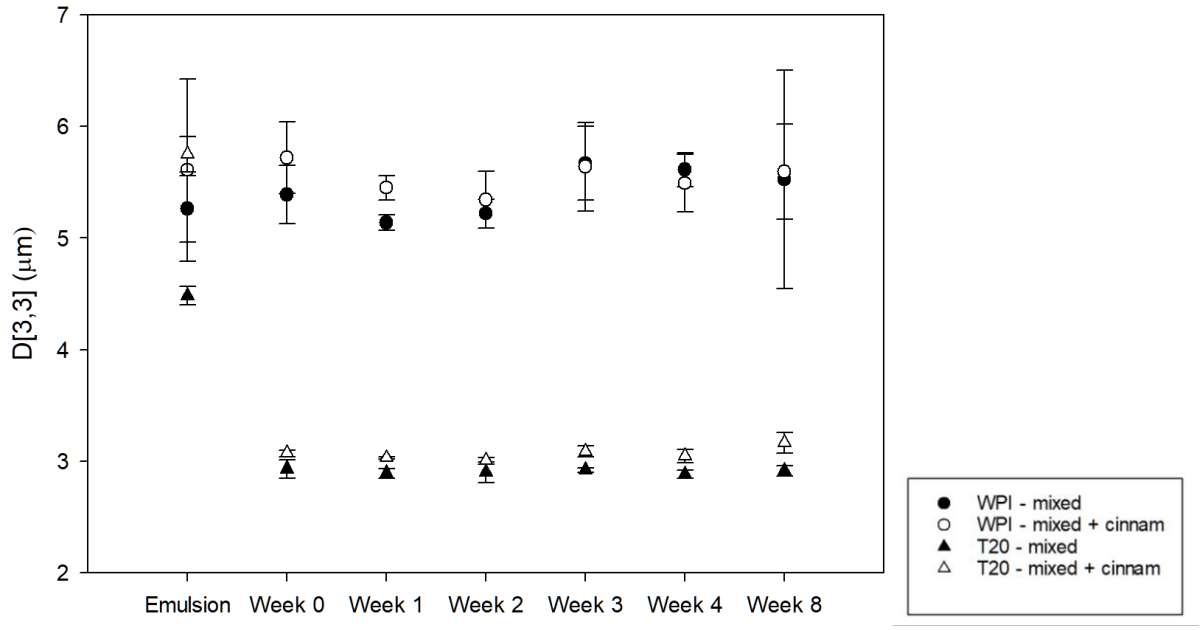

Appendix 8: TD-NMR over 8 weeks showing D3,3 values for κC-emulsion gels containing mixed micron and sub-micron scale emulsions with and without cinnamaldehyde

Appendix 9

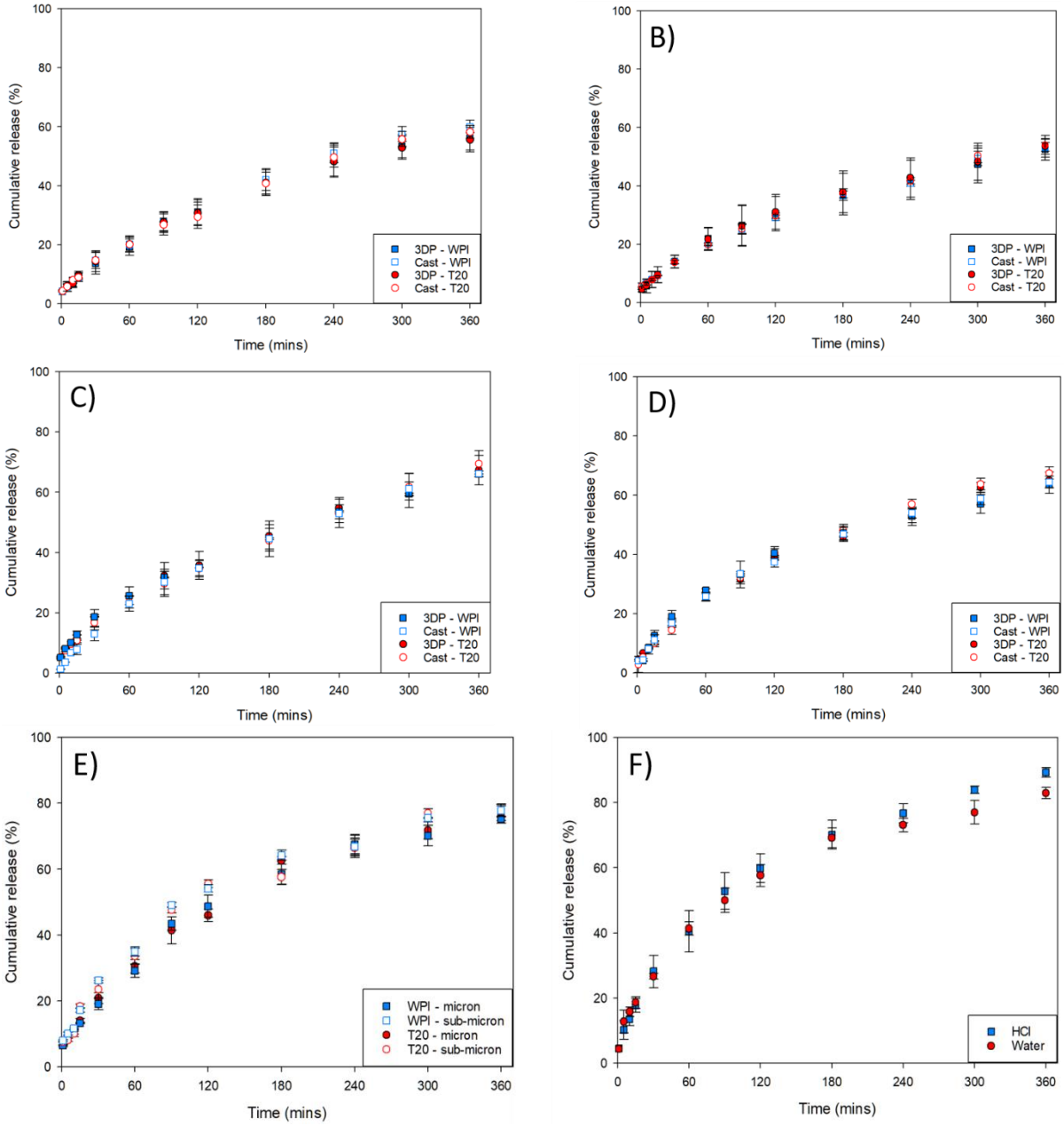

Appendix 9: A comparison of cumulative release rates of cinnamaldehyde from 3DP and cast κC-emulsion gels stabilised by T20 or WPI, at (A) 20 ˚C in water (B) PBS at 20 ˚C, (C) 0.1M HCl at 20 ˚C, (D) 1M KCl at 37 ˚C, (E) release from non-gelled emulsions in water and (F) release from cinnamaldehyde mixed with SFO in HCl and water at 37 ˚C